Rhodium "PONOP" Pincer Complexes for Amine-Borane Dehydrogenation

E. Anastasia K. Spearing-Ewyn

A thesis submitted in partial fulfilment of the requirements for the degree of

Doctor of Philosophy at the University of Oxford





St John's College

January 2020

The work presented in this thesis was carried out between October 2015 and June 2019 under the supervision of Professor Andrew S. Weller. All of the work is my own, unless otherwise stated, and has not been submitted previously for any degree at this, or any other, university.

E. Anastasia K. Spearing-Ewyn

January 2020

Acknowledgements

First and foremost, I am forever grateful for having Professor Andrew Weller as my DPhil supervisor. Thank you for going above and beyond for me, even before my first day in the lab, and continuing that support all the way through my DPhil studies and the hardships that have come to pass during this time. Thank you for your constant enthusiasm about my research which kept me motivated and thank you for helping me to see that elusive bigger picture. I will keep practising! I can honestly say I would not have got this far in my studies without you.

Thanks to all of the Weller group that I have worked with … and have put up with my crazy lab dancing/singing! I am so lucky to have worked with so many incredibly bright minded people. Thanks for all the help and advice, even after I have left the lab and am frantically trying to make this thesis make sense! Special shout out for Big Tone for believing in me during some of the toughest times in my life and always, always making time to help. I already miss the tea breaks and Magreller (is that how you spell it?) retreats. Enjoy the swanky new lab in York – I hope you are all settled in and loving it!

Outside the lab, thank you to all my friends at St John's for all the fun times, support and regular lunch dates. Thanks to Kelli (wowser!), Tunrayo (you're living your best life!), Ed and Angelika (the Love birds!), Osman and Razia (sort out the mess inside!), Gwen and Olivia for being awesome. Kelli, thank you for being my rock, for listening to my countless worries, for your solid advice and most of all, for your friendship.

Special thanks to Isobel for providing sanity from beyond the Oxford bubble and doing way more than your part in maintaining our friendship – I appreciate it so much. Thank you to Mabel Gubbins for getting me out of Oxford to go sword dancing each week. Special thanks to Jen for all of the amazing cake and for whisking me away even when rapper was cancelled. Thank you to Angela for all of the sound boarding and help in getting my life organised. You have helped me to develop my self-awareness and self-confidence, for which I am so grateful. Thank you to the Oxford salsa scene for all the dances, especially to the OUST 17-18 for all the smashing performances. Thank you to Sam, Jordan, Christoph, Nozzy, Adam, Charlotte, Alan, Ant, Bob and Jen, Jane and Andrew, Mark and Faye for all the board games, dances and support. Thank you to David and Kelley for letting me write up in paradise with Lady Sage, Chocolat, Croissant and all the other critters.

Last but not least, massive thanks to my mum and Jake. Jake, thank you for stepping into my life mid-DPhil chaos and taking it all on board with so much love, support and patience. Thank you for all the advice, for looking after me, helping me on my road to recovery and most importantly, for being wonderful! Mum, thank you for always being there for me, no matter what. It's going to be an end of an era and you were there every step of the way. I am glad I didn't turn back and kept on going, but I could not have done it without your constant love and support. Thanks team!

Abbreviations

Å	Angstrom
$[Al(O^tBu^F)_4]^-$	$[Al\{OC(CF_3)_3\}_4]^-$
Ar	aryl
atm	atmospheres
$[BAr^{Cl}{}_4]^-$	$[B\{3,5\text{-}C_6H_3Cl_2\}_4]^-$
$[BAr^F{}_4]^-$	$[B\{3,5\text{-}(CF_3)_2C_6H_3\}_4]^-$
Bn	benzyl
bpy	2,2'-bipyridine
Bz	benzoyl
calc.	calculated
COA	cyclooctane
cod	cyclooctadiene
COE	cyclooctene
Cp	cyclopentadienyl
Cp*	(pentamethyl)cyclopentadienyl
Cy	cyclohexyl
Cyp	cyclopentyl
°	degrees
°C	degrees Celsius
δ	chemical shift
ΔG	change in Gibb's free energy
DFT	density functional theory
DIPP	$2,6\text{-}^iPr_2C_6H_3N$
DIPP-nacnac	$CH((CMe)(2,6\text{-}^iPr_2C_6H_3N))_2$
Đ	dispersity index (M_w/M_n)
DMSO	dimethyl sulfoxide
DPEphos	bis(2-(diphenylphosphino)phenyl)ether)
dpp2 or dppe	bis(diphenylphosphino)ethane
dppm	$Ph_2PCH_2PPh_2$
ε	dielectric constant
EA	elemental analysis
EPR	electron paramagentic resonance
eq.	equivalent(s)
ESI-MS	electrospray ionisation mass spectrometry
Et	ethyl
g	gram
γ	gyromagnetic ratio
GC-MS	gas chromatography-mass spectrometry
GPC	gel permeation chromatography

h	hour
HBCat	catecholborane
HBPin	pinacolborane
Hz	Hertz
I	nuclear spin
^{i}Bu	isobutyl
IMes	*N,N'-bis*(2,4,6-trimethylphenyl)imidazol-2-ylidene
^{i}Pr	isopropyl
IR	infrared
I^{t}Bu	1,3-di-*tert*-butylimidazol-2-ylidene
J	joule
J	coupling constant in Hz
K	Kelvin
K_a	association constant
kcal	kilocalorie
KIE	kinetic isotope effect
L	ligand
M	metal or mol dm^{-3}
[M] or [Cat]	metal catalyst
Me	methyl
min	minute
mL	millilitre
M_n	number average molecular weight
mol	mole
mol%	percentage by mole
M_w	weight average molecular weight
m/z	mass to charge ratio
^{n}Bu	normal butyl
NHC	N-heterocyclic carbene
NMR	nuclear magnetic resonance
ν_{CO}	wavenumber in cm^{-1} of CO
ν_{max}	maximum rate
OAc	acetate
OMs	mesylate
OTf	triflate
PBP	bis-phosphinoboryl
$^{t\text{Bu}}$PCP	κ^3-C_6H_3-2,6-$(CH_2P^tBu_2)_2$
Ph	phenyl
$^{t\text{Bu}}$PNP	κ^3-C_5H_3N-2,6-$(CH_2P^tBu_2)_2$
$^{t\text{Bu}}$PNP’	κ^3-C_5H_3N-2-$(CH_2P^tBu_2)$-6-(CHP^tBu_2)
$^{i\text{Pr}}$PNP	$N(CH_2CH_2P^iPr_2)_2$
$^{i\text{Pr}}$PNP^{H}	$HN(CH_2CH_2P^iPr_2)_2$

$^{t\text{Bu}}$POCOP	κ^3-C_6H_3-2,6-$(OP^tBu_2)_2$
PONOP or $^{t\text{Bu}}$PONOP	κ^3-C_5H_3N-2,6-$(OP^tBu_2)_2$
$^{\text{Cy}}$PONOP	κ^3-C_6H_3-2,6-$(OPCy_2)_2$
$^{i\text{Pr}}$POSOP	$S(CH_2CH_2P^iPr_2)_2$
ppm	parts per million
r.t.	room temperature
s	second
S	solvent
σ-CAM	sigma complex assisted metathesis
t or T	time
TBE	*tert*-butylethylene
^{t}Bu	tertiary butyl
TEM	transmission electron microscopy
THF	tetrahydrofuran
TMEDA	tetramethylethylenediamine
TOF	turnover frequency
TON	turnover number
UV/Vis	ultraviolet/visible
VAM	vinyl acetate monomer
VTNA	Variable Time Normalisation Analysis
wt%	percentage by weight
Xantphos-Ph	4,5-bis(diphenylphosphino)-9,9-dimethylxanthene
Xantphos-Ph'	4-phenylphosphido-5-diphenylphosphino-9,9-dimethylxanthene
Xantphos-^{i}Pr	4,5-bis(diisopropylphosphino)-9,9-dimethylxanthene

NMR spectra analysis:

br	broad
d	doublet
m	multiplet
q	quartet
s	singlet
t	triplet

Abstract

This thesis explores the reactivity of the {Rh(PONOP)}$^{+}$ fragment with the tertiary amine-borane, $H_3B{\cdot}NMe_3$, and the secondary amine-borane, $H_3B{\cdot}NMe_2H$, with an overall aim of gaining mechanistic insight into the transition metal-catalysed dehydrocoupling of amine-boranes.

Chapter One provides a thorough outline of the background that the work reported in this thesis follows on from. Chapter Two describes the synthesis of several {Rh(PONOP)}$^{+}$–based complexes as potential pre-catalysts for amine-borane dehydrocoupling. Their stoichiometric reactivity with $H_3B{\cdot}NMe_3$ and $H_3B{\cdot}NMe_2H$ is described and an amine-borane sigma complex is isolated and fully characterised. A neutral, monohydride complex, Rh(PONOP)H, is also synthesised and fully characterised. At the end of this chapter, adaptation of the PONOP ligand is preliminarily investigated. Chapter Three builds upon Chapter Two and describes an in-depth study of the catalytic dehydrocoupling of $H_3B{\cdot}NMe_2H$ with {Rh(PONOP)}$^{+}$. Speciation studies, kinetic measurements and DFT calculations lead to a mechanistic proposal where neutral Rh(PONOP)H is a key intermediate. The roles of amine (NMe_2H), boronium ($[H_2B(NMe_2H)_2][BAr^F{}_4]$), and ammonium ($[NMe_2H_2][BAr^F{}_4]$) in catalysis are also probed. Finally, in Chapter Four the general reactivity of Rh(PONOP)H is explored. In particular, the potential of Rh(PONOP)H as a catalyst for the reduction of CO_2 is probed and Rh(PONOP)H is found to catalytically react with $H_3B{\cdot}NMe_2H$ in the presence of CO_2.

Contents

Declaration *ii*
Acknowledgements *iii*
Abbreviations *v*
Abstract *viii*
Contents *ix*

1 Introduction 1
1.1 Overview 1
1.2 Organotransition metal complexes 1
1.3 Rhodium: properties and application in catalysis 3
1.4 Phosphine ligands 5
1.4.1 Bonding in transition metal complexes 6
1.4.2 Chelating phosphines 8
1.5 Weakly coordinating anions and solvents 10
1.6 Amine-boranes 13
1.6.1 Dehydrocoupling of amine-boranes 14
1.6.2 General pathways for the dehydrocoupling of amine-boranes 15
1.7 Metal-catalysed dehydrocoupling of amine-boranes 17
1.7.1 Main group-catalysed dehydrocoupling of amine-boranes 17
1.7.2 Transition metal-catalysed dehydrocoupling of amine-boranes 20
1.7.2.1 Heterogeneous catalysis for the dehydrocoupling of amine-boranes 21
1.7.2.2 Homogeneous catalysis for the dehydrocoupling of amine-boranes 23
1.8 Sigma complexes 47
1.8.1 Dihydrogen sigma complexes 49
1.8.2 Amine-borane sigma complexes 51
1.9 Boronium as an intermediate in the dehydrocoupling of amine-boranes 54
1.10 Pincer ligands 61
1.11 Pincer-supported transition metal hydride complexes 66
1.12 Summary 72
1.13 References 73

2 {Rh(PONOP)}$^{+}$-based pre-catalysts for the dehydrogenation of amine-boranes 83

2.1 Introduction 83

2.2 Synthesis of potential catalysts: [Rh(PONOP)(η^2-H$_2$)][BAr$^F_4$] (1), [Rh(PONOP)(κ^1-N$_2$)][BAr$^F_4$] (2) and [Rh(PONOP)(κ^1-ClCH$_2$Cl)][BAr$^F_4$] (3) 85

2.3 Reactivity of complexes 1 and 2 with H$_2$ 91

2.4 Formation of [Rh(PONOP)(η^1-H$_3$B·NMe$_3$)][BAr$^F_4$] (4) 93

2.5 Reactivity of [Rh(PONOP)(η^1-H$_3$B·NMe$_3$)][BAr$^F_4$] (4) 99

2.5.1 Reaction of complex 4 with H$_2$ 99

2.5.2 Reaction of complex 4 with D$_2$ 100

2.5.3 Reaction of complex 4 with excess H$_3$B·NMe$_3$ 104

2.6 Stoichiometric reactivity of complexes 1, 2 and 4 with H$_3$B·NMe$_2$H 106

2.6.1 Reaction of complex 1 with H$_3$B·NMe$_2$H 107

2.6.2 Reaction of complex 2 with H$_3$B·NMe$_2$H 113

2.6.3 Reaction of complex 4 with H$_3$B·NMe$_2$H 118

2.7 Formation of Rh(PONOP)H (6) 121

2.8 Formation of ^{Cy}PONOP analogues 126

2.9 Conclusions 134

2.10 References 136

3 Catalytic dehydrogenation of H$_2$B·NMe$_2$H using [Rh(PONOP)(η^2-H$_2$)][BAr$^F_4$] 140

3.1 Introduction 140

3.2 Trial reactivity under catalytic conditions 142

3.3 Speciation studies under closed conditions 143

3.4 Role of Rh(PONOP)H (6) in catalysis 150

3.5 Probing H/D exchange during the induction period prior to catalysis 157

3.6 Catalysis under open conditions: H$_2$ evolution experiments 161

3.6.1 Speciation studies under open conditions 165

3.6.2 Tests for catalyst homogeneity 167

3.6.3 Kinetic isotope effects 171

3.6.4 Determining order in pre-catalyst 1 and H$_3$B·NMe$_2$H 174

3.7 Interactions of amine-borane with $[H_2B(NMe_2H)_2][BAr^F_4]$ and $[NMe_2H_2][BAr^F_4]$ 180
3.8 Role of NMe_2H in catalysis 188
3.9 Role of $[H_2B(NMe_2H)_2][BAr^F_4]$ and $[NMe_2H_2][BAr^F_4]$ in catalysis 194
3.10 Proposed mechanism for the catalytic dehydrocoupling of $H_3B{\cdot}NMe_2H$ with $[Rh(PONOP)(\eta^2\text{-}H_2)][BAr^F_4]$ (1) 202
3.11 Computational studies of catalytic pathways 205
3.12 Conclusions 210
3.13 Epilogue: further studies involving $[H_2B(NMe_2H)_2][BAr^F_4]$ 212
3.14 References 216
4 Reactivity of Rh(PONOP)H 219
4.1 Introduction 219
4.2 Solubility and stability of Rh(PONOP)H (6) 220
4.3 Protonation of Rh(PONOP)H (6) 223
4.4 Reaction of Rh(PONOP)H (6) with amine-boranes 225
4.4.1 Reaction of complex 6 with $H_3B{\cdot}NMe_3$ 226
4.4.2 Reaction of complex 6 with $H_3B{\cdot}NMe_2H$ 229
4.5 Reaction of complex 6 with H_2 and D_2 231
4.6 Reaction of Rh(PONOP)H (6) with CO_2 234
4.6.1 Formation of Rh(PONOP)OCOH (11) 236
4.6.2 Catalytic hydrogenation of CO_2 to form formic acid 240
4.7 Reaction of Rh(PONOP)OCOH (11) with amine-boranes 242
4.7.1 Reaction of complex 11 with $H_3B{\cdot}NMe_3$ 244
4.7.2 Reaction of complex 11 with $H_3B{\cdot}NMe_2H$ 245
4.8 Reaction of Rh(PONOP)H (6) with acetic acid 265
4.9 Reaction of Rh(PONOP)H (6) with triflic acid 268
4.10 Conclusions 271
4.11 References 272
5 Summary and future outlook 275
6 Experimental 277
6.1 Experimental techniques 277

6.2 Procedure for the addition of $H_2/N_2/D_2/CO_2$ to a reaction mixture 277
6.3 Nuclear Magnetic Resonance (NMR) spectroscopy 278
6.4 Mass spectrometry 278
6.5 Elemental microanalysis 279
6.6 Infrared spectroscopy 279
6.7 Synthesis and characterisation 279
6.7.1 Starting materials 279
6.7.2 Synthesis of [Rh(PONOP)(η^1-$H_3B{\cdot}NMe_3$)][$BAr^F{}_4$] (4) 280
6.7.3 Spectroscopic data for [Rh(PONOP)(η^1-$H_3B{\cdot}NMe_2H$)][$BAr^F{}_4$] (5) 281
6.7.4 Synthesis of Li[$H_3B{\cdot}NMe_2$] 281
6.7.5 Synthesis of Rh(PONOP)H (6) 282
6.7.6 Synthesis of Rh(^{Cy}PONOP)Cl (7) 283
6.7.7 Spectroscopic data for [Rh(^{Cy}PONOP)(κ^1-N_2)][$BAr^F{}_4$] (8) 283
6.7.8 Spectroscopic data for [Rh(^{Cy}PONOP)(η^2-H_2)][$BAr^F{}_4$] (9) 283
6.7.9 Synthesis of [Rh(^{Cy}PONOP)(η^1-$H_3B{\cdot}NMe_3$)][$BAr^F{}_4$] (10) 284
6.7.10 Synthesis of $D_3B{\cdot}NMe_2H$ 284
6.7.11 *In situ* synthesis of Rh(PONOP)(OCOH) (11) 285
6.7.12 Synthesis of $HMe_2N{\cdot}BH_2OCOH$ (12) 286
6.7.13 Synthesis of $HMe_2N{\cdot}BH(OCOH)_2$ (13) 287
6.7.14 Synthesis of Rh(PONOP)OAc (14) 288
6.7.15 Synthesis of Rh(PONOP)OTf (15) 288
6.8 General procedures for the catalytic dehydrogenation of $H_3B{\cdot}NMe_2H$ 289
6.8.1 Under closed/NMR tube conditions 289
6.8.2 Under H_2 evolution measurement conditions 290
6.9 Computational details 290
6.10 X-ray crystallography 291
6.10.1 Crystallographic data 293
6.11 References 296

1 Introduction

1.1 Overview

This thesis provides an in-depth analysis of the stoichiometric and catalytic reactivity of the {Rh(PONOP)}$^{+}$ fragment with amine-boranes, specifically $H_3B{\cdot}NMe_2H$. The synthesis and reactivity of the neutral rhodium hydride, Rh(PONOP)H is also investigated. This chapter introduces the areas of metal-based catalysis generally and amine-borane dehydrocoupling specifically, outlining the background and understanding needed for the rest of this thesis to build upon.

1.2 Organotransition metal complexes

Organotransition metal chemistry is the study of the interactions between organic molecules and transition metal centres. The resulting complexes contain *d* orbitals which, when empty, allow for the coordination of substrates and products. The presence of valence electrons in these *d* orbitals leads to the formation of variable oxidation states, which in turn facilitates bond activation processes such as oxidative addition and reductive elimination.[1,2] The accessibility of these reaction pathways allows organotransition metal complexes to act effectively as catalysts; whereas, main group organometallic complexes tend to be stoichiometric reagents (although the area of main group catalysis, operating via constant and variable oxidation state cycles, is rapidly developing).[3–5] The use of only catalytic amounts of organotransition metal complexes counterbalances the difference in cost of precious metal-based catalysts compared to much cheaper main group metal complexes used stoichiometrically. Organotransition metal complexes are essential

in the catalysis of organic reactions as such catalysts facilitate reactivity at lower temperatures and pressures and also limit waste products, such as inorganic salts.[6] In the pharmaceutical industry, chiral organotransition metal catalysts enable single pure enantiomers of a product to be obtained, which is extremely important if one enantiomer of a drug is highly active but the other is toxic.[7,8]

There are many other commercial processes that employ organotransition metal catalysts. For example, both rhodium and iridium complexes are used to catalyse the carbonylation of methanol to form acetic acid (the Monsanto and Cativa processes, respectively).[9] Acetic acid is a commodity chemical that is commonly used in the production of vinyl acetate monomer (VAM), which in turn has many uses such as in the production of paints and adhesives.[10] In the 1930s, Roelen discovered that $Co_2(CO)_8$ could be employed as a pre-catalyst for the hydroformylation of alkenes,[11] the process of converting alkenes to aldehydes using H_2 and CO. This process gave a mixture of primary and secondary aldehydes however, the addition of $P(^nBu)_3$ to the pre-catalyst was shown to not only offer greater selectivity for the primary aldehyde product, but also give a more active catalyst.[12] Other industrially important catalytic transformations that employ organotransition metal complexes include: olefin hydrogenation;[13] the hydrocyanation of alkenes;[14] olefin polymerisation[15] and cross coupling.[16] The widespread importance of organotransition metal catalysis is further highlighted by three Nobel prizes awarded for development in this area: in 2001 to Knowles, Noyori and Sharpless for their work developing asymmetric catalysts;[17] in 2005 to Chauvin, Grubbs and Schrock for their work on alkene metathesis;[18] and in 2010

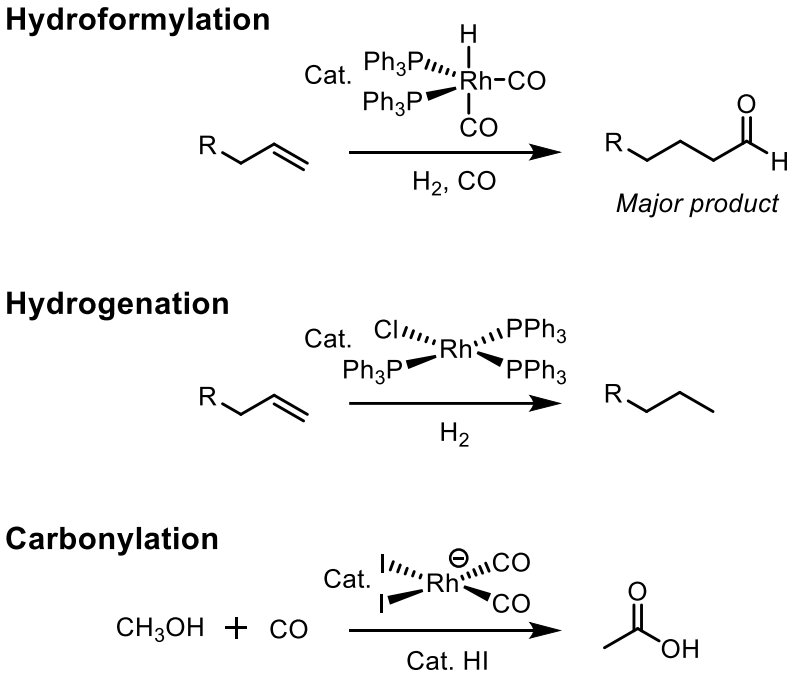
to Heck, Negishi and Suzuki for their work on palladium-catalysed cross coupling reaction.[19]

The main outcome of many of these organotransition metal-catalysed processes is the breaking or forming of carbon-element bonds. In contrast, the catalytic formation of other main group-main group bonds is relatively underdeveloped.[20] One such transformation, the catalytic formation of B–N bonds, is the focus of Chapters Two and Three.

1.3 Rhodium: properties and application in catalysis

Rhodium is a rare precious metal that occurs elementally or as part of a compound in the Earth's crust with a low natural abundance of 0.0002 ppm.[21] It has an electronic ground state of $[Kr]4d^8 5s^1$ placing it in group nine of the periodic table as a late, second row transition metal. Although rhodium has been found to exist in oxidation states from –III through to +VI, the extremes of this range are very unstable; for example, RhF_6 can react with glass.[21] Compared to early transition metals, rhodium has an increased electronegativity therefore the valence *d* electron orbitals are more stable and so only the low oxidation states are easily accessed, with the most commonly observed being +I and +III. These two oxidation states are both accessible and differ by a charge of two meaning rhodium can facilitate the two electron processes of oxidative addition and reductive elimination, making it an ideal transition metal catalyst.[1]

The main use of rhodium (greater than 80 % of global consumption) is in catalytic converters in the automobile industry in order to reduce harmful emissions such as nitrogen oxides, carbon monoxide and unburned hydrocarbons.[22] Rhodium complexes are also well-known as catalysts for many other industrial processes such as hydroformylation, hydrogenation and carbonylation (**Scheme 1.1**).



Scheme 1.1 Examples of industrially relevant reactions using rhodium-based complexes as catalysts.

As described in section 1.2, $Co_2(CO)_8$ has been employed as a pre-catalyst for the hydroformylation of alkenes. However, $RhH(CO)(PPh_3)_3$ was found to be a more active pre-catalyst for this process, with an even greater selectivity for the primary aldehyde product as well as reaction conditions reduced to 25 °C and atmospheric pressure.[23] Wilkinson's catalyst, $RhCl(PPh_3)_3$, is well-known to catalyse the hydrogenation of alkenes under ambient conditions,[13] as are the Schrock-Osborn

cationic rhodium complexes of the formula $[RhL_2(H)_2(S)_2]^+$ (where L_2 = two tertiary phosphine ligands or one bisphosphine and S = a polar solvent molecule).[24] Another industrially relevant process is the carbonylation of methanol to produce acetic acid, catalysed by the Rh^I complex, $[RhI_2(CO)_2]^-$.[25] The wide-ranging application of rhodium complexes goes on to include the catalytic hydrogenation of nitriles, aldehydes and ketones, the dehydrogenation of alkanes and alcohols and the carbonylation of alkyl halides and amines.[26] Chapters Two and Three will investigate the specific use of a rhodium complex to catalyse the dehydrocoupling of amine-boranes.

1.4 Phosphine ligands

Phosphines, PR_3, are some of the most commonly used ligands in organometallic chemistry. Tertiary phosphines easily form complexes with transition metals, especially late transition metals, as the lone pair on phosphorus can act as a Lewis base to a soft metal centre in a low oxidation state.[2] Thus there are a great number of known transition metal complexes containing a diverse range of phosphine ligands. By varying R in PR_3, the steric and electronic properties of the phosphine ligand can be predictably altered, affecting the reactivity of the metal centre in a transition metal complex. These steric and electronic effects can be exploited in order to improve the activity or selectivity of catalytic reactions. Another advantage of phosphine ligands is that the ^{31}P nucleus has a spin of ½ and 100 % isotopic abundance, meaning that any phosphine-containing organometallic complex can be studied using NMR spectroscopy.

1.4.1 Bonding in transition metal complexes

Phosphine ligands can act as both σ donors and π acceptors. The lone pair on phosphorus can donate into an empty metal *d* orbital of the appropriate symmetry forming a σ bond whilst filled metal d_π orbitals can back-donate into an empty hybrid orbital on the ligand (**Figure 1.1**).[27,28] This hybrid orbital is a mixture of the P–R σ* antibonding orbital and a vacant phosphorus d_π orbital and is of suitable energy to overlap with the filled metal d_π orbitals.

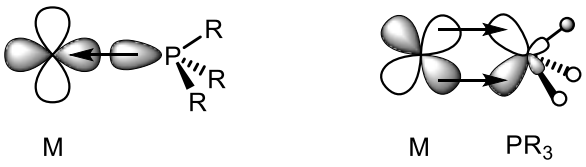


Figure 1.1 Bonding between a tertiary phosphine (PR_3) and a transition metal (M). *Left:* σ donation from lone pair on phosphorus. *Right:* π back-donation from filled metal d_π orbitals.

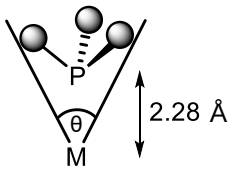
The ability of the phosphine ligand to accept π back-donation from the metal centre depends on the electronegativity of the R group.[1] A more electron withdrawing substituent lowers the energy of the P–R acceptor orbital and also increases the phosphorus 3*p* character of this orbital, which improves its directionality towards the metal, and so π back-bonding is enhanced, i.e. the ligand is a better π-acid. **Figure 1.2** depicts several common tertiary phosphines in order of π-acidity relative to CO.

$$PMe_3 \approx P(NR_2)_3 < PAr_3 < P(OR)_3 < PCl_3 < PF_3 \approx CO$$

Figure 1.2 Examples of tertiary phosphines arranged in order of increasing π-acidity, relative to CO.[1]

The electron donor-acceptor properties of a range of tertiary phosphines were quantified by Tolman, who measured how the highest frequency ν_{CO} band in $[Ni(CO)_3(PR_3)]$ varied for different R substituents.[29] Phosphines with greater π-acidity reduce the electron density at the metal centre and so reduce the back-bonding to the CO ligands leading to an increase in ν_{CO} compared to a value of ν_{CO} = 2056.1 cm^{-1} when R = ^{t}Bu.

As well as electronic effects, the steric effects of phosphine ligands can also have a major effect on the reactivity of organometallic complexes.[30] After studying competitive phosphorus ligand exchange in Ni^0 complexes, Tolman developed a structural parameter to quantify these steric properties called the cone angle, θ (**Figure 1.3**).[31] The Tolman cone angle is the angle between the outer edges of the substituents at phosphorus in a space filling model of M–PR_3 where the metal lies at the vertex of the cone, which is fixed at 2.28 Å from the centre of the phosphorus atom.



$PH_3 < PF_3 < PMe_3 < PMe_2Ph < PEt_3 < PPh_3 < PCy_3 < P^tBu_3$

Figure 1.3 *Top:* Tolman cone angle, θ. *Bottom:* Selected tertiary phosphines arranged in order of increasing steric bulk and therefore cone angle.

The Tolman cone angle is calculated based upon assumptions such as fixed bond lengths or the averaging of angles in the case of asymmetric ligands. A more accurate method for quantifying steric parameters, especially for more complex multidentate ligands, is the solid cone angle, Θ.[32] This parameter can be calculated based upon the exact geometry of the ligand if this is known from crystallography or computations.

1.4.2 Chelating phosphines

Chelating ligands are those that contain more than one donor atom connected by a bridge and can therefore bind to the metal through more than one site. These multidentate ligands are less prone to ligand displacement compared to their monodentate analogues due to the chelate effect.[1] In 1990, Casey and Whitaker developed a method to quantify chelating bisphosphine ligands called the "natural bite angle", β, which is defined as the "preferred chelation angle determined only by ligand backbone constraints" (**Figure 1.4**).[33] The longer the backbone of the chelating ligand, the larger the P–M–P angle or bite angle, β.

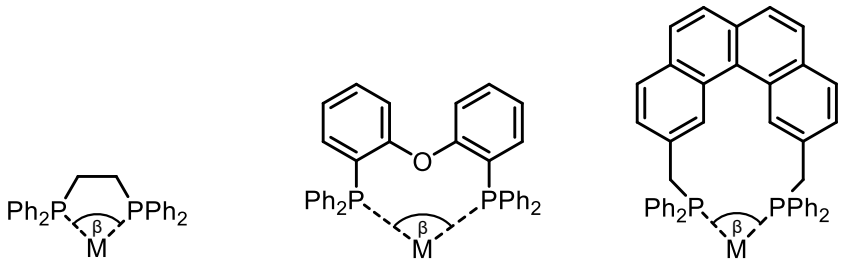


Figure 1.4 Natural bite angles, β, for selected chelating bisphosphine ligands: dpp2,[34] DPEphos[35] and Transphos.[33]

As the bite angle of a chelating phosphine is varied, the overall steric bulk of the ligand and also its electronic properties are affected, leading to a preference for certain geometries in a transition metal complex.[36] For example, chelating ligands with natural bite angles around 90°, such as bis(diphenylphosphino)ethane (which is referred to in this thesis as dpp2 in order to reflect the two carbon linker), will prefer *cis* coordination to the metal centre; whereas, ligands with a wider bite angle, such as transphos, can achieve *trans* geometries.[37]

The size of the bite angle of a chelating ligand can also strongly affect the reactivity and regioselectivity of an organometallic complex. For example, the Weller group have shown that for the dehydrogenation of $H_3B{\cdot}NMe_2H$ catalysed by $\{RhPPh_2(CH_2)_xPPh_2\}^+$, where x = 3 – 5, the smaller the bite angle the faster the rate.[38] Interestingly, when x = 2, no dehydrocoupling is observed as the amine-borane does not bind competitively to the metal centre when the ligand has such a small bite angle. Another example is the correlation between bite angle and regioselectivity of the aldehyde product in rhodium-catalysed hydroformylation

published by Casey *et al.*, which showed that selectivity for the linear product increased with a larger ligand bite angle.[34]

As well as bidentate chelating phosphines, multidentate analogues with an additional heteroatom (C, N, O) linkage are also commonly employed as ligands for organometallic complexes.[39] The ability to coordinate to the metal atom via a third donor atom achieves a classical pincer ligand geometry (see section 1.10), which offers another point of control over the reactivity of the complex.

1.5 Weakly coordinating anions and solvents

Rhodium-based complexes that are successful catalysts are usually able to form reactive low-coordinate cationic species. Such species are often proposed as intermediates during catalysis and so studying these species may increase the understanding of the relevant catalytic cycle. These low-coordinate, cationic complexes can be stabilised by weak interactions with solvent, the counterion or even agostic bonds (three-centre-two-electron M–H–C covalent bonds)[40] from ancillary ligands (**Figure 1.5**).[41] However, these stabilising agents need to form very labile bonds if the metal complex is to remain reactive and able to reveal a "vacant coordination site" in the presence of substrate.

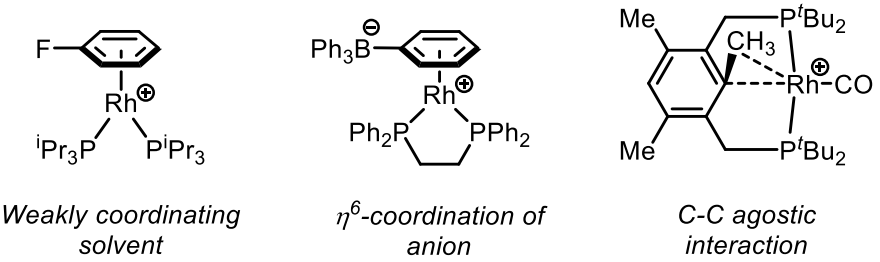


Figure 1.5 Examples of cationic, low-coordinate rhodium complexes stabilised by solvent (*left*),[42] anion (*middle*)[43] and an agostic interaction (*right*).[44] $[BAr^F_4]^-$ anions omitted for clarity.

When synthesising low-coordinate, cationic rhodium complexes, an appropriately weakly coordinating anion must be employed in order to allow any vacant sites at the metal centre to be easily accessible.[45] $[PF_6]^-$ and $[BF_6]^-$ are examples of weakly coordinating anions that are commonly used; however, under certain conditions they can be involved in competitive side reactions such as hydrolysis[46] or fluoride abstraction.[47,48] **Figure 1.6** depicts examples of other well-known, weakly coordinating anions, which are much less reactive.

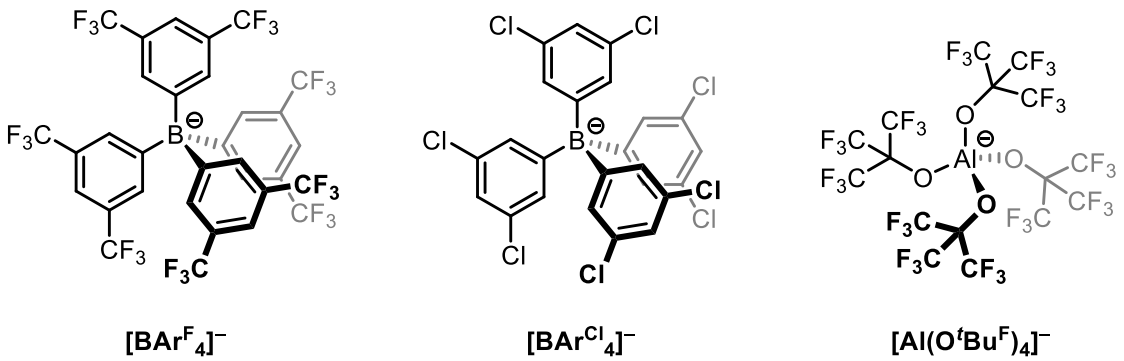


Figure 1.6 Examples of weakly coordinating anions.

The negative charge on the $[BAr^F_4]^-$ anion (Ar^F = 3,5-$C_6H_3(CF_3)_2$)[49] is delocalised across the multiple electronegative aryl groups. This diffusion of charge and the

large bulky aryl rings make $[BAr^F{}_4]^-$ an ideal counterion to low-valent cationic rhodium complexes.[41] Also, the synthesis of various salts of $[BAr^F{}_4]^-$ is relatively straight forward[50] and both boron ($^{10}B/^{11}B$) and fluorine (^{19}F) are NMR active nuclei, therefore $[BAr^F{}_4]^-$ is the main counteranion used in this thesis. $[BAr^{Cl}{}_4]^-$ (Ar^{Cl} = 3,5-$C_6H_3Cl_2$)[51] is similar to $[BAr^F{}_4]^-$ however, while the lack of CF_3 groups reduces rotational disorder observed in crystal structures obtained by single crystal X-ray diffraction, the anion is less straight forward to prepare and shows decreased solubility in its salts. The aluminium-based anion $[Al(O^tBu^F)_4]^-$, where $^tBu^F$ = $C(CF_3)_3$,[52] is another example of a bulky, weakly coordinating anion popularised by Krossing.

The choice of solvent for catalysis is also important.[1] A strongly coordinating solvent such as MeCN, pyridine or DMSO will most likely bind to the metal centre and prevent the substrate from coordinating, thus killing the catalyst. Solvents such as THF, acetone, water and ethanol are more weakly coordinating however, their nucleophilicity can still lead to undesirable coordination.[53] Halocarbon solvents can be oxidising and have been shown to coordinate to complexes.[54] Fluorinated arenes are even more weakly coordinating, though can bind in principle (as shown in **Figure 1.5**).[55] The majority of work in this thesis is carried out in 1,2-$F_2C_6H_4$: a weakly coordinating, non-nucleophilic solvent that is relatively chemically inert and has a large enough dielectric constant to dissolve a range of transition metal complexes (ε = 13.4 for 1,2-$F_2C_6H_4$, compared to ε = 9.1 for CH_2Cl_2).[56]

1.6 Amine-boranes

The complexation of Lewis-acidic boranes to Lewis-basic amines gives rise to the classical adducts that are amine-borane complexes ($R_3B{\cdot}NR_3$),[57] the majority of which are relatively air and moisture stable.[58] This class of inorganic molecules can be varied by substitution at both the boron and nitrogen atoms, the parent complex being ammonia-borane, $H_3B{\cdot}NH_3$. Amine-boranes are isoelectronic with olefins, their all-carbon analogues; however, due to the dipole generated between boron and nitrogen, amine-boranes have different properties.[59] Amine-boranes possess protic N–H bonds and hydridic B–H bonds, which can result in the formation of inter- or intramolecular B–H···H–N "non-classical" dihydrogen bonds, thus explaining why ammonia-borane is a solid at room temperature (melting point 109 °C) whereas the isoelectronic analogue ethane is a gas (melting point –183 °C).[60–62]

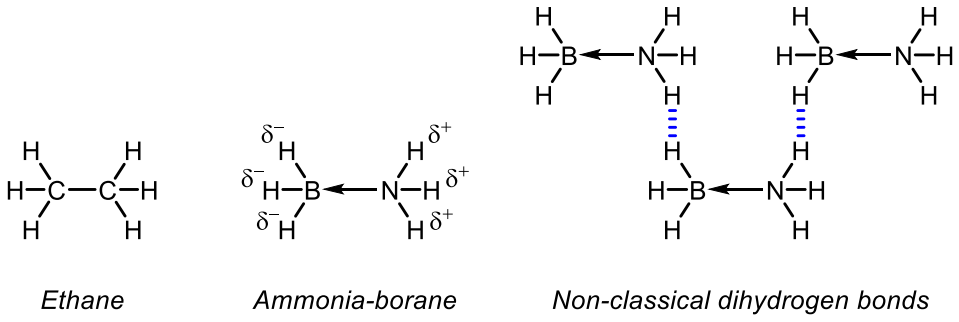


Figure 1.7 Comparison of the isoelectronic analogues, ethane and ammonia-borane.

1.6.1 Dehydrocoupling of amine-boranes

Dehydrocoupling is defined as the formation of a new element-element chemical bond accompanied by the simultaneous release of H_2.[63] Amine-boranes containing adjacent hydridic B–H and protic N–H bonds can undergo dehydrocoupling,[61] forming a new B–N bond. Dihydrogen loss is promoted by the B–H···H–N dihydrogen bonds making this process much more energetically feasible than for alkane analogues.[64,65] Although the B–N bond in ammonia-borane is rather weak (114 kJ mol^{-1}),[66] it is of sufficient strength that dehydrogenation can be favoured over dissociation to the respective amine and borane.[67]

Ammonia-borane is a molecule that has received significant interest over the last decade due to the combination of its low molecular weight (30.86 g mol^{-1}) and high gravimetric hydrogen capacity (19.6 wt%),[68] identifying it as a potential hydrogen storage material for use in fuel cells.[69] However, although liberation of hydrogen from ammonia-borane is relatively facile, the regeneration of ammonia-borane from the 'spent fuel' products is not yet energetically or economically viable.[57,66,70,71] Furthermore, as mentioned above, ammonia-borane is a solid at room temperature and as use of solid fuels is not currently common, major changes to infrastructure would be necessary for successful employment of hydrogen-based fuel cells. [72]

The products formed from the dehydrocoupling of amine-boranes have offered an alternative area of study due to their potential as novel materials. For example, polyaminoboranes, $[H_2BNRH]_n$, are products of dehydrocoupling that are

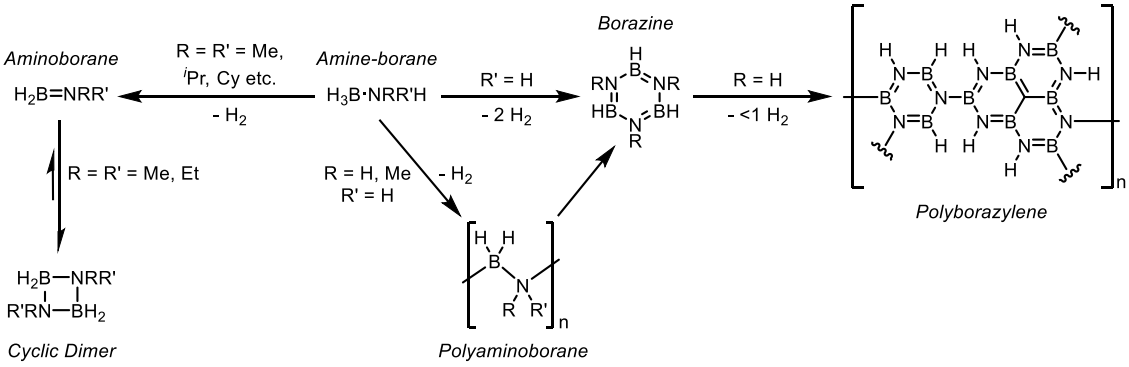
isoelectronic with societally ubiquitous polyolefins, the chemistry of which is well-understood.[57,73] These inorganic polymers already have a number of potential applications, such as precursors to high temperature boron-nitride ceramics, piezoelectric materials[74] and aluminium borate nanomaterials.[75] However, reliable syntheses of polyaminoboranes are relatively underdeveloped and the precise mechanism of their formation is still unknown.[76] Borazine, $[HBNR]_3$, and polyborazylene, BNH_x, are also products from the dehydrocoupling of amine-boranes and have shown to be precursors to the formation of hexagonal boron-nitride (*h*-BN).[77,78] *h*-BN, also known as 'white graphene', is a wide band gap insulator with many applications including in lubricants, cosmetics and graphene-based electronics.[79] Although much research has been carried out, understanding of these inorganic materials is still relatively limited compared to their organic analogues and so there is a demand for further mechanistic study into the process of dehydrocoupling in order to advance knowledge of this field.[63]

1.6.2 General pathways for the dehydrocoupling of amine-boranes

Amine-boranes can be thermally dehydrocoupled at temperatures greater than 100 °C, giving a mixture of BN coupled products;[80] however, the employment of transition metal catalysts allows for more control over dehydrogenation and subsequent coupling, allowing the use of lower temperatures and control of product distributions.[20]

Products from catalytic dehydrocoupling can vary depending on the nature of the parent amine-borane (**Scheme 1.2**).[81] Primary amine-boranes, $H_3B{\cdot}NRH_2$, can

undergo loss of one equivalent of hydrogen to form polyaminoboranes, $[H_2BNRH]_n$,[82] and loss of a further equivalent of hydrogen to yield borazine, $[HBNR]_3$, the thermodynamic product.[83] Ammonia-borane can be dehydrocoupled further to yield polyborazylene, BNH_x.[84] Secondary amine-boranes, $H_3B{\cdot}NR_2H$, can only release one equivalent of hydrogen forming the corresponding aminoborane (for example $H_2B{=}NMe_2$).[85] With non-bulky N-substituents (e.g. R = Me, Et), these aminoboranes are unstable and readily dimerise to yield the respective cyclic dimer, $[H_2BNR_2]_2$,[86] however, with bulkier substituents such as ^{i}Pr or Cy, the respective aminoborane is the final dehydrogenation product.[83,87]



Scheme 1.2 General pathways for the dehydrocoupling of primary and secondary amine-boranes. All steps can be mediated by metal catalysts.

The oligomeric and polymeric products of the dehydrocoupling of $H_3B{\cdot}NH_3$ and $H_3B{\cdot}NMeH_2$ are often formed in an insoluble and poorly defined mixture, rendering full characterisation and mechanistic study difficult.[82] Conversely, the intermediates and products from the dehydrocoupling of $H_3B{\cdot}NMe_2H$ are well-defined and soluble and selective formation of the cyclic dimer product, $[H_2BNR_2]_2$, is not greatly influenced by catalyst loadings. This makes speciation and kinetic

studies much easier to carry out. Therefore, $H_3B{\cdot}NMe_2H$ is often used as a model for investigating the dehydrocoupling of primary amine-boranes.[88]

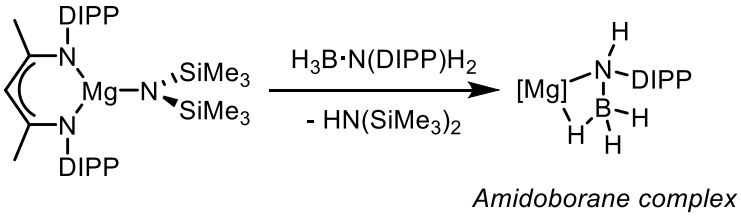
1.7 Metal-catalysed dehydrocoupling of amine-boranes

As described above, amine-boranes can be thermally dehydrocoupled to give a mixture of BN compounds; however, the use of transition metal-based catalysts for this process not only offers some control over these product distributions but also may negate the use of harsh reaction conditions.[76,89] In 1989, Roberts and co-workers were the first to report metal-catalysed amine-borane dehydrocoupling.[90] $H_3B{\cdot}N^tBuMeH$ was catalytically dehydrocoupled using 10 mol% palladium on charcoal at 120 °C. The product aminoborane, $H_2B{=}N^tBuMe$, is a volatile liquid that solidifies at room temperature to yield a mixture of two isomeric dimers, E/Z-$(H_2BN^tBuMe)_2$. However, catalytic dehydrocoupling of amine-boranes at lower temperatures was not reported until over a decade later when Manners and co-workers used $[Rh(1,5\text{-cod})(\mu\text{-Cl})]_2$ (cod = cyclooctadiene) to dehydrocouple both primary and secondary amine boranes at room temperature.[83,86] Since then, there have been many further examples of the use of transition metals[76,91,92] and also main group metals[81,93] as dehydrocoupling catalysts.

1.7.1 Main group-catalysed dehydrocoupling of amine-boranes

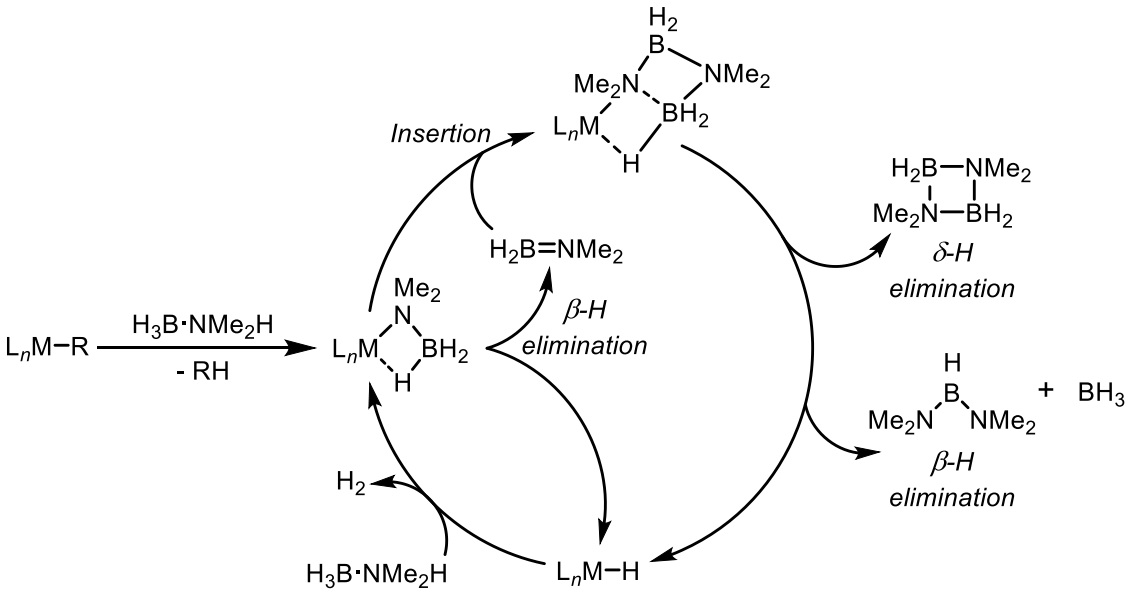
Alongside transition metal-based catalysts, a diverse range of main group metals have been employed as catalysts for the dehydrocoupling of amine-boranes, although lower turnovers are generally reported.

The first use of a main group metal for the catalytic dehydrocoupling of amine-boranes was reported in 2009 by Harder and co-workers.[94] A magnesium centre surrounded by the bulky β-diketiminate ligand DIPP-nacnac (DIPP-nacnac = $CH((CMe)(2,6\text{-}^{i}Pr_2C_6H_3N))_2$) was shown to catalyse the dehydrogenation of $H_3B{\cdot}N(DIPP)H_2$ to $HB(N(DIPP)H)_2$ and BH_3 (detected as B_2H_6) via a magnesium-amidoborane complex (**Scheme 1.3**).



Scheme 1.3 Formation of a magnesium-amidoborane complex that is proposed to be the active catalyst in the dehydrocoupling of $H_3B{\cdot}N(DIPP)H_2$.[94]

One year later, Hill and co-workers reported that alkyl magnesium and calcium complexes were active for the dehydrocoupling of $H_3B{\cdot}NMe_2H$ to $[H_2BNMe_2]_2$ and proposed a mechanism for this process (**Scheme 1.4**).[95]



Scheme 1.4 Proposed mechanism for the dehydrocoupling of $H_3B{\cdot}NMe_2H$ catalysed by group II metals.[95]

Throughout catalysis, $H_2B{=}NMe_2$ and $HB(NMe_2)_2$ were observed, along with a complex where the metal is bound to an anion, $[H_3B{\cdot}NMe_2BH_2{\cdot}NMe_2]^-$. It was proposed that initial N-H activation of $H_3B{\cdot}NMe_2H$ alongside protonation/decomplexation of the ligand yields an amidoborane complex, which can undergo β-H elimination to yield the observed $H_2B{=}NMe_2$ and a metal hydride. $H_2B{=}NMe_2$ can then insert into a further equivalent of the amidoborane complex to yield the amido species $LM[H_3B{\cdot}NMe_2BH_2{\cdot}NMe_2]$. β-H elimination of this species yields the observed $HB(NMe_2)_2$; whereas, δ-H elimination forms the product $[H_2BNMe_2]_2$.

More recently, the p-block metal bismuth has also been employed in the dehydrogenation of ammonia-borane.[96] A bismuthinidene complex was reported to catalyse the transfer-hydrogenation of azoarenes using ammonia-borane as a

hydrogen source, thus achieving simultaneous catalytic dehydrocoupling of the amine-borane. Interestingly, a catalytic cycle involving cycling between the Bi^{I} bismuthinidene complex and an unstable Bi^{III} dihydride was suggested. Such catalytic redox-activity is usually indicative of a transition metal catalyst.

There are many further examples of main group catalysts for the dehydrocoupling of amine-boranes that have been reported including catalysts based upon Al,[97,98] Mg,[99] Ca[100] and Sn.[101]

Although not officially main group elements, group three elements of the periodic table are occasionally included when discussing main group chemistry as they are electropositive and have only one main oxidation state, as in groups one and two. Complexes of scandium,[102] yttrium[102] and lanthanum[103] have been reported to catalyse the dehydrocoupling of amine-boranes. For example, the yttrium complex $(C_5H_5BMe)_2YCH(SiMe_3)_2$ rapidly dehydrocouples $H_3B{\cdot}NMe_2H$ to give the thermodynamic cyclic dimer product, $[H_2BNMe_2]_2$ (TOF = 1015 h^{-1}).[104]

1.7.2 Transition metal-catalysed dehydrocoupling of amine-boranes

There has been a great interest in transition metal complexes as catalysts for the dehydrocoupling of amine-boranes due to their high reactivity and ability to offer milder reaction conditions and product selectivity. A selection of examples from the literature will be visited in this section. But first, it is appropriate to highlight the various natures of a transition metal complex throughout catalysis. The metal complex initially added to the reaction mixture is often only a *pre-catalyst* and must

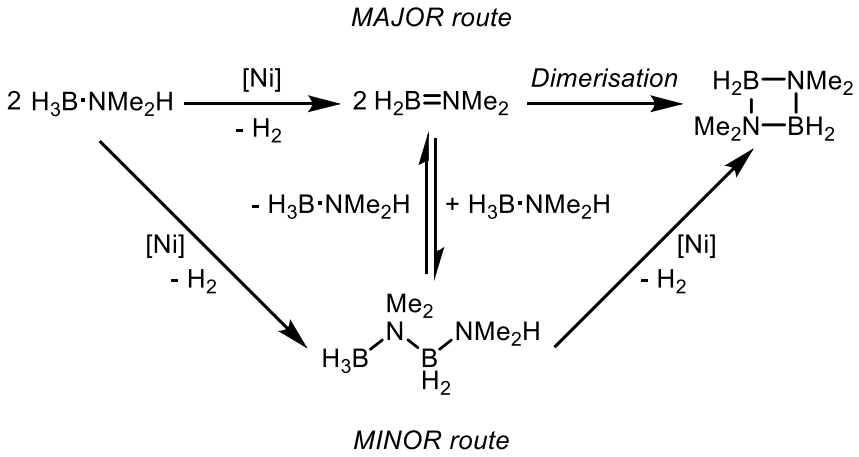
undergo a transformation to form the *active catalyst*, which is usually a far more reactive species. Such a transformation can form reactive metal colloids or nanoparticles, leading to heterogeneous catalysis, or the formation of a single highly active site, leading to homogeneous catalysis. Whether the catalyst is heterogeneous or homogeneous affects the nature of catalysis in terms of reactivity, selectivity and the separation of products.[105]

1.7.2.1 Heterogeneous catalysis for the dehydrocoupling of amine-boranes

One of the most attractive features of heterogeneous catalysis for the dehydrocoupling of amine-boranes is the ease of which the catalyst and products can be separated. As described in section 1.7, Manners and co-workers used $[Rh(1,5\text{-cod})(\mu\text{-Cl})]_2$ to facilitate the catalytic dehydrocoupling of primary and secondary amine-boranes.[86] A few years later, a more in-depth study revealed the nature of the catalyst to be heterogeneous.[83,105,106] Initially an induction period was observed during which a black precipitate was observed to form, which may indicate the slow formation of the active catalyst in the form of rhodium colloids. Analysis of this precipitate by transmission electron microscopy (TEM) showed the presence of ~2 nm rhodium clusters. A period of fast catalytic activity followed the induction period resulting in a sigmoidal kinetic curve, again indicative of heterogeneous catalysis.[107] Multiple tests, developed by Finke, to probe the heterogeneous nature of a catalyst were then performed.[108] Both mercury poisoning and filtration tests halted catalysis and addition of sub-stoichiometric amounts of PPh_3 slowed the rate of catalysis considerably. Later study by Autrey

and co-workers suggested that soluble Rh_6 clusters were in fact the active species.[109]

Manners and co-workers also reported the use of a heterogeneous catalyst in the form of skeletal nickel, which catalytically dehydrocoupled both $H_3B{\cdot}NMe_2H$ and $H_3B{\cdot}NMeH_2$ at 20 °C.[110] Catalytic dehydrocoupling of $H_3B{\cdot}NMe_2H$ to $[H_2BNMe_2]_2$ was shown to proceed mainly via the aminoborane intermediate, $H_2B{=}NMe_2$, but also via the linear diborazane, $H_3B{\cdot}NMe_2BH_2{\cdot}NMe_2H$, formed in low concentrations (**Scheme 1.5**).



Scheme 1.5 Proposed mechanism for the dehydrocoupling of $H_3B{\cdot}NMe_2H$ catalysed by skeletal nickel.[110]

Under similar catalytic conditions, $H_3B{\cdot}NMeH_2$ was shown to dehydrocouple to yield cyclic triborazane, $[H_2BNMeH]_3$; however, under stoichiometric conditions polyaminoborane, $[H_2BNMeH]_n$, was formed (M_n = 51, 300 g mol^{-1}, Đ = 1.5). This remarkable difference in product was attributed to a larger immediate

concentration of $H_2B{=}NMeH$ being formed at high catalyst loadings leading to polymerisation being kinetically favoured over cyclisation.

Heterogeneous catalysts are notably some of the fastest dehydrocoupling catalysts reported. For example, Morris and co-workers showed that iron(0) nanoparticles stabilised by PNNP ligands (PNNP = $(PPh_2C_6H_4CH{=}NCH_2)_2$) could successfully dehydrocouple $H_3B{\cdot}NH_3$ with a TOF of approximately 2, 400 h^{-1}.[111] A mixture of products was formed including borazine, polyborazylene and B–N oligomers.

1.7.2.2 Homogeneous catalysis for the dehydrocoupling of amine-boranes

Catalysis is defined as being homogeneous when the reactants and catalyst are in the same phase. Although heterogeneous catalysis can offer high turnover frequencies and easy product separation, homogeneous catalysis has been more widely studied due to the presence of well-defined coordination sites. These coordination sites can be adapted by making changes to the metal centre or surrounding ligands and therefore the flexibility of these systems allows for detailed study at the molecular level. This potential insight into the dehydrocoupling process may lead to catalyst development and optimisation.

There are two main types of mechanism to describe dehydrocoupling of amine-boranes by a homogeneous catalyst: outer sphere and inner sphere.

An outer sphere mechanism usually involves metal-ligand cooperativity, a process where the ligand environment participates in bond activation alongside the metal,

during the dehydrogenation step.[112,113] For example, in 2009 Schneider *et al*. reported the rapid dehydrocoupling of $H_3B{\cdot}NMe_2H$ to give $[H_2BNMe_2]_2$ using a ruthenium bifunctional catalyst, [Ru($^{i\text{Pr}}$PNP)(H)(PMe_3)] ($^{i\text{Pr}}$PNP = $N(CH_2CH_2P^iPr_2)_2$) (**Figure 1.8**).[114] An initial TOF of approximately 3, 600 h^{-1} was observed until about 70 % conversion, at which point a slower regime became apparent (TOF ~1.5 h^{-1}) suggesting a change in mechanism. The hydrogenated complex *trans*-[Ru($^{i\text{Pr}}$PNP$^{\text{H}}$)(H)$_2$(PMe_3)] ($^{i\text{Pr}}$PNP$^{\text{H}}$ = $HN(CH_2CH_2P^iPr_2)_2$) was observed to be the resting state during the fast regime and when used to dehydrocouple $H_3B{\cdot}NMe_2H$, catalysis proceeded with almost identical kinetics. Another ruthenium species was also observed during catalysis, assigned as [Ru($^{i\text{Pr}}$PNP^{BH_2NMe_2})(H)(PMe_3), which was shown to dehydrocouple $H_3B{\cdot}NMe_2H$ with a similar kinetic profile as observed in the slow regime. Both ruthenium intermediates, which were shown to be active dehydrocoupling catalysts, display ligand cooperativity and so function via an outer sphere mechanism.

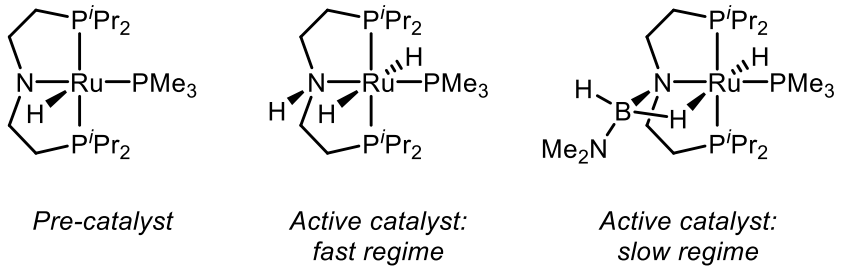
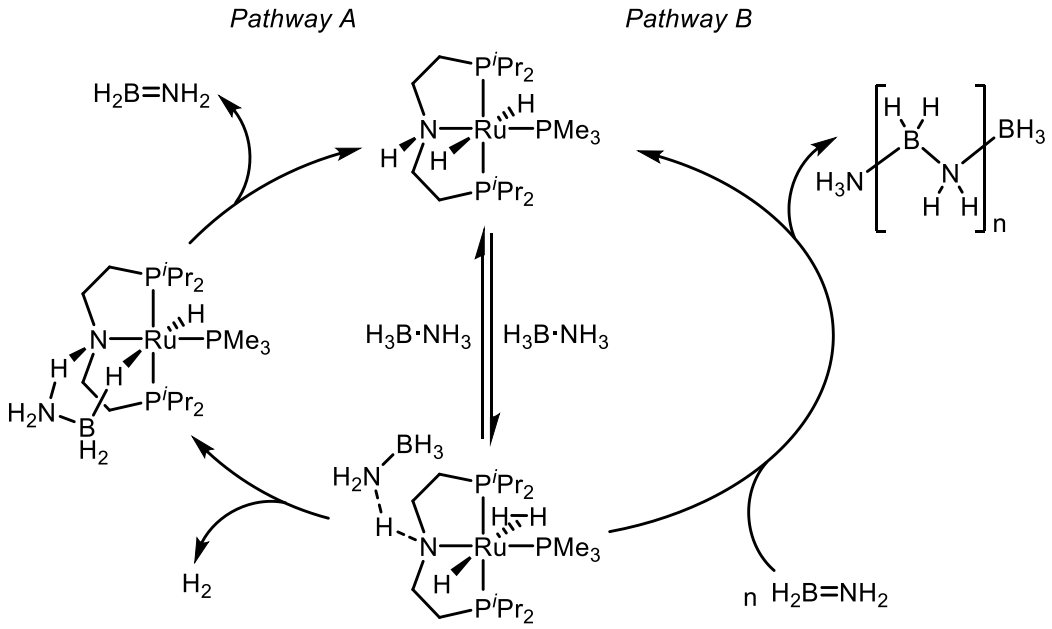


Figure 1.8 Bifunctional ruthenium complexes for the dehydrogenation of $H_3B{\cdot}NMe_2H$.[114]

At the same time, [Ru($^{i\text{Pr}}$PNP)(H)(PMe_3)] was also reported to rapidly dehydrocouple $H_3B{\cdot}NH_3$ to form $[H_2BNH_2]_n$ (TOF ~12, 000 h^{-1}) along with a small

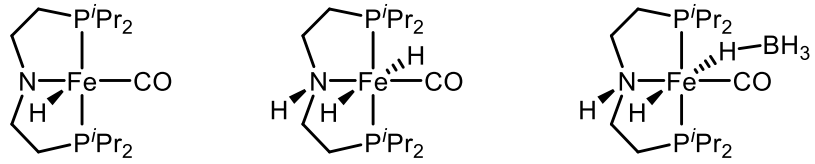
amount of borazine.[115] Again, *trans*-[Ru($^{i\text{Pr}}$PNP$^{\text{H}}$)(H)$_2$(PMe$_3$)] was observed as the resting state during catalysis. However, a more detailed study in 2013 suggested that [Ru($^{i\text{Pr}}$PNP)(H)(PMe$_3$)] and *trans*-[Ru($^{i\text{Pr}}$PNP$^{\text{H}}$)(H)$_2$(PMe$_3$)] actually dehydrocouple H$_3$B·NH$_3$ via different mechanisms.[113] In the case of *trans*-[Ru($^{i\text{Pr}}$PNP$^{\text{H}}$)(H)$_2$(PMe$_3$)], a mechanism was proposed that involves initial N–H activation to form H$_2$B=NH$_2$, which can then undergo metal-mediated oligomerisation (**Scheme 1.6**).



Scheme 1.6 Proposed mechanism for the dehydrocoupling of H$_3$B·NH$_3$ using [Ru($^{i\text{Pr}}$PNP)(H)(PMe$_3$)]. *Pathway A* depicts the dehydrogenation of H$_3$B·NH$_3$ to yield H$_2$B=NH$_2$ and *Pathway B* involves catalytic insertion of aminoborane into an N–H bond leading to oligomerisation.[113]

Schneider and co-workers also went on to report a related iron-based complex, [Fe($^{i\text{Pr}}$PNP)(H)(CO)] (**Figure 1.9**), as catalyst for the dehydrocoupling of H$_3$B·NH$_3$ to form linear polyaminoborane at room temperature.[116] Again, the analogous

dihydride complex, *trans*-[Fe($^{i\text{Pr}}$PNP$^{\text{H}}$)(H)$_2$(CO)], was observed to be the resting state during catalysis and the mechanism is similar to that in **Scheme 1.6** with both dehydrogenation to give $H_2B{=}NH_2$ and subsequent polymerisation being metal-mediated. Additionally, catalyst deactivation was shown to occur upon reaction of the iron-dihydride complex with BH_3, the latter being formed from the THF-promoted rearrangement of $H_2B{=}NH_2$ to give BH_3 and $HB(NH_2)_2$.[117]



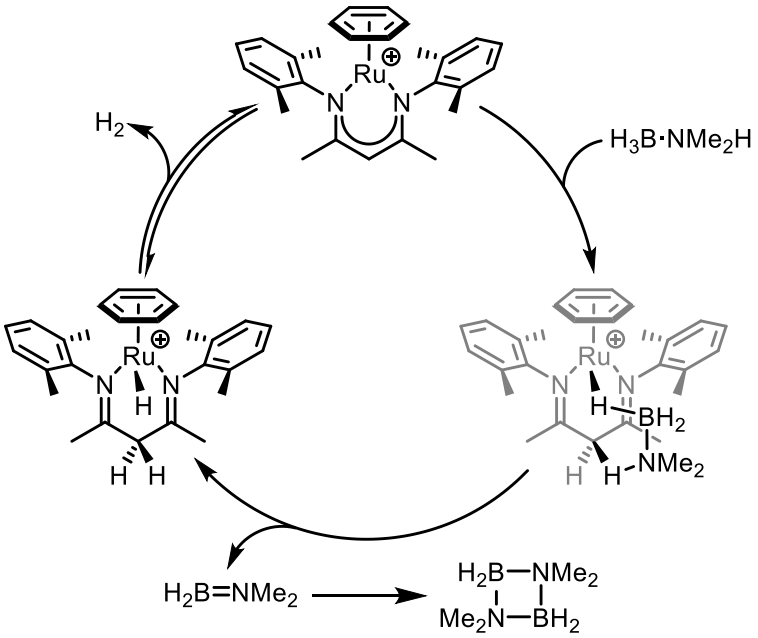
Pre-catalyst *Active catalyst* *Deactivated catalyst*

Figure 1.9 Iron complexes involved in the dehydrocoupling of $H_3B{\cdot}NH_3$ and $H_3B{\cdot}NMeH_2$.[116]

More recently, Bewaries *et al.* reported the dehydropolymerisation of the primary amine-borane $H_3B{\cdot}NMeH_2$ via the same iron-dihydride complex, *trans*-[Fe($^{i\text{Pr}}$PNP$^{\text{H}}$)(H)$_2$(CO)], with an analogous outer sphere mechanism as reported by Schneider.[118] However, the polymer produced remained unaffected by changing reaction conditions such as different catalyst loadings or increases in hydrogen concentration leading to the suggestion that polymerisation of the aminoborane intermediate, $H_2B{=}NMeH$, may actually proceed off-metal.

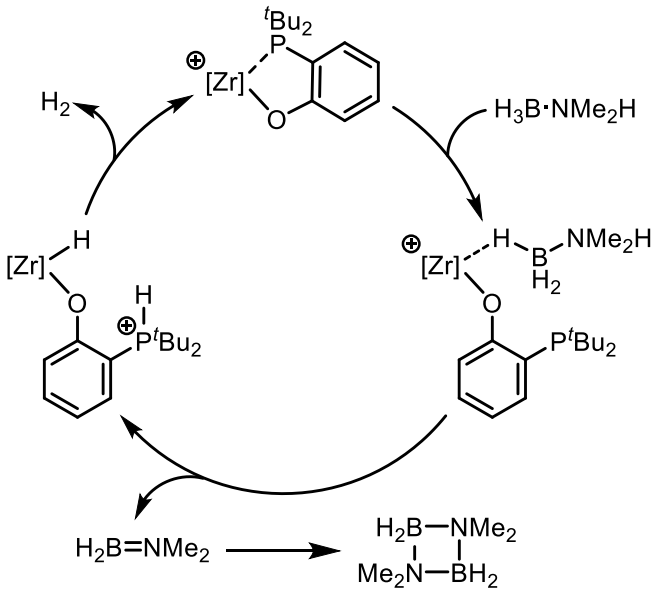
Another example of a ruthenium-based catalyst for the dehydrocoupling of amine-boranes via an outer sphere mechanism was reported by Philips and co-workers.[119] A bifunctional β-diketiminato(η^6-arene)-Ru$^{\text{II}}$ complex was shown to

catalyse both the dehydrocoupling of $H_3B{\cdot}NH_3$ and $H_3B{\cdot}NMe_2H$ at 42 °C with a catalyst loading of 0.5 mol%. As $H_3B{\cdot}NH_3$ was shown to liberate H_2 under these reaction conditions even in the absence of a catalyst, the dehydrocoupling of $H_3B{\cdot}NMe_2H$ was investigated instead to give mechanistic insight. The proposed mechanism involves initial hydride abstraction from the BH_3 fragment of $H_3B{\cdot}NMe_2H$ followed by the acidic proton of the NMe_2H fragment protonating the β-carbon of the β-diketiminato ligand (**Scheme 1.7**). This yields $H_2B{=}NMe_2$ that can go on to dimerise to give $[H_2BNMe_2]_2$ alongside the hydrogenated ruthenium complex, which had been previously shown to reversibly liberate H_2 to give the starting ruthenium complex.[120] An induction period prior to catalysis was observed for this system, which was noticeably reduced, along with an acceleration in dehydrogenation, when the reaction was repeated with H_2-saturated solvent. This suggests that the rate of catalysis is dependent on the formation of the hydrogenated metal complex.



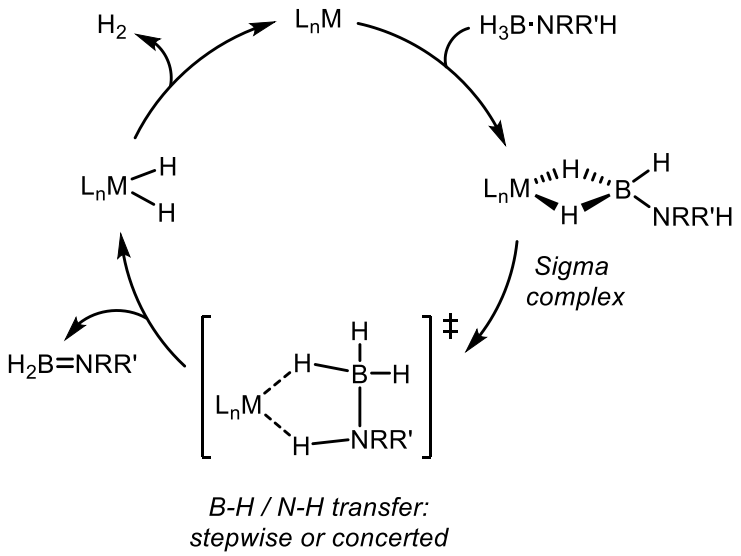
Scheme 1.7 Proposed mechanism for the dehydrocoupling of $H_3B{\cdot}NMe_2H$ using a bifunctional β-diketiminato(η^6-arene)-Ru^{II} complex. $[OTf]^-$ anions omitted for clarity.[119]

A further example of ligand cooperativity in the catalytic dehydrogenation of amine-boranes was reported by Wass and co-workers.[121] They extended the concept of main group 'frustrated' Lewis pairs (FLPs), which tend to have high reactivity under stoichiometric conditions, by replacing the Lewis acid fragment with an electrophilic Zr^{IV} centre to give the complex $[Cp_2ZrOC_6H_4P^tBu_2][B(C_6F_5)_4]$. This cationic zirconocene complex rapidly dehydrocoupled $H_3B{\cdot}NMe_2H$ to $[H_2BNMe_2]_2$ under catalytic conditions (1 mol% catalyst loading TOF ~600 h^{-1}) via an outer sphere mechanism as outlined in **Scheme 1.8**.



Scheme 1.8 Proposed mechanism for the dehydrocoupling of $H_3B{\cdot}NMe_2H$ using a cationic zirconocene complex. $[B(C_6F_5)_4]^-$ anions omitted for clarity.[121]

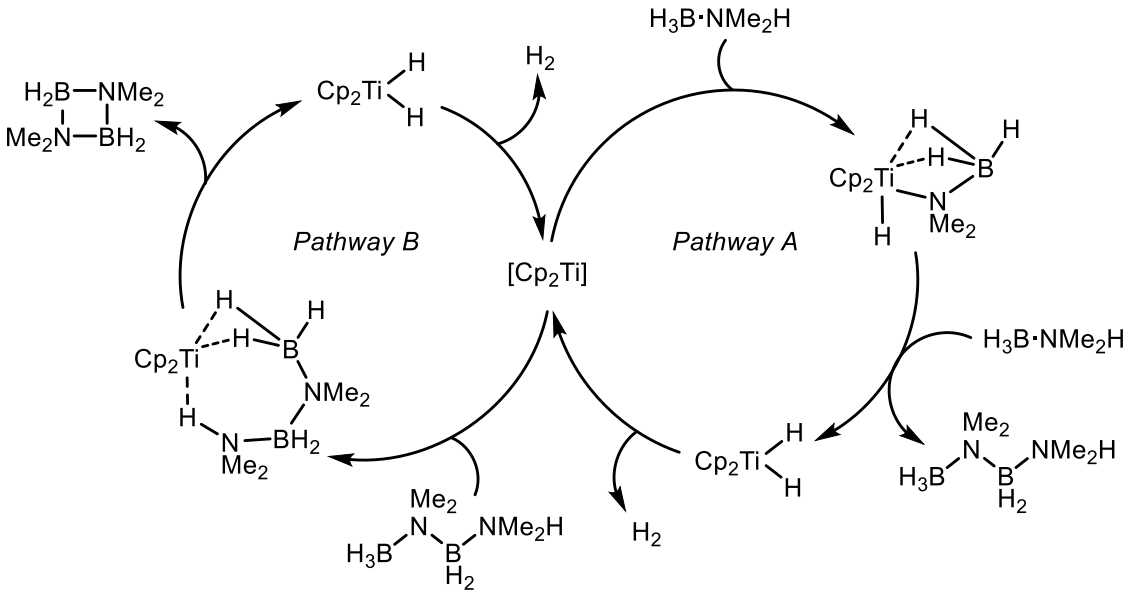
As mentioned before, another type of mechanism by which amine-boranes may be dehydrocoupled by homogeneous catalysts is an inner sphere mechanism. In contrast to the outer sphere mechanism, inner sphere mechanisms generally involve initial coordination of the amine-borane to the metal centre to form a sigma complex (see section 1.8). This is then followed by dehydrogenation of the amine-borane, without ligand assistance, via B–H/N–H transfer (concerted or stepwise) to give the resulting aminoborane (**Scheme 1.9**).



Scheme 1.9 Simplified, general mechanistic pathway for the inner sphere dehydrocoupling of amine-boranes.[81]

In 2006, Manners and co-workers reported the first example of well-defined homogeneous catalytic dehydrocoupling of amine-boranes.[122] $H_3B{\cdot}NMe_2H$ was dehydrocoupled to give $[H_2BNMe_2]_2$ using the $[Cp_2Ti]$ fragment (2 mol% catalyst loading) generated *in situ* from the reaction of Cp_2TiCl_2 with two equivalents of ^{n}BuLi. Later, an in-depth study into the mechanistic details of this process was reported, identifying linear diborazane as the main intermediate, and a two-cycle mechanism was proposed (**Scheme 1.10**).[123] Initial coordination of $H_3B{\cdot}NMe_2H$ to $[Cp_2Ti]$ is followed by N–H activation at the Ti^{II} centre to give the amidoborane complex, $[Cp_2Ti(H)(Me_2N{\cdot}BH_3)]$. This then reacts with a second equivalent of $H_3B{\cdot}NMe_2H$, generating $H_3B{\cdot}NMe_2H_2B{\cdot}NMe_2H$ alongside Cp_2TiH_2, which can lose H_2 to reform $[Cp_2Ti]$. Linear diborazane can then react with $[Cp_2Ti]$ to form a sigma complex that can undergo on-metal dehydrocyclisation yielding $[H_2BNMe_2]_2$ and Cp_2TiH_2. This proposed mechanism is consistent with the experimental observation

that, upon reaction of [Cp_2Ti] with independently synthesised $H_3B{\cdot}NMe_2H_2B{\cdot}NMe_2H$, complete conversion to $[H_2BNMe_2]_2$ occurs with only negligible amounts of $H_2B{=}NMe_2$ observed. This suggests that $H_3B{\cdot}NMe_2BH_2{\cdot}NMe_2H$ is likely the sole intermediate, not $H_2B{=}NMe_2$, during catalysis.



Scheme 1.10 Proposed two-cycle mechanism for the dehydrocoupling of $H_3B{\cdot}NMe_2H$ catalysed by [Cp_2Ti].[123]

Further research in this area suggested that paramagnetic Ti^{III} complexes may play a key role in the catalytic dehydrocoupling of $H_3B{\cdot}NMe_2H$ by [Cp_2Ti]. Manners and co-workers synthesised the Ti^{III} complexes [$Cp_2Ti(H_3B{\cdot}NMe_2)$] and [$Cp_2Ti(H_3B{\cdot}PPh_2)$] (**Figure 1.10**) and repeated catalysis under the same conditions as with the [Cp_2Ti] fragment.[124] Both complexes were found to be highly active pre-catalysts and, as before, $H_3B{\cdot}NMe_2H_2B{\cdot}NMe_2H$ was identified as the main intermediate, before forming $[H_2BNMe_2]_2$. Interestingly, the activity of [$Cp_2Ti(H_3B{\cdot}NMe_2)$] (TOF = 10.7 h^{-1}) was similar to that of [Cp_2Ti] (TOF = 12.5 h^{-1})

and furthermore, UV/Vis and EPR spectroscopic analyses of the reaction mixture catalysed by [Cp_2Ti] showed nearly identical spectra as those of isolated [$Cp_2Ti(H_3B{\cdot}NMe_2)$]. These results suggest that the mechanism of the dehydrocoupling of $H_3B{\cdot}NMe_2H$ catalysed by [Cp_2Ti] is more complex than the Ti^{II}/Ti^{IV} cycle depicted in **Scheme 1.10** and that the Ti^{III} complex [$Cp_2Ti(H_3B{\cdot}NMe_2)$] may be involved.

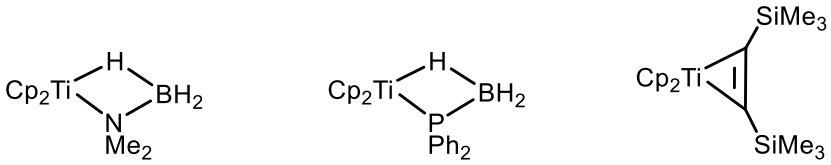


Figure 1.10 *Left* and *middle*: Ti^{III} complexes synthesised by Manners and co-workers.[124] *Right*: Ti^{II} pre-catalyst studied by Rosenthal and co-workers.[125]

In 2011, Rosenthal reported several related titanocene pre-catalysts for the dehydrocoupling of $H_3B{\cdot}NMe_2H$ via the [Cp_2Ti] fragment.[125] For the pre-catalyst [$Cp_2Ti(\eta^2\text{-}Me_3SiCCSiMe_3)$] (**Figure 1.10**), a TOF of 3 h^{-1} was observed; however, upon replacing Cp with Cp^* the resulting complex showed no dehydrocoupling activity. This change in activity was assigned to the influence of sterics on the system. Interestingly, upon replacing Cp with $C_5H_4{}^i\text{Pr}$, an improved activity was observed (TOF = 6 h^{-1}) suggesting electronic factors outweigh the additional steric effect in this case.[126] In contrast to the mechanism proposed by Manners (**Scheme 1.10**), only traces of linear diborazane were observed during catalysis suggesting [$(\eta^5\text{-}\ C_5H_4{}^i\text{Pr})_2Ti(\eta^2\text{-}Me_3SiCCSiMe_3)$] dehydrocouples $H_3B{\cdot}NMe_2H$ via a different mechanism.

In 2007, Chirik and co-workers reported that a bimetallic bis(cyclopentadienyl)titanium dinitrogen complex (**Figure 1.11**) was a particularly active pre-catalyst for the dehydrocoupling of $H_3B{\cdot}NMe_2H$ (TOF = 420 h^{-1}).[127] Following on from kinetic and isotopic labelling experiments, a mechanism was proposed involving initial reversible oxidative addition of B–H to the Ti^{II} centre followed by β-H elimination to yield $H_2B{=}NMe_2$, which can dimerise to form $[H_2BNMe_2]_2$.

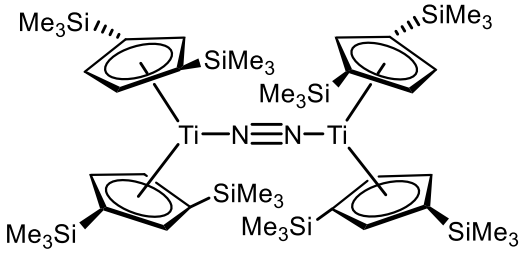


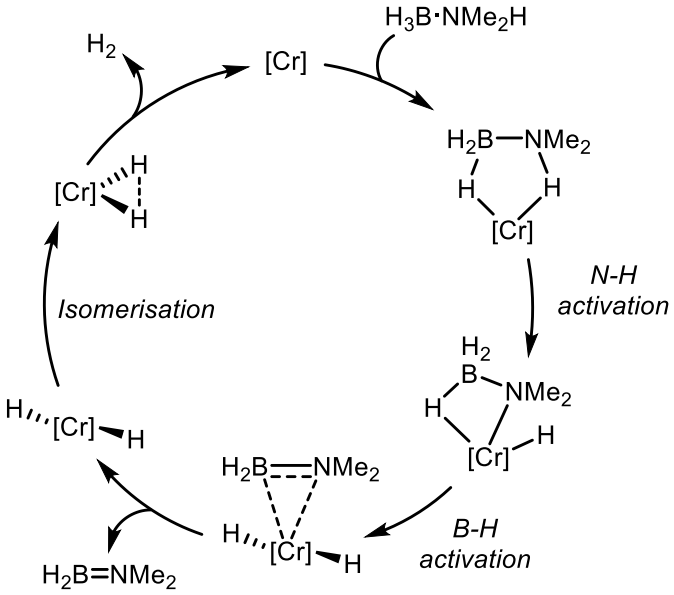
Figure 1.11 Bis(cyclopentadienyl)titanium dinitrogen complex studied by Chirik and co-workers.[127]

So far, these examples of dehydrocoupling following an inner sphere mechanism have shown the effectiveness of using early transition metal-based catalysts for the dehydrocoupling of $H_3B{\cdot}NMe_2H$. However, the use of such catalysts for the dehydrocoupling of the primary amine-borane $H_3B{\cdot}NMeH_2$ was not reported until as recently as 2018 by Manners and co-workers.[128] After several optimisation experiments, it was found that [Cp^*_2Ti], generated *in situ* from the reaction of $Cp^*_2TiCl_2$ and two equivalents of ^{n}BuLi, could catalyse the dehydropolymerisation of $H_3B{\cdot}NMeH_2$ at room temperature to yield high molecular weight polyaminoborane (M_n = 54, 000 g mol^{-1}, Đ = 1.6). Furthermore, the N-benzyl

substituted amine-borane $H_3B{\cdot}NBnH_2$ was also able to be dehydropolymerised under the same conditions yielding high molecular weight polymer (M_n = 101, 700 g mol^{-1}, Đ = 1.15).

Before this report by Manners and co-workers, early transition metal catalysts were found to only successfully catalyse the dehydrocoupling of secondary amine-boranes. However, mid-late transition metal catalysts had been shown to be effective for the dehydrocoupling of primary amine-boranes, as well as secondary.

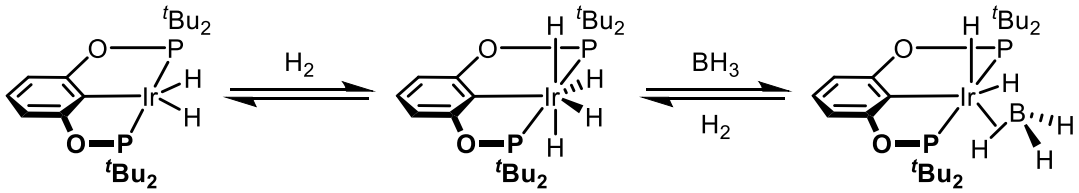
For example, in 2009 Shimoi and co-workers reported transition metal complexes of the type $[M(CO)_6]$ (M = Cr, Mo, W) acted as dehydrocoupling catalysts for both primary and secondary amine-boranes upon photoirradiation.[129] $H_3B{\cdot}NMe_2H$ was shown to be dehydrocoupled to form $[H_2BNMe_2]_2$ whilst bulkier analogues, such as $H_3B{\cdot}N^iPr_2H$ and $H_3B{\cdot}NCy_2H$, yielded the corresponding aminoboranes. Primary amine-boranes, such as $H_3B{\cdot}NMeH_2$ and $H_3B{\cdot}NEtH_2$, were dehydrocoupled to give a mixture of the corresponding oligomers, $[H_2BNRH]_n$, and borazines, $[HBNR]_3$. Mechanistic studies were carried out experimentally and using DFT calculations on the dehydrocoupling of $H_3B{\cdot}NMe_2H$ with $[Cr(CO)_6]$ (**Scheme 1.11**). Initial generation of the active catalyst $[Cr(CO)_4]$ is achieved by photoirradiation, which can then coordinate with $H_3B{\cdot}NMe_2H$ to form a sigma complex (see section 1.8). From here, N–H activation to form an amidoborane complex is followed by B–H activation to yield $H_2B{=}NMe_2$ that is released, along with an equivalent of H_2 to regenerate the active catalyst.



Scheme 1.11 Proposed mechanism by Shimoi *et al*. for the dehydrocoupling of $H_3B{\cdot}NMe_2H$. [Cr] = $[Cr(CO)_4]$.[129]

Late transition metal-based complexes have also been shown to successfully catalyse the dehydrocoupling of amine-boranes. In fact, the first transition metal complex shown to dehydropolymerise amine-boranes was based on iridium and was reported in 2006 by Heinekey and Goldberg. They employed Brookhart's iridium pincer complex Ir($^{t\text{Bu}}$POCOP)H_2 ($^{t\text{Bu}}$POCOP = κ^3-C_6H_3-2,6-(OP^{t}Bu$_2$)$_2$) to catalyse the dehydrocoupling of $H_3B{\cdot}NH_3$ to form a product initially proposed to be the cyclic pentamer $[H_2BNH_2]_5$ as assigned by IR spectroscopy and powder X-ray diffraction.[130] However, later Manners and co-workers went on to reassign this product as $[H_2BNH_2]_n$ (where n ~20) using solid state NMR spectroscopy.[131] The active catalyst for this process was determined to be an iridium tetrahydride species (**Scheme 1.12**) which, at low concentrations of H_2, was shown to react with BH_3 to from a catalytically dormant sigma complex, the structure of which was determined

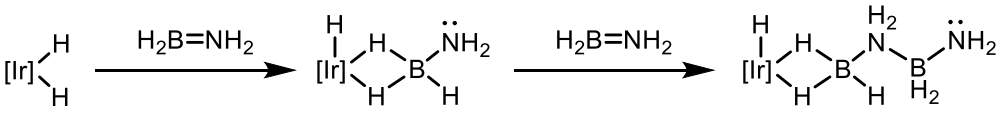
by neutron diffraction.[132] The active catalyst can be regenerated from the dormant species by addition of H_2.



Scheme 1.12 The active iridium tetrahydride species (*middle*) and dormant BH_3 sigma complex (*right*) involved in $H_3B{\cdot}NH_3$ dehydrocoupling catalysed by Brookhart's catalyst (*left*).[130]

Manners and co-workers further explored the use of Ir($^{t\text{Bu}}$POCOP)H_2 as a catalyst and in 2008 reported the first example of well-defined polyaminoborane.[82] At a catalyst loading of 0.3 mol% and high concentration of amine-borane (10 M), $H_3B{\cdot}NMeH_2$ was dehydropolymerised using Ir($^{t\text{Bu}}$POCOP)H_2 and high molecular weight polyaminoborane (M_n = 55, 200 g mol^{-1}, Đ = 2.9) was afforded. This polymer product was thoroughly characterised using several methods including NMR spectroscopy, IR spectroscopy, elemental analysis (EA) and gel permeation chromatography (GPC). Later studies explored the mechanistic detail of this system by using amine-borane conversion *versus* polymer molecular weight experiments and investigating different catalyst loadings.[131] High molecular weight polymer was observed at low monomer conversion (classical chain-growth); however, higher catalyst loadings led to higher polymer molecular weights (inconsistent with a single-site coordination/insertion mechanism). Therefore, a *modified* coordination/insertion chain-growth mechanism was proposed. This was explained

by slow initial dehydrogenation of $H_3B{\cdot}NMeH_2$ to yield the respective aminoborane, $H_2B{=}NMeH$, followed by fast insertion of this species on-metal to form a growing polymer chain, with both steps being metal-mediated. A computational study by Paul *et al*. on this system, using $H_3B{\cdot}NH_3$ as the substrate, also suggested a chain-growth mechanism for the polymerisation step.[133] However, rather than coordination/insertion as in Ziegler-Natta olefin polymerisation,[134] an alternative mechanism was proposed (**Scheme 1.13**), which involves the lone pair on the NH_2 group at the end of a growing polymer chain attached to the metal centre interacting with the Lewis acidic BH_2 group of a "free" aminoborane molecule, subsequently lengthening the polymer chain and revealing a new NH_2 end group. This mechanism can be considered a nucleophilic analogue of anionic polymerisation, which is a mechanism already commonly employed such as for the polymerisation of vinyl monomers.[135]



Scheme 1.13 Proposed chain growth mechanism by Paul *et al*. [Ir] = {Ir($^{t\text{Bu}}$POCOP)}.[133]

Another example of a late transition metal complex employed for the dehydrocoupling of amine-boranes is the Ni^{I} complex [Ni(trop$_2$NH)(OOCCF$_3$)] (trop$_2$NH = bistropylidenylamine) (**Figure 1.12**) reported by Grützmacher and co-workers as a particularly fast catalyst.[136] $H_3B{\cdot}NMe_2H$ was shown to be rapidly dehydrocoupled (TOF ~20, 000 h^{-1}) to form $[H_2BNMe_2]_2$ at a catalyst loading as low

as 0.3 mol%, in the presence of a basic co-catalyst K[NMe_2BH_3] (1–3 mol%). The base/catalyst ratio was highlighted as being crucial to the amount of amine-borane conversion; however, mechanistic details were not proposed.

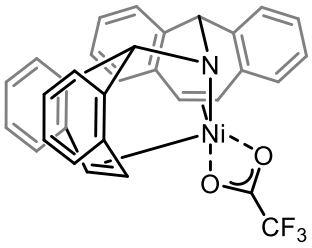
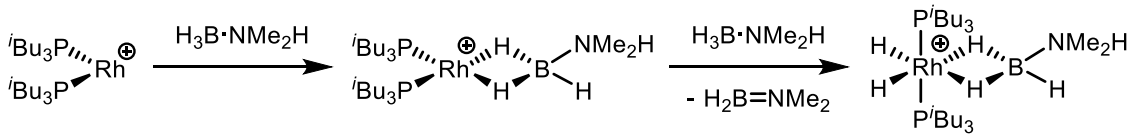


Figure 1.12 [Ni($trop_2NH$)($OOCCF_3$)] used for the rapid dehydrocoupling of $H_3B{\cdot}NMe_2H$.[136]

There are a multitude of further examples of transition metal catalysts for the dehydrocoupling of amine-boranes, such as those based upon: Re,[137] Fe,[138–140] Ru,[141–143] Os,[144] Co,[145] Ir,[146] Ni,[147] Pd,[148] and Pt.[149,150] However, the most relevant to this thesis are those examples based upon rhodium, which will be outlined in the rest of this section.

In 2008, [Rh(P^iBu_3)$_2$][BAr^F_4] was reported by Weller and co-workers as a homogeneous catalyst for the dehydrocoupling of $H_3B{\cdot}NMe_2H$ to give [H_2BNMe_2]$_2$ (5 mol% catalyst loading, TOF = 34 h^{-1}).[151] Initial coordination of $H_3B{\cdot}NMe_2H$ to the metal centre was shown to give the Rh^I sigma complex [Rh(P^iBu_3)$_2$(η^2-$H_3B{\cdot}NMe_2H$)][BAr^F_4] (**Scheme 1.14**) as a short-lived intermediate with the presence of further equivalents of amine-borane yielding the Rh^{III} sigma complex [Rh(P^iBu_3)$_2$(H)$_2$(η^2-$H_3B{\cdot}NMe_2H$)][BAr^F_4] along with [H_2BNMe_2]$_2$. Further studies by Weller and Hall suggested that the conversion of the Rh^I sigma complex to the Rh^{III}

sigma complex occurs via sequential B–H/N–H activation leading to loss of $H_2B{=}NMe_2$ to form the $\{Rh(P^iBu_3)_2(H)_2\}^+$ fragment which can then coordinate a further equivalent of $H_3B{\cdot}NMe_2H$.[152]



Scheme 1.14 Rh^I (*middle*) and Rh^{III} sigma complexes involved in the dehydrocoupling of $H_3B{\cdot}NMe_2H$. $[BAr^F{}_4]^-$ anions omitted for clarity.[151]

In 2011, Weller and Manners reported cationic rhodium catalysts $[Rh(PPh_2(CH_2)_xPPh_2)(\eta^6\text{-}C_6H_5F)][BAr^F{}_4]$ (x = 3–5) (**Figure 1.13**) for the dehydrocoupling of both $H_3B{\cdot}NMeH_2$ and $H_3B{\cdot}NMe_2H$.[38] $H_3B{\cdot}NMeH_2$ was dehydropolymerised to give high molecular weight polyaminoborane (when x = 4 M_n = 144, 000 g mol^{-1}, Đ = 1.3). A later study that also used deuterated isotopologues of $H_3B{\cdot}NMeH_2$ suggested an unusual hybrid coordination/insertion chain/step growth mechanism. At high concentrations of amine-borane (i.e. near the start of catalysis), medium polymer molecular weight was observed indicative of chain growth; however, at very low concentrations of amine-borane (towards the end of catalysis) a large increase in polymer molecular weight was observed suggesting step growth coupling of the already present polymer chains.[153]

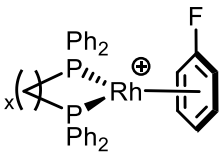


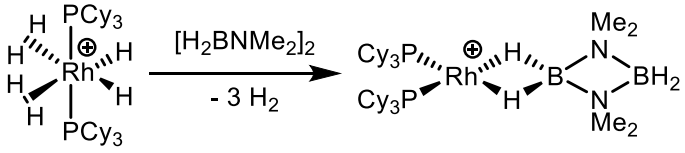
Figure 1.13 $[Rh(PPh_2(CH_2)_xPPh_2)(\eta^6\text{-}C_6H_5F)][BAr^F{}_4]$ where x = 3–5, for the dehydrocoupling of $H_3B{\cdot}NMeH_2$ and $H_3B{\cdot}NMe_2H$. $[BAr^F{}_4]^-$ anion omitted for clarity.[38]

Studies on the catalytic activity of $[Rh(PPh_2(CH_2)_xPPh_2)(\eta^6\text{-}C_6H_5F)][BAr^F{}_4]$ for the dehydrocoupling of $H_3B{\cdot}NMe_2H$ showed the presence of an induction period that increased with an increase in catalyst concentration. ESI-MS experiments suggested that this was due to initial formation of the inactive bimetallic species $[\{Rh(PPh_2(CH_2)_x)\}_2(H)(H_2BNMe_2)][BAr^F{}_4]$, possibly in equilibrium with an active monomeric rhodium dihydride species. The bite angle of the chelating phosphine backbone in $Rh(PPh_2(CH_2)_xPPh_2)(\eta^6\text{-}C_6H_5F)][BAr^F{}_4]$ was shown to correlate with the binding strength of the amine-borane by observation of the respective model sigma complexes $[Rh(PPh_2(CH_2)_xPPh_2)(\eta^2\text{-}H_3B{\cdot}NMe_3)][BAr^F{}_4]$; the smaller the bite angle, the more weakly bound the amine-borane. In terms of kinetics, a weaker Rh···H_3B interaction would suggest a higher activity and this is consistent with the observation that $H_3B{\cdot}NMe_2H$ is dehydrocoupled fastest when x = 3 (TOF ~1, 250 h^{-1}). However, when x = 2, no amine-borane complex is formed and so the limit in this trend is reached.

In 2012, Weller and Lloyd-Jones explored the dehydrocoupling of $H_3B{\cdot}NMe_2H$ in great detail using $\{Rh(PCy_3)_2L_n\}^+$ (L_n = solvent or agostic interaction) in an attempt to uncover a generic mechanism for this process.[88] Both stoichiometric and

catalytic experiments were carried out leading to many important observations. During catalysis, both $H_2B{=}NMe_2$ and the linear diborazane $H_3B{\cdot}NMe_2H_2B{\cdot}NMe_2H$ were observed as intermediates. Addition of two equivalents of $H_3B{\cdot}NMe_2H$ to $\{Rh(PCy_3)_2L_n\}^+$ yielded a Rh^I sigma complex (see section 1.8) followed quickly by a Rh^{III} sigma complex , analogous to those observed in **Scheme 1.14** for the reaction with $\{Rh(P^iBu_3)_2\}^+$. The Rh^{III} complex was shown to not lose H_2 easily when vacuum was applied suggesting it is stable relative to the Rh^I complex and therefore may be the resting state during catalysis. When five equivalents of $H_3B{\cdot}NMe_2H$ were reacted with the Rh^{III} sigma complex, dehydrocoupling occurred at a slower rate than observed during catalysis with $\{Rh(PCy_3)_2L_n\}^+$. This suggested that although the Rh^{III} sigma complex is an active dehydrocoupling catalyst, this slow Rh^{III}/Rh^{III} cycle is not the only route through which dehydrocoupling can occur.

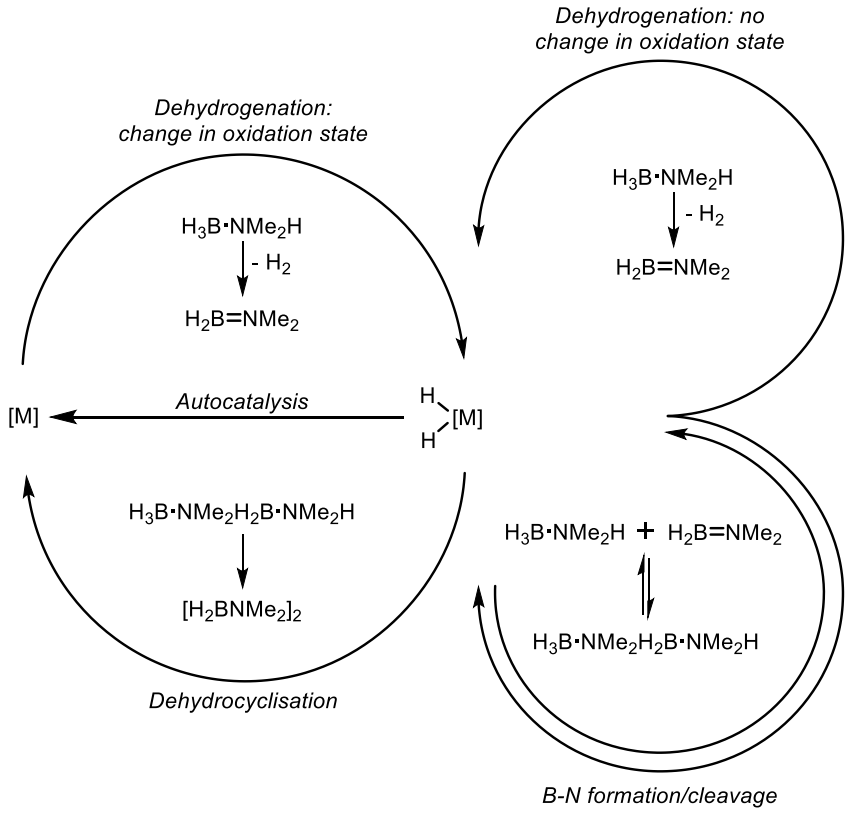
$[H_2BNMe_2]_2$ is the product of the dehydrocoupling of $H_3B{\cdot}NMe_2H$ and was found to have an autocatalytic role during catalysis. Addition of $[H_2BNMe_2]_2$ to the model Rh^{III} complex $[Rh(PCy_3)_2(H)_2(\eta^2\text{-}H_2)_2][BAr^F{}_4]$ resulted in the immediate formation of the Rh^I complex $[Rh(PCy_3)_2(\eta^2\text{-}(H_2BNMe_2)_2][BAr^F{}_4]$ (**Scheme 1.15**) showing that $[H_2BNMe_2]_2$ can initiate reductive elimination of H_2 from Rh^{III} complex to give a Rh^I species. Therefore, during catalysis $[H_2BNMe_2]_2$ can act as a modifier and enable a Rh^I/Rh^{III} cycle alongside the slow Rh^{III}/Rh^{III} cycle.



Scheme 1.15 Reduction from Rh^{III} to Rh^{I} by the addition of the product of dehydrocoupling $H_3B{\cdot}NMe_2H$, $[H_2BNMe_2]_2$. $[BAr^F{}_4]^-$ anions omitted for clarity.[88]

Furthermore, the role of $H_3B{\cdot}NMe_2H_2B{\cdot}NMe_2H$ was investigated in this system and it was found that it was in equilibrium with $H_3B{\cdot}NMe_2H$ and $H_2B{=}NMe_2$ with the B–N bond formation/cleavage mediated by the Rh^{III} species. This metal-mediated equilibrium was proposed in 2009 by Schneider *et al*. as part of the mechanism for the dehydrogenation of $H_3B{\cdot}NMe_2H$ catalysed by [Ru($^{i\text{Pr}}$PNP)(H)(PMe_3)].[114]

These, plus other observations, led to the proposal of a general mechanism for the dehydrocoupling of $H_3B{\cdot}NMe_2H$ (**Scheme 1.16**). $H_3B{\cdot}NMe_2H$ may be dehydrocoupled by a Rh^{III}/Rh^{III} cycle (slow) or a Rh^{I}/Rh^{III} cycle (fast) to give $H_2B{=}NMe_2$, which can dimerise off-metal to give the product $[H_2BNMe_2]_2$. $[H_2BNMe_2]_2$ can regenerate the Rh^{I} complex from the Rh^{III} complex leading to autocatalysis. $H_3B{\cdot}NMe_2H_2B{\cdot}NMe_2H$ may be formed, cleaved and dehydrocyclised to give $[H_2BNMe_2]_2$ during catalysis. This general mechanism includes many aspects of mechanisms proposed for other dehydrocoupling catalysts, as discussed in this section.

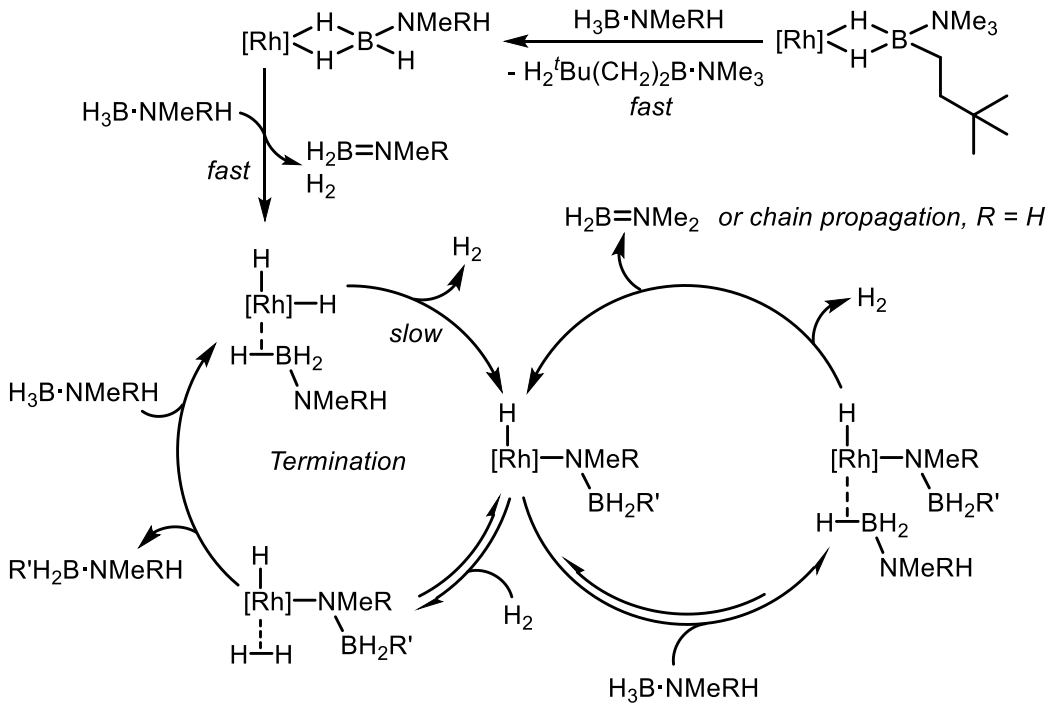


Scheme 1.16 General mechanistic pathways for the dehydrocoupling $H_3B{\cdot}NMe_2H$. [M] = metal catalyst.[88]

In addition to the above observations, an additional catalyst was observed in low concentrations and, due to the presence of chloride ions from the initial synthesis of $\{Rh(PCy_3)_2L_n\}^+$, was proposed to be the neutral species $Rh(PCy_3)_2(H)_2Cl$. A year later, the activity of this catalyst was investigated further and it was found to catalyse the dehydrocoupling of $H_3B{\cdot}NMe_2H$ (TOF = 28 h^{-1}, catalyst loading 2 mol%) via stepwise B–H/N–H activation with N–H activation being the turnover limiting step as deduced from kinetic isotope effect studies.[154]

In 2014 Weller, Manners and Lloyd-Jones reported the complex [Rh(κ²-P,P-Xantphos-Ph)(η²-$H_2B(CH_2CH_2{}^tBu){\cdot}NMe_3$)][$BAr^F{}_4$] (Xantphos-Ph = 4,5-

bis(diphenylphosphino)-9,9-dimethylxanthene), a source of the {Rh(Xantphos)}$^{+}$ fragment, as an active catalyst for the dehydrocoupling of $H_3B{\cdot}NMe_2H$ to $[H_2BNMe_2]_2$ (TOF ~1, 000 h^{-1}) and $H_3B{\cdot}NMeH_2$ to $[H_2BNMeH]_n$ (M_n = 22, 700 g mol^{-1}, Đ = 2.1).[155] The reaction profiles for the dehydrocoupling of both the primary and the secondary amine-boranes were very similar and a detailed mechanism was proposed (**Scheme 1.17**). Initial reaction of amine-borane with the starting rhodium complex rapidly forms a Rh^{III} dihydride species alongside loss of H_2 and $H_2B{=}NMeR$ (R = H, Me). An induction period was observed, during which N–H activation was found to be rate limiting, and so a rhodium amidoborane species was postulated to form during this time, suggested to be the active catalyst. Amine-borane can reversibly bind to this species, following which B–H/N–H transfer can occur to yield $H_2B{=}NMeR$ and regenerate the active catalyst. In the case of $H_2B{=}NMe_2$, dimerisation occurs to give $[H_2BNMe_2]_2$. For $H_2B{=}NMeH$, chain propagation was proposed to occur to yield polyaminoborane, via coordination/insertion steps similar to Ziegler-Natta olefin polymerisation.[134] Hydrogen was proposed to be involved in chain termination as catalysis in a closed system (where H_2 pressure is allowed to build up) yielded low molecular weight polymer (M_n = 2, 800 g mol^{-1}, Đ = 1.8).



Scheme 1.17 Proposed mechanism for the dehydrocoupling of $H_3B{\cdot}NMeRH$ (R = H, Me) using $[Rh(\kappa^2\text{-P,P-Xantphos-Ph})(\eta^2\text{-}H_2B(CH_2CH_2{}^tBu){\cdot}NMe_3)][BAr^F{}_4]$ as the pre-catalyst. [Rh] = $\{Rh(Xantphos\text{-}Ph)\}^+$, R' = H or growing polymer chain, $[BAr^F{}_4]^-$ anions omitted for clarity.[155]

The identity of the active catalyst, tentatively assigned as an amidoborane complex, was investigated further in later work and it was found that at the end of catalysis with $H_3B{\cdot}NMe_2H$, a bimetallic species $[(Rh(\kappa^2\text{-P,P-Xantphos-Ph'}))_2(\eta^2\eta^2\text{-}H_3BNMe_2BH_3)][BAr^F{}_4]$ could be isolated (**Figure 1.14**, *left*).[156] This complex was shown to be active in catalysis but with a longer induction period and slower overall rate. However, a related bimetallic complex (**Figure 1.14**, *right*) demonstrated a very similar kinetic profile and polymer output to that of the monometallic complex and so bimetallic complexes of this type were suggested to be close to, if not the active catalysts in these systems.

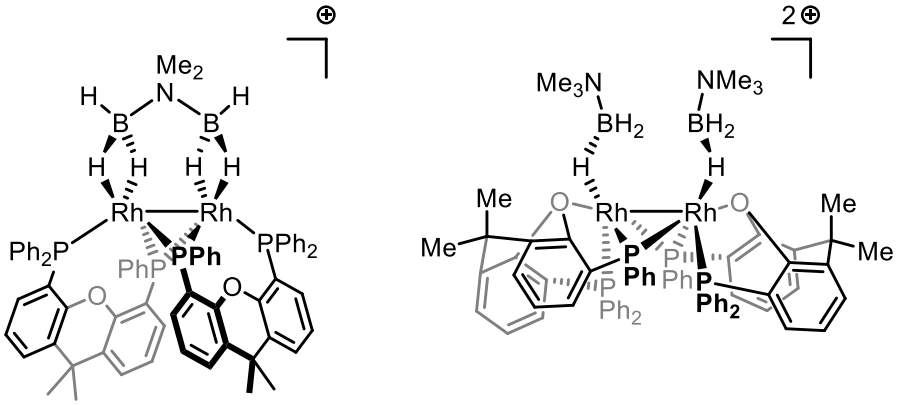


Figure 1.14 *Left*: Bimetallic [(Rh(κ²-P,P-Xantphos-Ph'))₂(η²η²-$H_3BNMe_2BH_3$)][BAr^F_4] end product. *Right*: Bimetallic [(Rh_2(κ³-P,O,P-Xantphos-Ph')₂(η¹-H_3BNMe_3)₂][BAr^F_4]₂, potential active catalyst. [BAr^F_4]⁻ omitted for clarity.[156]

More recently, further work was undertaken with the {Rh(Xantphos)} motif investigating neutral and cationic alkyl derivatives of the form {Rh(Xantphos-R)} where R = Et, ^{i}Pr and ^{t}Bu.[157] Systems where R = ^{i}Pr showed the most efficient dehydropolymerisation of $H_3B{\cdot}NMeH_2$ (TOF ~1, 500 h^{-1}) indicating the important effect of sterics. Interestingly, the neutral complex Rh(κ³-P,O,P-Xantphos-^{i}Pr)H yielded higher molecular weight polyaminoborane (M_n = 28,000 g mol^{-1}, Đ = 1.9) compared to the cationic complex [Rh(κ³-P,O,P-Xantphos-^{i}Pr)$(H)_2$(η¹-$H_3B{\cdot}NMe_3$)][BAr^F_4] (M_n = 9,000 g mol^{-1}, Đ = 2.9), demonstrating the effect of charge. In both cases, a classic chain growth process was reported, and a neutral rhodium hydride species implicated in the mechanism (see section 1.9).

Lastly, the analogous complex {Rh(DPEphos)}⁺ (DPEphos = bis(2-(diphenylphosphino)phenyl)ether) (**Figure 1.15**) was recently reported to dehydropolymerise $H_3B{\cdot}NMeH_2$ with some aspect of control of the product

molecular weight.[158] A polymer molecular weight range of 5,500–40,000 g mol^{-1} (Đ = 1.5–1.8) was achieved by varying catalyst loading (an inverse relationship) and H_2 pressure (due to H_2 contribution to chain termination). Importantly, NMe_2H was shown to bring the catalyst onto cycle and promote faster polymerisation. The mechanism proposed and effect of NMe_2H will be discussed further in section 1.9.

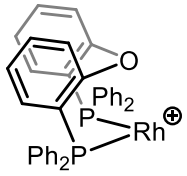


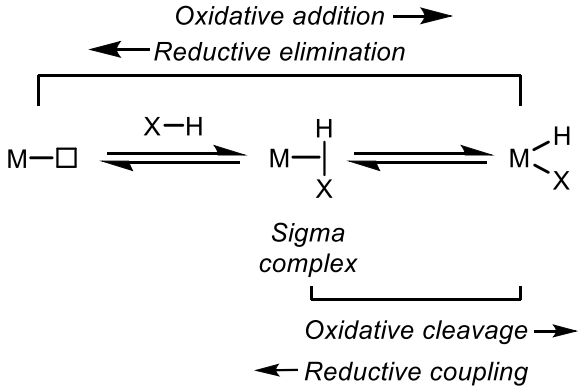
Figure 1.15 {Rh(DPEphos)}$^+$ employed in the dehydropolymerisation of $H_3B{\cdot}NMeH_2$. $[BAr^F{}_4]^-$ omitted for clarity.[158]

This section has provided a survey of the literature highlighting the work done to elucidate the mechanistic details surrounding the dehydrocoupling of amine-boranes. In many cases, model amine-boranes such as $H_3B{\cdot}NMe_2H$ have been studied in-depth in order to provide a greater insight into the more complex dehydrocoupling pathways of the primary amine-boranes $H_3B{\cdot}NMeH_2$ and $H_3B{\cdot}NH_3$. However, a universal mechanism that may apply to all amine-boranes and is not system dependent is yet to be uncovered.

1.8 Sigma complexes

A sigma complex is classed as containing an intermolecular neutral X–H ligand (where X = H, C, Si, B, Sn, etc.) that donates σ-bonding electrons to a metal centre and receives backdonation from the metal d_π orbital into the X–H σ* orbital forming a three-centre-two-electron bonding interaction.[1,159] The X–H ligand is able to

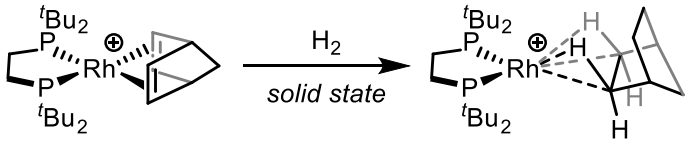
approach closely to the metal centre in order to achieve such backdonation as the hydrogen atom in X–H is so small. Too much backdonation leads to breaking of the X–H bond and thus sigma complexes are postulated as intermediates in the process of oxidative addition/reductive elimination (**Scheme 1.18**).[160] Therefore, investigation into the nature of sigma complexes could lead to further understanding of bond activation processes, which in turn could lead to the controlling of both rate and selectivity during catalysis.



Scheme 1.18 General pathways for oxidative addition and reductive elimination via a sigma complex. X = H, C, Si, B or Sn.

An agostic interaction describes a similar three-centre-two-electron bonding interaction, but where the bonding pair of electrons comes from a C–H ligand already coordinated to the metal centre. Examples of analogous interactions between a metal centre and C–C, Si–Si, B–B, Si–C or C–B bonds are also known and proposed as intermediates in the respective bond cleavage metal-mediated reactions.[161] Compared to complexes containing agostic interactions, sigma complexes tend to have limited stability and therefore tend to be difficult to

isolate.[40,162] Often such sigma complexes are only observed spectroscopically at low temperatures as intermediates; however, in 2012 Weller *et al*. isolated a sigma alkane complex using solid state single crystal to single crystal techniques (**Scheme 1.19**).[163]



Scheme 1.19 Synthesis of a sigma alkane complex using solid state techniques. $[BAr^F{}_4]^-$ omitted for clarity.[163]

1.8.1 Dihydrogen sigma complexes

The simplest type of sigma complex is formed from the complexation of H_2 to a metal centre. The first sigma complex was of this type, reported by Kubas and co-workers in 1983 (**Figure 1.16**),[164] and since then a multitude of other dihydrogen sigma complexes have been documented.[165]

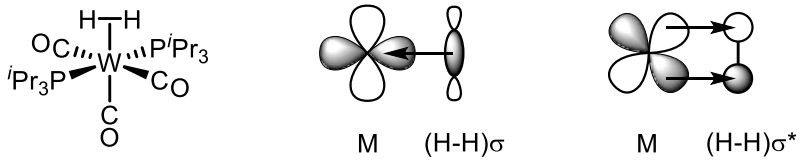


Figure 1.16 *Left*: Kubas' dihydrogen complex.[164] *Middle and right*: Bonding model for a sigma dihydrogen complex.

In a dihydrogen sigma complex, H_2 acts as a two-electron donor and donates these electrons from the H–H σ-bonding molecular orbital into a vacant and appropriately orientated d_π molecular orbital on the metal (**Figure 1.16**). Synergic backdonation

from a filled metal d_π molecular orbital to a H–H σ*-antibonding molecular orbital simultaneously occurs, much like in the Dewar-Chatt-Duncanson model.[166] This leads to side on binding of H_2 to the metal centre. Backbonding from the metal centre weakens the H–H σ bond and so the extent of this backdonation determines how elongated the H–H bond is in a sigma complex and whether oxidative cleavage occurs to generate a classical dihydride (**Figure 1.17**).[167] Reduction of electron density at the metal centre, such as from the presence of π-accepting CO ligands or a cationic charge, leads to less backdonation and so a sigma complex is favoured over the oxidative cleavage product. The contracted *d* orbitals of a first row metal compared to the more radially diffuse third row *d* orbitals also favour the formation of the sigma complex over the dihydride.

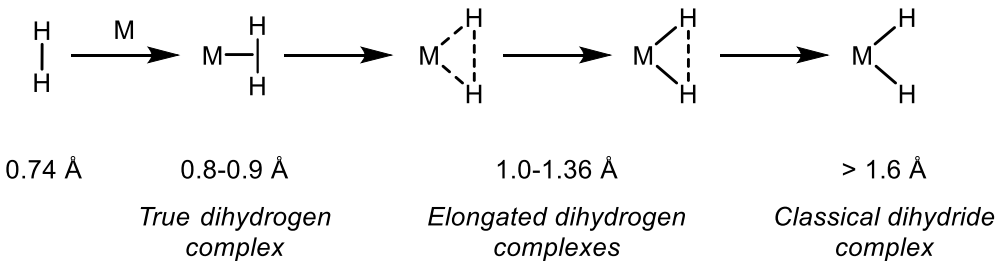


Figure 1.17 Transition from a dihydrogen complex to a dihydride complex upon increasing back donation from a transition metal centre.[167]

Characterisation of dihydrogen complexes by X-ray diffraction is challenging as the negligible electron density of the hydrogen atom makes locating it unreliable. Neutron diffraction is a more accurate, but challenging, alternative. Spectroscopically, an IR absorption at 2300–2900 cm^{-1} is assigned to the H–H stretch of a dihydrogen complex, however, it is not always observed. Two other

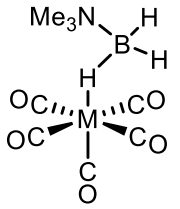
important characterisation techniques rely on ^{1}H NMR spectroscopy.[168,169] Firstly, if H_2 in the complex is replaced with HD then the H–D coupling constants can be compared: in free HD $^{1}J_{HD}$ = 43 Hz and so for dihydrogen complexes, where a degree of H···H interaction remains, $^{1}J_{HD}$ values greater than 25 Hz are often observed whereas for dihydride complexes, $^{2}J_{HD}$ values of less than 5 Hz are exhibited. Secondly, the efficiency of T_1 (spin-lattice) relaxation times for ^{1}H nuclei depend on the distance to other nearby relaxing nuclei and so at 500 MHz, T_1 times less than 160 ms indicate a dihydrogen complex whereas T_1 times greater than 300 ms suggest a dihydride complex (as the internuclear separation between the two hydrogen atoms in a dihydride complex is greater).

1.8.2 Amine-borane sigma complexes

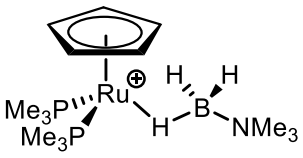
For many of the examples of inner sphere mechanisms for the dehydrocoupling of amine-boranes described in section 1.7.2.2, sigma complexes of amine-boranes are postulated as intermediates. Therefore, the synthesis and study of such complexes could give a great deal of mechanistic insight into the dehydrogenation pathways. Similar to dihydrogen sigma complexes (section 1.8.1), coordination of an amine-borane to a metal centre usually occurs via a three-centre-two-electron interaction with the B–H σ-bonding orbital donating to the metal.[170,171] However, in contrast to dihydrogen complexes, the B–H σ*-antibonding orbital is too high in energy to receive backdonation from the metal centre, resulting in end on binding (**Figure 1.18**). In tricoordinate boron complexes, such as $RuH_2(\eta^2,\eta^2\text{-}H_2B{\cdot}NH_2)(PCy_3)_2$,[170] backdonation from the metal centre into a vacant *p* orbital on boron is often able to occur. However, this is not possible for four coordinate boron as there is no empty

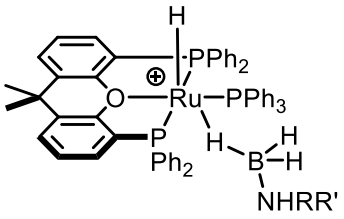
p orbital available. It is possible to isolate amine-borane sigma complexes using tertiary amine-boranes, $H_3B{\cdot}NR_3$, as the lack of N–H bonds renders the complex stable with respect to dehydrogenation and thus these complexes can act as a model for the interaction of primary and secondary amine-boranes with a metal centre.[151] For example, in 1999 Shimoi and co-workers reported the first amine-borane sigma complex $[M(CO)_5(\eta^1\text{-}H_3B{\cdot}NMe_3)]$ (M = Cr, Mo and W) generated from the photolysis of $[M(CO)_6]$ in the presence of $H_3B{\cdot}NMe_3$ (**Figure 1.18**).[171] Interestingly, although the amine-borane is bound through one B–H bond, both bridging and terminal B–H protons are in rapid exchange and so appear fluxional on an NMR timescale.[172]

η^1-amine-borane sigma complexes



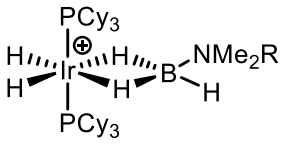
M = Cr, Mo, W



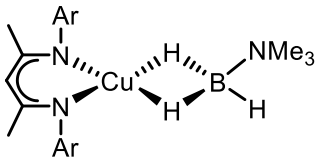


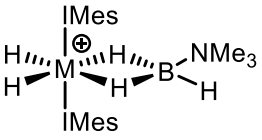
R = H, R' = H, ^{t}Bu
R = R' = Me

η^2,η^2-amine-borane sigma complexes



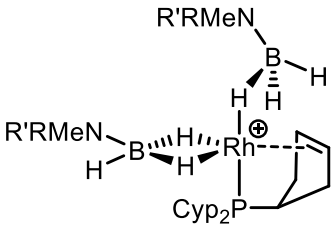
R = H, Me





M = Rh, Ir
IMes = N,N'-bis(2,4,6-trimethylphenyl) imidazol-2-ylidene

η^1-η^2,η^2-amine-borane sigma complex



R, R' = Me, H

Figure 1.18 Examples of selected sigma complexes: η^1[171,173,174], η^2,η^2[146,175,176] and η^1- η^2,η^2[177]. $[BAr^F{}_4]^-$ anions not shown.

Other examples of η^1-bound amine-borane sigma complexes have subsequently been reported (**Figure 1.18**).[155,173,174] Such η^1 complexes exhibit weak binding of the amine-borane mostly via the B–H proton, with relatively large M–H–B angles and long M···B distances.[178] Amine-boranes can also coordinate to the metal centre via an η^2 interaction, usually with two B–H bonds resulting in an η^2,η^2-sigma

complex (**Figure 1.18**).[38,146,151,155,158,175,176] Relative to an η^1 interaction, an η^2 bound amine-borane generally exhibits stronger binding to the metal centre via both boron and hydrogen in the B–H bond, a smaller M–H–B angle and a shorter M···B distance. A unique example of a rhodium sigma-complex containing both an η^1-bound and an η^2,η^2-bound amine-borane was reported by the Weller group.[177] Additionally, intermediates of amine-borane dehydrocoupling have also been observed bound to metal centres in the form of a sigma-complex (**Figure 1.19**).[64,152,179–182]

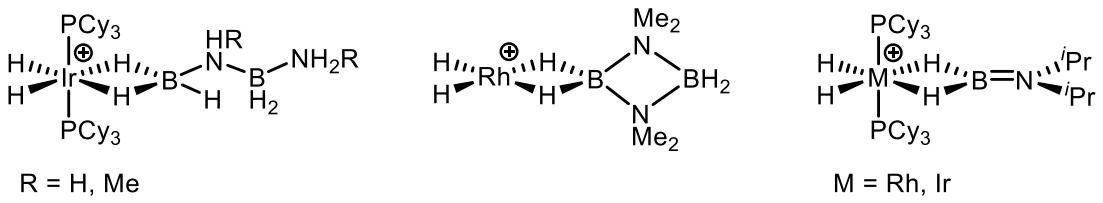


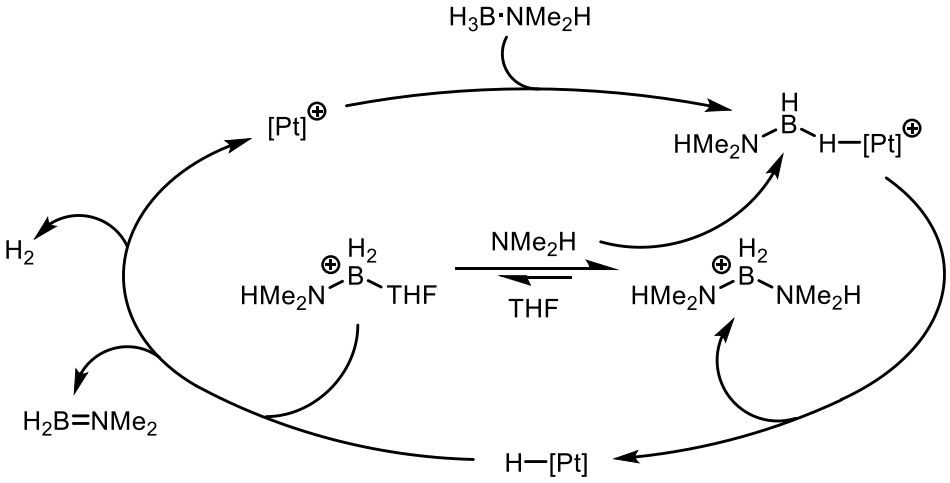
Figure 1.19 Selected sigma complexes of intermediates and products from amine-borane dehydrocoupling.[152,179,180] $[BAr^F{}_4]^-$ anions not shown.

1.9 Boronium as an intermediate in the dehydrocoupling of amine-boranes

In section 1.7.2.2, outer sphere and inner sphere mechanisms were outlined as two distinct pathways for the dehydrocoupling of amine-boranes in homogeneous systems. A third type of mechanism also exists that involves the formation of boronium cations such as $[H_2BLL']^+$ (where L and L' = NH_3, $NMeH_2$, NMe_2H, OTf, solvent, etc.), which can subsequently protonate an intermediate such as a metal hydride, generating aminoborane and the L/L' fragment.

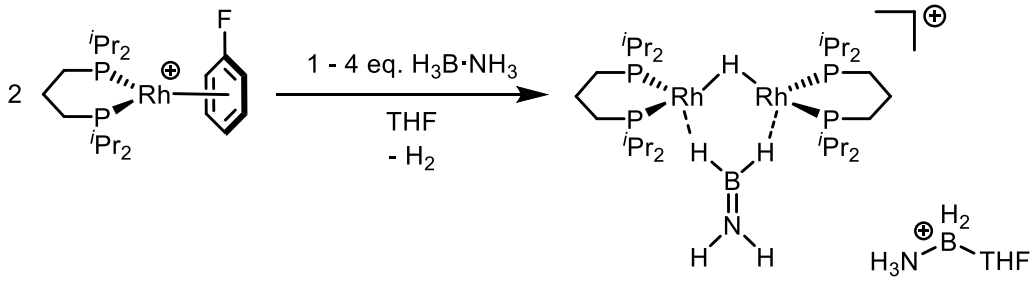
Jagirdar *et al*. reported the observation of the boronium species $H_2B(NMe_2H)(OTf)$ during the dehydrocoupling of $H_3B{\cdot}NMe_2H$ catalysed by the five-coordinated ruthenium complex $[RuCl(dppe)_2][OTf]$ (dppe = 1,2-bis(diphenylphosphine)ethane).[183] In 2007, boronium cations such as $\{H_2B(NH_2)(OSO_2CF_3)\}^+$ and $\{H_2B(NH_3)(OEt_2)\}^+$ were implicated as intermediates in the cationic dehydropolymerisation of $H_3B{\cdot}NH_3$ using strong Lewis and Brønsted acids.[184] However, it was Conejero and López-Serrano in 2013 who proposed a mechanism for the dehydrocoupling of amine-boranes involving boronium cations, which will be discussed in detail in this section.[149]

Conejero and López-Serrano reported $[Pt(I^tBu)(I^tBu')][BAr^F_4]$ (I^tBu = 1,3-di-*tert*-butylimidazol-2-ylidene, I^tBu' = cyclometallated I^tBu) as an efficient catalyst for the dehydrocoupling of $H_3B{\cdot}NMe_2H$ to $[H_2BNMe_2]_2$. A mechanism for this process was proposed, supported by DFT calculations using $H_3B{\cdot}NH_3$ as a model amine-borane (**Scheme 1.20**). Amine-borane initially coordinates to the platinum centre of $[Pt(I^tBu)(I^tBu')][BAr^F_4]$ to form an η^1-sigma complex. Free NMe_2H (arising from the B–N cleavage of $H_3B{\cdot}NMe_2H$) interacts with the η^1-sigma complex assisting in the formation of the neutral Pt^{II} hydride $Pt(I^tBu)(I^tBu')H$ along with the boronium cation $\{H_2B(NMe_2H)_2\}^+$. Calculations indicated that the addition of a Lewis base such as NMe_2H lowers the B–H activation barrier for the metal-bound amine-borane. $\{H_2B(NMe_2H)_2\}^+$ is shown to be in equilibrium with $\{H_2B(NMe_2H)(THF)\}^+$ in a solution of THF and it is this latter species that protonates the Pt^{II} hydride, releasing $H_2B{=}NMe_2$ and H_2 to regenerate the catalyst.



Scheme 1.20 Proposed mechanism for the dehydrocoupling of $H_3B{\cdot}NMe_2H$ with $[Pt(I^tBu)(I^tBu')][BAr^F{}_4]$ (= [Pt]). $[BAr^F{}_4]^-$ anions omitted for clarity.[149]

In section 1.7.2.2 the dehydrocoupling of both $H_3B{\cdot}NMeH_2$ and $H_3B{\cdot}NMe_2H$ using $[Rh(PPh_2(CH_2)_xPPh_2)(\eta^6\text{-}C_6H_5F)][BAr^F{}_4]$ was discussed. This complex, where x = 3, was investigated further in 2016, along with the ^{i}Pr analogue, where reaction with a slight excess of $H_3B{\cdot}NH_3$ yielded a novel bimetallic complex with a bridging $H_2B{=}NH_2$ fragment alongside the boronium cation $\{H_2B(NH_3)(THF)\}^+$ (**Scheme 1.21**).[185]



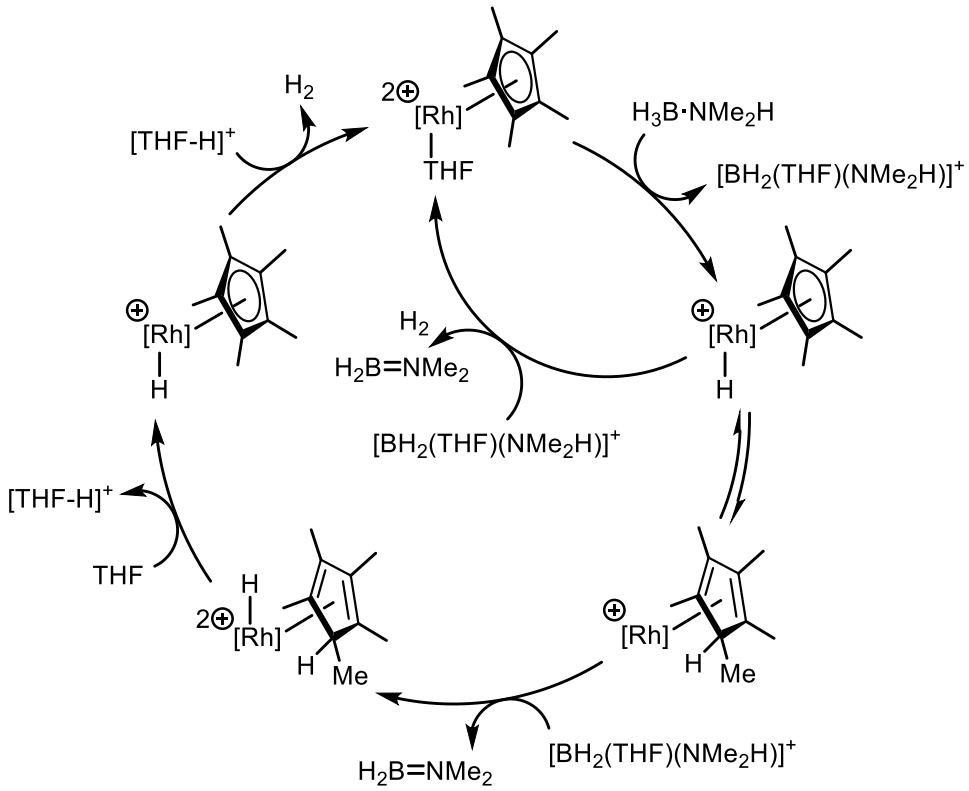
Scheme 1.21 Formation of a bimetallic rhodium complex with a bridging $H_2B{=}NH_2$ molecule. $[BAr^F{}_4]^-$ anions omitted for clarity.[185]

Interestingly, the phenyl derivative of the aminoborane-bridged dimer was shown to catalyse the dehydropolymerisation of $H_3B{\cdot}NMeH_2$ with a very similar kinetic profile as the monometallic species $[Rh(PPh_2(CH_2)_3PPh_2)(\eta^6\text{-}C_6H_5F)][BAr^F{}_4]$ discussed earlier. Therefore, whether the active catalyst in this system is mono- or bimetallic remains undetermined.

In 2017, Freixa *et al*. implied a similar role of boronium as proposed by Conejero and López-Serrano in the dehydrocoupling of $H_3B{\cdot}NH_3$ using [Ru(para-cymene)(bpy)Cl][Cl] (para-cymene = 4-isopropyltoluene, bpy = 2,2'-bipyridine).[186] THF promoted B–H activation at the metal centre to give the ruthenium monohydride alongside the boronium cation $\{H_2B(NH_3)(THF)\}^+$ was proposed, followed by reprotonation of the ruthenium hydride and aminoborane generation. Water stabilised boronium $\{H_2B(NH_3)(H_2O)\}^+$ was also implicated in the catalytic hydrolysis of amine-boranes using the same catalyst.

Boronium was also proposed by Nozaki *et al*. to be a key intermediate in the dehydrocoupling of $H_3B{\cdot}NMe_2H$ using $[Rh(Cp^*)(bpy)][OTf]_2$ in THF.[187] Two mechanistic pathways for this process were proposed, which both include formation of the boronium cation $\{H_2B(NMe_2H)(THF)\}^+$ alongside a Rh^{III} monohydride species (**Scheme 1.22**). From here, direct protonolysis to generate $H_2B{=}NMe_2$ can occur, or a second pathway can be followed involving Cp* non-innocence. Interestingly, catalysis using the analogous Ir^{III} complex was much slower (TOF ~2.8 h^{-1} compared to TOF ~60 h^{-1} for Rh^{III}). DFT calculations showed a high energy barrier for Cp* non-innocence in the Ir^{III} system, which can be

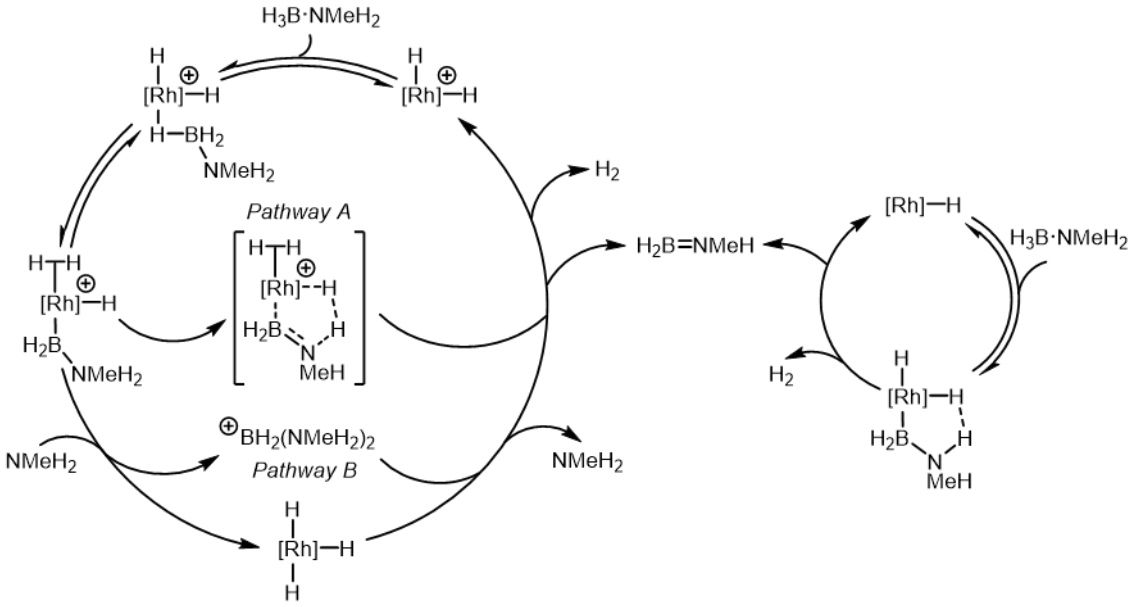
explained by the increased difficulty of breaking the Ir–H bond compared to the Rh–H bond in order to transfer a hydride to the Cp^* ligand. These results indicate that this ligand cooperative pathway is responsible for the higher activity observed in the Rh^{III} mediated system.



Scheme 1.22 Two pathways for the dehydrocoupling of $H_3B{\cdot}NMe_2H$, direct protonolysis and Cp* non-innocence, which involve boronium cations. $[OTf]^-$ anions omitted for clarity.[187]

In 2018, Weller in collaboration with Lloyd-Jones and Macgregor reported neutral and cationic alkyl derivatives of the {Rh(Xantphos)} motif for the catalytic dehydrocoupling of amine-boranes,[157] as described towards the end of section 1.7.2.2. Different mechanisms were proposed for the cationic Rh^{III} system and the neutral Rh^{I} system but neutral rhodium hydrides were identified as key

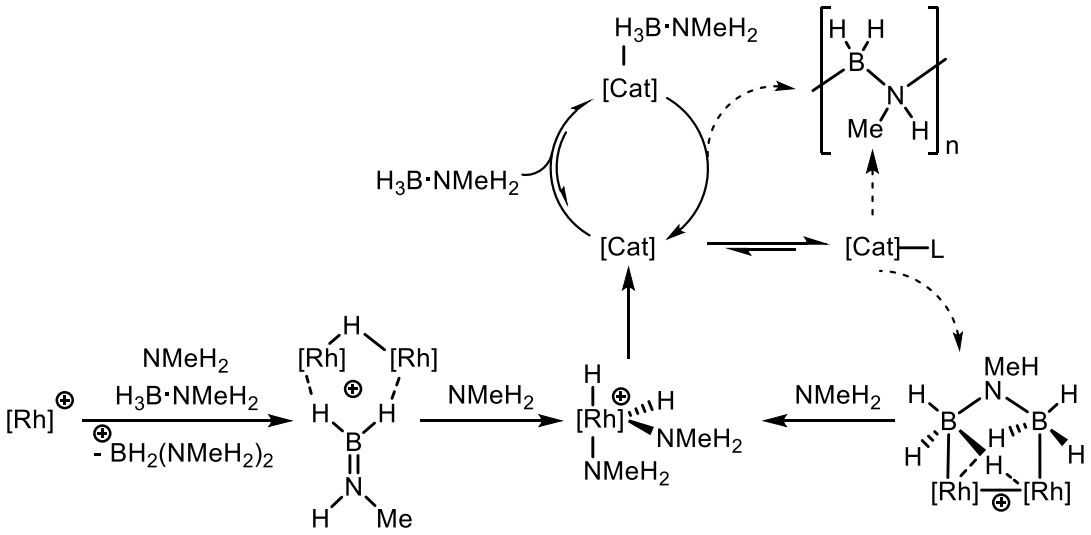
intermediates in both pathways (**Scheme 1.23**). For the cationic system, B–H activation of the bound amine-borane forms a boryl hydride dihydrogen species, which can undergo intramolecular N–H activation (Pathway A) to yield $H_2B{=}NMeH$, H_2 and a cationic rhodium dihydrogen species. Alternatively, the boronium cation $\{H_2B(NMeH_2)_2\}^+$ can be generated alongside a neutral rhodium trihydride species, which can then be protonated by boronium to yield $H_2B{=}NMeH$, H_2 and the cationic rhodium dihydrogen species (Pathway B).



Scheme 1.23 Proposed mechanistic pathways for the dehydrocoupling of $H_3B{\cdot}NMeH_2$ by a cationic Rh^I complex (Pathway A and B) and a neutral Rh^{III} complex where both catalysts are based upon {Rh(Xantphos)}. $[BAr^F{}_4]^-$ anions omitted for clarity.[157]

For the neutral system, the proposed mechanism involves stepwise B–H activation followed by N–H activation to yield $H_2B{=}NMeH$, H_2 and the starting monohydride.

Also discussed in section 1.7.2.2 was the analogous complex {Rh(DPEphos)}$^+$ for the dehydropolymerisation of $H_3B{\cdot}NMeH_2$.[158] An induction period was observed for this system, which increases with an increase in the concentration of the catalyst, during which initial formation of an aminoborane-bridged dimer alongside {$H_2B(NMeH_2)_2$}$^+$ was observed (**Scheme 1.24**), analogous to that observed in the [Rh($P^iPr_2(CH_2)_3P^iPr_2$)(η^6-C_6H_5F)][BAr^F_4] system (**Scheme 1.21**). Repeating catalysis under the same conditions but with the aminoborane-bridged dimer resulted in a similar kinetic profile but only a halving of the induction period, suggesting this species is only a precursor to the active catalyst. Speciation studies also revealed the formation of the amidodiboryl fragment {Rh_2(DPEphos)$_2$(σ,μ-$(H_2B)_2NMeH$)}$^+$ which, when used in catalysis, negated the induction period and yielded simpler first order kinetics. Interestingly, when two equivalents of $NMeH_2$ were added to catalysis the induction period was also removed and the kinetics simplified, along with the polymer yielded being of higher molecular weight than from undoped catalysis. $NMeH_2$ was shown to react rapidly with {Rh_2(DPEphos)$_2$(σ,μ-$(H_2B)_2NMeH$)}$^+$ to form {Rh(DPEphos)$(H)_2(NMeH)_2$}$^+$, which was suggested to be very similar to the still as yet unknown active catalyst. Addition of the boronium cation {$H_2B(NMeH_2)_2$}$^+$ to catalysis caused a significant reduction in rate suggesting boronium is not involved in a productive catalytic pathway, in contrast to that observed in the {Rh(Xantphos)} system (**Scheme 1.23**).



Scheme 1.24 Proposed mechanistic pathways for the dehydropolymerisation of $H_3B{\cdot}NMeH_2$ using {Rh(DPEphos)}$^+$-based pre-catalysts. [Cat] = [Rh]-polymeryl, L = [Cat] or $NMeH_2$. $[BAr^F{}_4]^-$ anions omitted for clarity.[158]

1.10 Pincer ligands

Pincer ligands are tridentate ligands that can coordinate to a metal centre at three meridional sites.[39,188] This coordinational geometry provides a framework around the metal centre of varying rigidity enhancing the stability of resulting complexes, even those that are coordinatively unsaturated.[189–191] The reactivity of the metal complex can also be finely tuned by altering the sterics and electronics of the surrounding pincer ligand, making these attractive complexes for catalytic processes as turnover numbers and product distributions can therefore be controlled. Due to these properties, there is a large precedent for a variety of pincer-based catalysts in the literature.[192] Particularly, those based upon PCP, PNP, POCOP and PONOP frameworks are often efficient catalysts for cross-coupling, dehydrogenation and hydrogenation reactions (**Figure 1.20**).[193–196]

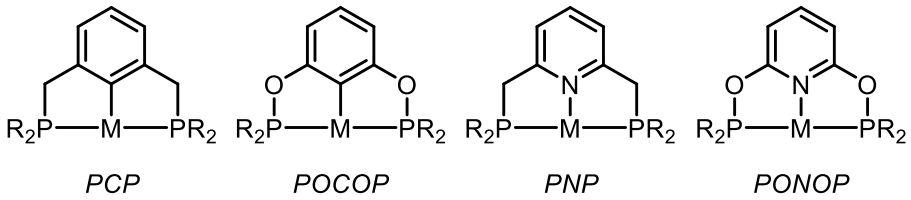


Figure 1.20 Variations of pincer ligands commonly employed in transition metal (M) catalysts.

Catalytic alkane dehydrogenation is a desirable process as it allows low value alkanes to be converted to synthetically important alkenes and PCP pincer complexes have been demonstrated as effective catalysts for this process.[197] In 1996, the iridium dihydride pincer complex $[Ir(H)_2(^{t\text{Bu}}PCP)]$ ($^{t\text{Bu}}PCP = \kappa^3\text{-}C_6H_3\text{-}2,6\text{-}(CH_2P^tBu_2)_2$) (**Figure 1.21**) was reported to catalyse the transfer dehydrogenation of cyclooctane (COA) to cyclooctene (COE) with *tert*-butylethylene (TBE) acting as a sacrificial H_2 acceptor.[198] Brookhart and co-workers improved upon this system by replacing the phosphines with phosphinite groups and making substitutions on the aromatic backbone to give $[Ir(H)(Cl)(p\text{-}X\text{-}^{t\text{Bu}}POCOP)]$ (X = OMe, Me, H, F and C_6H_5).[199] Initial turnover frequencies for the transfer dehydrogenation of COA were reported as between 1.6 – 2.4 s^{-1}; much faster than for $[Ir(H)_2(^{t\text{Bu}}PCP)]$ (TOF = 0.2 s^{-1}).

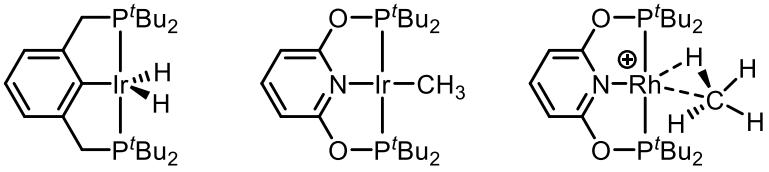
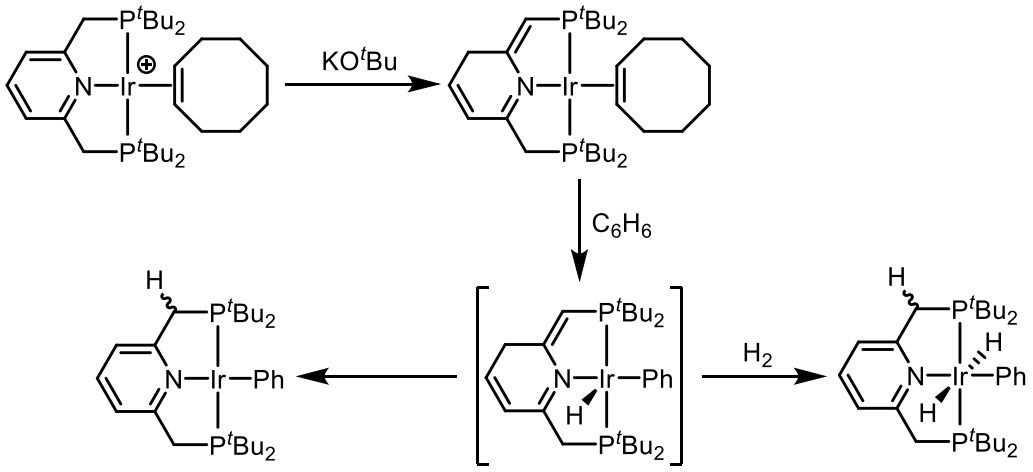


Figure 1.21 Examples of pincer-based complexes: [Ir(H)$_2$($^{t\text{Bu}}$PCP)] (*left*),[198] [Ir(Me)($^{t\text{Bu}}$PONOP)] (*centre*)[200] and {Rh(CH$_4$)($^{t\text{Bu}}$PONOP)}$^+$ (*right*, [BAr$^F{}_4$]$^-$ anion not shown).[201]

Goldman, Brookhart and co-workers went on to report the first use of a PONOP framework in the form of [Ir(R)($^{t\text{Bu}}$PONOP)] (R = Cl, Me, Ph and $^{t\text{Bu}}$PONOP = κ^3-C$_5$H$_3$N-2,6-(OP^{t}Bu$_2$)$_2$) to investigate the C–H bond activation process in alkane dehydrogenation.[200] Protonolysis of [Ir(Me)($^{t\text{Bu}}$PONOP)] (**Figure 1.21**) to give the Ir^{III} hydride {Ir(Me)(H)($^{t\text{Bu}}$PONOP)}$^+$ allowed reductive coupling and oxidative cleavage to be probed. In the same year, the rhodium analogues were used to fully characterise the methane sigma-complex intermediate {Rh(CH$_4$)($^{t\text{Bu}}$PONOP)}$^+$ in CDCl$_2$F at –110 °C (**Figure 1.21**).[201]

In 2001, Milstein and co-workers were the first to report several rhodium- and iridium-based complexes containing the $^{t\text{Bu}}$PNP pincer ligand ($^{t\text{Bu}}$PNP = κ^3-C$_5$H$_3$N-2,6-(CH$_2$P^{t}Bu$_2$)$_2$).[189] Interestingly it was shown that the CH$_2$ groups in the PNP backbone are susceptible to deprotonation leading to dearomatisation of the pyridine ring; for example, reaction of {Ir(COE)($^{t\text{Bu}}$PNP)}$^+$ with ^{t}BuOK rapidly yields the neutral species [Ir(COE)($^{t\text{Bu}}$PNP')] ($^{t\text{Bu}}$PNP' = κ^3-C$_5$H$_3$N-2-(CH$_2$P^{t}Bu$_2$)-6-(CHP^{t}Bu$_2$)) (**Scheme 1.25**).[202] The reactivity of this species was then investigated and shown to C–H activate benzene to yield the re-aromatised [Ir(Ph)($^{t\text{Bu}}$PNP)],

which can itself activate H_2 to exclusively form the *trans*-dihydride [Ir(Ph)(H)$_2$($^{t\text{Bu}}$PNP)]. Experimental and computational evidence confirmed that H_2 activation actually occurs via an Ir^{III} dearomatized complex [Ir(Ph)(H)($^{t\text{Bu}}$PNP')].[203]



Scheme 1.25 Reaction scheme demonstrating to the ability of PNP ligands to dearomatise. $[PF_6]^-$ anions omitted for clarity.[202]

There are many other chemical transformations efficiently catalysed by pincer ligand-based complexes reported in the literature, including: alkane metathesis,[204–206] reduction of CO_2,[207,208] hydrogenation of esters[209–211] and hydroboration.[212,213]

Specifically related to this thesis, it has been shown that incorporation of a pincer ligand into a metal catalyst for the dehydrocoupling of amine-boranes can increase the catalyst activity and even affect the overall polymeric characteristics of the resulting polyaminoborane.[131] Such pincer complexes based upon Ir, Rh, Ru and Fe have been discussed in section 1.7.2. Pincer complexes based upon other transition metals have also been reported as effective dehydrocoupling catalysts. For example,

in 2013 the palladium complex [Pd($^{t\text{Bu}}$PCP)(H_2O)][PF_6] was reported to dehydrocouple $H_3B{\cdot}NH_3$ to yield $[H_2BNH_2]_2$, releasing only one equivalent of H_2.[148] Furthermore, a unique example of a cobalt-based pincer complex, [Co($^{t\text{Bu}}$PBP)(N_2)] ($^{t\text{Bu}}$PBP = bis-phosphinoboryl), was reported by Peters and co-workers to facilitate the dehydrocoupling of $H_3B{\cdot}NMe_2H$ (TOF = 8 h^{-1}).[214] Later, computational work suggested the active catalyst for this process is the dihydride analogue [Co($^{t\text{Bu}}$PBP)($H)_2$] with the boron atom adjacent to the metal centre stabilising one of the hydride ligands.[215]

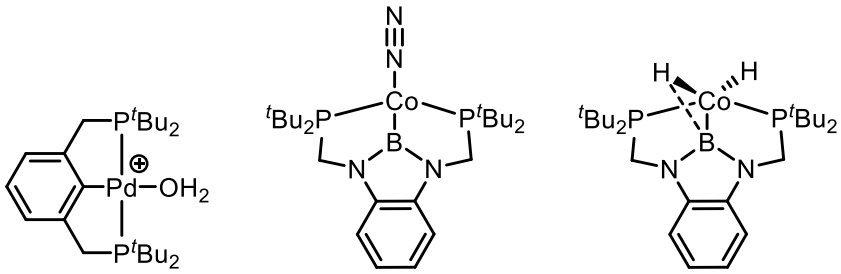


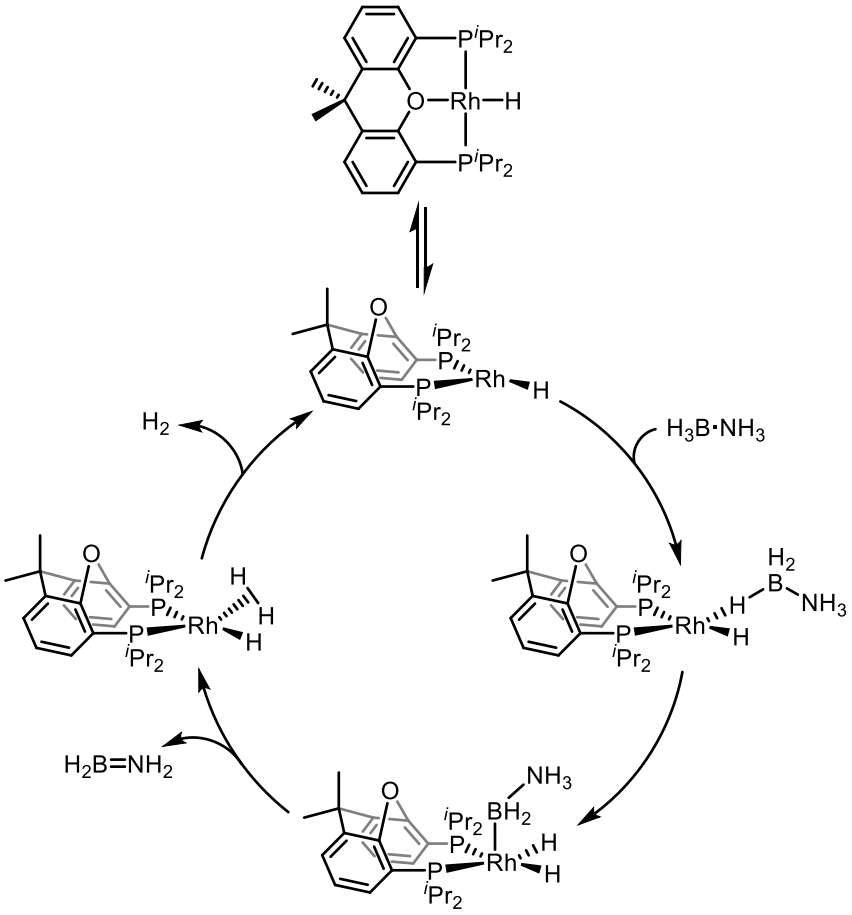
Figure 1.22 Examples of pincer-based complexes involved in the dehydrogenation of amine-boranes.[148,214,215] $[PF_6]^-$ anion not shown.

In summary, pincer ligands have been demonstrated as suitable ligands to support metal complexes for a multitude of catalytic processes. These versatile ligands provide a balance between stability and reactivity, which can be finely tuned by modifying the sterics, electronics, ligand rigidity and also the bite angle around the metal centre; all contributions that can greatly affect the reactivity and selectivity of the catalyst.

1.11 Pincer-supported transition metal hydride complexes

Transition metal hydride complexes have received significant interest as potential catalysts, mostly due to the M–H bond having such a wide range of polarisation leading to unusual and varied reactivity.[216] A transition metal hydride can react as a $H^{\bullet}$, H^{+} or H^{-} donor depending on the available stabilisation for the resulting radical, cationic or anionic metal species.[217]

Transition metal hydrides have been identified as potential intermediates, end products or even the active catalyst during many examples of catalytic dehydrocoupling of amine-boranes,[216] often forming alongside boronium cations (section 1.9).[95,149,157,186,187] However, studies have also been carried out investigating the activity of such hydrides upon direct reaction with amine-boranes. For example, in 2016 Esteruelas *et al*. reported the neutral rhodium monohydride Rh(κ^3-P,O,P-Xantphos-*i*Pr)H for the rapid dehydrocoupling of $H_3B{\cdot}NH_3$ to $[H_2BNH_2]_2$ (TOF = 3, 150 h^{-1}) and $H_3B{\cdot}NMe_2H$ to $[H_2BNMe_2]_2$ (TOF = 1, 725 h^{-1}).[218] The mechanism proposed for this process relies on the decoordination of the oxygen donor in the Xantphos ligand from the metal centre to allow a five-coordinate dihydride-boryl Rh^{III} intermediate (**Scheme 1.26**).



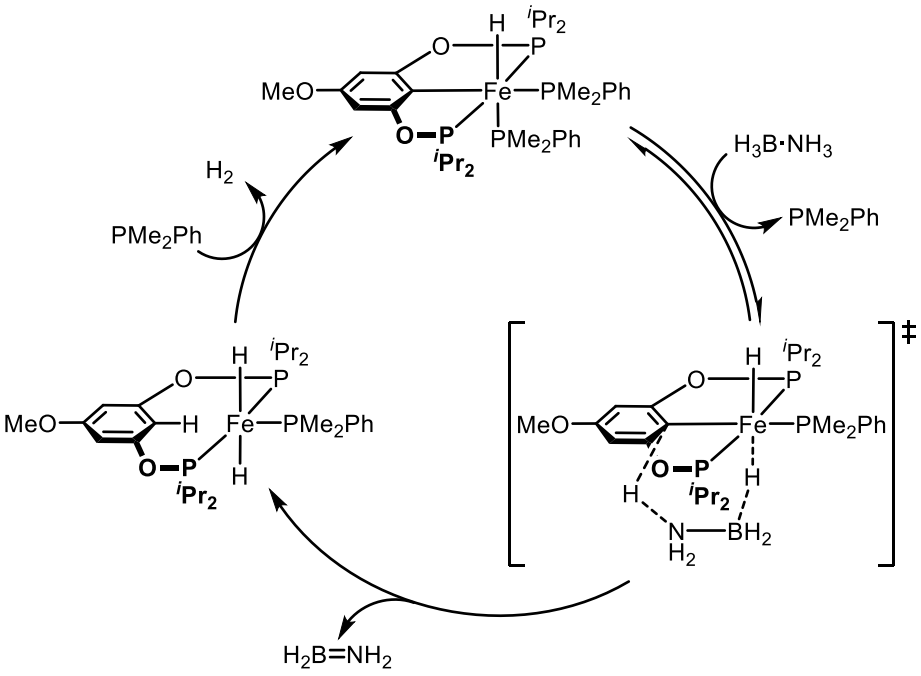
Scheme 1.26 A monohydride complex for the dehydrocoupling of $H_3B{\cdot}NH_3$.[218]

Another Xantphos-based complex, [Ru(κ^3-P,O,P-Xantphos-Ph)(H)(H$_2$O)(PPh$_3$)][BAr$^F{}_4$], was reported to catalyse the dehydrocoupling of $H_3B{\cdot}NMe_2H$ to $[H_2BNMe_2]_2$.[174] Spectroscopic studies showed that the η^1-sigma complex [Ru(κ^3-P,O,P-Xantphos-Ph)(H)(PPh$_3$)(η^1-$H_3B{\cdot}NMe_2H$)][BAr$^F{}_4$] (as in **Figure 1.18** in section 1.8) was the resting state throughout catalysis.

In 2013, Sgro and Stephan reported a range of ruthenium-based complexes with tridentate bis-phosphinite ligand supports for the dehydrocoupling of $H_3B{\cdot}NMe_2H$;

the most active identified being [Ru($^{i\text{Pr}}$POSOP)(H)(Cl)(Py)] ($^{i\text{Pr}}$POSOP = S($CH_2CH_2P^iPr_2$)$_2$) with a TOF ~4 h^{-1}.[219]

Iron hydrides tend to be fairly unstable and so only a few examples of such species as catalysts are known. One such example is the pincer ligand stabilised complex [Fe($^{i\text{Pr}}$POCOP-OMe)(H)(PMe_2Ph)$_2$ ($^{i\text{Pr}}$POCOP-OMe = C_6H_2-2,6-($^iPr_2PO$)$_2$-4-(OMe)), which proved to be extremely effective at catalysing the dehydrocoupling of $H_3B{\cdot}NH_3$.[220] Experimental observations led to a proposed mechanism that involves ligand cooperativity (**Scheme 1.27**).

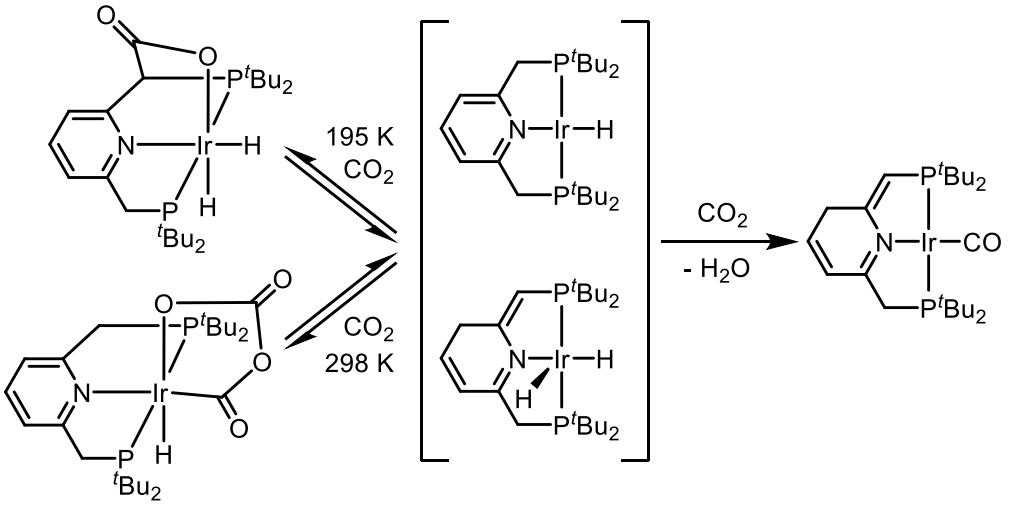


Scheme 1.27 Proposed mechanism for the dehydrocoupling of $H_3B{\cdot}NH_3$ using an iron-based pincer complex.[220]

Transition metal hydrides also have many other applications outside the dehydrocoupling of amine-boranes, including olefin hydrogenation,[221,222] ketone

hydrogenation[223] and hydrosilylation.[224] However, most relevant to this thesis is the transition metal hydride catalysis of the reduction of CO_2.

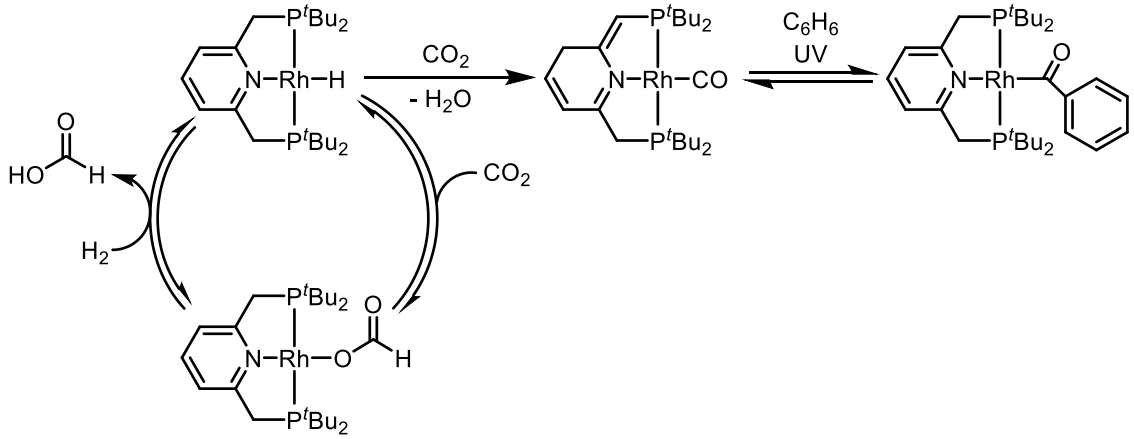
In 2016, Milstein and co-workers reported the reduction of CO_2 to CO and H_2O using a mixture of the iridium monohydride complex [Ir($^{t\text{Bu}}$PNP)(H)] and dihydride [Ir($^{t\text{Bu}}$PNP')(H)$_2$] ($^{t\text{Bu}}$PNP' = deprotonated $^{t\text{Bu}}$PNP).[225] The carbonyl complex [Ir($^{t\text{Bu}}$PNP')(CO)] was isolated as the final product and two CO_2 adducts were also observed to form reversibly. However, computational studies indicated these adducts were not intermediates, but rather reversibly formed side products (**Scheme 1.28**).



Scheme 1.28 Reaction pathways for iridium hydrides with CO_2.[225]

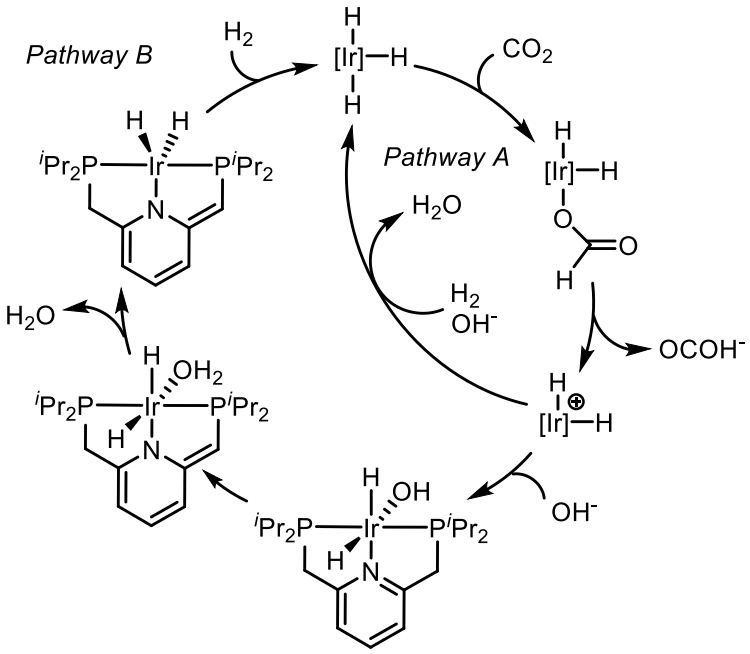
In the same year, the same group also reported the analogous rhodium monohydride complex [Rh($^{t\text{Bu}}$PNP)(H)] for the reduction of CO_2.[226] Upon reaction with CO_2, [Rh($^{t\text{Bu}}$PNP)(H)] was shown to undergo rapid insertion of CO_2 into the Rh–

H bond to give [Rh($^{t\text{Bu}}$PNP)(OCOH)], which could be hydrogenated back to the monohydride yielding formic acid. However, catalytic attempts at this process were thwarted by the eventual CO_2 cleavage to form the dearomatised product [Rh($^{t\text{Bu}}$PNP')(CO)] and water. Although this carbonyl complex halts catalysis, it is able to C–H activate benzene upon UV irradiation to form the benzoyl complex [Rh($^{t\text{Bu}}$PNP)(Bz)] which, upon protonation, yields benzaldehyde (**Scheme 1.29**).



Scheme 1.29 Reduction of CO_2 and the photocarbonylation of benzene using a rhodium monohydride complex. [226]

A highly active catalyst for the hydrogenation of CO_2 to produce formic acid was reported by Nozaki *et al*. in 2009.[208] The Ir^{III} trihydride complex [Ir($^{i\text{Pr}}$PNP)(H)$_3$] was shown to catalyse dehydrogenation of CO_2 in aqueous base (1 M KOH) with an unprecedented TOF of 150, 000 h^{-1}. An initial mechanism was proposed based upon experimental observations (pathway A, **Scheme 1.30**). However, in 2011 a more detailed computational studied reported that a second mechanism could be in competition (pathway B, **Scheme 1.30**).[227]

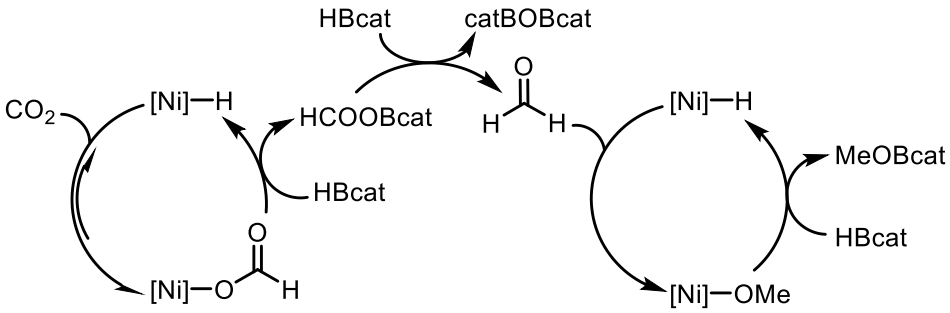


Scheme 1.30 Proposed mechanisms for the reduction of CO_2 using an iridium trihydride complex in the presence of KOH. [Ir] = [Ir($^{i\text{Pr}}$PNP)].[227]

CO_2 has also been shown to undergo facile insertion into a number of Ni^{II} and Pd^{II} hydride complexes, as demonstrated by Takase and co-workers.[228] CO_2 insertion was observed for those complexes supported by PCP and PSiP ligands, but not for PNP, suggesting that the rate of CO_2 insertion into the M–H bond can be increased by having a strong *trans* donor opposite the hydride. It was also reported that CO_2 insertion was more favourable for the Ni^{II} complexes than the Pd^{II} complexes, supposedly due to the ultimately generated Ni–O bond being stronger than the analogous Pd-O bond.

In 2010, the nickel monohydride complex [Ni($^{t\text{Bu}}$PONOP)(H)] was reported to efficiently reduce CO_2 via catalytic hydroboration (TOF = 495 h^{-1}).[229] When [Ni($^{t\text{Bu}}$PONOP)(H)] was reacted with CO_2 in the presence of catecholborane (HBcat),

initial insertion of CO_2 into the Ni–H bond is observed. [Ni(^{t}BuPONOP)(H)] is then regenerated via cleavage of the N–O bond to form HCOOBcat, which can be reduced to formaldehyde by another equivalent of HBcat. A second cycle can also operate, which involves the [Ni(^{t}BuPONOP)(H)] catalysed hydroboration of formaldehyde to give CH_3OBcat (**Scheme 1.31**).



Scheme 1.31 Catalytic reduction of CO_2 via hydroboration using a nickel monohydride. [Ni] = [Ni(^{t}BuPONOP)].[229]

1.12 Summary

This introduction has outlined the fundamentals of organotransition metal catalysis, with an emphasis on the reactivity of rhodium-based complexes. The importance of transition metal complexes as catalysts for a variety of chemical transformations has been highlighted, with an especial focus on the dehydrogenation of amine-boranes, which has been discussed in detail. Intermediates within this process, such as sigma complexes and boronium cations, have been considered and literature examples outlined. Pincer ligands have been highlighted as a popular choice of framework to stabilise transition metal catalysts and so will be the basis for the catalysts presented in this thesis.

Chapters Two and Three will build upon the research presented in this chapter on the dehydrogenation of amine-boranes, specifically focusing on a thorough investigation into the dehydrocoupling of $H_3B{\cdot}NMe_2H$. Mechanistic insight into this process will contribute to the overall aim of elucidating a universal mechanism for the dehydrogenation of amine-boranes in general. With this knowledge, fine tuning of catalysts to generate desirable product distributions under mild conditions may become facile potentially leading to a range of novel materials and processes. A catalyst based upon the $\{Rh(PONOP)\}^+$ fragment will be employed in this thesis as both rhodium and pincer ligands have been components of some of the most successful amine-borane dehydrocoupling catalysts reported.

In Chapter Four, the reactivity of the related neutral complex Rh(PONOP)H is explored. Its potential as a catalyst for the reduction of CO_2 is investigated due to the progress made by Milstein *et al*. in this area using the analogous Rh(PNP)H analogue. The substitution of a PNP ligand for a PONOP ligand may result in different reactivity due to the inability of PONOP to be deprotonated and therefore dearomatised.

1.13 References

[1] R. H. Crabtree, *The Organometallic Chemistry of the Transition Metals*, Wiley, **2014**.
[2] J. F. Hartwig, *Organotransition Metal Chemistry: From Bonding to Catalysis*, University Science Books, **2010**.
[3] A. J. Kasparian, C. Savarin, A. M. Allgeier, S. D. Walker, *J. Org. Chem.* **2011**, *76*, 9841–9844.
[4] R. J. Less, R. L. Melen, D. S. Wright, *RSC Advances* **2012**, *2*, 2191–2199.
[5] O. Planas, F. Wang, M. Leutzsch, J. Cornella, *Science* **2020**, *367*, 313–317.
[6] R. A. Sheldon, *Chem. Commun.* **2008**, 3352–3365.

[7] C. A. Busacca, D. R. Fandrick, J. J. Song, C. H. Senanayake, *Advanced Synthesis & Catalysis* **2011**, *353*, 1825–1864.
[8] *Chirality* **1992**, *4*, 338–340.
[9] I. Omae, *Applied Organometallic Chemistry* **2009**, *23*, 91–107.
[10] J. A. Dubin, in *Studies in Consumer Demand — Econometric Methods Applied to Market Data*, Springer US, **1998**, pp. 61–76.
[11] B. Cornils, W. A. Herrmann, M. Rasch, *Angewandte Chemie International Edition in English* **1994**, *33*, 2144–2163.
[12] L. H. Slaugh, R. D. Mullineaux, *Journal of Organometallic Chemistry* **1968**, *13*, 469–477.
[13] J. A. Osborn, F. H. Jardine, J. F. Young, G. Wilkinson, *J. Chem. Soc. A* **1966**, 1711–1732.
[14] C. A. Tolman, *J. Chem. Educ.* **1986**, *63*, 199.
[15] G. Cecchin, G. Morini, F. Piemontesi, in *Kirk-Othmer Encyclopedia of Chemical Technology*, American Cancer Society, **2003**.
[16] Yin, J. Liebscher, *Chem. Rev.* **2007**, *107*, 133–173.
[17] "The Nobel Prize in Chemistry 2001,"
[18] "The Nobel Prize in Chemistry 2005,"
[19] "The Nobel Prize in Chemistry 2010,"
[20] T. J. Clark, K. Lee, I. Manners, *Chem. Eur. J.* **2006**, *12*, 8634–8648.
[21] N. N. Greenwood, A. Earnshaw, *Chemistry of the Elements*, Butterworth Heinemann, **1997**.
[22] M. L. Zientek, P. J. Loferski, H. L. Parks, R. F. Schulte, R. R. Seal II, *Platinum-Group Elements*, Reston, VA, **2017**.
[23] D. Evans, J. A. Osborn, G. Wilkinson, *J. Chem. Soc. A* **1968**, 3133–3142.
[24] R. R. Schrock, J. A. Osborn, *J. Am. Chem. Soc.* **1976**, *98*, 2134–2143.
[25] D. Forster, in *Advances in Organometallic Chemistry*, Academic Press, **1979**, pp. 255–267.
[26] M. C. Simpson, D. J. Cole-Hamilton, *Coordination Chemistry Reviews* **1996**, *155*, 163–207.
[27] P. B. Dias, M. E. M. de Piedade, J. A. M. Simões, *Coordination Chemistry Reviews* **1994**, *135–136*, 737–807.
[28] A. G. Orpen, N. G. Connelly, *J. Chem. Soc., Chem. Commun.* **1985**, 1310–1311.
[29] C. A. Tolman, *J. Am. Chem. Soc.* **1970**, *92*, 2953–2956.
[30] C. A. Tolman, *Chem. Rev.* **1977**, *77*, 313–348.
[31] C. A. Tolman, *J. Am. Chem. Soc.* **1970**, *92*, 2956–2965.
[32] J. A. Bilbrey, A. H. Kazez, J. Locklin, W. D. Allen, *J. Chem. Theory Comput.* **2013**, *9*, 5734–5744.
[33] C. P. Casey, G. T. Whiteker, *Israel Journal of Chemistry* **1990**, *30*, 299–304.
[34] C. P. Casey, G. T. Whiteker, M. G. Melville, L. M. Petrovich, J. A. Gavney, D. R. Powell, *J. Am. Chem. Soc.* **1992**, *114*, 5535–5543.
[35] P. Dierkes, P. W. N. M. van Leeuwen, *J. Chem. Soc., Dalton Trans.* **1999**, 1519–1530.
[36] M.-N. B. (née Gensow), Z. Freixa, P. W. N. M. van Leeuwen, *Chem. Soc. Rev.* **2009**, *38*, 1099–1118.

[37] N. J. DeStefano, D. K. Johnson, R. M. Lane, L. M. Venanzi, *Helvetica Chimica Acta* **1976**, *59*, 2674–2682.
[38] R. Dallanegra, A. P. M. Robertson, A. B. Chaplin, I. Manners, A. S. Weller, *Chem. Commun.* **2011**, *47*, 3763–3765.
[39] K. J. Szabó, O. F. Wendt, *Pincer and Pincer-Type Complexes Applications in Organic Synthesis and Catalysis.*, Wiley-VCH, **2014**.
[40] M. Brookhart, M. L. H. Green, G. Parkin, *PNAS* **2007**, *104*, 6908–6914.
[41] S. H. Strauss, *Chem. Rev.* **1993**, *93*, 927–942.
[42] A. B. Chaplin, A. I. Poblador-Bahamonde, H. A. Sparkes, J. A. K. Howard, S. A. Macgregor, A. S. Weller, *Chem. Commun.* **2009**, 244–246.
[43] P. Albano, M. Aresta, M. Manassero, *Inorg. Chem.* **1980**, *19*, 1069–1072.
[44] A. Vigalok, B. Rybtchinski, L. J. W. Shimon, Y. Ben-David, D. Milstein, *Organometallics* **1999**, *18*, 895–905.
[45] I. Krossing, I. Raabe, *Angewandte Chemie International Edition* **2004**, *43*, 2066–2090.
[46] R. L. Paul, A. J. Amoroso, P. L. Jones, S. M. Couchman, Z. R. Reeves, L. H. Rees, J. C. Jeffery, J. A. McCleverty, M. D. Ward, *J. Chem. Soc., Dalton Trans.* **1999**, 1563–1568.
[47] S. Kannan, M. A. Moody, C. L. Barnes, P. B. Duval, *Inorg. Chem.* **2006**, *45*, 9206–9212.
[48] P. de Frémont, N. Marion, S. P. Nolan, *Journal of Organometallic Chemistry* **2009**, *694*, 551–560.
[49] H. Kobayashi, T. Sonoda, H. Iwamoto, M. Yoshimura, *Chem. Lett.* **1981**, *10*, 579–580.
[50] A. J. Martínez-Martínez, A. S. Weller, *Dalton Trans.* **2019**, *48*, 3551–3554.
[51] A. B. Chaplin, A. S. Weller, *Eur. J. Inorg. Chem.* **2010**, *2010*, 5124–5128.
[52] I. Krossing, *Chemistry – A European Journal* **2001**, *7*, 490–502.
[53] P. Wasserscheid, C. Hilgers, W. Keim, *Journal of Molecular Catalysis A: Chemical* **2004**, *214*, 83–90.
[54] G. M. Adams, F. M. Chadwick, S. D. Pike, A. S. Weller, *Dalton Trans.* **2015**, *44*, 6340–6342.
[55] S. D. Pike, M. R. Crimmin, A. B. Chaplin, *Chem. Commun.* **2017**, *53*, 3615–3633.
[56] T. R. O'Toole, J. N. Younathan, B. P. Sullivan, T. J. Meyer, *Inorg. Chem.* **1989**, *28*, 3923–3926.
[57] E. M. Leitao, T. Jurca, I. Manners, *Nat Chem* **2013**, *5*, 817–829.
[58] R. O. Hutchins, K. Learn, B. Nazer, D. Pytlewski, A. Pelter, *Organic Preparations and Procedures International* **1984**, *16*, 335–372.
[59] Z. Liu, T. B. Marder, *Angewandte Chemie International Edition* **2008**, *47*, 242–244.
[60] R. H. Crabtree, *Science* **1998**, *282*, 2000–2001.
[61] S. Aldridge, A. J. Downs, C. Y. Tang, S. Parsons, M. C. Clarke, R. D. L. Johnstone, H. E. Robertson, D. W. H. Rankin, D. A. Wann, *J. Am. Chem. Soc.* **2009**, *131*, 2231–2243.
[62] W. T. Klooster, T. F. Koetzle, P. E. M. Siegbahn, T. B. Richardson, R. H. Crabtree, *J. Am. Chem. Soc.* **1999**, *121*, 6337–6343.
[63] R. Waterman, *Chem. Soc. Rev.* **2013**, *42*, 5629–5641.

[64] A. Kumar, H. C. Johnson, T. N. Hooper, A. S. Weller, A. G. Algarra, S. A. Macgregor, *Chem. Sci.* **2014**, *5*, 2546–2553.
[65] D. A. Dixon, M. Gutowski, *J. Phys. Chem. A* **2005**, *109*, 5129–5135.
[66] D. J. Grant, D. A. Dixon, *J. Phys. Chem. A* **2006**, *110*, 12955–12962.
[67] F. H. Stephens, V. Pons, R. T. Baker, *Dalton Trans.* **2007**, 2613–2626.
[68] Y. J. Choi, E. C. E. Rönnebro, S. Rassat, A. Karkamkar, G. Maupin, J. Holladay, K. Simmons, K. Brooks, *Phys. Chem. Chem. Phys.* **2014**, *16*, 7959–7968.
[69] T. B. Marder, *Angewandte Chemie International Edition* **2007**, *46*, 8116–8118.
[70] A. D. Sutton, A. K. Burrell, D. A. Dixon, E. B. Garner, J. C. Gordon, T. Nakagawa, K. C. Ott, J. P. Robinson, M. Vasiliu, *Science* **2011**, *331*, 1426–1429.
[71] S. Bhunya, T. Malakar, G. Ganguly, A. Paul, *ACS Catal.* **2016**, *6*, 7907–7934.
[72] D. J. Grant, M. H. Matus, K. D. Anderson, D. M. Camaioni, S. R. Neufeldt, C. F. Lane, D. A. Dixon, *J. Phys. Chem. A* **2009**, *113*, 6121–6132.
[73] A. Staubitz, A. P. M. Robertson, M. E. Sloan, I. Manners, *Chem. Rev.* **2010**, *110*, 4023–4078.
[74] S. M. Nakhmanson, M. B. Nardelli, J. Bernholc, *Phys. Rev. Lett.* **2004**, *92*, 115504.
[75] V. A. Du, T. Jurca, G. R. Whittell, I. Manners, *Dalton Trans.* **2016**, *45*, 1055–1062.
[76] A. L. Colebatch, A. S. Weller, *Chem. Eur. J.* **2019**, *25*, 1379–1390.
[77] S. Bernard, C. Salameh, P. Miele, *Dalton Trans.* **2016**, *45*, 861–873.
[78] S.-K. Kim, H. Cho, M. J. Kim, H.-J. Lee, J. Park, Y.-B. Lee, H. C. Kim, C. W. Yoon, S. W. Nam, S. O. Kang, *J. Mater. Chem. A* **2013**, *1*, 1976–1981.
[79] Z. Liu, L. Song, S. Zhao, J. Huang, L. Ma, J. Zhang, J. Lou, P. M. Ajayan, *Nano Lett.* **2011**, *11*, 2032–2037.
[80] G. E. Ryschkewitsch, J. W. Wiggins, *Inorg. Chem.* **1970**, *9*, 314–317.
[81] H. C. Johnson, T. N. Hooper, A. S. Weller, *Top.Organomet.Chem* **2015**, 153.
[82] A. Staubitz, A. Presa Soto, I. Manners, *Angewandte Chemie International Edition* **2008**, *47*, 6212–6215.
[83] C. A. Jaska, K. Temple, A. J. Lough, I. Manners, *J. Am. Chem. Soc.* **2003**, *125*, 9424–9434.
[84] P. J. Fazen, J. S. Beck, A. T. Lynch, E. E. Remsen, L. G. Sneddon, *Chem. Mater.* **1990**, *2*, 96–97.
[85] H. C. Johnson, A. S. Weller, *Journal of Organometallic Chemistry* **2012**, *721–722*, 17–22.
[86] C. A. Jaska, K. Temple, A. J. Lough, I. Manners, *Chem. Commun.* **2001**, 962–963.
[87] L. Euzenat, D. Horhant, Y. Ribourdouille, C. Duriez, G. Alcaraz, M. Vaultier, *Chem. Commun.* **2003**, 2280–2281.
[88] L. J. Sewell, G. C. Lloyd-Jones, A. S. Weller, *J. Am. Chem. Soc.* **2012**, *134*, 3598–3610.
[89] N. E. Stubbs, A. Schäfer, A. P. M. Robertson, E. M. Leitao, T. Jurca, H. A. Sparkes, C. H. Woodall, M. F. Haddow, I. Manners, *Inorg. Chem.* **2015**, *54*, 10878–10889.
[90] I. G. Green, K. M. Johnson, B. P. Roberts, *J. Chem. Soc., Perkin Trans. 2* **1989**, 1963–1972.
[91] D. Han, F. Anke, M. Trose, T. Beweries, *Coordination Chemistry Reviews* **2019**, *380*, 260–286.

[92] C. W. Hamilton, R. T. Baker, A. Staubitz, I. Manners, *Chem. Soc. Rev.* **2008**, *38*, 279–293.
[93] R. L. Melen, *Chem. Soc. Rev.* **2016**, *45*, 775–788.
[94] J. Spielmann, M. Bolte, S. Harder, *Chem. Commun.* **2009**, 6934–6936.
[95] D. J. Liptrot, M. S. Hill, M. F. Mahon, D. J. MacDougall, *Chemistry – A European Journal* **2010**, *16*, 8508–8515.
[96] F. Wang, O. Planas, J. Cornella, *J. Am. Chem. Soc.* **2019**, *141*, 4235–4240.
[97] H. J. Cowley, M. S. Holt, R. L. Melen, J. M. Rawson, D. S. Wright, *Chem. Commun.* **2011**, *47*, 2682–2684.
[98] M. M. Hansmann, R. L. Melen, D. S. Wright, *Chem. Sci.* **2011**, *2*, 1554–1559.
[99] P. Bellham, M. S. Hill, G. Kociok-Köhn, D. J. Liptrot, *Chem. Commun.* **2013**, *49*, 1960–1962.
[100] P. Bellham, M. S. Hill, G. Kociok-Köhn, *Organometallics* **2014**, *33*, 5716–5721.
[101] K. A. Erickson, D. S. Wright, R. Waterman, *Journal of Organometallic Chemistry* **2014**, *751*, 541–545.
[102] M. S. Hill, G. Kociok-Köhn, T. P. Robinson, *Chem. Commun.* **2010**, *46*, 7587–7589.
[103] P. Cui, T. P. Spaniol, L. Maron, J. Okuda, *Chemistry – A European Journal* **2013**, *19*, 13437–13444.
[104] E. Lu, Y. Yuan, Y. Chen, W. Xia, *ACS Catal.* **2013**, *3*, 521–524.
[105] C. A. Jaska, I. Manners, *J. Am. Chem. Soc.* **2004**, *126*, 9776–9785.
[106] C. A. Jaska, I. Manners, *J. Am. Chem. Soc.* **2004**, *126*, 1334–1335.
[107] M. A. Watzky, R. G. Finke, *J. Am. Chem. Soc.* **1997**, *119*, 10382–10400.
[108] J. A. Widegren, R. G. Finke, *Journal of Molecular Catalysis A: Chemical* **2003**, *198*, 317–341.
[109] Y. Chen, J. L. Fulton, J. C. Linehan, T. Autrey, *J. Am. Chem. Soc.* **2005**, *127*, 3254–3255.
[110] A. P. M. Robertson, R. Suter, L. Chabanne, G. R. Whittell, I. Manners, *Inorg. Chem.* **2011**, *50*, 12680–12691.
[111] J. F. Sonnenberg, R. H. Morris, *ACS Catal.* **2013**, *3*, 1092–1102.
[112] J. R. Khusnutdinova, D. Milstein, *Angewandte Chemie International Edition* **2015**, *54*, 12236–12273.
[113] A. N. Marziale, A. Friedrich, I. Klopsch, M. Drees, V. R. Celinski, J. Schmedt auf der Günne, S. Schneider, *J. Am. Chem. Soc.* **2013**, *135*, 13342–13355.
[114] A. Friedrich, M. Drees, S. Schneider, *Chemistry – A European Journal* **2009**, *15*, 10339–10342.
[115] M. Käß, A. Friedrich, M. Drees, S. Schneider, *Angewandte Chemie International Edition* **2009**, *48*, 905–907.
[116] A. Glüer, M. Förster, V. R. Celinski, J. Schmedt auf der Günne, M. C. Holthausen, S. Schneider, *ACS Catal.* **2015**, *5*, 7214–7217.
[117] T. Malakar, S. Bhunya, A. Paul, *Chemistry – A European Journal* **2015**, *21*, 6340–6345.
[118] F. Anke, D. Han, M. Klahn, A. Spannenberg, T. Beweries, *Dalton Trans.* **2017**, *46*, 6843–6847.
[119] D. F. Schreiber, C. O'Connor, C. Grave, Y. Ortin, H. Müller-Bunz, A. D. Phillips, *ACS Catal.* **2012**, *2*, 2505–2511.

[120] A. D. Phillips, G. Laurenczy, R. Scopelliti, P. J. Dyson, *Organometallics* **2007**, *26*, 1120–1122.
[121] A. M. Chapman, M. F. Haddow, D. F. Wass, *J. Am. Chem. Soc.* **2011**, *133*, 8826–8829.
[122] T. J. Clark, C. A. Russell, I. Manners, *J. Am. Chem. Soc.* **2006**, *128*, 9582–9583.
[123] M. E. Sloan, A. Staubitz, T. J. Clark, C. A. Russell, G. C. Lloyd-Jones, I. Manners, *J. Am. Chem. Soc.* **2010**, *132*, 3831–3841.
[124] H. Helten, B. Dutta, J. R. Vance, M. E. Sloan, M. F. Haddow, S. Sproules, D. Collison, G. R. Whittell, G. C. Lloyd-Jones, I. Manners, *Angewandte Chemie International Edition* **2013**, *52*, 437–440.
[125] T. Beweries, S. Hansen, M. Kessler, M. Klahn, U. Rosenthal, *Dalton Trans.* **2011**, *40*, 7689–7692.
[126] T. Beweries, J. Thomas, M. Klahn, A. Schulz, D. Heller, U. Rosenthal, *ChemCatChem* **2011**, *3*, 1865–1868.
[127] D. Pun, E. Lobkovsky, P. J. Chirik, *Chem. Commun.* **2007**, *0*, 3297–3299.
[128] T. Jurca, T. Dellermann, N. E. Stubbs, D. A. Resendiz-Lara, G. R. Whittell, I. Manners, *Chem. Sci.* **2018**, *9*, 3360–3366.
[129] Y. Kawano, M. Uruichi, M. Shimoi, S. Taki, T. Kawaguchi, T. Kakizawa, H. Ogino, *J. Am. Chem. Soc.* **2009**, *131*, 14946–14957.
[130] M. C. Denney, V. Pons, T. J. Hebden, D. M. Heinekey, K. I. Goldberg, *J. Am. Chem. Soc.* **2006**, *128*, 12048–12049.
[131] A. Staubitz, M. E. Sloan, A. P. M. Robertson, A. Friedrich, S. Schneider, P. J. Gates, J. S. auf der Günne, I. Manners, *J. Am. Chem. Soc.* **2010**, *132*, 13332–13345.
[132] T. J. Hebden, M. C. Denney, V. Pons, P. M. B. Piccoli, T. F. Koetzle, A. J. Schultz, W. Kaminsky, K. I. Goldberg, D. M. Heinekey, *J. Am. Chem. Soc.* **2008**, *130*, 10812–10820.
[133] S. Bhunya, T. Malakar, A. Paul, *Chem. Commun.* **2014**, *50*, 5919–5922.
[134] H. G. Alt, A. Köppl, *Chem. Rev.* **2000**, *100*, 1205–1222.
[135] R. P. Quirk, in *Encyclopedia of Polymer Science and Technology*, American Cancer Society, **2002**.
[136] M. Vogt, B. de Bruin, H. Berke, M. Trincado, H. Grützmacher, *Chem. Sci.* **2011**, *2*, 723–727.
[137] Y. Jiang, O. Blacque, T. Fox, C. M. Frech, H. Berke, *Organometallics* **2009**, *28*, 5493–5504.
[138] C. Lichtenberg, L. Viciu, M. Adelhardt, J. Sutter, K. Meyer, B. de Bruin, H. Grützmacher, *Angewandte Chemie International Edition* **2015**, *54*, 5766–5771.
[139] J. R. Vance, A. Schäfer, A. P. M. Robertson, K. Lee, J. Turner, G. R. Whittell, I. Manners, *J. Am. Chem. Soc.* **2014**, *136*, 3048–3064.
[140] R. T. Baker, J. C. Gordon, C. W. Hamilton, N. J. Henson, P.-H. Lin, S. Maguire, M. Murugesu, B. L. Scott, N. C. Smythe, *J. Am. Chem. Soc.* **2012**, *134*, 5598–5609.
[141] C. J. Wallis, H. Dyer, L. Vendier, G. Alcaraz, S. Sabo-Etienne, *Angewandte Chemie International Edition* **2012**, *51*, 3646–3648.
[142] T. Miyazaki, Y. Tanabe, M. Yuki, Y. Miyake, Y. Nishibayashi, *Organometallics* **2011**, *30*, 2394–2404.
[143] C. Boulho, J.-P. Djukic, *Dalton Trans.* **2010**, *39*, 8893–8905.

[144] M. A. Esteruelas, I. Fernández, A. M. López, M. Mora, E. Oñate, *Organometallics* **2014**, *33*, 1104–1107.
[145] S. Todisco, L. Luconi, G. Giambastiani, A. Rossin, M. Peruzzini, I. E. Golub, O. A. Filippov, N. V. Belkova, E. S. Shubina, *Inorg. Chem.* **2017**, *56*, 4296–4307.
[146] C. J. Stevens, R. Dallanegra, A. B. Chaplin, A. S. Weller, S. A. Macgregor, B. Ward, D. McKay, G. Alcaraz, S. Sabo-Etienne, *Chem. Eur. J.* **2011**, *17*, 3011–3020.
[147] R. J. Keaton, J. M. Blacquiere, R. T. Baker, *J. Am. Chem. Soc.* **2007**, *129*, 1844–1845.
[148] A. Rossin, G. Bottari, A. M. Lozano-Vila, M. Paneque, M. Peruzzini, A. Rossi, F. Zanobini, *Dalton Trans.* **2013**, *42*, 3533–3541.
[149] M. Roselló-Merino, J. López-Serrano, S. Conejero, *J. Am. Chem. Soc.* **2013**, *135*, 10910–10913.
[150] M. Roselló-Merino, R. J. Rama, J. Díez, S. Conejero, *Chem. Commun.* **2016**, *52*, 8389–8392.
[151] T. M. Douglas, A. B. Chaplin, A. S. Weller, *J. Am. Chem. Soc.* **2008**, *130*, 14432–14433.
[152] T. M. Douglas, A. B. Chaplin, A. S. Weller, X. Yang, M. B. Hall, *J. Am. Chem. Soc.* **2009**, *131*, 15440–15456.
[153] A. L. Colebatch, B. W. Hawkey Gilder, G. R. Whittell, N. L. Oldroyd, I. Manners, A. S. Weller, *Chemistry – A European Journal* **2018**, *24*, 5450–5455.
[154] L. J. Sewell, M. A. Huertos, M. E. Dickinson, A. S. Weller, G. C. Lloyd-Jones, *Inorg. Chem.* **2013**, *52*, 4509–4516.
[155] H. C. Johnson, E. M. Leitao, G. R. Whittell, I. Manners, G. C. Lloyd-Jones, A. S. Weller, *J. Am. Chem. Soc.* **2014**, *136*, 9078–9093.
[156] H. C. Johnson, A. S. Weller, *Angewandte Chemie International Edition* **2015**, *54*, 10173–10177.
[157] G. M. Adams, A. L. Colebatch, J. T. Skornia, A. I. McKay, H. C. Johnson, G. C. Lloyd−Jones, S. A. Macgregor, N. A. Beattie, A. S. Weller, *J. Am. Chem. Soc.* **2018**, *140*, 1481–1495.
[158] G. M. Adams, D. E. Ryan, N. A. Beattie, A. I. McKay, G. C. Lloyd-Jones, A. S. Weller, *ACS Catal.* **2019**, *9*, 3657–3666.
[159] J. C. Green, M. L. H. Green, G. Parkin, *Chem. Commun.* **2012**, *48*, 11481–11503.
[160] D. Devarajan, D. H. Ess, *Inorg. Chem.* **2012**, *51*, 6367–6375.
[161] M. Etienne, A. S. Weller, *Chem. Soc. Rev.* **2013**, *43*, 242–259.
[162] I. Castro-Rodriguez, H. Nakai, P. Gantzel, L. N. Zakharov, A. L. Rheingold, K. Meyer, *J. Am. Chem. Soc.* **2003**, *125*, 15734–15735.
[163] S. D. Pike, A. L. Thompson, A. G. Algarra, D. C. Apperley, S. A. Macgregor, A. S. Weller, *Science* **2012**, *337*, 1648–1651.
[164] G. J. Kubas, R. R. Ryan, B. I. Swanson, P. J. Vergamini, H. J. Wasserman, *J. Am. Chem. Soc.* **1984**, *106*, 451–452.
[165] G. J. Kubas, *Chem. Rev.* **2007**, *107*, 4152–4205.
[166] J. Chatt, L. A. Duncanson, *J. Chem. Soc.* **1953**, 2939–2947.
[167] G. J. Kubas, *Catal Lett* **2005**, *104*, 79–101.
[168] D. M. Heinekey, W. J. Oldham, *Chem. Rev.* **1993**, *93*, 913–926.
[169] G. S. McGrady, G. Guilera, *Chemical Society Reviews* **2003**, *32*, 383.

[170] G. Alcaraz, S. Sabo-Etienne, *Angewandte Chemie International Edition* **2010**, *49*, 7170–7179.
[171] M. Shimoi, S. Nagai, M. Ichikawa, Y. Kawano, K. Katoh, M. Uruichi, H. Ogino, *J. Am. Chem. Soc.* **1999**, *121*, 11704–11712.
[172] A. G. Algarra, L. J. Sewell, H. C. Johnson, S. A. Macgregor, A. S. Weller, *Dalton Trans.* **2014**, *43*, 11118–11128.
[173] Y. Kawano, M. Hashiva, M. Shimoi, *Organometallics* **2006**, *25*, 4420–4426.
[174] A. E. W. Ledger, C. E. Ellul, M. F. Mahon, J. M. J. Williams, M. K. Whittlesey, *Chemistry – A European Journal* **2011**, *17*, 8704–8713.
[175] A. E. Nako, A. J. P. White, M. R. Crimmin, *Dalton Trans.* **2015**, *44*, 12530–12534.
[176] C. Y. Tang, A. L. Thompson, S. Aldridge, *J. Am. Chem. Soc.* **2010**, *132*, 10578–10591.
[177] R. Dallanegra, A. B. Chaplin, A. S. Weller, *Angewandte Chemie International Edition* **2009**, *48*, 6875–6878.
[178] A. S. Weller, F. M. Chadwick, A. I. McKay, in *Advances in Organometallic Chemistry* (Ed.: P.J. Pérez), Academic Press, **2016**, pp. 223–276.
[179] H. C. Johnson, A. P. M. Robertson, A. B. Chaplin, L. J. Sewell, A. L. Thompson, M. F. Haddow, I. Manners, A. S. Weller, *J. Am. Chem. Soc.* **2011**, *133*, 11076–11079.
[180] G. Alcaraz, A. B. Chaplin, C. J. Stevens, E. Clot, L. Vendier, A. S. Weller, S. Sabo-Etienne, *Organometallics* **2010**, *29*, 5591–5595.
[181] A. B. Chaplin, A. S. Weller, *Inorg. Chem.* **2010**, *49*, 1111–1121.
[182] R. Dallanegra, A. B. Chaplin, J. Tsim, A. S. Weller, *Chem. Commun.* **2010**, *46*, 3092–3094.
[183] R. Kumar, B. R. Jagirdar, *Inorg. Chem.* **2013**, *52*, 28–36.
[184] F. H. Stephens, R. T. Baker, M. H. Matus, D. J. Grant, D. A. Dixon, *Angewandte Chemie International Edition* **2007**, *46*, 746–749.
[185] A. Kumar, N. A. Beattie, S. D. Pike, S. A. Macgregor, A. S. Weller, *Angewandte Chemie International Edition* **2016**, *55*, 6651–6656.
[186] A. Telleria, C. Vicent, V. San Nacianceno, M. A. Garralda, Z. Freixa, *ACS Catal.* **2017**, *7*, 8394–8405.
[187] S. Pal, S. Kusumoto, K. Nozaki, *Organometallics* **2018**, *37*, 906–914.
[188] D. Morales-Morales, C. M. Jensen, *The Chemistry of Pincer Compounds*, Elsevier, Amsterdam, **2007**.
[189] D. Hermann, M. Gandelman, H. Rozenberg, L. J. W. Shimon, D. Milstein, *Organometallics* **2002**, *21*, 812–818.
[190] M. E. van der Boom, D. Milstein, *Chem. Rev.* **2003**, *103*, 1759–1792.
[191] A. Kumar, T. M. Bhatti, A. S. Goldman, *Chem. Rev.* **2017**, *117*, 12357–12384.
[192] G. van Koten, in *Organometallic Pincer Chemistry* (Eds.: G. van Koten, D. Milstein), Springer Berlin Heidelberg, Berlin, Heidelberg, **2013**, pp. 1–20.
[193] M. Findlater, K. M. Schultz, W. H. Bernskoetter, A. Cartwright-Sykes, D. M. Heinekey, M. Brookhart, *Inorg. Chem.* **2012**, *51*, 4672–4678.
[194] J. Choi, A. H. R. MacArthur, M. Brookhart, A. S. Goldman, *Chem. Rev.* **2011**, *111*, 1761–1779.
[195] N. Selander, K. J. Szabó, *Chem. Rev.* **2011**, *111*, 2048–2076.

[196] C. Gunanathan, D. Milstein, *Chem. Rev.* **2014**, *114*, 12024–12087.
[197] D. Morales-Morales, *Pincer Compounds: Chemistry and Applications*, Elsevier, **2018**.
[198] M. Gupta, C. Hagen, R. J. Flesher, W. C. Kaska, C. M. Jensen, *Chem. Commun.* **1996**, 2083–2084.
[199] I. Göttker-Schnetmann, P. White, M. Brookhart, *J. Am. Chem. Soc.* **2004**, *126*, 1804–1811.
[200] W. H. Bernskoetter, S. K. Hanson, S. K. Buzak, Z. Davis, P. S. White, R. Swartz, K. I. Goldberg, M. Brookhart, *J. Am. Chem. Soc.* **2009**, *131*, 8603–8613.
[201] W. H. Bernskoetter, C. K. Schauer, K. I. Goldberg, M. Brookhart, *Science* **2009**, *326*, 553–556.
[202] E. Ben-Ari, G. Leitus, L. J. W. Shimon, D. Milstein, *J. Am. Chem. Soc.* **2006**, *128*, 15390–15391.
[203] M. A. Iron, E. Ben-Ari, R. Cohen, D. Milstein, *Dalton Trans.* **2009**, 9433–9439.
[204] A. S. Goldman, A. H. Roy, Z. Huang, R. Ahuja, W. Schinski, M. Brookhart, *Science* **2006**, *312*, 257–261.
[205] R. Ahuja, S. Kundu, A. S. Goldman, M. Brookhart, B. C. Vicente, S. L. Scott, *Chem. Commun.* **2007**, 253–255.
[206] S. Kundu, Y. Choliy, G. Zhuo, R. Ahuja, T. J. Emge, R. Warmuth, M. Brookhart, K. Krogh-Jespersen, A. S. Goldman, *Organometallics* **2009**, *28*, 5432–5444.
[207] W. C. Kaska, S. Nemeh, Ata. Shirazi, Suzan. Potuznik, *Organometallics* **1988**, *7*, 13–15.
[208] R. Tanaka, M. Yamashita, K. Nozaki, *J. Am. Chem. Soc.* **2009**, *131*, 14168–14169.
[209] J. Zhang, G. Leitus, Y. Ben-David, D. Milstein, *Angewandte Chemie International Edition* **2006**, *45*, 1113–1115.
[210] T. Zell, Y. Ben-David, D. Milstein, *Angewandte Chemie International Edition* **2014**, *53*, 4685–4689.
[211] N. A. Espinosa-Jalapa, A. Nerush, L. J. W. Shimon, G. Leitus, L. Avram, Y. Ben-David, D. Milstein, *Chemistry – A European Journal* **2017**, *23*, 5934–5938.
[212] J. V. Obligacion, S. P. Semproni, P. J. Chirik, *J. Am. Chem. Soc.* **2014**, *136*, 4133–4136.
[213] G. Zhang, H. Zeng, J. Wu, Z. Yin, S. Zheng, J. C. Fettinger, *Angewandte Chemie International Edition* **2016**, *55*, 14369–14372.
[214] T.-P. Lin, J. C. Peters, *J. Am. Chem. Soc.* **2013**, *135*, 15310–15313.
[215] G. Ganguly, T. Malakar, A. Paul, *ACS Catal.* **2015**, *5*, 2754–2769.
[216] A. Rossin, M. Peruzzini, *Chem. Rev.* **2016**, *116*, 8848–8872.
[217] R. G. Pearson, *Chemical Reviews* **1985**, *85*, 41–49.
[218] M. A. Esteruelas, P. Nolis, M. Oliván, E. Oñate, A. Vallribera, A. Vélez, *Inorg. Chem.* **2016**, *55*, 7176–7181.
[219] M. J. Sgro, D. W. Stephan, *Dalton Trans.* **2013**, *42*, 10460–10472.
[220] P. Bhattacharya, J. A. Krause, H. Guan, *J. Am. Chem. Soc.* **2014**, *136*, 11153–11161.
[221] D. Evans, J. A. Osborn, F. H. Jardine, G. Wilkinson, *Nature* **1965**, *208*, 1203.
[222] C. O'Connor, G. Wilkinson, *J. Chem. Soc. A* **1968**, 2665–2671.

[223] R. Langer, G. Leitus, Y. Ben-David, D. Milstein, *Angewandte Chemie International Edition* **2011**, *50*, 2120–2124.
[224] P. Bhattacharya, J. A. Krause, H. Guan, *Organometallics* **2011**, *30*, 4720–4729.
[225] M. Feller, U. Gellrich, A. Anaby, Y. Diskin-Posner, D. Milstein, *J. Am. Chem. Soc.* **2016**, *138*, 6445–6454.
[226] A. Anaby, M. Feller, Y. Ben-David, G. Leitus, Y. Diskin-Posner, L. J. W. Shimon, D. Milstein, *Journal of the American Chemical Society* **2016**, *138*, 9941–9950.
[227] R. Tanaka, M. Yamashita, L. W. Chung, K. Morokuma, K. Nozaki, *Organometallics* **2011**, *30*, 6742–6750.
[228] H.-W. Suh, T. J. Schmeier, N. Hazari, R. A. Kemp, M. K. Takase, *Organometallics* **2012**, *31*, 8225–8236.
[229] S. Chakraborty, J. Zhang, J. A. Krause, H. Guan, *Journal of the American Chemical Society* **2010**, *132*, 8872–8873.

2 {Rh(PONOP)}$^{+}$-based pre-catalysts for the dehydrogenation of amine-boranes

2.1 Introduction

Over the last decade, the dehydrogenation of amine-boranes, $H_3B{\cdot}NRR'H$ (R, R' = H, alkyl), has been an area of significant interest. This was originally due to the potential of amine-boranes as H_2 storage materials.[1] However, more recently this interest has been refocused on the synthesis of new materials containing B–N bonds, such as polyaminoboranes, $[H_2BNRH]_n$, which are isoelectronic with societally and technologically ubiquitous polyolefins.[2] However, reliable syntheses of polyaminoboranes are less well developed and the precise mechanistic details for their formation is still unknown.[3]

As outlined in section 1.7.2, transition metal complexes have been successfully employed as pre-catalysts for the dehydrogenation of amine-boranes. In 2008, Manners *et al*. reported the neutral, dihydrogen pincer complex Ir(POCOP)H_2 (POCOP = κ^3-C_6H_3-2,6-(OP^tBu_2)$_2$) (**Figure 2.1**), known as "Brookhart's catalyst",[4] to be the first catalyst to dehydropolymerise $H_3B{\cdot}NMeH_2$, yielding high molecular weight polymer (M_n = 55, 200 g mol^{-1}, Đ = 2.9).[5,6] Since then, there have been a number of reports of pincer-based catalysts for the dehydrocoupling of amine-boranes.[7–10] However, even though sigma amine-borane complexes have been postulated as key intermediates in the catalytic cycle[11] (section 1.8.2), no such complexes have been isolated for these neutral systems so far.

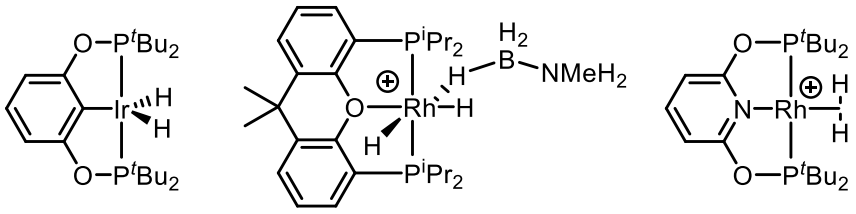


Figure 2.1 *Left*: Brookhart's catalyst, Ir(POCOP)H_2.[4] *Middle*: {Rh(Xantphos)}$^+$-based amine-borane sigma complex.[12] *Right*: {Rh(PONOP)}$^+$-based dihydrogen complex.[13] $[BAr^F{}_4]^-$ anions omitted for clarity.

In contrast, there are several examples of cationic rhodium pincer complexes, such as those based upon {Rh(Xantphos)}$^+$, which not only act as catalysts for the dehydrogenation of amine-boranes, but also support the formation of isolatable sigma complexes with amine-boranes (**Figure 2.1**).[12,14–16] These sigma complexes can be active intermediates during catalysis or they can be pre-catalysts, which do not lie on the catalytic cycle, but they are all relevant to the dehydrocoupling of amine-boranes.

In order to optimise the catalytic dehydrogenation of amine-boranes, further understanding of the mechanism involved is required. The isolation of relevant amine-borane sigma complexes and investigation into their reactivity is a key method used to provide mechanistic insight and also direct entry into the catalytic cycle. In this thesis, complexes based on the {Rh(PONOP)}$^+$ fragment (**Figure 2.1**) are employed to investigate the mechanistic details of the dehydrogenation of amine-boranes. The {Rh(PONOP)}$^+$ fragment combines both cationic and pincer ligand motifs, which are attributes of successful dehydrogenation catalysts reported in the literature.

This chapter describes the synthesis of several {Rh(PONOP)}$^{+}$ complexes, their reactivity with $H_3B{\cdot}NMe_3$ and stoichiometric reactivity with $H_3B{\cdot}NMe_2H$. These preliminary studies provide the groundwork for a thorough investigation into the catalytic dehydrocoupling of $H_3B{\cdot}NMe_2H$, detailed in Chapter Three. Also in this chapter, the synthesis and characterisation of the monohydride complex Rh(PONOP)H is outlined. This neutral complex is observed during the catalytic dehydrocoupling of $H_3B{\cdot}NMe_2H$, as detailed in Chapter Three, and its reactivity investigated in detail in Chapter Four. The last section of this chapter details a preliminary investigation into the substitution of ^{t}Bu groups on the PONOP ligand for the less sterically bulky Cy groups.

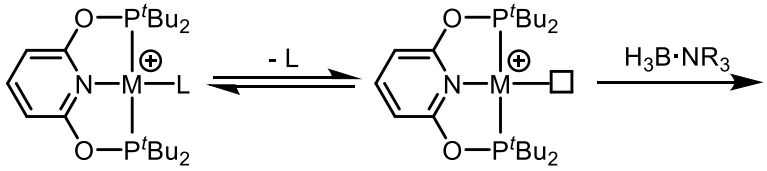
2.2 Synthesis of potential catalysts: [Rh(PONOP)(η²-H₂)][BAr$^{F}_4$] (1), [Rh(PONOP)(κ¹-N₂)][BAr$^{F}_4$] (2) and [Rh(PONOP)(κ¹-ClCH₂Cl)][BAr$^{F}_4$] (3)

The PONOP ligand (PONOP = κ^3-C_5H_3N-2,6-(OP^{t}Bu$_2$)$_2$) was first reported in 2009 by Goldberg and Brookhart *et al*. as a supporting ligand in an iridium complex used to investigate C–H bond activation in hydrocarbons.[13] Since then it has been employed as a ligand set in a number of transition metal catalysts used for olefin isomerisation,[17] hydrogenation[18–20] and hydrosilylation.[21] The PONOP ligand has also been reported to stabilise the formation of transition metal-based sigma complexes,[22,23] such as the breakthrough rhodium(I) sigma-methane complex [Rh(PONOP)(CH_4)][BAr$^{F}_4$].[24]

The PONOP ligand is structurally similar to the POCOP ligand that, as part of the catalyst Ir(POCOP)H_2, has been shown to be successful for amine-borane dehydropolymerisation.[5,6] However, the use of pyridine as a modular component in the PONOP ligand allows for the synthesis of cationic complexes, which may favour the stabilisation of sigma-bound intermediates due to the improved energy match between the metal centre and the low-lying B–H σ orbital.[25] Another advantage of employing cationic complexes as catalysts is the potential to observe the fate of the catalytic species via electrospray ionisation mass spectrometry techniques (ESI-MS).[26] Furthermore, the PONOP ligand is also structurally similar to the PNP ligand (PNP = κ^3-C_5H_3N-2,6-($CH_2P^tBu_2$)$_2$), which is another ligand used to support transition metal catalysts.[27–29] However, the two methylene groups in the PNP ligand are susceptible to deprotonation leading to dearomatisation of the pyridine unit.[30,31] The substitution of these CH_2 groups with oxygen atoms to give the PONOP ligand mitigates this process and also reduces the electron density at the metal centre, contributing to favourable formation of sigma complexes.[22] With these attributes in mind, the PONOP ligand has therefore been selected as a suitable ligand to further investigate the mechanism of transition metal-catalysed amine-borane dehydrogenation.

Low-coordinate metal complexes with vacant coordination sites are often proposed as intermediates along a catalytic pathway (see section 1.5).[32] These vacant sites allow incoming substrates to approach the metal centre, and subsequently react with it. Such low-coordinate, reactive metal complexes require stabilisation, which can come from the coordination of solvent molecules, counterions or other ligands,

effectively "masking" the vacant site. For the metal complex to still be reactive in the presence of the substrate, these masking ligands must be so weakly bound that they are easily displaced by the substrate, revealing a vacant coordination site (**Scheme 2.1**). Therefore, latent, low-coordinate metal complexes that contain suitably weakly bound masking ligands were selected as pre-catalysts to further investigate the catalysis of amine-borane dehydrocoupling.



Scheme 2.1 A latent, low-coordinate complex showing ligand L masking vacant site □ which, when revealed, allows amine-borane $H_3B{\cdot}NR_3$ to react with the metal centre. Anion omitted for clarity.

Several rhodium-based cationic PONOP pincer complexes that would be appropriate to synthesise as potential pre-catalysts have been reported in the literature: [Rh(PONOP)(η^2-H_2)][$BAr^F{}_4$][22] (**1**); [Rh(PONOP)(κ^1-N_2)][$BAr^F{}_4$][33] (**2**) and [Rh(PONOP)(κ^1-$ClCH_2Cl$)][$BAr^F{}_4$][33] (**3**) (**Figure 2.2**).

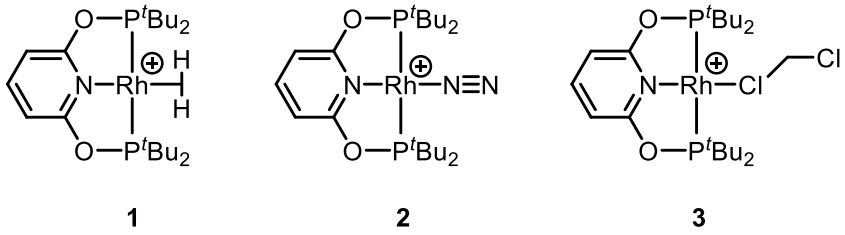
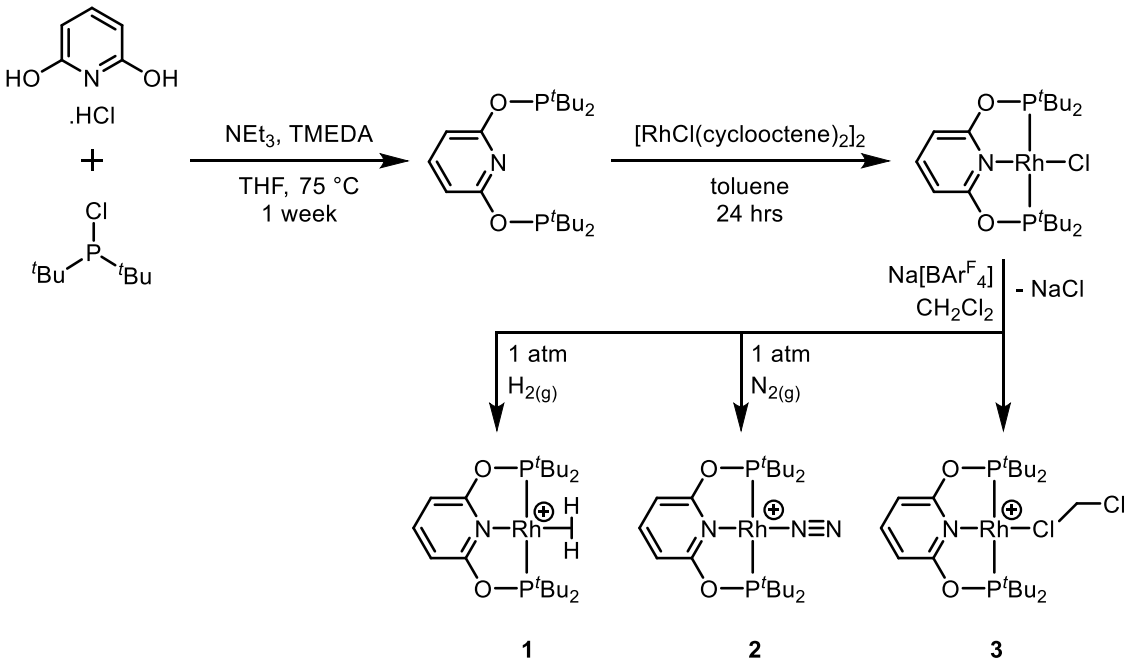


Figure 2.2 Structures of target pre-catalysts. [$BAr^F{}_4$]$^-$ anions omitted for clarity.

The anion of choice for the complexes in this thesis is $[BAr^F_4]^-$ (Ar^F = 3,5-$C_6H_3(CF_3)_2$), which is a weakly coordinating anion (see section 1.5) and thus is unlikely to competitively bind to or react with the metal catalyst.[34–36] All three complexes contain a ligand that is only weakly coordinated to the metal centre (H_2, N_2 or CH_2Cl_2), effectively masking a vacant coordination site. During the initial steps of catalysis, amine-borane substrates need to be able to displace these weakly bound ligands.[37–39]

Complexes **1**, **2** and **3** were all synthesised in good yields following literature procedures as outlined in **Scheme 2.2**.[21,22,24,33,36,40] The key synthetic intermediate here is the known neutral chloride Rh(PONOP)Cl.[41]



Scheme 2.2 Synthetic scheme for the synthesis of [Rh(PONOP)(η^2-H_2)][BAr^F_4] (**1**); [Rh(PONOP)(κ^1-N_2)][BAr^F_4] (**2**) and [Rh(PONOP)(κ^1-$ClCH_2Cl$)][BAr^F_4] (**3**). [BAr^F_4]$^-$ anions omitted for clarity.

[Rh(PONOP)(κ^1-ClCH$_2$Cl)][BAr$^F_4$] (**3**) was synthesised by the addition of Rh(PONOP)Cl to Na[BAr$^F_4$] in CH_2Cl_2, according to the literature procedure.[33] The solution was filtered and the solvent removed *in vacuo* to yield a pale orange powder. However, as found in the literature,[33] NMR spectroscopy of the isolated product revealed the presence of [Rh(PONOP)(κ^1-N$_2$)][BAr$^F_4$] (**2**) as a minor product (~8 %), proposed to be from the small amounts of N_2 impurity in the inert argon gas supply. The inability to obtain [Rh(PONOP)(κ^1-ClCH$_2$Cl)][BAr$^F_4$] pure rendered this complex unsuitable for the speciation and kinetic studies necessary to probe effectively the mechanism of amine-borane dehydrogenation. Therefore, even though the instability of complex **3** suggested the CH_2Cl_2 ligand could be easily displaced, this complex was not used further in these studies.

Complexes **1** and **2** were similarly synthesised by the addition of Rh(PONOP)Cl to Na[BAr$^F_4$] in CH_2Cl_2, but the solution was then freeze-pump-thaw degassed three times and placed under one atmosphere of either H_2 or N_2 gas. The reaction mixture was then stirred for four hours under the appropriate atmosphere, filtered and the solvent removed *in vacuo* to yield the isolated complexes **1** and **2** respectively. NMR spectroscopy was consistent with that reported in the literature: $^{31}P\{^1H\}$ NMR spectroscopic data (298 K, CD_2Cl_2) for complex **1**,[22] δ 224.6 ppm (d, $^1J_{RhP}$ = 126 Hz) and for complex **2**,[33] δ 211.0 ppm (d, $^1J_{RhP}$ = 132 Hz).

Both complexes **1** and **2** demonstrated limited stability in CH_2Cl_2 under an argon atmosphere with respect to the formation of complex **3** (~25 % complex **3** present in CH_2Cl_2 solutions of complexes **1** and **2** within one hour). In THF, complex **2**

immediately decomposed to a mixture of unidentified species as observed by $^{31}P\{^{1}H\}$ NMR spectroscopy. The fluorinated arene 1,2-$F_2C_6H_4$ was trialled as an alternative solvent due to its inertness (section 1.5). Both complexes **1** and **2** were synthesised successfully and proved stable (for at least one week) in 1,2-$F_2C_6H_4$ and so this solvent was used henceforth for further synthesis and reactivity studies.

It should be noted that isolated [Rh(PONOP)(η^2-H_2)][BAr^F_4] (**1**) that had been stored under an inert argon atmosphere showed approximately 20 % reaction to form [Rh(PONOP)(κ^1-N_2)][BAr^F_4] (**2**) after one month. This was postulated to be due to trace amounts (1–2 ppm) of nitrogen present in the argon atmosphere used, as previously reported in the literature,[42] and subsequently complex **1** was only synthesised in small batches when required and used within a week.

The solid state structure of complex **2** has been reported[33] and shows an N–N bond length of 1.063(5) Å, which is very similar to that of free N_2 (1.09 Å). This similarity indicates only a slight activation of the N_2 ligand upon coordination to the rhodium centre suggesting that the ligand is weakly bound. This is a desirable property for a catalyst as the more weakly bound the ligand, the more easily amine-borane substrate can displace it and interact with the metal centre.

Although [Rh(PONOP)(η^2-H_2)][BAr^F_4] (**1**) has been fully characterised using NMR spectroscopic techniques, the solid state structure of complex **1** has not yet been reported. Attempts to recrystallise this complex by layering a solution of complex **1** in 1,2-$F_2C_6H_4$ with pentane at 298 K were unsuccessful. However, reported NMR

spectroscopic data for this complex yielded a T_1 relaxation time of 33 ms and a $^1J_{HD}$ coupling value of 30 Hz for the HD isotopologue, both indicating an η^2-bound dihydrogen complex rather than a dihydride (section 1.8).[22]

Both complexes **1** and **2** exhibit suitable stability in a 1,2-$F_2C_6H_4$ solution and contain weakly bound ligands to the rhodium centre, which may be easily displaced by incoming amine-borane substrate during catalytic amine-borane dehydrogenation. Therefore, both of these complexes were investigated further in stoichiometric and catalytic reactivity with amine-boranes.

2.3 Reactivity of complexes 1 and 2 with H_2

Both [Rh(PONOP)(η^2-H_2)][BAr^F_4] (**1**) and [Rh(PONOP)(κ^1-N_2)][BAr^F_4] (**2**) were selected as suitable complexes for probing the catalytic dehydrocoupling of amine-boranes. As hydrogen gas is evolved during the dehydrogenation of amine-boranes, the reactivity of both complexes **1** and **2** with hydrogen was investigated.

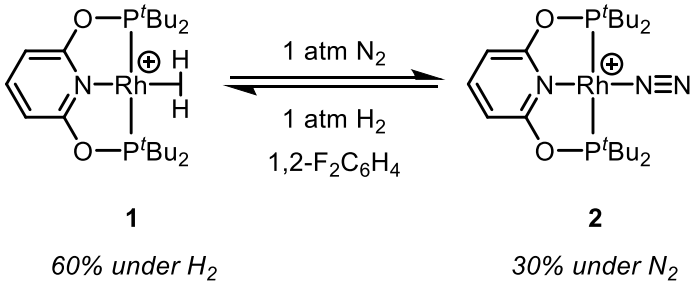
In 2006, the tetrahydride species Ir(POCOP)$(H)_4$ was observed during the dehydrogenation of $H_3B{\cdot}NH_3$ catalysed by Brookhart's catalyst, Ir(POCOP)$(H)_2$.[43] Ir(POCOP)$(H)_4$ was determined to be formed from the reaction of Ir(POCOP)$(H)_2$ with hydrogen generated during the reaction. This example suggests the potential for complexes **1** and **2** to access a Rh^{III} oxidation state with the addition of H_2. However, when a solution of complex **1** in 1,2-$F_2C_6H_4$ was placed under one atmosphere of H_2, NMR spectroscopy of the hydrogenated solution indicated no

further reaction. This result is consistent with the relative accessibilities of the Rh^{III} and Ir^{III} oxidations states.[32]

Interestingly, when a solution of complex **2** in 1,2-$F_2C_6H_4$ was placed under one atmosphere of H_2 and analysed using NMR spectroscopy, comparison of the $^{31}P\{^1H\}$ NMR integrals showed a 10 % conversion to complex **1** in 30 minutes, increasing to a 60 % conversion in 24 hours.

The reverse reaction was then probed by placing a solution of the same concentration of complex **1** under one atmosphere of N_2 and analysing the solution via NMR spectroscopy. In 24 hours, 30 % conversion to complex **2** was observed.

These results suggest that both complexes **1** and **2** are in equilibrium with each other and the position of that equilibrium depends upon the concentrations of H_2 and N_2 present (**Scheme 2.3**).



Scheme 2.3 [Rh(PONOP)(η^2-H_2)][$BAr^F{}_4$] (**1**) and [Rh(PONOP)(κ^1-N_2)][$BAr^F{}_4$] (**2**) in equilibrium in solution. [$BAr^F{}_4$]$^-$ anions are omitted for clarity.

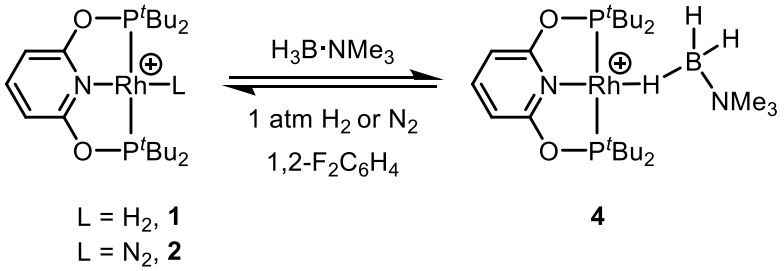
Other factors that would affect the equilibrium would include the respective solubilities of H_2 and N_2 in 1,2–$F_2C_6H_4$. If these solubilities were assumed to be the same, the results suggest complex **1** is marginally more stable than complex **2** under these conditions (also assuming both samples were mixed identically and both NMR tubes contained the exact same headspace volume).

2.4 Formation of [Rh(PONOP)(η¹-H₃B·NMe₃)][BArᶠ₄] (4)

Amine-boranes have been shown to bind to metal centres via three-centre-two-electron interactions, thus forming a variety of sigma complexes (section 1.8.2),[25,44] some of which have been observed as resting states during the catalytic dehydrogenation of amine-boranes.[45] It is possible to isolate such complexes using tertiary amine-boranes, $H_3B{\cdot}NR_3$, as the lack of N–H bonds renders the complex stable with respect to dehydrogenation and thus these complexes can act as models for the interaction of primary and secondary amine-boranes with the metal centre. Consequently, the tertiary amine-borane sigma complex [Rh(PONOP)($H_3B{\cdot}NMe_3$)][BAr^F_4] (**4**) was targeted.

A solution of [Rh(PONOP)(η²-H_2)][BAr^F_4] (**1**) in 1,2-$F_2C_6H_4$ was reacted with one equivalent of $H_3B{\cdot}NMe_3$ in a sealed NMR tube and the reaction monitored using NMR spectroscopy. Upon time of mixing (i.e. the time of the first NMR spectrum to be recorded, immediately after mixing of reagents and inserting of the sample into the NMR spectrometer), a new signal was observed in the $^{31}P\{^1H\}$ NMR spectrum (~30 %) and was assigned to [Rh(PONOP)(η¹-$H_3B{\cdot}NMe_3$)][BAr^F_4] (**4**). This signal

slowly increased in intensity over 24 hours, as the signal for complex **1** decreased, forming complex **4** in quantitative yield (**Scheme 2.4**).



Scheme 2.4 Synthesis of [Rh(PONOP)(η^1-H$_3$B·NMe$_3$)][BAr$^F{}_4$] (**4**). [BAr$^F{}_4$]$^-$ anions omitted for clarity.

Complex **4** was isolated and characterised fully by NMR spectroscopy, electrospray ionisation mass spectrometry (ESI-MS), elemental microanalysis and single crystal X-ray diffraction. Complex **4** was also synthesised under the same conditions using [Rh(PONOP)(κ^1-N$_2$)][BAr$^F{}_4$] (**2**); however, ^{31}P{^{1}H} NMR spectroscopy indicated only 35 % conversion to complex **4** after 15 minutes of reactivity, compared to 55 % conversion after 15 minutes when starting from complex **1**. Complex **4** is stable in a solution of 1,2-F$_2$C$_6$H$_4$ for at least 24 hours, as measured by ^{31}P{^{1}H} NMR spectroscopy.

The ^{31}P{^{1}H} NMR spectrum (298 K, CD$_2$Cl$_2$) of complex **4** (**Figure 2.3**) exhibits a single doublet at δ 208.9 ppm with a coupling constant consistent with a Rh^I centre ($^1J_{RhP}$ = 142 Hz)[46] similar to the Rh^I coupling constants for complexes **1** ($^1J_{RhP}$ = 126 Hz) and **2** ($^1J_{RhP}$ = 132 Hz).

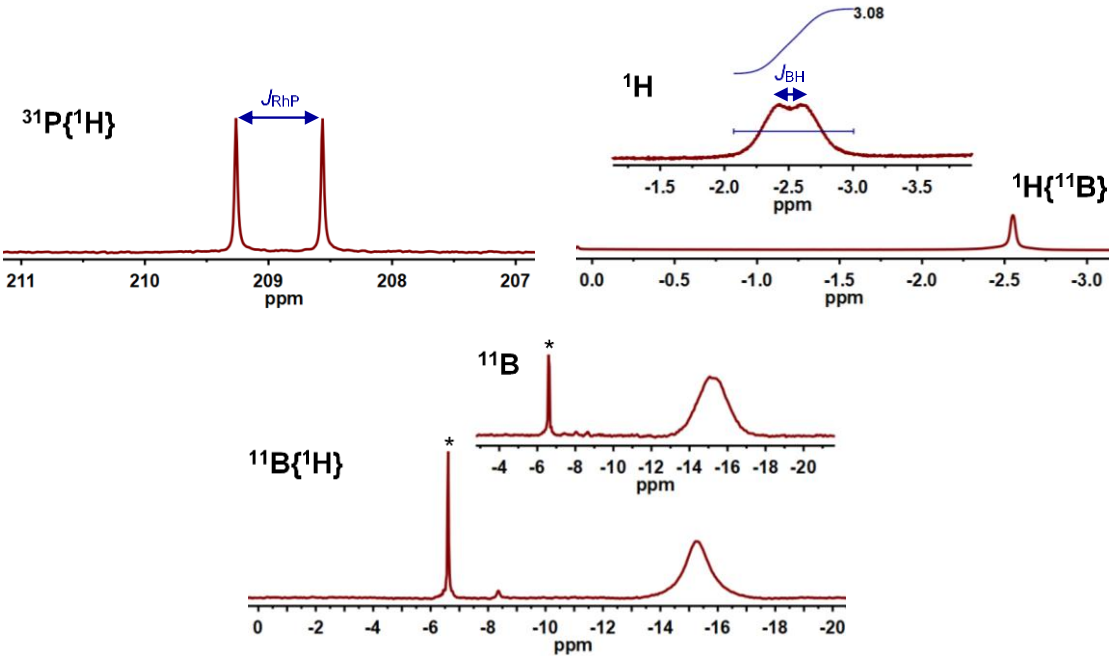


Figure 2.3 Partial $^{31}P\{^{1}H\}$ (202 MHz), ^{1}H and $^{1}H\{^{11}B\}$ (showing the hydride region) (500 MHz) and ^{11}B and $^{11}B\{^{1}H\}$ NMR spectra (160 MHz) of complex **4** (CD_2Cl_2, 298 K). * = $[BAr^F_4]^-$ anion.

In the ^{1}H NMR spectrum, a broad signal of relative integral 3 H is observed in the hydride region at δ –2.6 ppm. This peak is quadrupolar broadened and sharpens upon ^{11}B decoupling, indicative of the bound BH_3 group with the terminal and bridging B–H protons undergoing rapid exchange compared to the NMR timescale.[47–49] The chemical shift of –2.6 ppm is as expected for a weighted average of the chemical shifts for terminal B–H protons (typically 1–2 ppm) and metal-bound B–H protons (typically –10 ppm), again indicating all B–H protons are undergoing rapid exchange.[44] Due to the quadrupolar nature of boron, the B–H ^{1}H NMR resonances are often too broad for any B–H coupling to be observed in such complexes.[50] However, in this case an apparent coupling constant of $^{1}J_{BH}$ = 90 Hz is observed. This is a reduced B–H coupling constant compared to that of unbound

$H_3B{\cdot}NMe_3$ ($^1J_{BH}$ = 98 Hz), and thus indicates a significant interaction between the B–H orbitals of the amine-borane and those of the metal due to coordination via a three-centre-two-electron bond. [51–53] Other amine-borane sigma complexes that show a reduced $^1J_{BH}$ coupling constant (by ~10 Hz) compared to that of the respective free amine-borane include $[M(CO)_5(\eta^1\text{-}H_3B{\cdot}L)]$ (M = Cr, W and L = NMe_3, PMe_3 or PPh_3).[44] For these complexes, real values of the $^1J_{BH}$ coupling constants for the bridging B–H bonds were estimated by assuming the apparent $^1J_{BH}$ coupling constant is an average of the terminal and bridging B–H $^1J_{BH}$ values and that the terminal $^1J_{BH}$ value is the same as that for unbound amine-borane. Therefore, $^1J_{BH}$ values for the bridging B–H bonds were calculated to be between 55–82 % of the $^1J_{BH}$ value for the respective free amine-boranes. Following the same principle, the $^1J_{BH}$ coupling constant for the bridging B–H in complex **4** was estimated at 74 Hz, which corresponds to a reduction percentage of 76 %, falling into the same range as for the other η^1-borane complexes.

^{1}H NMR spectroscopy across the temperature range 173 K –298 K showed no decoalescence of the broad signal for the BH_3 group suggesting the B–H protons remain fluxional even at such low temperatures and so the interaction between the rhodium centre and amine-borane must be relatively weak.[44,52]

In the ^{11}B NMR spectrum, a broad signal at δ –15.2 ppm is observed, which sharpens upon ^{1}H decoupling, and is assigned to the bound BH_3 group. This signal is shifted to a lower frequency compared to that of unbound $H_3B{\cdot}NMe_3$ (δ –7.3 ppm)[14] and so implies η^1 coordination (section 1.8.2) of the amine-borane, as observed for

analogous η^1-complexes: [CpRu(PMe_3)(η^1-H_3B·dppm)][PF_6] ^{11}B NMR signal exhibits a low frequency shift of 7.3 ppm compared to unbound H_3B·dppm (dppm = $Ph_2PCH_2PPh_2$);[52] and [$Cr(CO)_5$(η^1-H_2PhB·NMe_3)] ^{11}B NMR signal exhibits a low frequency shift of 4.8 ppm.[54] In contrast, a ^{11}B NMR chemical shift of higher frequency than that for free H_3B·NMe_3 would be indicative of an η^2-bound amine-borane,[50] such as observed for [Cp*Ru(η^2,η^2-H_3B·dppm)][PF_6],[52] where the ^{11}B NMR signal is shifted to a higher frequency by 52.7 ppm compared to unbound H_3B·dppm, and also for [Rh(P^iBu_3)$_2$(η^2,η^2-H_3B·NMe_3)][BAr^F_4],[45] the ^{11}B NMR signal for which is shifted to a higher frequency by 30.4 ppm compared to unbound H_3B·NMe_3.

Diffusion of a solution of complex **4** in 1,2-$F_2C_6H_4$ into pentane at 298 K afforded dark yellow crystals suitable for single crystal X-ray diffraction. The solid state structure of **4** (**Figure 2.4**) is in agreement with the η^1-binding mode of the amine-borane to the metal centre as observed in the solution NMR spectra. The BH_3 hydrogen atoms were located and freely refined.

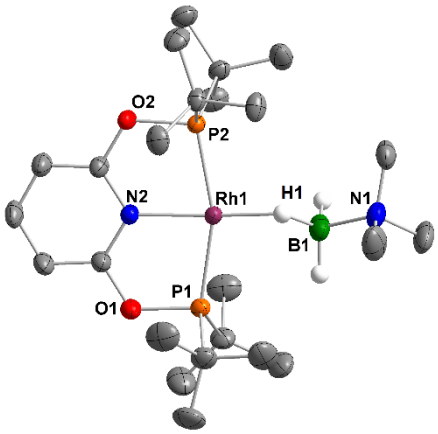
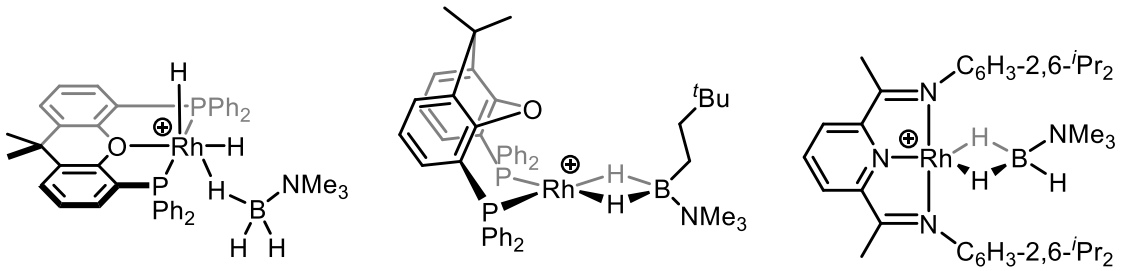


Figure 2.4 Solid state structure of the cationic portion of [Rh(PONOP)(η^1-$H_3B{\cdot}NMe_3$)][$BAr^F{}_4$] (**4**). Displacement ellipsoids are drawn at the 30 % probability level. Carbon-bound hydrogen atoms are omitted for clarity. Selected bond lengths (Å) and angles (°): Rh1–B1, 2.567(5); Rh1–P1, 2.2832(9); Rh1–P2, 2.2594(9); Rh1–N2, 2.026(3); B1–N1, 1.631(6); Rh1–H1, 1.72(5); P1–Rh1–P2, 161.63(3); N2–Rh1–H1, 172.6(17); Rh1–H1–B1, 121(4).

The solid state structure of complex **4** shows one of the three BH_3 hydrogens relatively close to the metal centre (Rh–H1 = 1.72(5) Å) with the other two hydrogens significantly more distant (2.8 – 2.9 Å), consistent with η^1 coordination. As expected for an η^1 structure (section 1.8.2), complex **4** exhibits a long Rh···B distance (2.567(5) Å) and a relatively large Rh–H–B angle (121(4)°).[53,55] This Rh···B distance is only slightly shorter than that observed in [Rh(Xantphos)$(H)_2$(η^1-$H_3B{\cdot}NMe_3$)][$BAr^F{}_4$][56] (2.759(6) Å) and the Rh–H–B angle is very similar (120(6)°) (**Figure 2.5**, *left*). In comparison, reported η^2 sigma complexes show significantly shorter Rh···B distances and more acute Rh–H–B angles, such as in [Rh(Xantphos)(η^2,η^2-$H_2(CH_2CH_2{}^tBu)B{\cdot}NMe_3$)][$BAr^F{}_4$][56] (2.162(5) Å, 87(8)°) (**Figure 2.5**, *middle*), and [Rh(NNN)(η^2,η^2-$H_3B{\cdot}NMe_3$)][$BAr^F{}_4$][57] (NNN = 2,6-bis-[1-(2,6-diisopropylphenylimino)ethyl]pyridine) (2.306(5) Å, 93(3)°) (**Figure 2.5**,

right). The longer Rh···B distances observed for η^1 complexes compared to those of η^2 geometry imply that amine-borane fragments are more weakly bound to the metal centre when coordinated via an η^1 binding mode. As the amine-borane in complex **4** is bound in an η^1 geometry it can be expected that $H_3B{\cdot}NMe_3$ may be easily displaced, ideal for enabling other amine-borane substrates to interact with the metal centre.



η^1 — Rh···B = 2.759(6) Å, Rh-H-B = 120(6)°

η^2,η^2 — Rh···B = 2.162(5) Å, Rh-H-B = 87(8)°

η^2,η^2 — Rh···B = 2.306(5) Å, Rh-H-B = 93(3)°

Figure 2.5 Comparison of η^1[56] and η^2,η^2[56,57] amine-borane sigma complexes.

2.5 Reactivity of [Rh(PONOP)(η^1-$H_3B{\cdot}NMe_3$)][BAr^F_4] (4)

2.5.1 Reaction of complex 4 with H_2

In order to investigate how easily $H_3B{\cdot}NMe_3$ can be displaced from complex **4** under catalytic conditions where H_2 is generated, the stability of this amine-borane complex in the presence of H_2 was studied.

A solution of **4** (8.7 mM, 1,2-$F_2C_6H_4$) in a high pressure NMR tube was freeze-pump-thaw degassed three times before being cooled to 73 K by immersion in liquid N_2 and backfilled with H_2 at a pressure of one atmosphere. The NMR tube was then

sealed and warmed to room temperature, causing the internal H_2 pressure to become approximately four atmospheres, and the reaction progress followed by NMR spectroscopy. The relative integrals in the $^{31}P\{^1H\}$ NMR spectra indicated an immediate conversion to complex **1**, in the ratio 4:1 (complex **1**:complex **4**). As expected, the ^{11}B NMR spectra showed signals for both complex **4** (broad peak at δ –15.2 ppm) as well as unbound $H_3B{\cdot}NMe_3$ (sharp quartet at δ –7.3 ppm, $^1J_{BH}$ = 98 Hz).

After degassing the solution to remove H_2 and backfilling the headspace of the NMR tube with argon, NMR spectroscopy of the solution showed the return of complex **4** as the major component (3:2, complex **4**:complex **1**). These results indicate that both complex **4** and complex **1** are in equilibrium with each other and that the binding of $H_3B{\cdot}NMe_3$ to the $\{Rh(PONOP)\}^+$ fragment is in fact reversible (as shown earlier in **Scheme 2.4**).

These experimental results are consistent with DFT calculations undertaken by Dr Nicholas A. Beattie and Professor Stuart A. Macgregor (Heriot-Watt University, Edinburgh). The computed ΔG for the transformation of complex **4** to complex **1** was calculated as being –1.2 kcal mol^{-1}, close to thermoneutral.

2.5.2 Reaction of complex 4 with D_2

B–H activation of an amine-borane is a key step during the metal-mediated dehydrocoupling of amine-boranes (section 1.7.2).[2] To probe such a process, H/D

exchange at the boron centre in the model amine-borane complex **4** was investigated using exogeneous D_2 to intercept any Rh–B or Rh–H intermediates.

In an NMR tube, a solution of **4** (17.4 mM, 1,2-$F_2C_6H_4$) was placed under one atmosphere of D_2 and the reaction progress was monitored by NMR spectroscopy. Initially, the ^{11}B NMR spectra showed a mixture of complex **4** and unbound $H_3B{\cdot}NMe_3$ indicating that deuterium is a competitive ligand for the $\{Rh(PONOP)\}^+$ fragment. After 30 minutes of reactivity, evidence for deuterium scrambling was observed in the resulting NMR spectra (**Figure 2.6**).

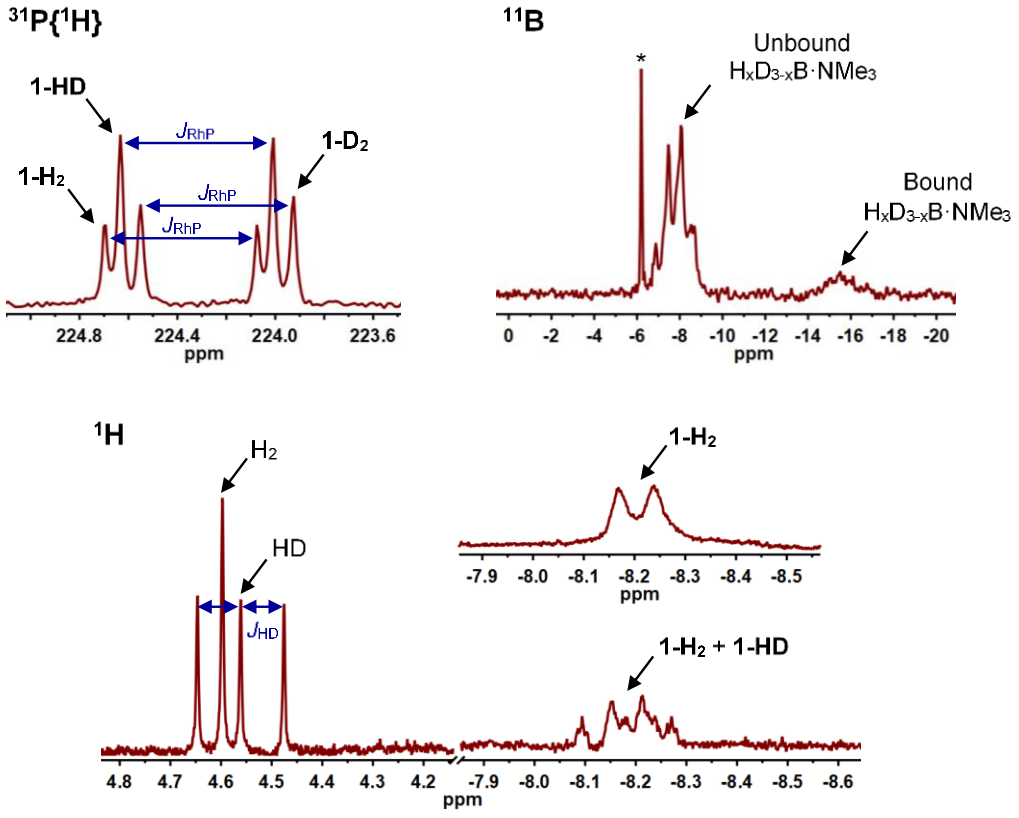


Figure 2.6 Partial $^{31}P\{^1H\}$ (202 MHz), ^{11}B (160 MHz) and ^1H NMR (500 MHz) spectra (1,2-$F_2C_6H_4$, 298 K) of the reaction of complex **4** with 1 atmosphere D_2 after 30 minutes from time of mixing. J_{RhP} = 126 Hz, J_{HD} = 43 Hz and * = $[BAr^F{}_4]^-$.

After 30 minutes from time of mixing, a broadening of the characteristic quartet for unbound $H_3B{\cdot}NMe_3$ was observed in the ^{11}B NMR spectra due to additional overlapping signals from the presence of a mixture of amine-boranes with various amounts of deuteration, $H_xD_{3-x}B{\cdot}NMe_3$ (**Figure 2.6**, **^{11}B**). Broadening of the $H_xD_{3-x}B$ signal also occurs due to the reduction of observable coupling for B–D signals as compared to those for B–H, explained by the fact that isotopic coupling constants are proportional to their gyromagnetic ratios (γ) and so $^1J_{BD}$ is smaller than $^1J_{BH}$ by approximately 1/6 ($\gamma_H = 6.5\gamma_D$).[58] The incorporation of deuterium into $H_3B{\cdot}NMe_3$ indicates the occurrence of B–H activation.

In the ^{1}H NMR spectrum, small amounts of both dissolved H_2 (δ 4.59 ppm) and HD (δ 4.56 ppm, $^1J_{HD}$ = 43 Hz)[47,59] were observed (**Figure 2.6**, **^{1}H**), consistent with deuterium scrambling. In the high field region of the ^{1}H NMR spectrum, an overlapping set of signals resulting in a complex splitting pattern were observed and assigned to a mixture of complex **1** and the HD–isotopologue [Rh(PONOP)(HD)][BAr^F_4] (**1-HD**). Complex **1** can be observed as a broad doublet at δ –8.19 ppm ($^1J_{RhH}$ = 28 Hz), assigned by comparison to independently synthesised complex **1** (d, δ –8.21 ppm, $^1J_{RhH}$ = 28 Hz) (**Figure 2.6**, ^{1}H NMR insert). In both cases the doublet observed is broad due to the small unresolved two-bond coupling to phosphorus (reported as $^2J_{PH}$ = 5 Hz).[22] Overlapping with the signal for complex **1** is the splitting pattern observed for complex **1-HD**, arising from the coupling of Rh–H (d, $^1J_{RhH}$ = 28 Hz), H–D (1:1:1 triplet, $^1J_{HD}$ = 30 Hz) and P–H (t, $^1J_{PH}$ = 5 Hz) as reported by Brookhart *et al*.[22] Consistent with this assignment, a very similar set of signals were reported for the mixture of the analogous complexes

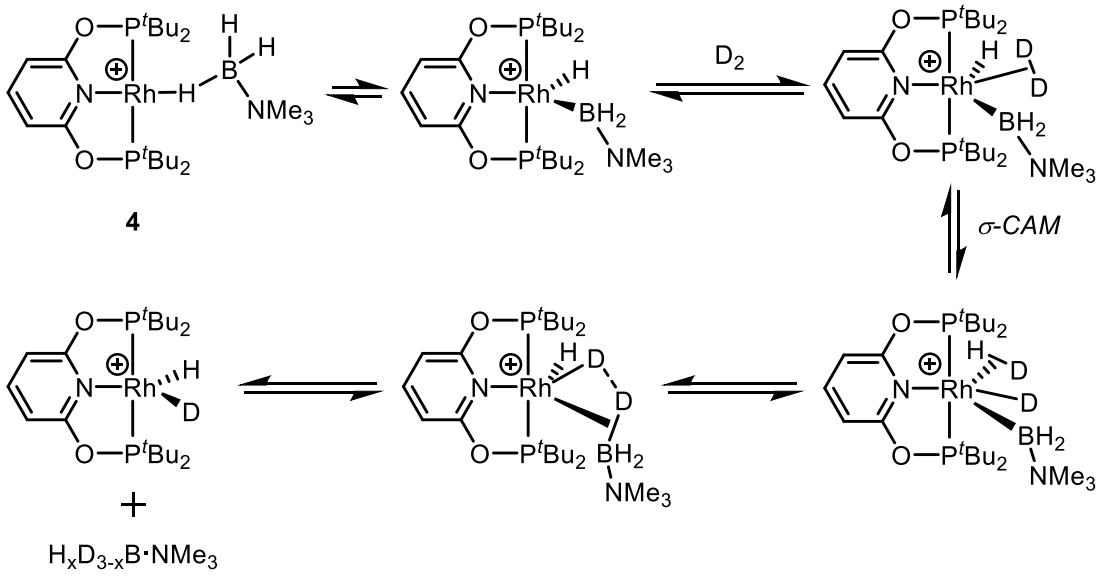
[Rh(PNP)(H_2)][BAr^F_4] (dt, δ = –10.79 ppm, $^1J_{RhH}$ = 27 Hz, $^2J_{PH}$ = 5 Hz) and [Rh(PNP)(HD)][BAr^F_4] (PNP = κ^3-C_5H_3N-2,6-($CH_2P^tBu_2$)$_2$) (qt, δ –10.73 ppm, $^1J_{RhH}$ = 27 Hz , $^1J_{HD}$ = 27 Hz, $^2J_{PH}$ = 6 Hz).[60]

Complex **1-HD** was also observed in the $^{31}P\{^1H\}$ NMR spectra, along with complex **1** (i.e. **1-H_2**) and the D_2–isotopologue [Rh(PONOP)(D_2)][BAr^F_4] (**1-D_2**) (**Figure 2.6**). The three isotopologues can be distinguished in the $^{31}P\{^1H\}$ NMR spectrum due to their slight differences in chemical shift caused by isotopic perturbation. Complex **1-H_2** was assigned by comparison to the $^{31}P\{^1H\}$ NMR spectral data from independent synthesis of this complex (d, δ 224.4 ppm, $^1J_{RhP}$ = 126 Hz). The $^{31}P\{^1H\}$ NMR signal assigned to complex **1-D_2** (d, δ 224.2 ppm, $^1J_{RhP}$ = 126 Hz) matches that observed during the reaction of complex **1-H_2** with 25 equivalents of $D_3B{\cdot}NMe_2D$, which is described in Chapter Three (section 3.5). During this reaction, when $^{31}P\{^1H\}$ NMR spectra showed the presence of complex **1-D_2**, the corresponding ^1H NMR spectra showed no signals in the hydride region, as expected. With these two assignments in mind, the third doublet observed in the $^{31}P\{^1H\}$ NMR spectrum in **Figure 2.6** (δ 224.3 ppm, $^1J_{RhP}$ = 126 Hz) was deduced to be complex **1-HD** due to its similarity to complexes **1-H_2** and **1-D_2** and as **1-HD** is observed in the hydride region of the corresponding ^1H NMR spectra, as described.

Equivalent H/D exchange was observed when a solution of complex **1** (9 mM, 1,2-$F_2C_6H_4$) was reacted with one equivalent of $D_3B{\cdot}NMe_3$ in an NMR tube. The same products of dissolved H_2 and HD were observed in the ^1H NMR spectra and the

complexes **1**, **1-HD** and **1-D$_2$** were observed in the $^{31}P\{^1H\}$ NMR spectra during the first 30 minutes of reactivity.

These results indicate that complex **4** is able to undergo B–H activation in the presence of one atmosphere of D_2, leading to H/D exchange. The deuterium scrambling observed most likely involves reversible oxidative cleavage of the B–H bond or bound D_2 at the metal centre, followed by H/D exchange via a σ-complex assisted metathesis (σ-CAM) mechanism (**Scheme 2.5**).[61]

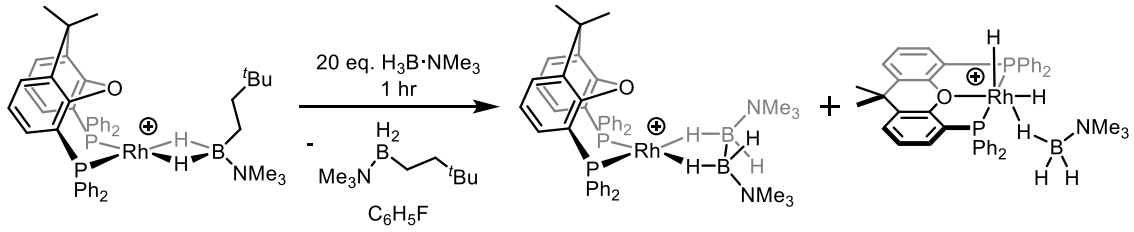


Scheme 2.5 One proposed mechanism for H/D exchange between complex **4** and D_2 via a σ-CAM mechanism. $[BAr^F{}_4]^-$ anions omitted for clarity. Not all pathways and H/D combinations possible are shown.

2.5.3 Reaction of complex 4 with excess $H_3B{\cdot}NMe_3$

The dehydrocoupling of amine-boranes generally leads to the formation of products containing new B–N bonds; however, it is possible for dehydrogenative homocoupling to occur and for new B–B bonds to form.[62,63] Well-defined examples

of such homocoupling mediated by transition metals are limited to polyhedral boranes,[64,65] guanidine bases[66] and catecholborane.[67] However, in 2013 the first fully characterised boron homocoupling product from an amine-borane was reported.[56] Addition of 20 equivalents of $H_3B{\cdot}NMe_3$ to [Rh(Xantphos)(η^2,η^2-$H_2(CH_2CH_2{}^tBu)B{\cdot}NMe_3$)][$BAr^F{}_4$] resulted in the slow formation of [Rh(Xantphos)(η^2,η^2-$H_4B_2{\cdot}2NMe_3$)][$BAr^F{}_4$], which contains the diborane ligand $Me_3N{\cdot}BH_2BH_2{\cdot}NMe_3$ sigma-bound to the rhodium centre (**Scheme 2.6**). [Rh(Xantphos)$(H)_2$(η^1-$H_3B{\cdot}NMe_3$)][$BAr^F{}_4$] was also produced in this reaction, in a 1:1 ratio with the homocoupled product.



Scheme 2.6 Dehydrogenative homocoupling of $H_3B{\cdot}NMe_3$.[56] $[BAr^F{}_4]^-$ anions omitted for clarity.

To investigate whether complex **4** is also able to undergo boron homocoupling, a solution of complex **4** (17.4 mM, 1,2-$F_2C_6H_4$) was reacted with 20 equivalents of $H_3B{\cdot}NMe_3$ and the reaction mixture was monitored using NMR spectroscopy. However, no reaction was observed, even after 21 hours. DFT calculations for the homocoupling mechanism observed for [Rh(Xantphos)(η^2,η^2-$H_2(CH_2CH_2{}^tBu)B{\cdot}NMe_3$)][$BAr^F{}_4$] suggest that this process operates through sequential B–H activations, with the first B–H activation having a low energy barrier (ΔG = +1.6 kcal mol^{-1}). Although, B–H activation has been shown to occur in complex

4 as measured by H/D exchange (section 2.5.2), clearly the steric and electronic requirements of the PONOP ligand do not support B–B homocoupling under these conditions.

2.6 Stoichiometric reactivity of complexes 1, 2 and 4 with $H_3B{\cdot}NMe_2H$

In section 2.4, $H_3B{\cdot}NMe_3$ was shown to successfully displace the weakly bound ligands H_2 and N_2 from complexes **1** and **2** respectively and subsequently bind to the metal centre. The ability of this tertiary amine-borane to interact with the metal centre demonstrates the potential of these rhodium complexes to act as catalysts for the dehydrocoupling of primary and secondary amine-borane analogues (i.e. those containing N–H bonds).

However, challenges remain in studying the precise mechanism of the dehydrocoupling of amine-boranes.[3] These include: the difficulty in conducting speciation studies when selective polymer production requires low catalyst loadings; the insolubility of the final product if it is a polymeric mixture of high molecular weight and/or heavily cross-linked; and the complex kinetics that result from the presence of induction periods or if the hydrogen co-product is involved in the mechanism.

With these challenges in mind, the dehydrocoupling of the secondary amine-borane $H_3B{\cdot}NMe_2H$ offers a simplified model for mechanistic study compared to the dehydropolymerisation reactions of the primary amine-borane $H_3B{\cdot}NMeH_2$.

$H_3B{\cdot}NMe_2H$ can be dehydrocoupled to give the well-defined, soluble dimer $[H_2BNMe_2]_2$, the selectivity of which is not greatly influenced by catalyst loading (compared to the polymeric products yielded from $H_3B{\cdot}NMeH_2$). Therefore, the catalyst speciation and reaction kinetics are easier to study meaning $H_3B{\cdot}NMe_2H$ can act as a suitable model for detailed investigation of dehydrocoupling of amine-boranes.

2.6.1 Reaction of complex 1 with $H_3B{\cdot}NMe_2H$

In order to probe the potential of $[Rh(PONOP)(\eta^2\text{-}H_2)][BAr^F{}_4]$ (**1**) as a catalyst for the dehydrocoupling of amine-boranes and to preliminarily investigate the mechanism of this process, the reaction of complex **1** with the secondary amine-borane $H_3B{\cdot}NMe_2H$ was studied.

In an NMR tube, approximately one equivalent of $H_3B{\cdot}NMe_2H$ was added to a solution of complex **1** (36 mM, 1,2-$F_2C_6H_4$) and the reaction progress was monitored using $^{31}P\{^1H\}$ NMR spectroscopy (**Figure 2.7**). This reaction was then repeated under the same conditions and followed by ^{11}B NMR spectroscopy (**Figure 2.8**). In both cases, as soon as the reagents had been added to the NMR tube, the vessel was sealed and immersed in liquid N_2 in order to freeze the solution and prevent reactivity until the NMR spectrometer was available for use. At this point, the NMR spectrometer was set up for the required experiments and when ready, the sample was thawed, placed inside the magnet and recordings begun. Even under this protocol, spectra labelled as being recorded at the same time for each sample cannot be directly compared in this experiment due to multiple reasons. The first is that

there are small differences in the length of reaction time prior to the first NMR spectrum being recorded for each sample, depending on how quickly each sample is sealed and frozen or put into the magnet after thawing. Therefore, even though the first NMR spectrum in the figures below is labelled with "Time of mixing", this spectrum will have been recorded 1-2 minutes after the reagents were actually combined. Another discrepancy comes from the difficulty in mixing each sample in a uniform and reproducible way in such a narrow reaction vessel. Differences in mixing would lead to differences in reaction progression compared to time. Furthermore, the time labels for the spectra shown below indicate when the recording for that spectrum was started compared to the first recording (time of mixing). For the $^{31}P\{^{1}H\}$ NMR spectra, the data for each spectrum took three minutes to collect and so what is observed is an average across those three minutes, but for the ^{11}B NMR spectra, each spectrum was produced from one minute of recording. Therefore with these points in mind, the $^{31}P\{^{1}H\}$ NMR spectra and ^{11}B NMR spectra discussed below should not be directly compared as a function of time. However, these data do give a valuable insight into the speciation of these stoichiometric reactions in a qualitative sense, rather than quantitative. When investigating speciation under catalytic conditions in Chapter Three, many of the described issues are addressed and comparisons between phosphorus and boron species are made.

Figure 2.7 depicts selected $^{31}P\{^{1}H\}$ NMR spectra showing the progress of the reaction of complex **1** with $H_3B{\cdot}NMe_2H$. Upon time of mixing, $^{31}P\{^{1}H\}$ NMR spectroscopy showed the presence of a new organometallic species, labelled as complex **5**, as the major product (> 95 %) with the minor product being complex **1**.

After three minutes of reactivity, the $^{31}P\{^{1}H\}$ NMR spectra showed the return of complex **1** as the major organometallic product (~97 %), with complex **5** becoming observable only in trace amounts after nine minutes of reactivity.

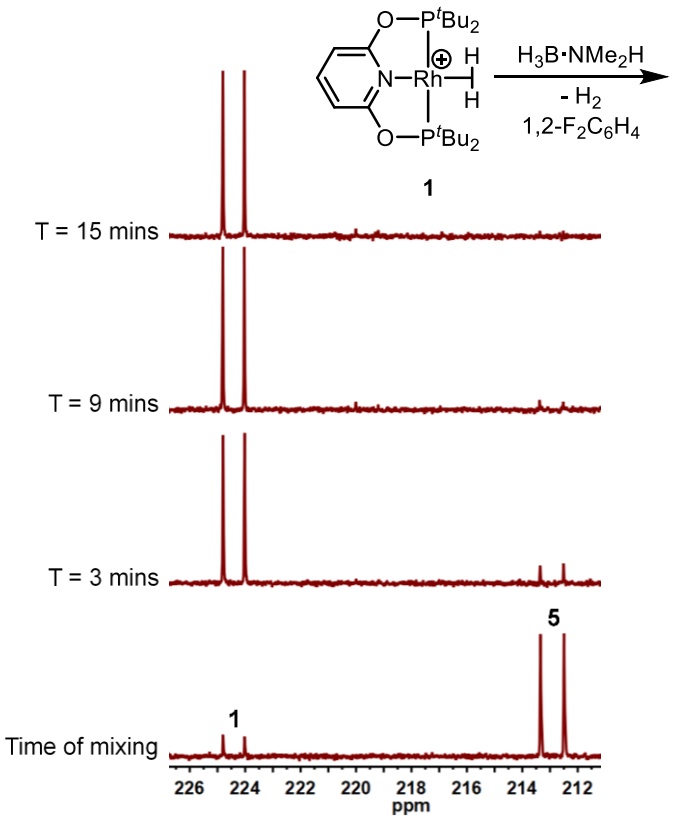


Figure 2.7 Stacked $^{31}P\{^{1}H\}$ NMR spectra (162 MHz, 1,2-$F_2C_6H_4$, 298 K) over time of the reaction of complex **1** with one equivalent of $H_3B{\cdot}NMe_2H$.

Complex **5** was assigned as the amine-borane sigma complex [Rh(PONOP)(η^1-$H_3B{\cdot}NMe_2H$)][$BAr^F{}_4$] (**5**) (**Scheme 2.7**), analogous to complex **4**, due to the similarities between the respective NMR spectroscopic data. In the $^{31}P\{^{1}H\}$ NMR spectrum, a single environment for complex **5** was observed (d, δ 212.9 ppm, $^{1}J_{RhP}$ = 138 Hz) with a coupling constant indicative of a Rh^{I} centre[46] and of similar size to that of complex **4** (d, δ 208.9 ppm, $^{1}J_{RhP}$ = 142 Hz). In the ^{1}H NMR spectrum, a broad

signal of relative integral 3 H (compared to C–H signals in the aromatic region for this complex) was observed at δ –1.98 ppm in the hydride region. This broad signal is analogous to that observed for complex **4** (δ –2.6 ppm) and is consistent with rapid exchange of the BH_3 protons. The ^{11}B NMR spectra exhibited a broad peak at δ –21.3 ppm (**Figure 2.8**), significantly low frequency shifted from that of unbound $H_3B{\cdot}NMe_2H$ (δ –13.2 ppm), consistent with the amine-borane bound to the metal-centre via an η^1 binding mode (section 1.8.2). By comparison to the ^{11}B NMR spectrum for complex **4**, it can be noted that the chemical shifts for both complex **4** (δ –15.2 ppm) and complex **5** (δ –21.3 ppm) are shifted to a lower frequency by approximately 8 ppm compared to the chemical shift of the respective unbound amine-borane ($H_3B{\cdot}NMe_3$ = δ –7.3 ppm, $H_3B{\cdot}NMe_2H$ = δ –13.2 ppm).

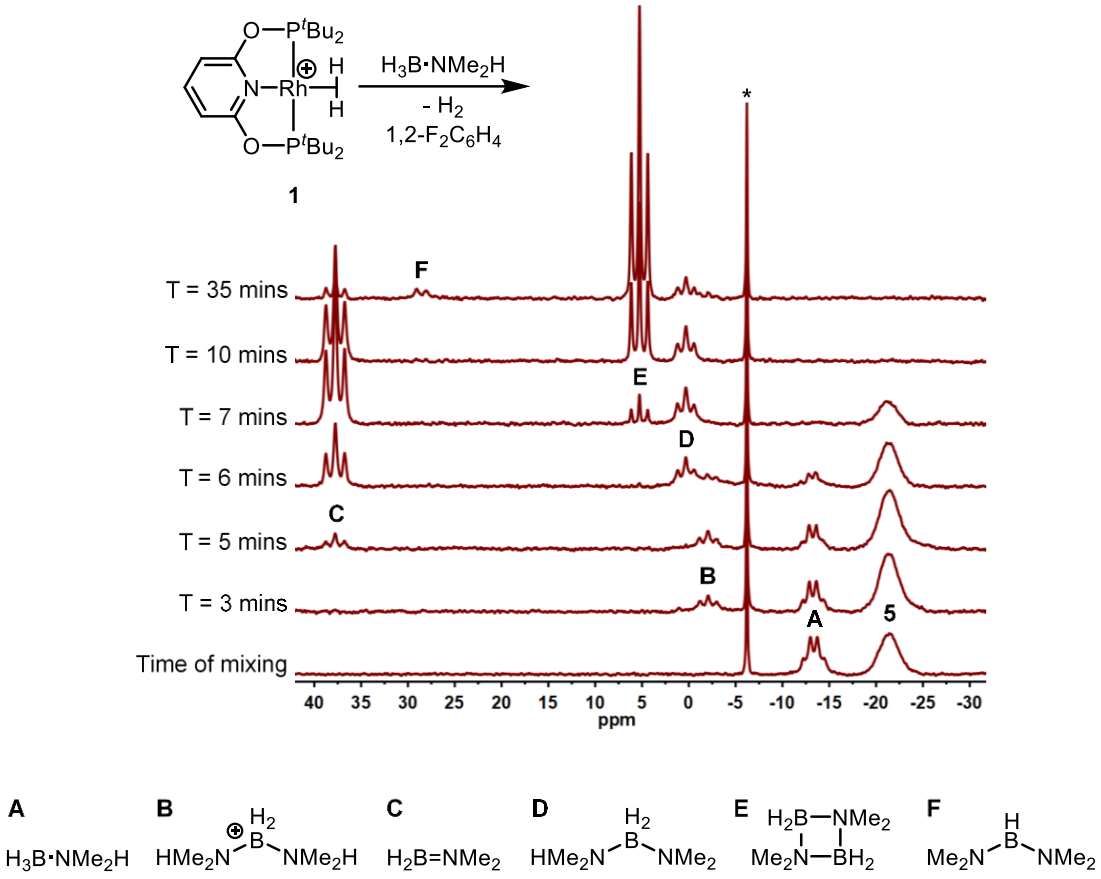


Figure 2.8 Stacked ^{11}B NMR spectra (128 MHz, 1,2-$F_2C_6H_4$, 298 K) over time of the reaction of complex **1** with one equivalent of $H_3B{\cdot}NMe_2H$. * = $[BAr^F{}_4]^-$.

After three minutes from time of mixing, the ^{11}B NMR spectra showed the appearance of a new signal (**B**) in the form of a triplet (~5 %) at δ –2.04 ppm ($^1J_{BH}$ = 115 Hz), identified as the boronium salt $[H_2B(NMe_2H)_2][BAr^F{}_4]$ by comparison to an independently-prepared sample in 1,2-$F_2C_6H_4$.[68,69]

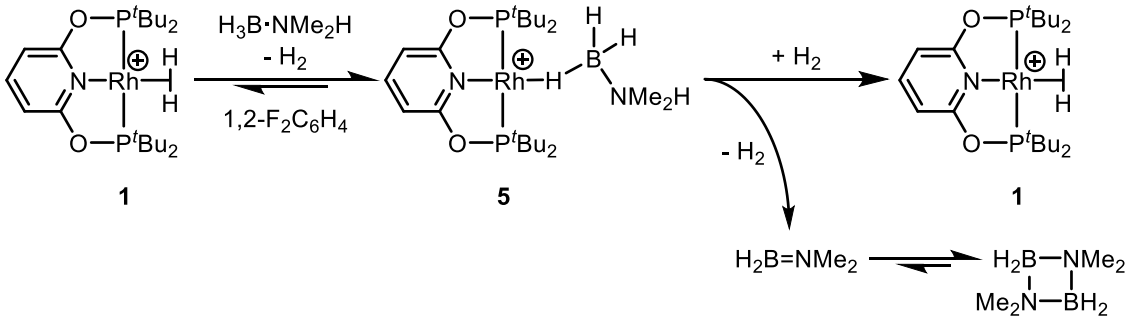
After five minutes from the time of mixing, a signal (**C**) for the formation of aminoborane, $H_2B{=}NMe_2$ (t, δ 37.8 ppm, $^1J_{BH}$ = 129 Hz),[38,70,71] was observed in the ^{11}B NMR spectra. Transient aminoborane formation is indicative of the occurrence of dehydrocoupling of $H_3B{\cdot}NMe_2H$. The appearance of this signal was shortly

followed by the observation of a new triplet (**D**) in the ^{11}B NMR spectra (δ 0.36 ppm, $^{1}J_{BH}$ = 110 Hz), similar in appearance to that of the boronium cation $\{H_2B(NMe_2H)_2\}^+$, but high frequency shifted by approximately two ppm compared to boronium. This boronium-like species was postulated to be the neutral analogue $H_2B(NMe_2)_2H$.[72,73] During the next five minutes, the signals for unbound $H_3B{\cdot}NMe_2H$ (**A**), complex **5** and $[H_2B(NMe_2H)_2][BAr^F{}_4]$ (**B**) were observed to diminish as those for $H_2B{=}NMe_2$ (**C**) and $H_2B(NMe_2)_2H$ (**D**) (maximum ~15 %) were observed to increase in intensity. The dimer $[H_2BNMe_2]_2$ (t, δ 5.3 ppm, $^{1}J_{BH}$ = 112 Hz),[45] product from the dehydrocoupling of $H_3B{\cdot}NMe_2H$, was also observed at this time in the ^{11}B NMR spectra (**E**). As the reaction progressed, the intensity of the signal for $[H_2BNMe_2]_2$ increased as the signal for $H_2B{=}NMe_2$ decreased reflecting the slow dimerisation of $H_2B{=}NMe_2$ to form the thermodynamic product $[H_2BNMe_2]_2$.[38]

After 35 minutes from the time of mixing, the major boron-containing product was observed to be $[H_2BNMe_2]_2$ in the ^{11}B NMR spectrum. Another minor product (~2 %) was also observed in the form of a doublet at δ 28.7 ppm ($^{1}J_{BH}$ = 130 Hz) (**F**), identified as the diaminoborane $HB(NMe_2)_2$.[45,74] $HB(NMe_2)_2$ is often observed as a minor product in such reactions and is formed from the dehydrocoupling reaction between $H_3B{\cdot}NMe_2H$ and NMe_2H.[68,75,76]

From the results of these speciation experiments, it can be proposed that complex **1** reacts with one equivalent of $H_3B{\cdot}NMe_2H$ to yield the intermediate amine-borane sigma complex **5**, which can undergo dehydrogenation to yield the transient

aminoborane $H_2B{=}NMe_2$ and subsequently $[H_2BNMe_2]_2$ (**Scheme 2.7**). Complex **1** can be regenerated from reaction of H_2, evolved from the dehydrogenation process, with $\{Rh(PONOP)\}^+$. Other boron-containing species are observed throughout the reaction and will be discussed in detail when these speciation studies are returned to in Chapter Three under catalytic conditions.



Scheme 2.7 Suggested reaction pathway for the reaction of complex **1** with one equivalent $H_3B{\cdot}NMe_2H$. $[BAr^F{}_4]^-$ anions omitted for clarity.

It should be noted that complex **5** was unable to be isolated and fully characterised due to the rapid dehydrocoupling of $H_3B{\cdot}NMe_2H$ that occurs in solution, leading to the reformation of complex **1**.

2.6.2 Reaction of complex 2 with $H_3B{\cdot}NMe_2H$

As with complex **1**, $[Rh(PONOP)(\kappa^1\text{-}N_2)][BAr^F{}_4]$ (**2**) was similarly investigated as a potential catalyst for the dehydrocoupling of $H_3B{\cdot}NMe_2H$.

A solution of complex **2** (36 mM, $1,2\text{-}F_2C_6H_4$) was reacted with approximately one equivalent of $H_3B{\cdot}NMe_2H$ in an NMR tube and the reaction progress was followed using $^{31}P\{^1H\}$ NMR spectroscopy (**Figure 2.9**). This reaction was repeated under the

same conditions and followed using ^{11}B NMR spectroscopy (**Figure 2.10**). The same caveats that render the $^{31}P\{^{1}H\}$ NMR and ^{11}B NMR spectroscopic data unable to be directly compared as a function of time, as described for the reaction of complex **1** with $H_3B{\cdot}NMe_2H$ in the previous section, apply for these experiments as well.

The reaction of complex **2** with one equivalent of $H_3B{\cdot}NMe_2H$ initially follows the same course as with the stoichiometric reaction of complex **1** with $H_3B{\cdot}NMe_2H$. Upon time of mixing, complex **5** was again observed in the $^{31}P\{^{1}H\}$ NMR spectra (**Figure 2.9**). However, at this point complex **5** is the minor organometallic product (~35 %) and the major remains complex **2**, as judged by comparison of the respective integrals of the NMR signals. During the next three minutes of reactivity, the signal for complex **5** was observed to increase in intensity as it became the major complex, consistent with the relatively slow displacement of N_2 by $H_3B{\cdot}NMe_2H$. Interestingly, a signal for complex **1** was also observed during this time. As the reaction progressed, the intensity of the signal for complex **5** diminished as that for complex **1** increased before the signals for complex **1** and **2** became of equal intensity and remained such for the rest of the reaction. Furthermore, a new signal **X** (d, δ 219.6 ppm, $^{1}J_{RhP}$ = 132 Hz) for an as yet unidentified species was observed early on during the reaction and remained at low levels of concentration.

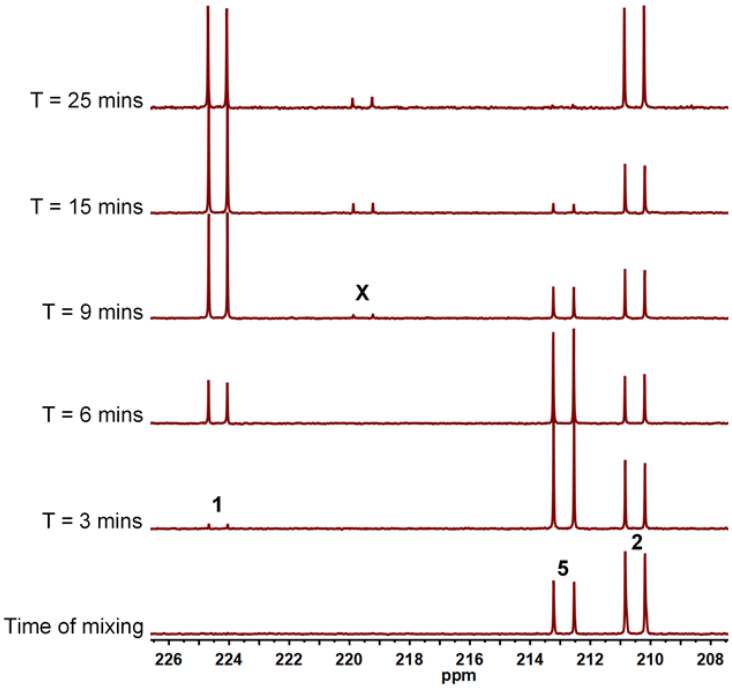


Figure 2.9 Stacked $^{31}P\{^{1}H\}$ NMR spectra (202 MHz, 1,2-$F_2C_6H_4$, 298 K) over time of the reaction of complex **2** with one equivalent of $H_3B{\cdot}NMe_2H$. **X** = unidentified species.

The ^{11}B NMR spectra recorded throughout this reaction (**Figure 2.10**) showed similar results to those observed for the reaction of complex **1** with $H_3B{\cdot}NMe_2H$. Along with unbound $H_3B{\cdot}NMe_2H$ and complex **5**, $[H_2B(NMe_2H)_2][BAr^F{}_4]$ was initially observed followed by signals for $H_2B(NMe_2)_2H$, $H_2B{=}NMe_2$ and $[H_2BNMe_2]_2$. Towards the end of the reaction, a small amount of $HB(NMe_2)_2$ (~5 %) was again observed.

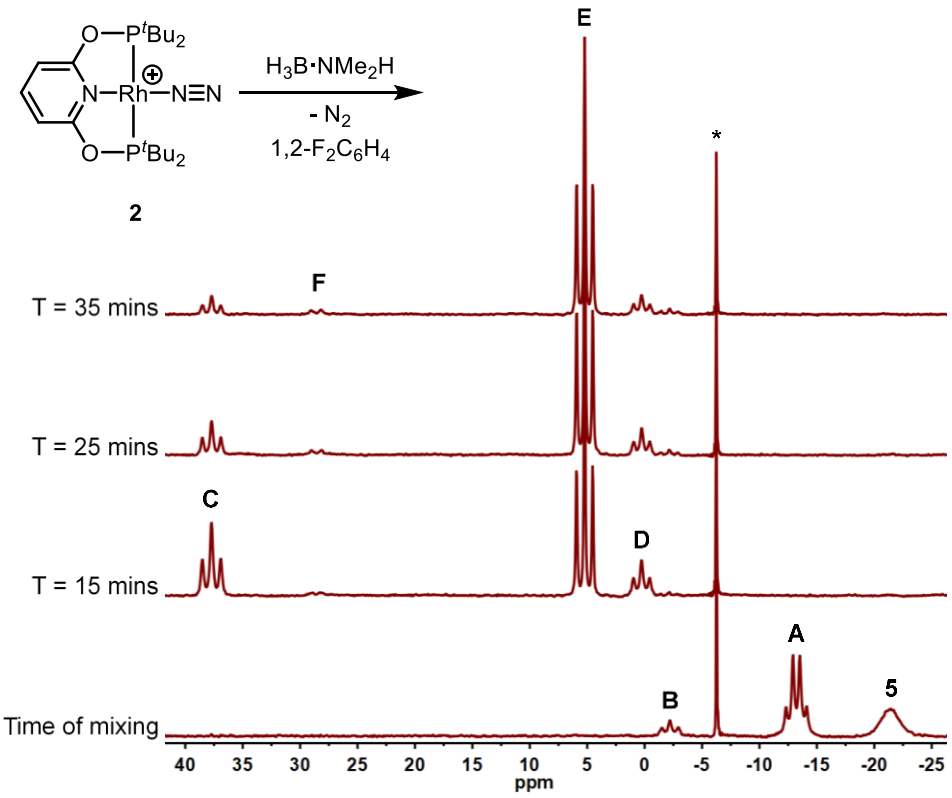
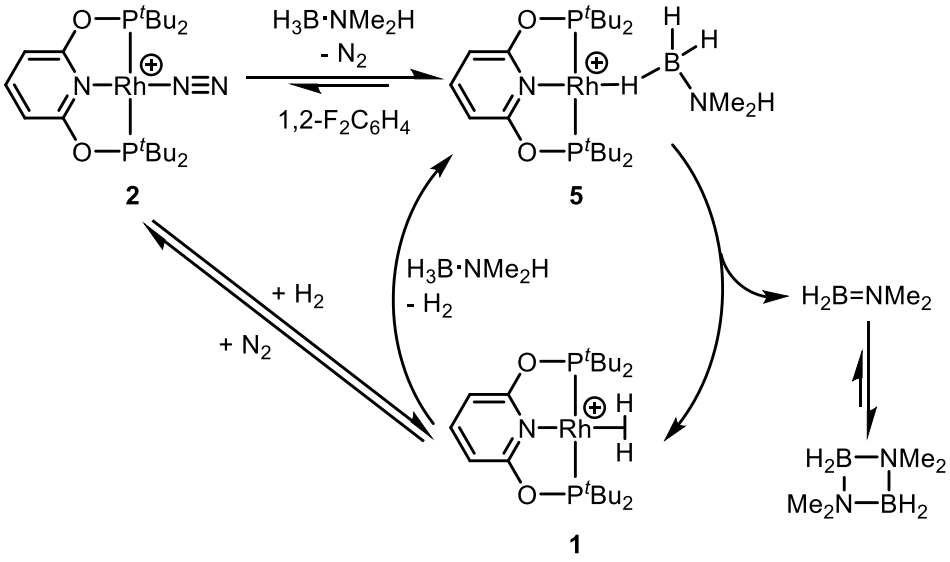


Figure 2.10 Stacked ^{11}B NMR spectra (160 MHz, 1,2-$F_2C_6H_4$, 298 K) over time of the reaction of complex **2** with one equivalent of $H_3B{\cdot}NMe_2H$. **A** = $H_3B{\cdot}NMe_2H$, **B** = $\{H_2B(NMe_2H)_2\}^+$, **C** = $H_2B{=}NMe_2$, **D** = $H_2B(NMe_2)_2H$, **E** = $[H_2BNMe_2]_2$, **F** = $HB(NMe_2)_2$ and * = $[BAr^F{}_4]^-$.

From analysis of the NMR spectra recorded during the reaction of complex **2** and $H_3B{\cdot}NMe_2H$, it can be seen that $H_3B{\cdot}NMe_2H$ is successfully dehydrocoupled under these conditions. A proposed reaction pathway is outlined in **Scheme 2.8**. The generation of complex **1** during this reaction is proposed to be from the reaction of H_2, produced from the dehydrocoupling of the amine-borane, with the metal centre. This is consistent with the stoichiometric studies with complex **1** in the previous section. Displacement of N_2 from complex **2** with H_2 evolved during the reaction could also generate complex **1**, consistent with the equilibrium between these two complexes shown in section 2.3. The presence of complex **2** throughout the reaction,

rather than being wholly consumed by reaction with $H_3B{\cdot}NMe_2H$, can be explained in a two ways: N_2 in the sealed system may react with the $\{Rh(PONOP)\}^+$ fragment to reform complex **2**; or $H_3B{\cdot}NMe_2H$ may react preferentially with complex **1** formed *in situ* compared to complex **2**, leaving a proportion of complex **2** unreacted. This latter explanation is consistent with the slower reactivity observed for the reaction of the tertiary amine-borane $H_3B{\cdot}NMe_3$ with complex **2** compared to that with complex **1** (section 2.4).



Scheme 2.8 Suggested pathway for the reaction of complex **2** with one equivalent of $H_3B{\cdot}NMe_2H$. $[BAr^F{}_4]^-$ anions omitted for clarity.

It was also observed that the signal intensities for both complexes **1** and **2** became approximately the same by the end of the reaction. This result may be explained by the presence of both one equivalent of N_2 (from the starting complex **2**) and one equivalent of H_2 (from the dehydrocoupling of $H_3B{\cdot}NMe_2H$) in the closed system of

the NMR tube causing both complexes **1** and **2** to be in equilibrium, as shown in section 2.3.

2.6.3 Reaction of complex 4 with $H_3B{\cdot}NMe_2H$

There are multiple reports in the literature of cationic amine-borane sigma complexes successfully employed as pre-catalysts for the dehydrocoupling of primary and secondary amine-boranes.[12,15,16] The weakly bound amine-borane ligands in such complexes can be easily displaced to reveal an unsaturated catalytically active complex. Thus, the potential of complex **4** as an active dehydrocoupling catalyst was probed.

Following the same procedure as outlined in the rest of this section, a solution of complex **4** (36 mM, 1,2-$F_2C_6H_4$) was added to one equivalent of the secondary amine-borane $H_3B{\cdot}NMe_2H$ in an NMR tube and the subsequent reaction was followed by $^{31}P\{^1H\}$ NMR spectroscopy (**Figure 2.11**) and ^{11}B NMR spectroscopy.

Upon time of mixing, the $^{31}P\{^1H\}$ NMR spectrum showed the presence of complex **1** (~20 %) alongside complex **4** (**Figure 2.11**). Three minutes later the signal intensities for these complexes had reached the ratio 3:2 (complex **1**:complex **4**) and remained as such for the rest of the reaction. ^{11}B NMR spectra of the reaction mixture confirmed the dehydrocoupling of $H_3B{\cdot}NMe_2H$ to $H_2B{=}NMe_2$ and $[H_2BNMe_2]_2$ as before.

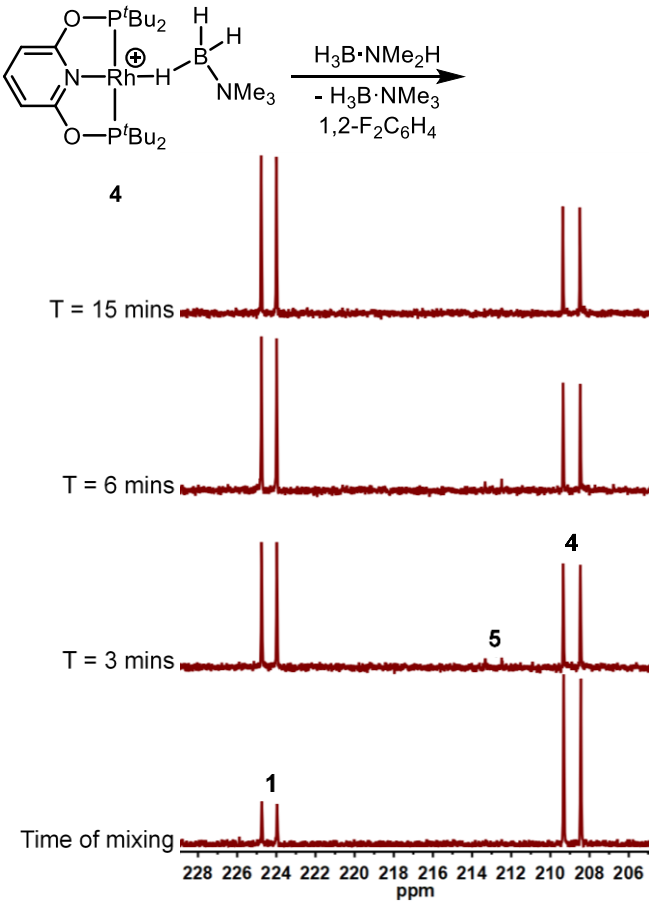
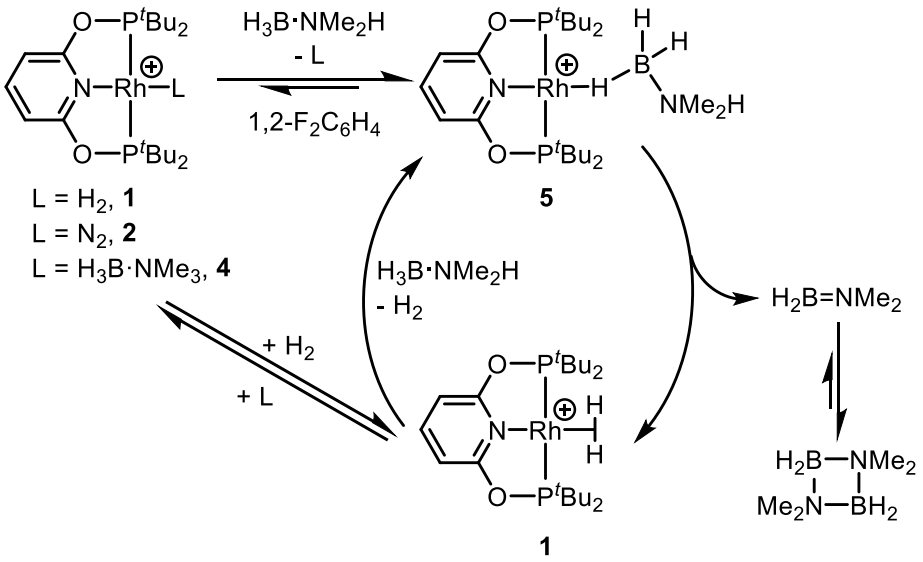


Figure 2.11 Stacked $^{31}P\{^1H\}$ NMR spectra (162 MHz, 1,2-$F_2C_6F_4$, 298 K) over time of the reaction of complex **4** with one equivalent of $H_3B{\cdot}NMe_2H$.

The observation of complex **1** during this reaction is consistent with the observations for the stoichiometric reactions previously described, starting with complex **1** and with complex **2**. As when starting from complex **2**, a proportion of starting complex **4** remains unreacted throughout the reaction, which may indicate that $H_3B{\cdot}NMe_2H$ reacts preferentially with complex **1** formed *in situ*.

Interestingly, complex **5** was observed in small quantities (as judged by relative integrals in the $^{31}P\{^1H\}$ NMR spectra) and only after three minutes from the time of mixing. These results are different to those recorded for the analogous reactions

with complexes **1** and **2** where complex **5** was observed initially upon time of mixing and also to be the major organometallic species early on in both reactions. The fact that complex **5** is observed in such low concentrations could indicate the rate of formation of complex **5** is matched by the rate of subsequent dehydrocoupling. This suggests that the tertiary amine-borane $H_3B{\cdot}NMe_3$ may bind more strongly to the metal centre than $H_3B{\cdot}NMe_2H$.



Scheme 2.9 Overall suggested pathway for the reaction of [Rh(PONOP)(L)][BAr^F_4] (L = H_2, N_2 or $H_3B{\cdot}NMe_3$) with $H_3B{\cdot}NMe_2H$. [BAr^F_4]$^-$ anions omitted for clarity.

In summary, complexes **1**, **2** and **4** have all been shown to react stoichiometrically with $H_3B{\cdot}NMe_2H$ yielding the intermediate aminoborane $H_2B{=}NMe_2$ followed by the dimer product $[H_2BNMe_2]_2$ (**Scheme 2.9**). In all three cases, complex **1** was observed to form during the reaction. However, a proportion of complexes **2** and **4** remained unreacted at the end of the reactions where these were the starting complexes, suggesting complex **1** reacts more readily with $H_3B{\cdot}NMe_2H$ than **2** and

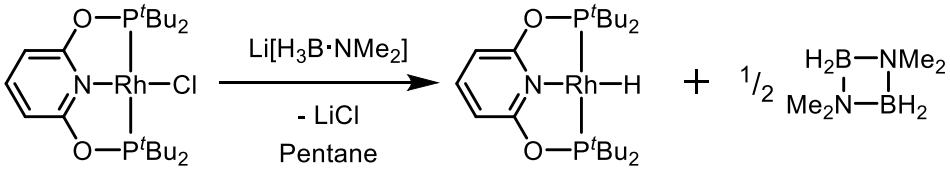
4. For this reason, and due to the simplicity of the reaction mixture observed in the $^{31}P\{^{1}H\}$ NMR spectra for reactivity with complex **1** compared to **2** and **4** making speciation studies easier, complex **1** was employed further to investigate the mechanistic detail of the dehydrocoupling of $H_3B{\cdot}NMe_2H$ as outlined in Chapter Three.

2.7 Formation of Rh(PONOP)H (6)

Chapter Three details a thorough investigation into the dehydrocoupling of $H_3B{\cdot}NMe_2H$ as catalysed by complex **1**. NMR spectroscopic data recorded during speciation studies under catalytic conditions indicated the presence of an organometallic intermediate, which contained a metal hydride unit. This species was not observed under the stoichiometric conditions reported in this chapter. Neutral metal hydrides, such as Pt(I^{t}Bu)(I^{t}Bu')H,[68] have been postulated as intermediates during the catalytic dehydrocoupling of amine-boranes (section 1.11). Therefore, the analogous neutral monohydride complex Rh(PONOP)H (**6**) was targeted, and subsequently identified as the intermediate observed during catalysis. In this section, the synthesis and characterisation that led to the assignment of this species is described. The role of complex **6** in catalysis is described later in section 3.4.

Many routes were initially trialled to synthesise Rh(PONOP)H (**6**). These included the reactions of Rh(PONOP)Cl with hydride transfer reagents such as LiH, NaH, KH or $Li[BEt_3H]$ under H_2 and also the reaction of $[Rh(PONOP)(\eta^2\text{-}H_2)][BAr^F{}_4]$ (**1**) with 1,8-bis(dimethylamino)naphthalene (proton sponge) in an effort to deprotonate

the dihydrogen ligand. However, these pathways were unsuccessful, resulting in mixtures of products. Instead, complex **6** was synthesised by the reaction of Rh(PONOP)Cl with lithium amidoborane, $Li[H_3B{\cdot}NMe_2]$,[77] in pentane (**Scheme 2.10**). $[H_2BNMe_2]_2$ was formed alongside as a side product, which could simply be removed *in vacuo*, resulting in the isolation of complex **6** as a red powder (81 % yield).



6

Scheme 2.10 Synthesis of Rh(PONOP)H (**6**).

Complex **6** was isolated and characterised fully by NMR spectroscopy, elemental microanalysis and single crystal X-ray diffraction.

The $^{31}P\{^1H\}$ NMR spectrum of complex **6** (**Figure 2.12**) displays one environment at δ 226.2 ppm (d, $^1J_{RhP}$ = 171 Hz). In the ^1H NMR spectrum, a triplet of doublets of relative integral 1 H is observed in the hydride region (δ –9.60 ppm, $^1J_{RhH}$ = 20 Hz and $^1J_{PH}$ = 23 Hz). Upon decoupling of ^{31}P, this signal collapses into a doublet ($^1J_{RhH}$ = 20 Hz). The single environment observed in the $^{31}P\{^1H\}$ NMR spectrum and the symmetric splitting pattern in the ^1H NMR spectrum suggest a square planar geometry for complex **6**.

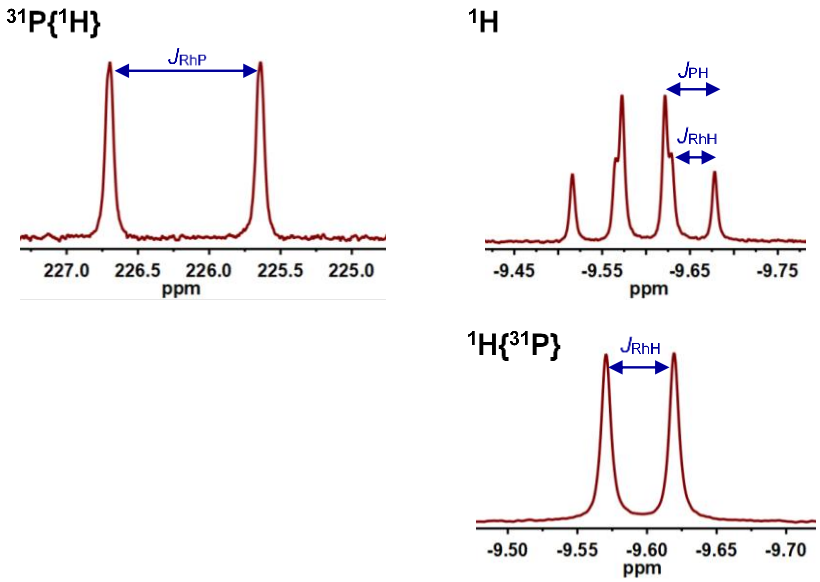


Figure 2.12 Partial $^{31}P\{^{1}H\}$ (162 MHz), ^{1}H and $^{1}H\{^{31}P\}$ (400 MHz) NMR spectra (C_6D_6, 298 K) of complex **6**.

Recrystallisation of a solution of complex **6** in neat methylcyclohexane at –20 °C afforded red crystals suitable for single crystal X-ray diffraction. The solid state structure of complex **6** (**Figure 2.13**) is in agreement with the NMR spectroscopic data and shows a pseudo-square planar geometry around the rhodium centre (the N1–Rh1–H1 bond angle 178.4(12) is nearly linear). This planar geometry is consistent with that of the small number of other pincer monohydride complexes reported in the literature.[78–81] The hydride ligand was located and freely refined.

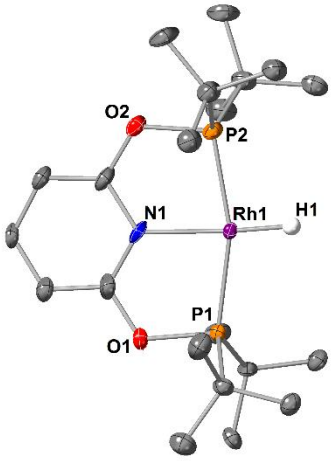


Figure 2.13 Solid state structure of complex **6**. Displacement ellipsoids are drawn at the 30 % probability level. Carbon-bound hydrogen atoms are omitted for clarity. Selected bond lengths (Å) and angles (°): Rh1–H1, 1.54(5); Rh1–P1, 2.2179(17); Rh1–P2, 2.2020(17); Rh1–N1, 2.046(6); P1–Rh1–P2, 162.80(7); N1–Rh1–H1, 178.4(12).

The mechanism of the hydride transfer to form complex **6** could operate via the initial formation of an amidoborane intermediate (**Figure 2.14**, **I**). This intermediate could then undergo β-H elimination to generate complex **6** alongside an equivalent of $H_2B{=}NMe_2$, which is experimentally observed as the dimer $[H_2BNMe_2]_2$. This pathway is consistent to that reported for the dehydrocoupling of $H_3B{\cdot}NMe_2H$ catalysed by the β-diketiminate complex $[HC\{(Me)CN(Dipp)\}_2Mg^nBu]$ (section 1.7.1).[82] However, in this case the β-H elimination of the amidoborane species is thermally induced by raising the temperature of the reaction mixture to 60 °C. Later work in this area found β-H elimination in group two amidoborane complexes to be relatively high in energy and instead, a second molecule of $H_3B{\cdot}NMe_2H$ is necessary to promote this process.[83] These results suggest β-H elimination of the proposed amidoborane complex Rh(PONOP)($Me_2N{\cdot}BH_3$) may be inaccessible. This supposition is supported by the report that ethyl analogues, such

as M(PONOP)(CH_2CH_3) (M = Rh, Ir), have been shown to be stable with regard to β-H elimination at 298 K.[23]

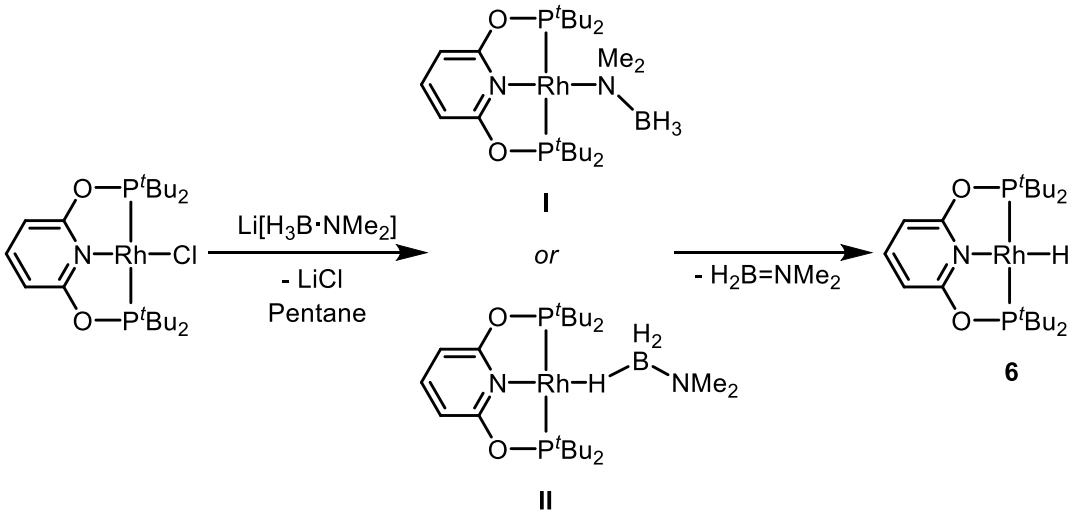


Figure 2.14 Possible intermediates (**I** and **II**) during the synthesis of complex **6** from the reaction of Rh(PONOP)Cl with Li[$H_3B{\cdot}NMe_2$].

Alternatively, the formation of complex **6** could proceed via the formation of the sigma-amidoborane complex as shown in **Figure 2.14**, **II**. In this case, Li[$H_3B{\cdot}NMe_2$] would act as a direct hydride source, leading to the elimination of LiCl along with $H_2B{=}NMe_2$. This pathway is supported by DFT calculations undertaken by Dr Nicholas A. Beattie and Professor Stuart A. Macgregor (Herriot-Watt University), which calculate the boron-bound isomer to be 9.3 kcal mol^{-1} more stable than the nitrogen-bound amidoborane complex. Furthermore, the barrier to B–H bond cleavage of the boron-bound complex, leading to the formation of complex **6**, is calculated to be only 1.1 kcal mol^{-1}. Therefore, it is proposed that complex **6** is more likely to be formed via the more energetically favourable pathway involving the formation of boron-bound isomer as an intermediate (**Figure 2.14**, **II**).

2.8 Formation of ^{Cy}PONOP analogues

The PONOP ligand (PONOP = κ^3-C_5H_3N-2,6-$(OPR_2)_2$) is a popular choice for the ligand framework of a number of transition metal catalysts[17–22] due to its ability to stabilise coordinatively unsaturated species.[41,84] In this thesis, the *tert*-butyl-substituted PONOP ligand, ^{tBu}PONOP (referred to as simply PONOP outside of this section), is employed in all rhodium complexes discussed. However, by varying the R groups in the PR_2 group of the PONOP ligand, the steric and electronic properties of the PONOP ligand can be altered resulting in a change in stability and reactivity of the transition metal complex.[85,86] For example, the relative rate of substitution of the PCy_3 ligand in [Rh(^{R}PNP)(PCy_3)][BAr^F_4] (PNP = κ^3-C_5H_3N-2,6-$(CH_2PR_2)_2$)by MeCN is slower when R = Cy ($t_{1/2}$ = 6.2 ± 0.5 h at 333 K) than for when R = ^{t}Bu (< 5 min at 298 K).[60] This is due to the increase in steric pressure between the pincer and PCy_3 groups when R = ^{t}Bu.

As quantified by the Tolman cone angle, θ, (section 1.4.1),[87] the PCy_3 group (θ = 170°) is less sterically bulky than the P^tBu_3 phosphine (θ = 182°).[88] Therefore, substitution between P^tBu_3 and PCy_3 in the rhodium-based PONOP complexes employed in this thesis may have an effect on the resulting reactivity and provide interesting comparisons.

Analogous to the synthesis described already in this chapter, the cyclohexyl-substituted complex Rh(^{Cy}PONOP)Cl (**7**) was initially targeted. The ^{Cy}PONOP ligand used for this synthesis had been previously synthesised by F. M. Chadwick (according to the literature procedure for other PONOP ligands)[21] and was

available for group use. Complex **7** was synthesised by the reaction of the ^{Cy}PONOP ligand with $[Rh(COE)_2Cl]_2$ in toluene over 24 hours, analogous to the literature procedure for the synthesis of Rh(^{tBu}PONOP)Cl (**Figure 2.15**).[41]

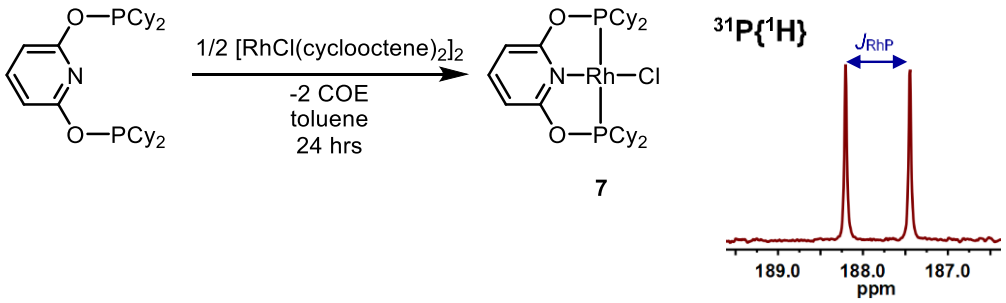
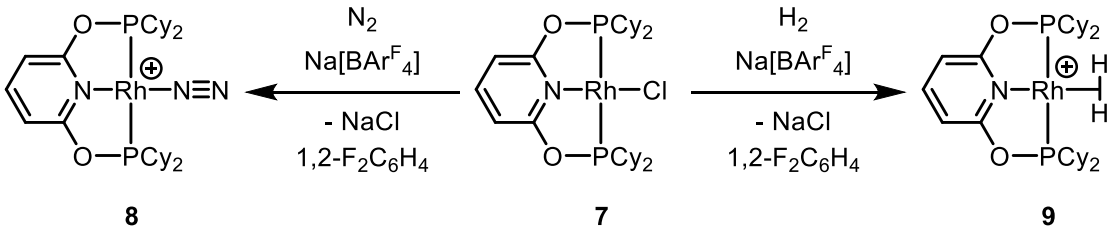


Figure 2.15 Synthesis and partial $^{31}P\{^1H\}$ NMR spectrum (202 MHz, C_6D_6, 298 K) of complex **7.** J_{RhP} = 154 Hz.

The $^{31}P\{^1H\}$ NMR spectrum of complex **7** depicts a single doublet at 187.8 ppm with a coupling of 154 Hz, identical coupling to the ^{t}Bu-analogue Rh(^{tBu}PONOP)Cl (198.7 ppm, $^1J_{RhP}$ = 154 Hz).[41] A concentrated solution of complex **7** in methylcyclohexane was placed at –20 °C for over a week in an attempt to yield single crystals suitable for X-ray diffraction however none were formed.

Following the same synthetic pathway as outlined in section 2.2 for the formation of $[Rh(PONOP)(\eta^2\text{-}H_2)][BAr^F{}_4]$[22] (**1**), $[Rh(PONOP)(\kappa^1\text{-}N_2)][BAr^F{}_4]$[33] (**2**) and $[Rh(PONOP)(\kappa^1\text{-}ClCH_2Cl)][BAr^F{}_4]$[33] (**3**), the analogous H_2 and N_2 complexes with the ^{Cy}PONOP ligand were targeted. In a J. Young flask, a solution of complex **7** (31 mM, 1,2-$F_2C_6H_4$) was reacted with one equivalent of $Na[BAr^F{}_4]$ and the solution was freeze-pump-thaw degassed three times before being backfilled with one atmosphere of N_2 (**Scheme 2.11**, *left*). The reaction mixture was stirred for four

hours before being filtered and the solvent removed *in vacuo*. $^{31}P\{^{1}H\}$ NMR spectroscopy of the product in 1,2-$F_2C_6H_4$ indicated all of complex **7** had reacted and revealed multiple doublets indicating a mixture of organometallic products. The major product (~60 %) was assigned as the desired N_2 adduct [Rh(^{Cy}PONOP)(κ^1-N_2)][BAr^F_4] (**8**) due to the similarity of the $^{31}P\{^{1}H\}$ NMR spectroscopic data (d, 194.5 ppm, $^{1}J_{RhP}$ = 132 Hz) to that for the analogous complex [Rh(PONOP)(κ^1-N_2)][BAr^F_4] (**2**) (d, 211.0 ppm, $^{1}J_{RhP}$ = 132 Hz).[33] This assignment was confirmed using ESI-MS: *m/z* 634.23 (calculated 634.22 for {Rh(^{Cy}PONOP)(κ^1-N_2)}$^+$). The other species observed in the $^{31}P\{^{1}H\}$ NMR spectrum remain uncharacterised. A repeat of this reaction but with leaving the reaction mixture to stir under an atmosphere of N_2 for three days rather than four hours again resulted in multiple products observed in the $^{31}P\{^{1}H\}$ NMR spectrum with complex **8** only present in a small amount (~6 %). Recrystallisation attempts were unsuccessful.



Scheme 2.11 Attempted synthesis of [Rh(^{Cy}PONOP)(κ^1-N_2)][BAr^F_4] (*left*) and [Rh(^{Cy}PONOP)(η^2-H_2)][BAr^F_4] (*right*). [BAr^F_4]$^-$ anions omitted for clarity.

The synthesis of [Rh(^{Cy}PONOP)(η^2-H_2)][BAr^F_4] (**9**) was also attempted. One equivalent of Na[BAr^F_4] was added to a J. Young flask containing a solution of complex **7** (50 mM, 1,2-$F_2C_6H_4$) (**Scheme 2.11**, *right*). The reaction mixture was freeze-pump-thaw degassed three times and stirred under an atmosphere of H_2 for

four hours, before being filtered and the solvent removed *in vacuo*. $^{31}P\{^{1}H\}$ NMR spectroscopy of the product in 1,2-$F_2C_6H_4$ showed multiple signals, including some unreacted complex **7** (~37 %). A doublet at 208.0 ppm, $^{1}J_{RhP}$ = 127 Hz, (present at ~19 % of the total phosphorus containing species) was assigned as the desired complex **9** due to the similarity to the NMR spectroscopic data for [Rh(PONOP)(η^2-H_2)][BAr^F_4] (**1**) (d, 224.6 ppm, $^{1}J_{RhP}$ = 126 Hz).[22] Further confirmation of this assignment came from the observation of a doublet in the ^{1}H NMR spectrum (–8.16 ppm, $^{1}J_{RhH}$ = 28 Hz), which is very similar to the analogous doublet observed for complex **1** (–8.21 ppm, $^{1}J_{RhH}$ = 28 Hz). ESI-MS was also conducted on the sample and yielded a signal for complex **9**: *m/z* 608.22 (calculated 608.23 for {Rh(^{Cy}PONOP)(η^2-H_2)}$^+$). Attempted recrystallisations of complex **9** were unsuccessful. The other organometallic species observed within the $^{31}P\{^{1}H\}$ NMR spectrum remain uncharacterised. Repeating the reaction to synthesise complex **9**, but leaving the reaction mixture to stir under an atmosphere of H_2 for three days rather than four hours, resulted in all of complex **7** being consumed as observed using $^{31}P\{^{1}H\}$ NMR spectroscopy. As before, a mixture of products was observed in the $^{31}P\{^{1}H\}$ NMR spectrum including complex **9** (~26 %) and also complex **8** (~30 %). Although a greater proportion of the products was complex **9** when the reaction mixture was left under H_2 for longer, complex **9** was still unable to be isolated due to other similar products being present. The formation of complex **8** under these conditions is proposed to be due to N_2 impurities in the H_2 atmosphere and the fact complex **8** is present in a significant amount indicates that complex **8** is more stable than complex **9**. An analogous increase in stability is observed for [Rh(PONOP)(κ^1-

N_2)][BAr^F_4][33][33][33] (**2**) over [Rh(PONOP)(η^2-H_2)][BAr^F_4] (**1**) as discussed in section 2.4.

Earlier in this chapter (section 2.4), the synthesis of the amine-borane sigma complex [Rh(PONOP)(η^1-$H_3B{\cdot}NMe_3$)][BAr^F_4] (**4**) was reported, from the reaction of either complex **1** or **2** with $H_3B{\cdot}NMe_3$. For comparison to complex **4**, the analogous complex containing Cy groups rather than ^{t}Bu groups was targeted. However, as the Cy analogues to complexes **1** and **2** (**9** and **8**, respectively) could not be cleanly isolated, a different synthetic route was employed. One equivalent of each Na[BAr^F_4] and $H_3B{\cdot}NMe_3$ were added to an NMR tube containing a solution of complex **7** (31 mM, CD_2Cl_2) and the sample was mixed via rotation for three hours before being analysed by NMR spectroscopy (**Figure 2.16**). The $^{31}P\{^1H\}$ NMR spectrum showed a doublet at 199.5 ppm ($^1J_{RhP}$ = 142 Hz) as the major organometallic product (~93 %). This signal was assigned to the desired amine-borane sigma complex [Rh(^{Cy}PONOP)(η^1-$H_3B{\cdot}NMe_3$)][BAr^F_4] (**10**) upon comparison to the identical Rh–P coupling in the corresponding *tert*-butyl complex [Rh(^{tBu}PONOP)(η^1-$H_3B{\cdot}NMe_3$)][BAr^F_4] (**4**) ($^1J_{RhP}$ = 142 Hz). One other signal was observed in the $^{31}P\{^1H\}$ NMR spectrum at 193.2 ppm ($^1J_{RhP}$ = 137 Hz), which was also observed as a minor product during the syntheses of complexes **8** and **9**, and remains uncharacterised, but may be derived from impurities in complex **7**, which is a reagent for all these reactions.

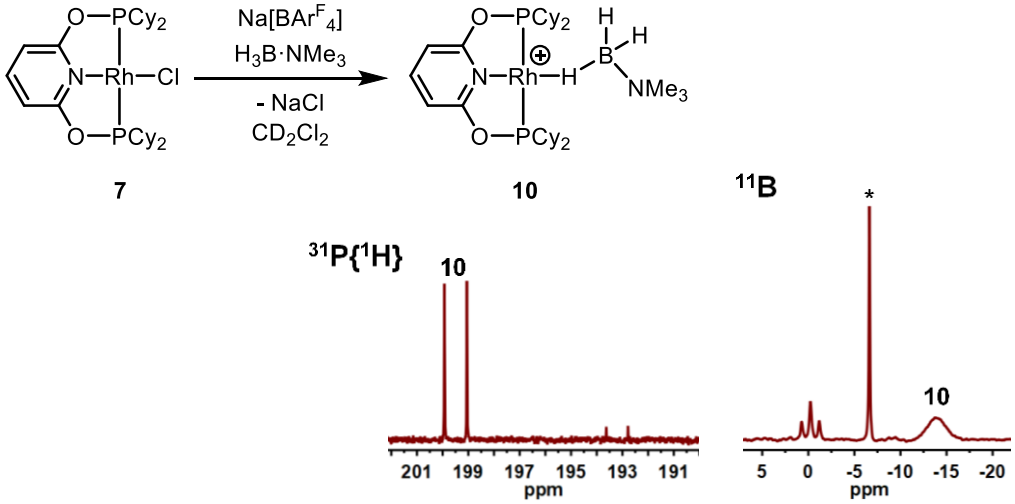


Figure 2.16 Partial $^{31}P\{^{1}H\}$ (162 MHz) and ^{11}B (128 MHz) NMR spectra (CD_2Cl_2, 298 K) for the reaction of complex **7** with $Na[BAr^F_4]$ and $H_3B{\cdot}NMe_3$. * = $[BAr^F_4]^-$ (not shown in scheme for clarity).

The ^{11}B NMR spectrum of this reaction revealed a broad singlet at –14.0 ppm, which sharpens upon decoupling of ^{1}H nuclei, consistent with the formation of an amine-borane sigma complex such as complex **10**. This signal is low frequency shifted from that of free $H_3B{\cdot}NMe_3$ (δ –7.3 ppm)[14] and so implies η^1 coordination (section 1.8.2) of the amine-borane, as observed for the analogous complex **4** (br s, –15.2 ppm). Also present is the ^{11}B NMR spectrum is an as yet uncharacterised triplet at –0.23 ppm ($^{1}J_{BH}$ = 123 Hz), which has similar NMR spectroscopic data to the literature reported $HMe_2N{\cdot}BH_2(OTf)$ (–0.4 ppm, $^{1}J_{BH}$ = 121 Hz)[69] indicating a similar deprotonated analogue of $H_3B{\cdot}NMe_3$ may be present, which may also be linked to the formation of the side organometallic product observed in the $^{31}P\{^{1}H\}$ NMR spectrum. The ^{1}H NMR spectrum of this reaction showed a broad signal in the hydride region at –2.5 ppm (3 H), comparable to that of complex **4** (–2.6 ppm) and again consistent with the presence of a sigma-bound amine-borane.

Diffusion of a concentrated 1,2-$F_2C_6H_4$ solution of the reaction of complex **7** with $Na[BAr^F{}_4]$ and $H_3B{\cdot}NMe_3$ into pentane at room temperature yielded orange crystals of complex **10** suitable for single crystal X-ray diffraction. The solid state structure of complex **10** is depicted in **Figure 2.17**. The BH_3 hydrogen atoms could not be located, although they were observed via NMR spectroscopy, and so they were placed in calculated positions.

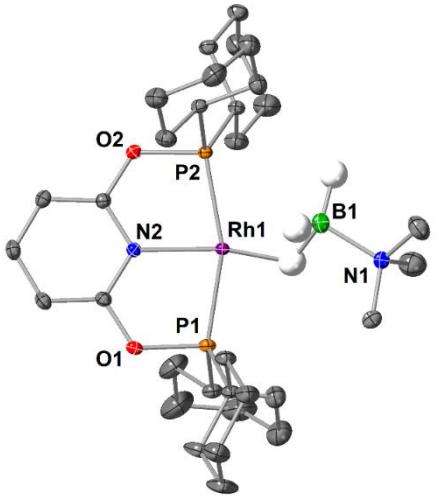


Figure 2.17 Solid state structure of the cationic portion of [Rh(^{Cy}PONOP)(η^1-$H_3B{\cdot}NMe_3$)][$BAr^F{}_4$] (**10**). Displacement ellipsoids are drawn at the 30 % probability level. Carbon-bound hydrogen atoms are omitted for clarity. Selected bond lengths (Å) and angles (°): Rh1–B1, 2.380(4); Rh1–P1, 2.2483(6); Rh1–P2, 2.2546(6); Rh1–N2, 2.030(2); B1–N1, 1.629(5); P1–Rh1–P2, 160.91(3).

The calculated positions of the BH_3 hydrogens are consistent with η^1 coordination of the amine-borane, with one hydrogen situated relatively close to the metal centre (Rh1–H = 1.649 Å) and the other two hydrogens further away (2.365 and 3.070 Å). A Rh···B distance of 2.380(4) Å is exhibited in complex **10**, which is shorter than that observed in the ^{t}Bu-analogue complex **4** (2.567(5) Å) and in the reported η^1 complex [Rh(Xantphos)$(H)_2$(η^1-$H_3B{\cdot}NMe_3$)][$BAr^F{}_4$][56] (2.759(6) Å). This shorter

Rh···B distance implies that the amine-borane fragment in complex **10** is more strongly bound to the metal centre than in complex **4**, suggesting complex **10** may be slightly less reactive. Short Rh···B distances in amine-borane sigma complexes are often indicative of η^2 complexes such as [Rh(Xantphos)(η^2,η^2-$H_2B{\cdot}NMe_3$)][$BAr^F{}_4$][56] (2.162(5) Å) and [Rh(NNN)(η^2,η^2-$H_2(CH_2CH_2{}^tBu)B{\cdot}NMe_3$)][$BAr^F{}_4$][57] (NNN = 2,6-bis-[1-(2,6-diisopropylphenylimino)ethyl]pyridine) (2.306(5) Å). Therefore, the short Rh···B distance in complex **10** may suggest η^2 binding of the amine-borane fragment rather than η^1. However, η^2 complexes also tend to exhibit acute Rh–H–B angles, for example; 87(8) ° for [Rh(Xantphos)(η^2,η^2-$H_2B{\cdot}NMe_3$)][$BAr^F{}_4$] and 93(3) ° for [Rh(NNN)(η^2,η^2-$H_2(CH_2CH_2{}^tBu)B{\cdot}NMe_3$)][$BAr^F{}_4$]. The calculated Rh–H–B angle for complex **10** is 104.6 °, which is significantly larger than for a typical η^2 complex, consistent with an η^1 binding mode.

The environment around the metal centre in complex **10** exhibits the expected pseudo-square planar geometry, with a near linear P1–Rh1–P2 angle (160.91(3) °) and calculated N2–Rh1–H angle (162.7 °). In comparison, complex **4** exhibits slightly more square planar geometry as the respective P1–Rh1–P2 (161.63(3) °) and N2–Rh1–H1 angles (172.6(17) °) are closer to 180 °. The Rh–P bond distances are also slightly longer in complex **4** (2.2832(9) and 2.2594(9) Å) compared to complex **10** (2.2483(6) and 2.2546(6) Å). These differences may be explained by the increased steric pressure from the ^{t}Bu groups compared to the Cy groups forcing a more square planar geometry in complex **4** compared to that of complex **10**.

As described, synthesis of complex **10** did not form pure material and recrystallisation techniques produced very low yields. Therefore, due to the difficulty in isolating complex **10** and time constraints, the reactivity of complex **10** was not investigated.

In summary, this section has probed the substitution of the *tert*-butyl groups in the $^{t\text{Bu}}$PONOP ligand for cyclohexyl groups. Rh($^{\text{Cy}}$PONOP)Cl (**7**) was synthesised and employed in the attempted synthesis of [Rh($^{\text{Cy}}$PONOP)(κ^1-N_2)][BAr^F_4] (**8**) and [Rh($^{\text{Cy}}$PONOP)(η^2-H_2)][BAr^F_4] (**9**), which led to the observation of complexes **8** and **9** by NMR spectroscopy and ESI-MS; however, complexes **8** and **9** were unable to be isolated. The amine-borane sigma-complex [Rh($^{\text{Cy}}$PONOP)(η^1-$H_3B{\cdot}NMe_3$)][BAr^F_4] (**10**) was also synthesised and characterised by NMR spectroscopy and single crystal X-ray diffraction; however, complex **10** was unable to be isolated in sufficient yields to allow further study.

2.9 Conclusions

In this chapter, a novel η^1 sigma amine-borane complex, [Rh(PONOP)(η^1-$H_3B{\cdot}NMe_3$)][BAr^F_4] (**4**), has been synthesised and fully characterised. This complex can act as a model for other amine-borane sigma complexes that are postulated as intermediates during the dehydrocoupling of amine-boranes. Upon reaction of complex **4** with H_2 or D_2, it was found that the weakly bound $H_3B{\cdot}NMe_3$ could be easily displaced, highlighting the potential of the cationic fragment {Rh(PONOP)}$^+$ as a catalyst for the dehydrocoupling of amine-boranes. Also, H/D exchange was observed to occur with complex **4** in the presence of D_2, suggesting B–H activation

is possible. However, boron-boron homocoupling did not take place when complex **4** was reacted with an excess of $H_3B{\cdot}NMe_3$, proposed to be due to the lack of favourable steric and electronic properties when using the PONOP ligand.

Reactions of complexes **1**, **2** and **4** with one equivalent of $H_3B{\cdot}NMe_2H$ all yielded the thermodynamic dehydrocoupled product $[H_2BNMe_2]_2$. Several intermediates were observed during the reactions using ^{11}B NMR spectroscopy, such as $H_2B{=}NMe_2$, $[H_2B(NMe_2H)_2][BAr^F{}_4]$, $H_2B(NMe_2)_2H$ and $HB(NMe_2)_2$. The novel amine-borane complex $[Rh(PONOP)(\eta^1\text{-}H_3B{\cdot}NMe_2H)][BAr^F{}_4]$ (**5**) was also observed and identified through comparison of NMR spectroscopic data to the analogous complex **4**. $^{31}P\{^1H\}$ NMR spectroscopy revealed complex mixtures of organometallic species during the reactions with complexes **2** and **4**, but not for **1**, where complex **5** was observed to form before complex **1** was regenerated. Therefore, it was decided to only use complex **1** to investigate the mechanistic pathways for the catalytic dehydrocoupling of $H_3B{\cdot}NMe_2H$, as detailed in Chapter Three.

The synthesis and full characterisation of the neutral complex Rh(PONOP)H (**6**) was also described in this chapter and the mechanism of its formation discussed. The importance of this complex as an intermediate in the catalytic dehydrocoupling of $H_3B{\cdot}NMe_2H$ is described in detail in Chapter Three. A thorough investigation into the reactivity of complex **6** under multiple conditions is outlined in Chapter Four.

Finally, the substitution of the *tert*-butyl groups in the $^{t\text{Bu}}$PONOP ligand for cyclohexyl groups was preliminarily probed with the aim of altering the steric

properties of the PONOP ligand and investigating any subsequent change on the reactivity of PONOP-supported transition metal complexes. Rh(^{Cy}PONOP)Cl (**7**) was initially synthesised and employed in the synthesis of Rh(^{Cy}PONOP)(κ^1-N_2)][BAr^F_4] (**8**), [Rh(^{Cy}PONOP)(η^2-H_2)][BAr^F_4] (**9**) and [Rh(^{Cy}PONOP)(η^1-$H_3B{\cdot}NMe_3$)][BAr^F_4] (**10**). Although complexes **8**, **9** and **10** were all observed and characterised, they were unable to be isolated cleanly and so comparisons in reactivity to the analogous complexes **1**, **2** and **4** have not yet been probed.

2.10 References

[1] T. B. Marder, *Angewandte Chemie International Edition* **2007**, *46*, 8116–8118.
[2] H. C. Johnson, T. N. Hooper, A. S. Weller, *Top.Organomet.Chem* **2015**, 153.
[3] A. L. Colebatch, A. S. Weller, *Chem. Eur. J.* **2019**, *25*, 1379–1390.
[4] I. Göttker-Schnetmann, P. S. White, M. Brookhart, *Organometallics* **2004**, *23*, 1766–1776.
[5] A. Staubitz, A. Presa Soto, I. Manners, *Angewandte Chemie International Edition* **2008**, *47*, 6212–6215.
[6] A. Staubitz, M. E. Sloan, A. P. M. Robertson, A. Friedrich, S. Schneider, P. J. Gates, J. S. auf der Günne, I. Manners, *J. Am. Chem. Soc.* **2010**, *132*, 13332–13345.
[7] E. M. Titova, E. S. Osipova, A. A. Pavlov, O. A. Filippov, S. V. Safronov, E. S. Shubina, N. V. Belkova, *ACS Catal.* **2017**, *7*, 2325–2333.
[8] P. Bhattacharya, J. A. Krause, H. Guan, *J. Am. Chem. Soc.* **2014**, *136*, 11153–11161.
[9] T.-P. Lin, J. C. Peters, *J. Am. Chem. Soc.* **2013**, *135*, 15310–15313.
[10] D. Han, M. Joksch, M. Klahn, A. Spannenberg, H.-J. Drexler, W. Baumann, H. Jiao, R. Knitsch, M. R. Hansen, H. Eckert, et al., *Dalton Trans.* **2016**, *45*, 17697–17704.
[11] S. Bhunya, T. Malakar, G. Ganguly, A. Paul, *ACS Catal.* **2016**, *6*, 7907–7934.
[12] G. M. Adams, A. L. Colebatch, J. T. Skornia, A. I. McKay, H. C. Johnson, G. C. Lloyd−Jones, S. A. Macgregor, N. A. Beattie, A. S. Weller, *J. Am. Chem. Soc.* **2018**, *140*, 1481–1495.
[13] W. H. Bernskoetter, S. K. Hanson, S. K. Buzak, Z. Davis, P. S. White, R. Swartz, K. I. Goldberg, M. Brookhart, *J. Am. Chem. Soc.* **2009**, *131*, 8603–8613.
[14] R. Dallanegra, A. P. M. Robertson, A. B. Chaplin, I. Manners, A. S. Weller, *Chem. Commun.* **2011**, *47*, 3763–3765.
[15] H. C. Johnson, E. M. Leitao, G. R. Whittell, I. Manners, G. C. Lloyd-Jones, A. S. Weller, *J. Am. Chem. Soc.* **2014**, *136*, 9078–9093.
[16] G. M. Adams, D. E. Ryan, N. A. Beattie, A. I. McKay, G. C. Lloyd-Jones, A. S. Weller, *ACS Catal.* **2019**, *9*, 3657–3666.

[17] R. Castro-Rodrigo, S. Chakraborty, L. Munjanja, W. W. Brennessel, W. D. Jones, *Organometallics* **2016**, *35*, 3124–3131.
[18] S. Mazza, R. Scopelliti, X. Hu, *Organometallics* **2015**, *34*, 1538–1545.
[19] W. Li, J.-H. Xie, H. Lin, Q.-L. Zhou, *Green Chem.* **2012**, *14*, 2388–2390.
[20] M. Rubio, A. Suárez, E. Vega, E. Álvarez, J. Díez, M. P. Gamasa, A. Pizzano, *European Journal of Inorganic Chemistry* **2012**, *2012*, 655–663.
[21] S. Kundu, W. W. Brennessel, W. D. Jones, *Inorg. Chem.* **2011**, *50*, 9443–9453.
[22] M. Findlater, K. M. Schultz, W. H. Bernskoetter, A. Cartwright-Sykes, D. M. Heinekey, M. Brookhart, *Inorg. Chem.* **2012**, *51*, 4672–4678.
[23] M. D. Walter, P. S. White, C. K. Schauer, M. Brookhart, *J. Am. Chem. Soc.* **2013**, *135*, 15933–15947.
[24] W. H. Bernskoetter, C. K. Schauer, K. I. Goldberg, M. Brookhart, *Science* **2009**, *326*, 553–556.
[25] G. Alcaraz, S. Sabo-Etienne, *Angewandte Chemie International Edition* **2010**, *49*, 7170–7179.
[26] A. T. Lubben, J. S. McIndoe, A. S. Weller, *Organometallics* **2008**, *27*, 3303–3306.
[27] R. Langer, G. Leitus, Y. Ben-David, D. Milstein, *Angewandte Chemie International Edition* **2011**, *50*, 2120–2124.
[28] J. Zhang, G. Leitus, Y. Ben-David, D. Milstein, *Angewandte Chemie International Edition* **2006**, *45*, 1113–1115.
[29] R. J. Trovitch, E. Lobkovsky, P. J. Chirik, *Inorg. Chem.* **2006**, *45*, 7252–7260.
[30] C. Gunanathan, D. Milstein, *Acc. Chem. Res.* **2011**, *44*, 588–602.
[31] M. A. Iron, E. Ben-Ari, R. Cohen, D. Milstein, *Dalton Trans.* **2009**, 9433–9439.
[32] J. F. Hartwig, *Organotransition Metal Chemistry: From Bonding to Catalysis*, University Science Books, **2010**.
[33] G. M. Adams, F. M. Chadwick, S. D. Pike, A. S. Weller, *Dalton Trans.* **2015**, *44*, 6340–6342.
[34] S. H. Strauss, *Chem. Rev.* **1993**, *93*, 927–942.
[35] H. Kobayashi, T. Sonoda, H. Iwamoto, M. Yoshimura, *Chem. Lett.* **1981**, *10*, 579–580.
[36] A. J. Martínez-Martínez, A. S. Weller, *Dalton Trans.* **2019**, *48*, 3551–3554.
[37] G. Alcaraz, A. B. Chaplin, C. J. Stevens, E. Clot, L. Vendier, A. S. Weller, S. Sabo-Etienne, *Organometallics* **2010**, *29*, 5591–5595.
[38] C. J. Stevens, R. Dallanegra, A. B. Chaplin, A. S. Weller, S. A. Macgregor, B. Ward, D. McKay, G. Alcaraz, S. Sabo-Etienne, *Chem. Eur. J.* **2011**, *17*, 3011–3020.
[39] Y. Gloaguen, G. Bénac-Lestrille, L. Vendier, U. Helmstedt, E. Clot, G. Alcaraz, S. Sabo-Etienne, *Organometallics* **2013**, *32*, 4868–4877.
[40] A. Van Der Ent, A. L. Onderdelinden, R. A. Schunn, in *Inorganic Syntheses*, John Wiley & Sons, Inc., **1990**, pp. 90–92.
[41] W. H. Bernskoetter, C. K. Schauer, K. I. Goldberg, M. Brookhart, *Science* **2009**, *326*, 553–556.
[42] H. Aneetha, M. Jiménez-Tenorio, M. C. Puerta, P. Valerga, K. Mereiter, *Organometallics* **2002**, *21*, 628–635.
[43] M. C. Denney, V. Pons, T. J. Hebden, D. M. Heinekey, K. I. Goldberg, *J. Am. Chem. Soc.* **2006**, *128*, 12048–12049.

[44] M. Shimoi, S. Nagai, M. Ichikawa, Y. Kawano, K. Katoh, M. Uruichi, H. Ogino, *J. Am. Chem. Soc.* **1999**, *121*, 11704–11712.
[45] T. M. Douglas, A. B. Chaplin, A. S. Weller, X. Yang, M. B. Hall, *J. Am. Chem. Soc.* **2009**, *131*, 15440–15456.
[46] P. S. Pregosin, *NMR in Organometallic Chemistry*, Wiley-VCH, **2012**.
[47] A. G. Algarra, L. J. Sewell, H. C. Johnson, S. A. Macgregor, A. S. Weller, *Dalton Trans.* **2014**, *43*, 11118–11128.
[48] Y. Kawano, T. Kakizawa, K. Yamaguchi, M. Shimoi, *Chem. Lett.* **2006**, *35*, 568–569.
[49] Y. Kawano, M. Hashiva, M. Shimoi, *Organometallics* **2006**, *25*, 4420–4426.
[50] G. Alcaraz, S. Sabo-Etienne, *Coordination Chemistry Reviews* **2008**, *252*, 2395–2409.
[51] G. J. Kubas, *Metal Dihydrogen and σ-Bond Complexes*, Springer US, **2001**.
[52] N. Merle, G. Koicok-Köhn, M. F. Mahon, C. G. Frost, G. D. Ruggerio, A. S. Weller, M. C. Willis, *Dalton Trans.* **2004**, 3883–3892.
[53] A. S. Weller, F. M. Chadwick, A. I. McKay, in *Advances in Organometallic Chemistry* (Ed.: P.J. Pérez), Academic Press, **2016**, pp. 223–276.
[54] Y. Kawano, K. Yamaguchi, S. Miyake, T. Kakizawa, M. Shimoi, *Chemistry – A European Journal* **2007**, *13*, 6920–6931.
[55] A. J. Martínez-Martínez, B. E. Tegner, A. I. McKay, A. J. Bukvic, N. H. Rees, G. J. Tizzard, S. J. Coles, M. R. Warren, S. A. Macgregor, A. S. Weller, *J. Am. Chem. Soc.* **2018**, *140*, 14958–14970.
[56] H. C. Johnson, C. L. McMullin, S. D. Pike, S. A. Macgregor, A. S. Weller, *Angew. Chem. Int. Ed.* **2013**, *52*, 9776–9780.
[57] A. Johnson, A. J. Martínez-Martínez, S. A. Macgregor, A. S. Weller, *Dalton Trans.* **2019**, *48*, 9776–9781.
[58] Peter. J. Hore, *Nuclear Magnetic Resonance*, Oxford University Press, Oxford, New York, **1994**.
[59] J. Y.-C. Chen, A. A. Martí, N. J. Turro, K. Komatsu, Y. Murata, R. G. Lawler, *J. Phys. Chem. B* **2010**, *114*, 14689–14695.
[60] A. B. Chaplin, A. S. Weller, *Organometallics* **2011**, *30*, 4466–4469.
[61] R. N. Perutz, S. Sabo-Etienne, *Angewandte Chemie International Edition* **2007**, *46*, 2578–2592.
[62] H. Braunschweig, R. D. Dewhurst, *Angewandte Chemie International Edition* **2013**, *52*, 3574–3583.
[63] S.-K. Kim, W.-S. Han, T.-J. Kim, T.-Y. Kim, S. W. Nam, M. Mitoraj, Ł. Piekoś, A. Michalak, S.-J. Hwang, S. O. Kang, *J. Am. Chem. Soc.* **2010**, *132*, 9954–9955.
[64] E. W. Corcoran, L. G. Sneddon, *J. Am. Chem. Soc.* **1984**, *106*, 7793–7800.
[65] E. W. Corcoran, L. G. Sneddon, *J. Am. Chem. Soc.* **1985**, *107*, 7446–7450.
[66] O. Ciobanu, E. Kaifer, M. Enders, H.-J. Himmel, *Angewandte Chemie International Edition* **2009**, *48*, 5538–5541.
[67] H. Braunschweig, C. Claes, F. Guethlein, *Journal of Organometallic Chemistry* **2012**, *706–707*, 144–145.
[68] M. Roselló-Merino, J. López-Serrano, S. Conejero, *J. Am. Chem. Soc.* **2013**, *135*, 10910–10913.

[69] O. J. Metters, A. M. Chapman, A. P. M. Robertson, C. H. Woodall, P. J. Gates, D. F. Wass, I. Manners, *Chem. Commun.* **2014**, *50*, 12146–12149.
[70] H. Nöth, H. Vahrenkamp, *Chemische Berichte* **1967**, *100*, 3353–3362.
[71] T. M. Douglas, A. B. Chaplin, A. S. Weller, *J. Am. Chem. Soc.* **2008**, *130*, 14432–14433.
[72] D. K. Srivastava, L. K. Krannich, C. L. Watkins, *Inorg. Chem.* **1991**, *30*, 2441–2444.
[73] L. K. Krannich, C. L. Watkins, D. K. Srivastava, R. K. Kanjolia, *Coordination Chemistry Reviews* **1992**, *112*, 117–129.
[74] H. Nöth, H. Vahrenkamp, *Chemische Berichte* **1966**, *99*, 1049–1067.
[75] P. Bellham, M. S. Hill, G. Kociok-Köhn, D. J. Liptrot, *Chem. Commun.* **2013**, *49*, 1960–1962.
[76] M. Roselló-Merino, R. J. Rama, J. Díez, S. Conejero, *Chem. Commun.* **2016**, *52*, 8389–8392.
[77] G. B. Fisher, J. C. Fuller, J. Harrison, S. G. Alvarez, E. R. Burkhardt, C. T. Goralski, B. Singaram, *J. Org. Chem.* **1994**, *59*, 6378–6385.
[78] S. P. Semproni, C. Milsmann, P. J. Chirik, *J. Am. Chem. Soc.* **2014**, *136*, 9211–9224.
[79] M. Feller, U. Gellrich, A. Anaby, Y. Diskin-Posner, D. Milstein, *Journal of the American Chemical Society* **2016**, *138*, 6445–6454.
[80] L. M. Guard, T. J. Hebden, D. E. Linn, D. M. Heinekey, *Organometallics* **2017**, *36*, 3104–3109.
[81] W. D. Bailey, W. Kaminsky, R. A. Kemp, K. I. Goldberg, *Organometallics* **2014**, *33*, 2503–2509.
[82] D. J. Liptrot, M. S. Hill, M. F. Mahon, D. J. MacDougall, *Chemistry – A European Journal* **2010**, *16*, 8508–8515.
[83] P. Bellham, M. D. Anker, M. S. Hill, G. Kociok-Köhn, M. F. Mahon, *Dalton Trans.* **2016**, *45*, 13969–13978.
[84] M. E. van der Boom, D. Milstein, *Chem. Rev.* **2003**, *103*, 1759–1792.
[85] M. Mastalir, M. Glatz, B. Stöger, M. Weil, E. Pittenauer, G. Allmaier, K. Kirchner, *Inorganica Chimica Acta* **2017**, *455*, 707–714.
[86] S. R. M. M. de Aguiar, B. Stöger, E. Pittenauer, G. Allmaier, L. F. Veiros, K. Kirchner, *Dalton Trans.* **2016**, *45*, 13834–13845.
[87] C. A. Tolman, *J. Am. Chem. Soc.* **1970**, *92*, 2956–2965.
[88] P. B. Dias, M. E. M. de Piedade, J. A. M. Simões, *Coordination Chemistry Reviews* **1994**, *135–136*, 737–807.

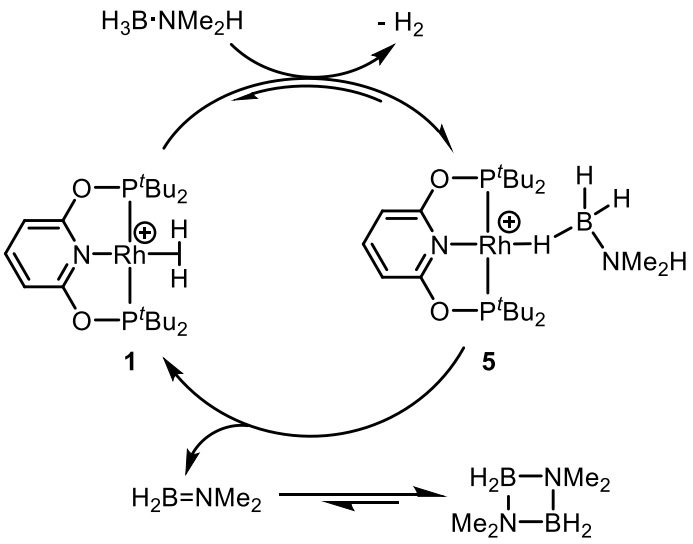
3 Catalytic dehydrogenation of $H_2B{\cdot}NMe_2H$ using $[Rh(PONOP)(\eta^2\text{-}H_2)][BAr^F{}_4]$

3.1 Introduction

Polyaminoboranes, $[H_2BNRH]_n$, are novel materials that are isoelectronic with societally and technologically ubiquitous polyolefins.[1] They are formed from the dehydrocoupling of primary amine-boranes, $H_3B{\cdot}NRH_2$, via the loss of one equivalent of H_2.[2] In order to optimise the catalytic synthesis of polyaminoboranes, understanding of the precise mechanistic detail of the catalytic cycles operating is required. There are several challenges that are presented in the study of the mechanism of dehydropolymerisation of the primary amine-borane $H_3B{\cdot}NMeH_2$. For example, the necessity for low catalyst loadings in order to avoid borazine ($[HBNR]_3$) formation makes catalyst speciation studies challenging.[3] Also, there is potential for insoluble polymeric products. Employing the secondary amine-borane, $H_3B{\cdot}NMe_2H$, instead allows for in-depth mechanistic study of the dehydrocoupling of amine-boranes due to the dehydrocoupling product, $[H_2BNMe_2]_2$, being well-defined, soluble and relatively unaffected by catalyst loadings. In addition, the putative intermediate, $H_2B{=}NMe_2$, is longer lived than the primary analogue, $H_2B{=}NMeH$, and can be easily observed by NMR spectroscopy.[4,5]

Chapter Two described the stoichiometric reactions of the tertiary amine-borane $H_3B{\cdot}NMe_3$ and the secondary amine-borane $H_3B{\cdot}NMe_2H$ with the cationic rhodium complex $[Rh(PONOP)(\eta^2\text{-}H_2)][BAr^F{}_4]$ (**1**). Sigma amine-borane complex formation to give $[Rh(PONOP)(\eta^1\text{-}H_3B{\cdot}NMe_2R)][BAr^F{}_4]$ (R = Me (**4**) or H (**5**)), via the loss of H_2,

was observed in both cases. B–H activation and competitive H_2 binding was also demonstrated. For the reaction with $H_3B{\cdot}NMe_2H$, the amine-borane was fully dehydrocoupled to give $[H_2BNMe_2]_2$ and complex **1** was reformed (**Scheme 3.1**).



Scheme 3.1 Initial suggested pathway for the reaction of complex **1** with $H_3B{\cdot}NMe_2H$ in 1,2-$F_2C_6H_4$. $[BAr^F{}_4]^-$ anions omitted for clarity.

Following on from the stoichiometric reactivity between complex **1** and these model amine-boranes, this chapter presents a detailed study on the reactivity between complex **1** and $H_3B{\cdot}NMe_2H$ under catalytic conditions. Speciation studies and kinetic measurements are described and the potential roles of amine (NMe_2H), boronium ($[H_2B(NMe_2H)_2][BAr^F{}_4]$), ammonium ($[NMe_2H_2][BAr^F{}_4]$) and Rh(PONOP)H (**6**) are investigated. Ultimately a mechanism is proposed for catalytic dehydrocoupling of $H_3B{\cdot}NMe_2H$ with complex **1**.

3.2 Trial reactivity under catalytic conditions

In order to probe [Rh(PONOP)(η²-H₂)][BArᶠ₄] (**1**) as a pre-catalyst for the dehydrocoupling of H₃B·NMe₂H under catalytic conditions, a repeat of the stoichiometric reactivity described in section 2.6.1 was carried out, but with the addition of 10 equivalents of H₃B·NMe₂H.

In a high pressure NMR tube, complex **1** (36 mM in 1,2-F₂C₆H₄, 10 mol% catalyst loading) catalysed the dehydrocoupling of H₃B·NMe₂H (0.36 M) fully within 15 minutes to yield [H₂BNMe₂]₂ as the major product, as observed by ¹¹B NMR spectroscopy (**Figure 3.1**).

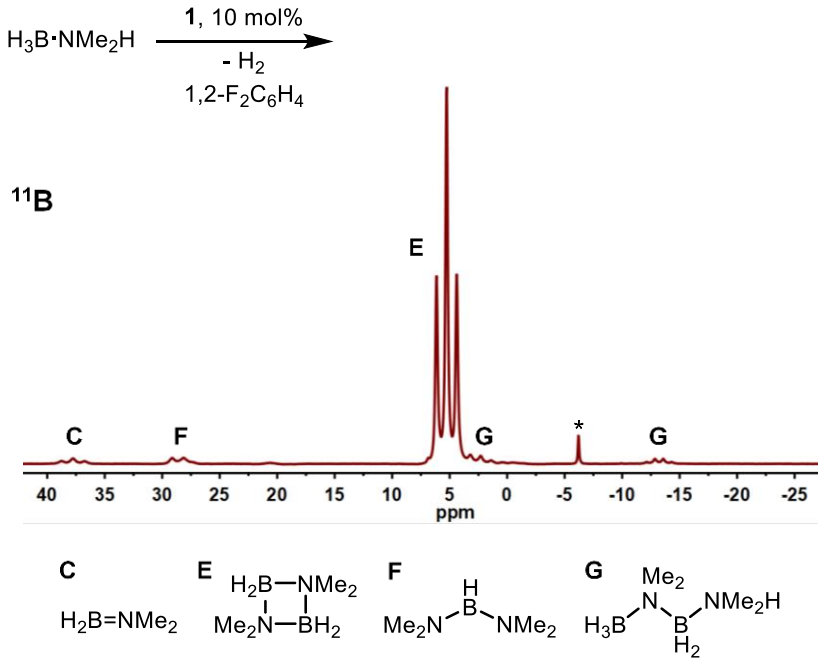


Figure 3.1 ¹¹B NMR spectrum (128 MHz, 1,2-F₂C₆H₄, 298 K) after 15 minutes of reactivity between complex **1** and 10 eq. H₃B·NMe₂H. * = [BArᶠ₄]⁻ anion.

In the ^{11}B NMR spectrum depicted in **Figure 3.1**, $[H_2BNMe_2]_2$ can be observed as the major product at δ 5.3 ppm (t, $^1J_{BH}$ = 112 Hz).[6] A small amount (~3 %) of the transient intermediate $H_2B{=}NMe_2$ (δ 37.8 ppm, t, $^1J_{BH}$ = 129 Hz)[4,7] remains at the end of catalysis, which is expected as $H_2B{=}NMe_2$ dimerises to give $[H_2BNMe_2]_2$ under a second order rate law and so would be expected to be persistent at low concentrations.[4] The side product, $HB(NMe_2)_2$ (d, δ 28.7 ppm, $^1J_{BH}$ = 130 Hz)[8] is also observed along with a very small amount (~3 %) of the linear diborazane, $H_3B{\cdot}NMe_2H_2B{\cdot}NMe_2H$ (δ 2.3 ppm, t, $^1J_{BH}$ = 110 Hz, BH_2 and δ –13.2 ppm, q, $^1J_{BH}$ = 94 Hz, BH_3).[6] Linear diborazane has been previously reported as a viable intermediate in the transition metal-catalysed dehydrocoupling of $H_3B{\cdot}NMe_2H$.[9–11] For example, $H_3B{\cdot}NMe_2H_2B{\cdot}NMe_2H$ may be formed, cleaved and dehydrocyclised to give $[H_2BNMe_2]_2$ during the catalytic dehydrocoupling of $H_3B{\cdot}NMe_2H$ with $\{Rh(PCy_3)L_n\}^+$ (L_n = solvent or agostic interaction).[12] However, other than $[H_2BNMe_2]_2$, these products are observed in such small amounts that they are considered not to be important in describing the gross mechanism.

Given the ability of complex **1** to successfully catalyse the dehydrocoupling of $H_3B{\cdot}NMe_2H$, further studies were undertaken to elucidate the precise mechanism of this process.

3.3 Speciation studies under closed conditions

In order to gain insight into the organometallic species that are formed during the catalytic dehydrocoupling of $H_3B{\cdot}NMe_2H$ with $[Rh(PONOP)(\eta^2\text{-}H_2)][BAr^F{}_4]$ (**1**),

speciation studies were carried out, which involved following the reaction progress using NMR spectroscopy.

In a high pressure NMR tube, a solution of complex **1** in 1,2-$F_2C_6H_4$ (2.9 mM, 4 mol% catalyst loading) was added to 25 equivalents of $H_3B{\cdot}NMe_2H$ (72 mM). The reaction mixture was frozen in liquid N_2 until the NMR spectrometer was available at which point the solution was thawed and the reaction progress followed *in situ* using $^{31}P\{^1H\}$ NMR spectroscopy. The time course plot for the reaction is depicted in **Figure 3.2**. The concentrations of the organometallic species are derived from the relative integrals in the $^{31}P\{^1H\}$ NMR spectra, assuming no leaching of phosphorus into NMR-silent material during catalysis.

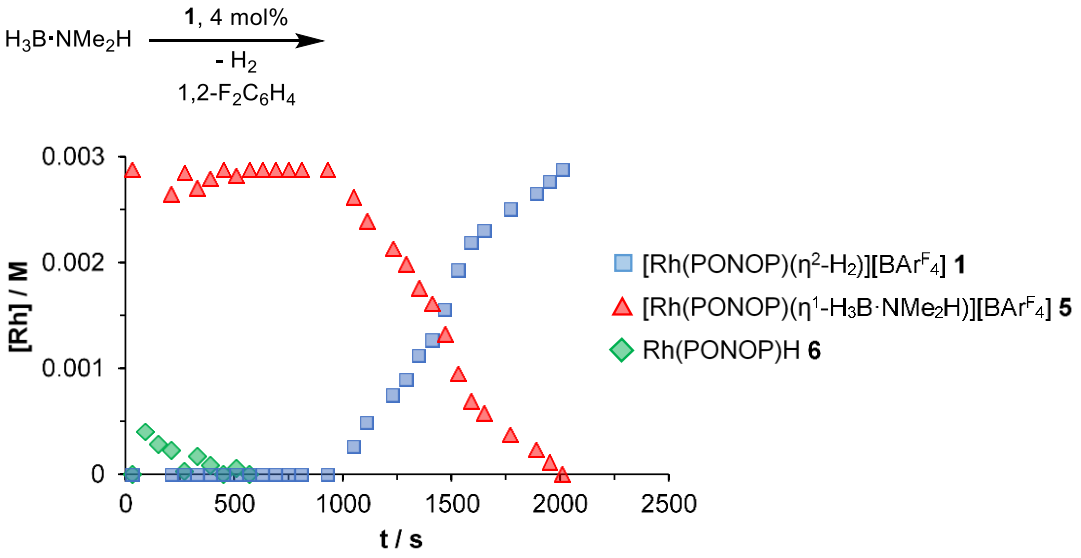


Figure 3.2 Time course plot for the catalytic dehydrocoupling of $H_3B{\cdot}NMe_2H$ (72 mM, 1,2-$F_2C_6H_4$, 298 K) with complex **1** (2.9 mM, 4 mol%) as measured *in situ* using $^{31}P\{^1H\}$ NMR spectroscopy.

The $^{31}P\{^{1}H\}$ NMR spectra recorded during catalysis showed the reaction going to completion in ~2010 s and essentially the same reaction progress is observed as during the stoichiometric reaction between complex **1** and $H_3B{\cdot}NMe_2H$ as described in section 2.6.1. Initially, immediate formation of the amine-borane sigma complex [Rh(PONOP)(η^1-$H_3B{\cdot}NMe_2H$)][BAr^F_4] (**5**) is observed, with no signal present for complex **1**, suggesting complex **5** is the resting state on the catalytic cycle at high concentrations of $H_3B{\cdot}NMe_2H$. After 15 minutes, complex **1** begins to reform as $H_3B{\cdot}NMe_2H$ is dehydrocoupled, potentially due to H_2 build up in the reaction headspace. Complex **1** remains the major organometallic species for the rest of catalysis, suggesting it is the resting state at low to medium concentrations of $H_3B{\cdot}NMe_2H$. During the early stages of the reaction, a third complex with a signal at δ 225.4 ppm (d, 170 Hz) is observed in the $^{31}P\{^{1}H\}$ NMR spectra in a small amount (~10 %) and is then consumed before complex **1** starts to reform. The ^{1}H NMR spectra of a repeat reaction show a broad signal in the hydride region at δ –10.13 ppm that follows the same profile. This species is identified as the neutral monohydride Rh(PONOP)H (**6**), by comparison with independently synthesised **6** (described in section 2.7). There is a slight difference in chemical shift between complex **6** observed in catalysis and independently synthesised **6** ($^{31}P\{^{1}H\}$ δ 226.2 ppm, ^{1}H δ –9.6 ppm), suggesting the possibility of secondary [Rh]–H···H–X interactions during catalysis.[13] This will be discussed further at the end of this chapter (section 3.11).

Catalysis was repeated under identical conditions and the reaction progress was monitored by ^{11}B NMR spectroscopy instead. The resulting time course plot for the boron-containing species is depicted below in **Figure 3.3**.

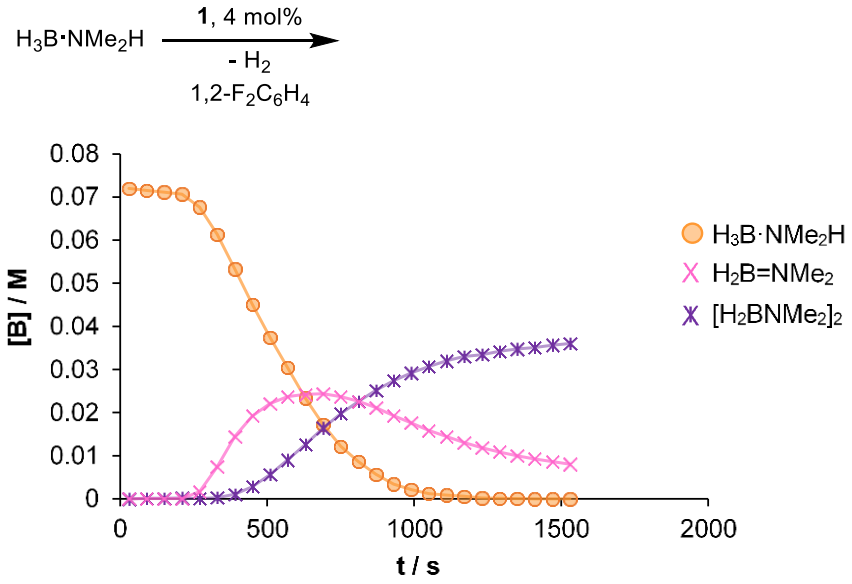


Figure 3.3 Time course plot for the catalytic dehydrocoupling of $H_3B{\cdot}NMe_2H$ (72 mM, 1,2-$F_2C_6H_4$, 298 K) with complex **1** (4 mol%) as measured *in situ* using ^{11}B NMR spectroscopy.

The time course plot derived from ^{11}B NMR spectra reflects the overall reaction progress discussed in Chapter Two (section 2.6.1) for the stoichiometric reaction between complex **1** and $H_3B{\cdot}NMe_2H$, with the expected consumption of $H_3B{\cdot}NMe_2H$ throughout the reaction to yield $[H_2BNMe_2]_2$. The gradual formation and then consumption of $H_2B{=}NMe_2$ is also observed, consistent with the profile of an intermediate. An induction period of approximately 200 s is revealed, before $H_2B{=}NMe_2$ is observed. For this sample, all of the starting amine-borane is

consumed by approximately 1300 s; however, $H_2B{=}NMe_2$ still remains due to the slow rate of dimerisation to give $[H_2BNMe_2]_2$ at low concentrations of $H_2B{=}NMe_2$.[4]

In order to investigate how the speciation of the organometallic species and the boron containing species relate to each other during catalysis, catalysis was repeated in a high pressure NMR tube and the reaction followed by interleaved $^{31}P\{^1H\}$ and ^{11}B NMR spectroscopy. As both $^{31}P\{^1H\}$ NMR spectra and ^{11}B NMR spectra were recorded for the same sample, the time course plots for both the organometallic species and the boron species can be directly compared (**Figure 3.4**). This method addresses the issues preventing the comparison of $^{31}P\{^1H\}$ NMR spectra from one sample and ^{11}B NMR spectra from another of the same reaction, as discussed for the stoichiometric reactions in section 2.6.

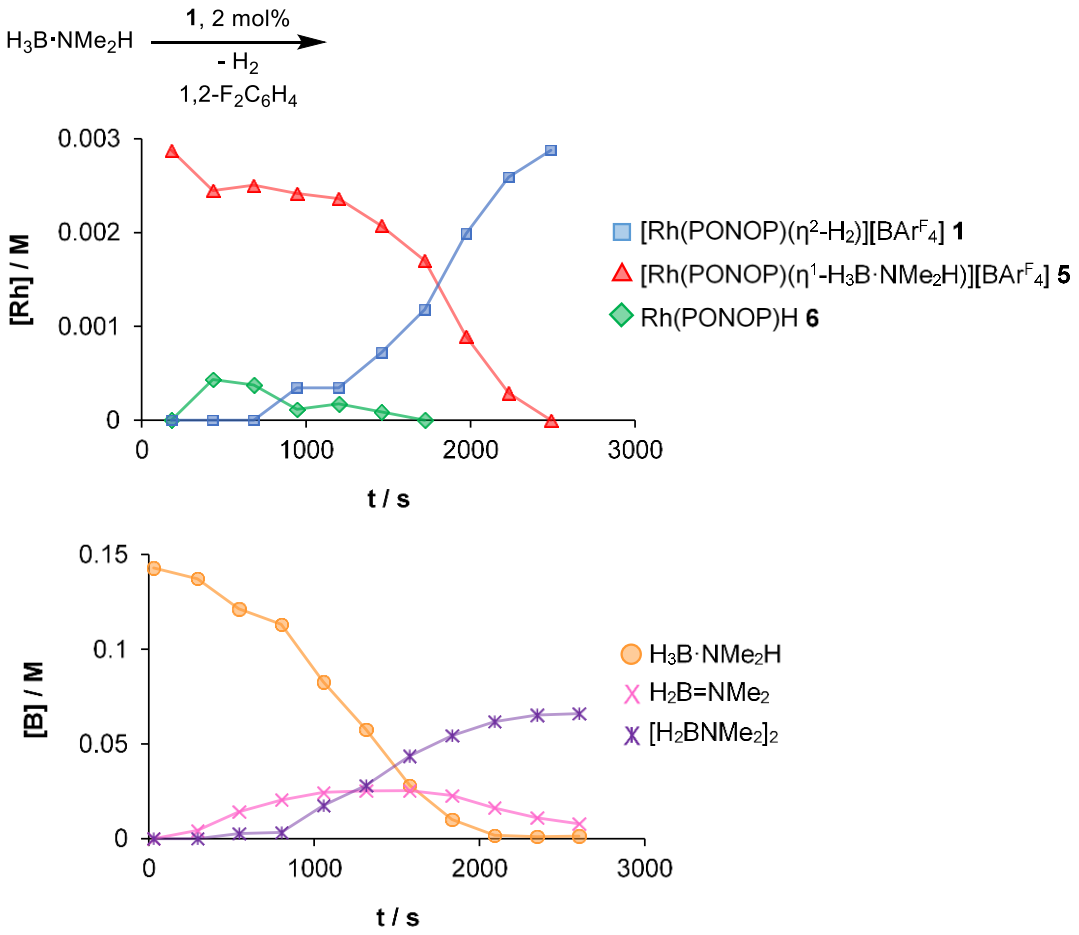


Figure 3.4 Time course plots for the dehydrocoupling of $H_3B{\cdot}NMe_2H$ (0.144 M, 1,2-$F_2C_6H_4$, 298 K) with complex **1** (2.9 mM, 2 mol%) as measured *in situ* using $^{31}P\{^1H\}$ NMR and ^{11}B NMR spectroscopy.

The time course plot for the organometallic species depicts the same overall trends as observed before (**Figure 3.2** and **Figure 3.3**). **Figure 3.4** depicts the presence of an induction period (~300 s) in the ^{11}B NMR spectra, before $H_2B{=}NMe_2$ is observed, during which time complex **5** is the major organometallic species observed in solution by $^{31}P\{^1H\}$ NMR spectroscopy. This again suggests that the amine-borane sigma complex **5** is the resting state on the catalytic cycle at high concentrations of $H_3B{\cdot}NMe_2H$. Complex **1** is only observed to reform after approximately half of

$H_3B{\cdot}NMe_2H$ has been consumed, at which point the concentration of $H_2B{=}NMe_2$ plateaus indicating catalysis is beginning to slow. This observation agrees with the suggestion that complex **1** formation depends upon the build up of H_2, produced from the dehydrocoupling of $H_3B{\cdot}NMe_2H$, and so is the resting state at low concentrations of $H_3B{\cdot}NMe_2H$. A small amount of $HB(NMe_2)_2$ (<1 %) is observed near the end of catalysis, as is also observed in stoichiometric reactions (section 2.6), however is of too small a concentration to include in the time course plots.

Further comparison of the two time course plots in **Figure 3.4** reveals that initial formation of complex **6** coincides with the initial observation of $H_2B{=}NMe_2$, which may indicate complex **6** is involved in the formation of the aminoborane intermediate. Furthermore, a signal for $H_2B(NMe_2)_2H$ (δ 0.36 ppm, $^1J_{BH}$ = 110 Hz), as observed in the stoichiometric reactions discussed in section 2.6, could also been seen to form at a similar time to, and to follow the same trend as, complex **6** (**Figure 3.5** – the concentration of $H_2B(NMe_2)_2H$ is too low compared to the other boron containing species (< 2 %) to depict clearly in **Figure 3.4**). The similarity in the concentrations and temporal profiles of complex **6** and $H_2B(NMe_2)_2H$ indicate that their formation may also be linked.

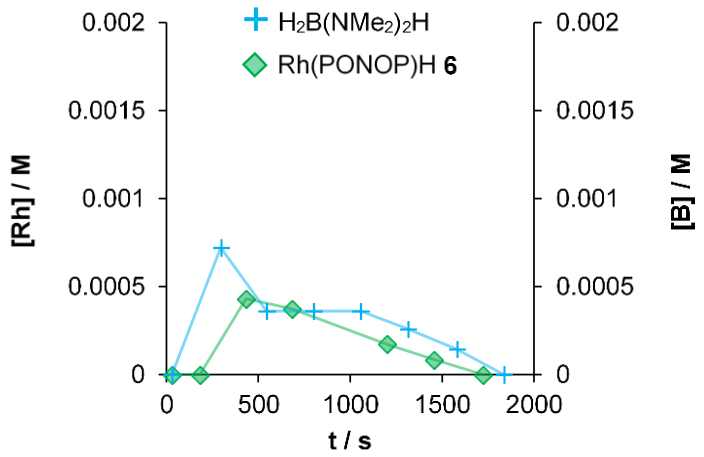
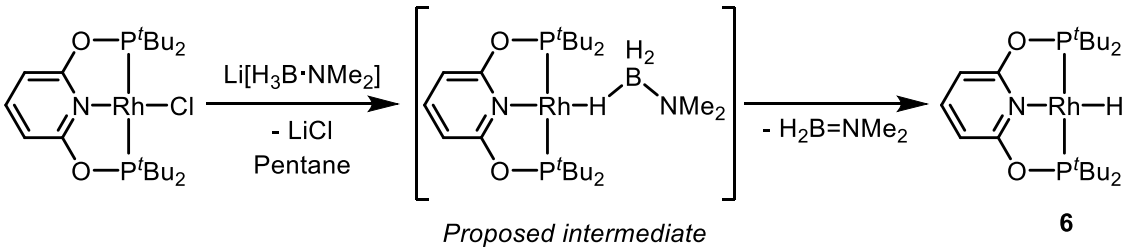


Figure 3.5 Time course plot for the dehydrocoupling of $H_3B{\cdot}NMe_2H$ (0.144 M, 1,2-$F_2C_6H_4$, 298 K) with complex **1** (2 mol%) as measured *in situ* using $^{31}P\{^1H\}$ NMR and ^{11}B NMR spectroscopy. Showing the temporal profile for complex **6** and $H_2B(NMe_2)_2H$.

3.4 Role of Rh(PONOP)H (6) in catalysis

The neutral rhodium monohydride Rh(PONOP)H (**6**) forms at the onset of the catalytic dehydrocoupling of $H_3B{\cdot}NMe_2H$ with complex **1** (2.9 mM, 2 and 4 mol%, 1,2-$F_2C_6H_4$) under closed conditions (in a sealed NMR tube), as observed by $^{31}P\{^1H\}$ NMR spectroscopy in the speciation studies discussed in section 3.3. Complex **6** was assigned by comparison to the NMR spectroscopic data of the independently-synthesised complex **6** from the reaction of Rh(PONOP)Cl with $Li[H_3B{\cdot}NMe_2]$ in pentane (section 2.7) (**Scheme 3.2**). The formation of complex **6** via this synthetic route is proposed to be via the sigma-amidoborane intermediate Rh(PONOP)(η^1-$H_3B{\cdot}NMe_2$), leading to the elimination of $H_2B{=}NMe_2$. Computational studies support this mechanistic pathway, rather than the less energetically favoured β-H

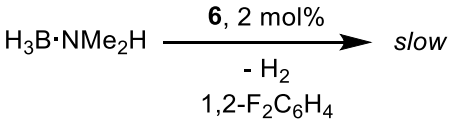
elimination from the nitrogen-bound amidoborane intermediate Rh(PONOP)($Me_2N{\cdot}BH_3$).



Scheme 3.2 Synthetic scheme for the for the stoichiometric formation of complex **6**, including the proposed amidoborane intermediate.

As complex **6** was observed to form and be present early on in catalysis, it was initially probed for its potential as the active catalyst for the dehydrocoupling of $H_3B{\cdot}NMe_2H$ (**Scheme 3.3**). In a high pressure NMR tube, complex **6** (1.44 mM, 2 mol%, 1,2-$F_2C_6H_4$) was reacted with 50 equivalents of $H_3B{\cdot}NMe_2H$ (72 mM) and the reaction progress monitored by ^{11}B and $^{31}P\{^1H\}$ NMR spectroscopy. Dehydrocoupling of $H_3B{\cdot}NMe_2H$ was observed to occur, with the ^{11}B NMR spectra showing signals for both $H_2B{=}NMe_2$ and the final product $[H_2BNMe_2]_2$. However, the reaction progressed very slowly, with consumption of only 3 % of $H_3B{\cdot}NMe_2H$ 40 minutes after time of mixing (as determined by relative integrals in the ^{11}B NMR spectra). In comparison, catalysis with complex **1** under the same conditions yielded complete consumption of $H_3B{\cdot}NMe_2H$ in the same time. Other boron-containing species, such as $H_2B(NMe_2)_2H$, $[H_2B(NMe_2H)_2][BAr^F{}_4]$ and $HB(NMe_2)_2$, which had previously been observed during the stoichiometric and catalytic speciation studies

already discussed, were not observed in the ^{11}B NMR spectra when complex **6** was used as the catalyst.

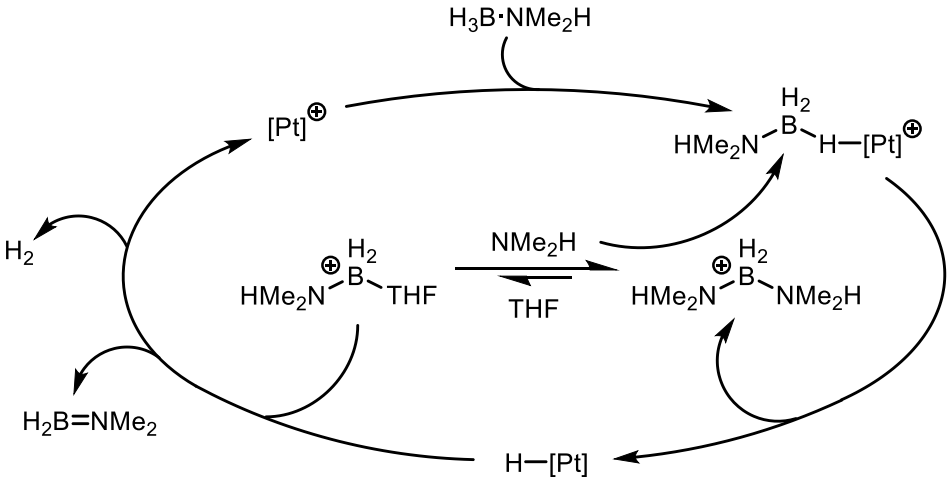


Scheme 3.3 Dehydrocoupling of complex $H_3B{\cdot}NMe_2H$ with complex **6**.

$^{31}P\{^1H\}$ NMR spectroscopy revealed that complex **6** remained the sole organometallic species present. This is different to that observed for catalysis with complex **1**, where complex **6** is only observed in small amounts (<10 %). In conclusion, the slower rate of catalysis and the variation in speciation observed suggest that Rh(PONOP)H (**6**) is a poor catalyst and is not the species responsible for the dehydrocoupling of $H_3B{\cdot}NMe_2H$ that occurs upon its reaction with complex **1**. DFT calculations discussed at the end of this chapter (section 3.11) are consistent with complex **6** being a poor dehydrocoupling catalyst.

As complex **6** is therefore not acting as the sole active species for the dehydrocoupling of $H_3B{\cdot}NMe_2H$ in the presence of complex **1**, the precise role of complex **6** (in terms of formation and reactivity) was investigated further. Hydride transfer from amine-boranes to cation transition metal centres to yield neutral hydride complexes has been reported in the literature.[14,15] There have also been several reports of the formation of neutral monohydrides alongside the formation of boronium species.[16–18] For example, in 2013 Conejero *et al*. proposed a mechanism for the catalytic dehydrocoupling of $H_3B{\cdot}NMe_2H$ with a platinum-based

system involving the formation of a neutral platinum monohydride alongside the boronium cation, $\{H_2B(NMe_2H)_2\}^+$ (**Scheme 3.4**).[19]

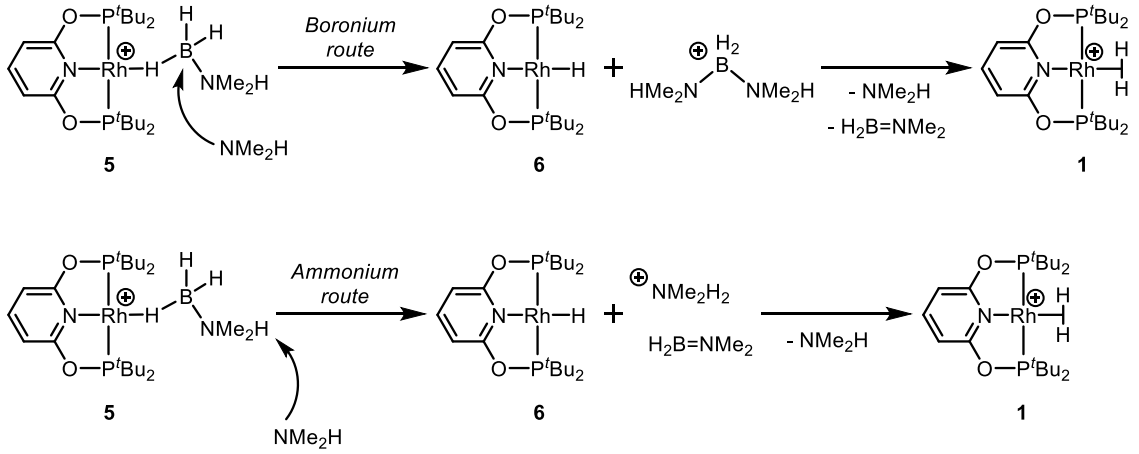


Scheme 3.4 Proposed mechanism for the dehydrocoupling of $H_3B{\cdot}NMe_2H$ with $[Pt(I^tBu)(I^tBu')][BAr^F_4]$ (= [Pt]).[19] $[BAr^F_4]^-$ anions omitted for clarity.

In this instance, and for other examples such as catalysis with $\{Rh(Xantphos)\}^+$[20] and $\{Rh(DPEphos)\}^+$[21] systems, free amine (from the B–N bond cleavage of amine-borane) is proposed to interact with an amine-borane sigma complex and promote the formation of the monohydride alongside a boronium species. Furthermore, for the $\{Rh(DPEphos)\}^+$ catalysed dehydropolymerisation of $H_3B{\cdot}NMeH_2$ it was shown that the addition of $NMeH_2$ removed the induction period that had been observed prior to significant product production.[21]

As an induction period was observed during the speciation studies for the catalytic dehydrocoupling of $H_3B{\cdot}NMe_2H$ with complex **1** (section 3.3), a similar mechanistic pathway as reported in the literature could be occurring for this system. Furthermore, the boronium cation $\{H_2B(NMe_2H)_2\}^+$ was observed in the ^{11}B NMR

spectra (albeit in relatively low concentration) early on in the stoichiometric reaction between $H_3B{\cdot}NMe_2H$ and complex **1**, again suggesting a similar boronium-based route as depicted in **Scheme 3.4**; however, this may not be the only route available. Such a "boronium route" could operate by attack of NMe_2H (from the dissociation of amine-borane in solution)[22,23] at the boron in the amine-borane sigma complex $[Rh(PONOP)(\eta^1\text{-}H_3B{\cdot}NMe_2H)][BAr^F{}_4]$ (**5**) to yield the rhodium monohydride (**6**) alongside boronium (**Scheme 3.5**). This could be followed by reprotonation of complex **6** by boronium to regenerate complex **1** alongside $H_2B(NMe_2)_2H$, which releases $H_2B{=}NMe_2$ and regenerates NMe_2H. However, an alternative mechanistic pathway, that up until this point had not been considered by ourselves or others, may also be viable: the so called "ammonium route" (**Scheme 3.5**). This could involve the deprotonation of complex **5** by free amine to form ammonium $[NMe_2H_2][BAr^F{}_4]$, $H_2B{=}NMe_2$ and complex **6**. In this case ammonium may act to reprotonate complex **6** to regenerate complex **1** alongside NMe_2H.



Scheme 3.5 Possible mechanistic pathways for the formation of complex **6** from the reaction of complex **1** $H_3B{\cdot}NMe_2H$ in 1,2-$F_2C_6H_5$. $[BAr^{F}{}_4]^-$ anions omitted for clarity.

In order to probe the viability of each of these routes, complex **6** was reacted stoichiometrically with boronium and with ammonium to investigate the regeneration of complex **1** from **6**.

In an NMR tube, complex **6** (0.04 M, 1,2-$F_2C_6H_4$) was reacted with one equivalent of $[H_2B(NMe_2H)_2][BAr^{F}{}_4]$ and the reaction progress was monitored *in situ* using NMR spectroscopy (**Figure 3.6**).

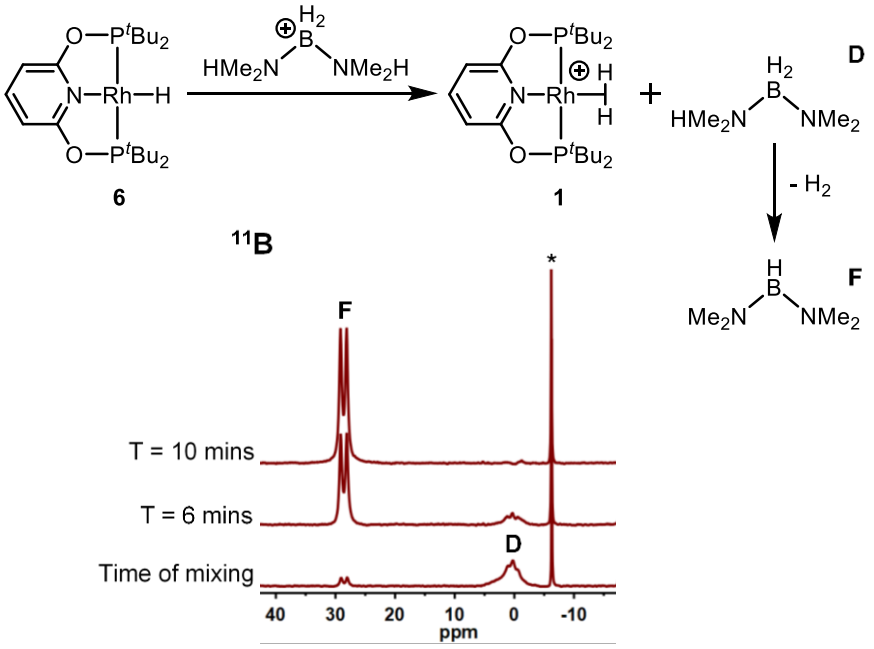


Figure 3.6 Reaction of complex **6** (0.04 M, 1,2-$F_2C_6H_4$) with 1 eq. $[H_2B(NMe_2H)_2][BAr^F{}_4]$. Stacked ^{11}B NMR spectra (128 MHz, 1,2-$F_2C_6H_4$, 298 K) over time. * = $[BAr^F{}_4]^-$ (anions omitted from scheme for clarity).

$^{31}P\{^1H\}$ NMR spectra showed the immediate and total formation of complex **1**, demonstrating the ease at which complex **1** can be regenerated by the addition of boronium. In the ^{11}B NMR, a triplet corresponding to $H_2B(NMe_2)_2H$ (**D**), the deprotonated analogue of boronium, was also immediately observed as the major product. The minor product was observed to be $HB(NMe_2)_2$ (**F**), formed from the loss of H_2 from $H_2B(NMe_2)_2H$ (via $H_2B{=}NMe_2$ and NMe_2H). During the 10 minutes after time of mixing, the signal for $HB(NMe_2)_2$ was observed to increase until it was the sole boron-containing product as $H_2B(NMe_2)_2H$ was consumed. The formation of $HB(NMe_2)_2$ as the major product, rather than $[H_2BNMe_2]_2$, can be explained by the fact that both $H_2B{=}NMe_2$ and NMe_2H moieties are formed in high concentration under these stoichiometric conditions and so NMe_2H can rapidly trap out $H_2B{=}NMe_2$

before dimerisation occurs. Under catalytic conditions, $HB(NMe_2)_2$ is only observed in small amounts at the end of catalysis, when the concentration of $H_2B{=}NMe_2$ is low (and therefore persistent due to dimerisation of $H_2B{=}NMe_2$ being a second order process). Furthermore, under catalytic conditions, other processes that consume NMe_2H are available, such as the reaction of NMe_2H with complex **5**.

The analogous stoichiometric reaction of complex **6** with $[NMe_2H_2][BAr^F{}_4]$ was carried out by Timothy M. Boyd in the Weller group and, as for the reaction with boronium, complex **1** was immediately regenerated.[24]

As both $[H_2B(NMe_2H)_2][BAr^F{}_4]$ and $[NMe_2H_2][BAr^F{}_4]$ have been shown to readily protonate complex **6** to yield complex **1**, both the "boronium route" and the "ammonium route" remain viable pathways for the catalytic dehydrocoupling of $H_3B{\cdot}NMe_2H$ with complex **1**. The challenge of distinguishing between which route is operating is discussed later in this chapter.

3.5 Probing H/D exchange during the induction period prior to catalysis

During the transition metal-mediated dehydrocoupling of amine-boranes, B–H activation has been shown to be a key step in the catalytic process.[1] In Chapter Two (section 2.5.2), $[Rh(PONOP)(\eta^2\text{-}H_2)][BAr^F{}_4]$ (**1**) was shown to undergo reversible binding of the tertiary amine-borane $H_3B{\cdot}NMe_3$ to form the sigma complex $[Rh(PONOP)(\eta^1\text{-}H_3B{\cdot}NMe_3)][BAr^F{}_4]$ (**4**). B–H bond activation in complex **4** was proposed due to the observation of H/D exchange in the presence of D_2. Equivalent

H/D exchange was observed when complex **1** was reacted with the deuterated amine-borane $D_3B{\cdot}NMe_3$.

In order to further investigate the reaction mechanism for the catalytic dehydrocoupling of $H_3B{\cdot}NMe_2H$ with complex **1**, H/D exchange at the metal centre was probed. Catalysis was carried out using different isotopomers of $H_3B{\cdot}NMe_2H$ in order to gain insight into the possibility of B–H and/or N–H bond activation at the metal centre during the induction period.

In a high pressure NMR tube, a solution of complex **1** (2.9 mM, 4 mol%, 1,2-$F_2C_6H_4$) was reacted with 25 equivalents of fully deuterated $D_3B{\cdot}NMe_2D$ and the reaction progress was monitored *in situ* using NMR spectroscopy. The ^{11}B NMR spectra revealed an induction period of approximately 600 s before a broad singlet corresponding to $D_2B{=}NMe_2$ (δ 37.5 ppm) was observed. The loss of resolvable coupling leading to a singlet rather than a triplet as observed for $H_2B{=}NMe_2$ (δ 37.8 ppm, $^1J_{BH}$ = 129 Hz) is due to $^1J_{BD}$ being smaller than $^1J_{BH}$.[25] There is also a slight difference in chemical shift between $H_2B{=}NMe_2$ and $D_2B{=}NMe_2$ (~0.3 ppm) due to isotopic perturbation of chemical shift.

During this induction period, the $^{31}P\{^1H\}$ NMR spectra showed a doublet at 212.7 ppm ($^1J_{RhP}$ = 138 Hz) as the sole organometallic species present (**Figure 3.7**). This signal is almost identical to that for sigma complex **5** (d, δ 212.9 ppm, $^1J_{RhP}$ = 138 Hz) and is assigned as [Rh(PONOP)(η^1-$D_3B{\cdot}NMe_2D$)][$BAr^F{}_4$] (**5-D**) due to the slight isotopic perturbation in chemical shift. A similar change in chemical shift to a lower

frequency upon deuteration can be observed upon comparison of the $^{31}P\{^{1}H\}$ NMR spectroscopic data of complex **1-H$_2$** (δ 224.4 ppm) and complex **1-D$_2$** (δ 224.2 ppm) (section 2.5.2). The ^{11}B NMR signal for **5-D** (br s, δ –21.7 ppm) is similarly low frequency shifted compared to that for **5-H** (br s, δ –21.3 ppm).

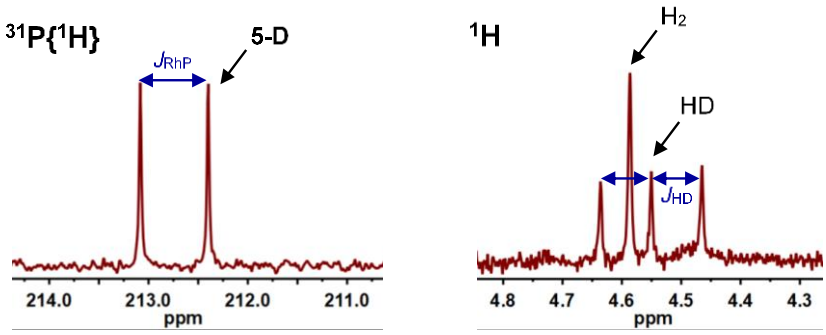


Figure 3.7 Selected NMR spectra (500 MHz, 1,2-$F_2C_6H_4$, 298 K) during the induction period of catalysis with $D_3B{\cdot}NMe_2D$ (72 mM) and complex **1** (2.9 mM, 4 mol%). J_{RhP} = 138 Hz and J_{HD} = 43 Hz.

The ^{1}H NMR spectra during the induction period showed no signals in the hydride region, consistent with there being no complex **1** or undeuterated complex **5** (i.e. **5-H**) present. This result does not exclude the possibility of H/D exchange occurring as if it were, the amount of protonation of complex **5-D** would be too small to be observed due to the excess of deuterium in the system from adding 25 equivalents of $D_3B{\cdot}NMe_2D$. In fact, evidence of H/D exchange at the metal centre in complex **5-D** during the induction period occurring is indicated by the presence of a mixture of dissolved H_2 and HD in the ^{1}H NMR spectra at this time (**Figure 3.7**). HD (and likely D_2, although not observed) can be generated either through B–D activation in complex **5-D**, or N–D activation or potentially both.

Catalysis was repeated in a closed system with the mono-deuterated isotopologue $H_3B{\cdot}NMe_2D$ (72 mM, catalyst loading of 4 mol%, 1,2-$F_2C_6H_4$) and the reaction progress followed *in situ* using NMR spectroscopy. A similar induction period was observed (~540 s) during which a doublet matching that for complex **5-H**, rather than **5-D**, was the only signal observed in the $^{31}P\{^1H\}$ NMR spectra (**Figure 3.8**). The ^{11}B NMR spectra showed a sharp quartet consistent with full protonation around the boron centre as in $H_3B{\cdot}NMe_2D$, along with a broad singlet at δ –21.3 ppm as observed for complex **5-H**. However, contrary to the reaction with $D_3B{\cdot}NMe_2D$, the ^1H NMR spectra during the induction period showed no signals for dissolved HD, only for H_2 (**Figure 3.8**) Only after evidence of dehydrogenation was observed in the ^{11}B NMR spectra did signals for dissolved HD appear in the ^1H NMR spectra.

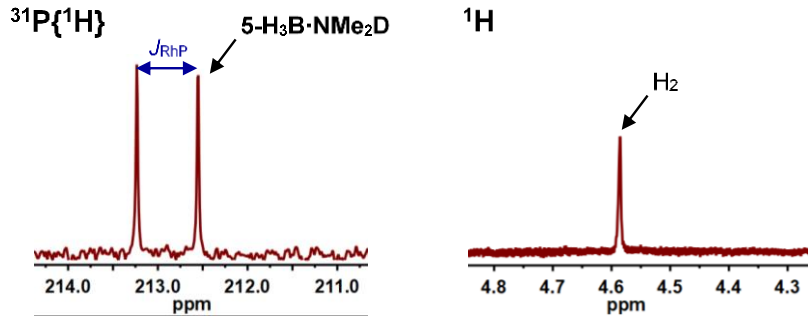


Figure 3.8 Selected NMR spectra (500 MHz, 1,2-$F_2C_6H_4$, 298 K) during the induction period of catalysis with $H_3B{\cdot}NMe_2D$ (72 mM) and complex **1** (2.9 mM, 4 mol%). J_{RhP} = 138 Hz.

In summary, no dissolved HD was observed in the ^1H NMR spectra during the induction period of catalysis with $H_3B{\cdot}NMe_2D$, but HD was observed with $D_3B{\cdot}NMe_2D$. This suggests that H/D exchange at the metal centre during the induction period is able to occur via B–H activation in amine-borane sigma complex

5, but not via N–H activation. Such deuterium scrambling to produce HD is proposed to be via B–D activation at the metal centre, followed by H/D exchange via a σ-CAM mechanism,[26] as discussed in Chapter Two for the analogous complex [Rh(PONOP)(η^1-$H_3B{\cdot}NMe_3$)][$BAr^F{}_4$] (**4**) (section 2.5.2).

Interestingly, computational studies carried out by Professor Stuart A. Macgregor and Dr Nicholas A. Beattie (Heriot-Watt University) indicated that unassisted B–H and N–H activation at the metal centre in complex **5** were energetically unfavourable, with no intermediates for B–H activation being located. Therefore, even though B–H activation has been shown to occur experimentally, DFT calculations suggest that this pathway would not be competitive and indicate that catalysis (i.e. reactivity post induction period) may occur via a different mechanistic pathway. This is discussed in more detail towards the end of this chapter and compared to calculations for amine-assisted B–H/N–H activation, as would occur in the "boronium route" and "ammonium route" respectively.

3.6 Catalysis under open conditions: H_2 evolution experiments

So far in this thesis, experiments to probe the catalytic dehydrocoupling of $H_3B{\cdot}NMe_2H$ with [Rh(PONOP)(η^2-H_2)][$BAr^F{}_4$] (**1**) have been carried out under closed conditions, i.e. in a sealed NMR tube. This method allows the monitoring of the reaction progress by NMR spectroscopy and so is useful for revealing speciation of the reaction. Another method of carrying out catalysis is under open conditions, i.e. a controlled and constant argon gas flow through the reaction mixture, meaning there is no build up of H_2. This may affect catalysis, for example [Rh(κ^2-P,P-

Xantphos-Ph)(η^2-$H_2B(CH_2CH_2{}^tBu)\cdot NMe_3$)][$BAr^F{}_4$] (Xantphos-Ph = 4,5-bis(diphenylphosphino)-9,9-dimethylxanthene) has been shown to catalyse the dehydropolymerisation of $H_3B\cdot NMeH_2$ to yield polyaminoboranes of different molecular weights depending on the reaction conditions (open: M_n = 22, 700 g mol^{-1}, Đ = 2.1, closed: M_n = 2, 800 g mol^{-1}, Đ = 1.8).[27]

Another type of open condition for catalysis that has been developed in the Weller group is a H_2 evolution measurement experiment. This particular method allows for the indirect measurement of the concentration of $H_2B{=}NMe_2$ present in the reaction mixture as a function of time and therefore can offer an insight into the kinetics of catalysis. A H_2 evolution experiment consists of carrying out catalysis in a jacketed two-neck Schlenk flask connected to a recirculating cooler to maintain a constant reaction temperature (in this case, set to 25 °C). The flask is also connected to a water-filled 100.0 mL gas burette via Teflon tubing and the argon supply to the flask turned off. Any gas evolved during catalysis will increase the pressure in the system and thus displace the water in the burette, allowing the volume of gas evolved to be recorded as a function of time.

The data collected in a H_2 evolution experiment can be manipulated as follows in order to plot the temporal profile of the dehydrogenation of amine-borane, in this case $H_3B\cdot NMe_2H$, over time (**Figure 3.9**). The H_2 evolved during catalysis is measured in mL and these measurements are converted to moles using the ideal gas law (n=PV/RT where P = 101325 Pa, V = volume of H_2 released in m^3, R = 8.314 J K^{-1} mol^{-1} and T = 298 K). It is assumed that exactly one equivalent of H_2 is evolved

during catalysis due to the efficient dehydrogenation of all $H_3B{\cdot}NMe_2H$ to form $H_2B{=}NMe_2$. In practice, however, the volume of evolved H_2 may not be exactly one equivalent due to small amounts (<5 %) of side products being formed that require further loss of H_2, such as $HB(NMe_2)_2$, or experimental errors, such as recording volume measurements before the pressure between the reaction flask and the burette has fully equalised. Therefore, the moles of evolved H_2 calculated is normalised relative to the number of moles of $H_3B{\cdot}NMe_2H$ at the beginning of catalysis (**Equation 3.1**).

$$n(H_2)_{normalised} = \frac{n(H_2)_t \times n(H_3B{\cdot}NMe_2H)_0}{n(H_2)_{total}}$$

Equation 3.1 Normalisation of the moles of H_2 evolved in a H_2 evolution experiment. $n(H_2)_{normalised}$ = normalised number of moles H_2 evolved at time t; $n(H_2)_t$ = number of moles H_2 evolved at time t; $n(H_3B{\cdot}NMe_2H)_0$ = initial number of moles $H_3B{\cdot}NMe_2H$ at the onset of catalysis (t=0); $n(H_2)_{total}$ = total number of moles H_2 evolved.

Using the normalised value for the number of moles of H_2 evolved at a specific time ($n(H_2)_{normalised}$) and assuming all H_2 evolved is from the formation of $H_2B{=}NMe_2$ from $H_3B{\cdot}NMe_2H$, the normalised concentration of $H_2B{=}NMe_2$ at that time ($[H_2B{=}NMe_2]$) may also be calculated (**Equation 3.2**).

$$[H_2B{=}NMe_2] = \frac{1000 \times n(H_2)_{normalised}}{V}$$

Equation 3.2 Normalised concentration of $H_2B{=}NMe_2$ (M) in a H_2 evolution experiment. V = volume of reaction mixture (mL).

The temporal profile of the formation of $H_2B{=}NMe_2$ during catalysis can then be plotted as $[H_2B{=}NMe_2]$ formed as a function of time (**Figure 3.9**). Such a temporal plot is used to discuss the catalytic dehydrocoupling of $H_3B{\cdot}NMe_2H$ with complex **1** in the rest of this chapter.

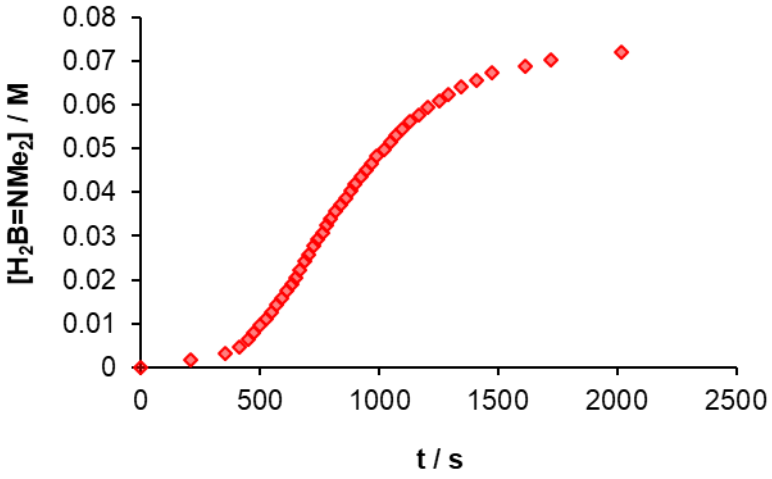


Figure 3.9 Temporal profile for the dehydrocoupling of $H_3B{\cdot}NMe_2H$ (72 mM, 1,2-$F_2C_6H_4$, 298 K) with complex **1** (2 mol%) as measured by H_2 evolution.

As mentioned before, H_2 evolution measurement experiments can be valuable tools allowing insight into the kinetics of catalysis. In order to do this, the maximum rate of formation of $H_2B{=}NMe_2$ was calculated and compared for multiple H_2 evolution experiments described in the remainder of this chapter. Due to the presence of an induction period, initial rates were not deemed a reliable method for the comparison of kinetics.[28] The method for the calculation of maximum rate for each H_2 evolution experiment was developed by T. M. Boyd (Weller group, University of Oxford) and is as follows. For each data set of $[H_3B{\cdot}NMe_2H]$ vs. time (where $[H_3B{\cdot}NMe_2H]_t = [H_3B{\cdot}NMe_2H]_0 - [H_2B{=}NMe_2]_t$), the anaconda software distribution

package was used to run Python 3 and fit the kinetic data to a polynomial.[29,30] A sixth order polynomial was determined by inspection to give the best fit around the point of maximum rate and fitted to the data using the SciPy packages.[31] This gave a maximum rate of catalysis (ν_{max}) for each temporal profile, which was then used to compare different kinetic regimes. For a single experiment under certain experimental conditions, no error was derived; however, where multiple experiments were carried out under identical conditions, an average ν_{max} was calculated along with the standard error of the mean, which is quoted where applicable.

3.6.1 Speciation studies under open conditions

Before using H_2 evolution measurement studies to investigate the kinetics of the catalytic dehydrocoupling of $H_3B{\cdot}NMe_2H$ with complex **1**, a speciation study under H_2 evolution conditions was carried out in order to see if the change in conditions altered the reactivity previously observed in the closed system.

Dehydrogenation of $H_3B{\cdot}NMe_2H$ (72 mM, 1,2-$F_2C_6H_4$) catalysed by complex **1** (4 mol% catalyst loading) was carried out under the H_2 evolution conditions previously described. An aliquot of the reaction mixture was removed by syringe, added to an NMR tube and frozen at four different intervals during the reaction (**Figure 3.10**). These samples were then later analysed by NMR spectroscopy at 298 K. From the relative integrals of the signals observed in the $^{31}P\{^1H\}$ NMR spectra for each sample, a temporal profile could be plotted (**Figure 3.11**).

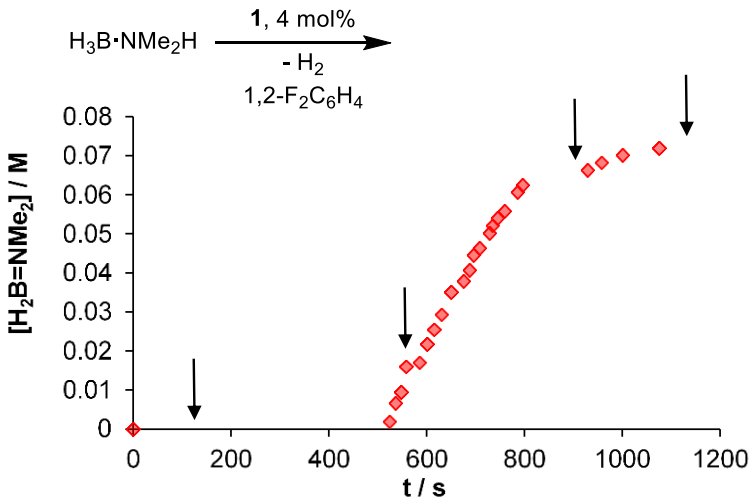


Figure 3.10 Temporal profile for the dehydrocoupling of $H_3B{\cdot}NMe_2H$ (72 mM, 1,2-$F_2C_6H_4$, 298 K) with complex **1** (2.9 mM, 4 mol%) as measured by H_2 evolution. Arrows mark when aliquots of reaction mixture were removed.

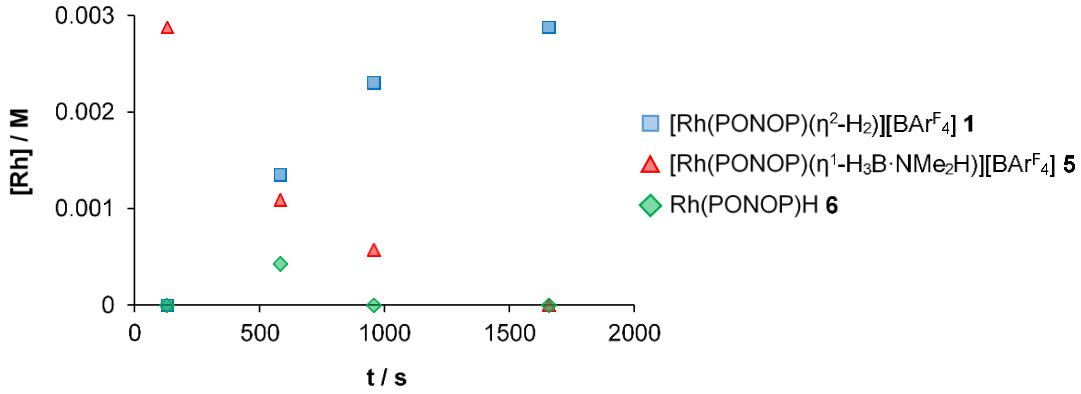


Figure 3.11 Time course plot for the dehydrocoupling of $H_3B{\cdot}NMe_2H$ (72 mM, 1,2-$F_2C_6H_4$, 298 K) with complex **1** (2.9 mM, 4 mol%) H_2 evolution conditions as measured using $^{31}P\{^1H\}$ NMR spectroscopy.

Under H_2 evolution conditions, an induction period of ~500 s was observed before any H_2 evolution was observed (before the first bubble of gas was observed to displace water in the burette). The limited $^{31}P\{^1H\}$ NMR spectroscopic data density does not allow the induction period to be clearly observed; however, the H_2

evolution plot reveals its existence. $^{31}P\{^{1}H\}$ NMR spectroscopy of the sample taken during the induction period showed the amine-borane sigma complex (**5**) as the sole organometallic species. As the reaction progressed and H_2 was evolved, the $^{31}P\{^{1}H\}$ NMR spectra of the remaining samples showed the consumption of complex **5**, the regeneration of complex **1** and the appearance of complex **6** in low concentrations early on in catalysis. The presence of an induction period and the fate of the organometallic species during catalysis are all consistent with what was observed during the speciation studies under closed conditions (section 3.3). Therefore, it can be assumed that catalysis operates via very similar mechanistic pathways under closed conditions (in a sealed NMR tube) and under H_2 evolution conditions.

3.6.2 Tests for catalyst homogeneity

Every H_2 evolution experiment carried out for the catalytic dehydrocoupling of $H_3B{\cdot}NMe_2H$ with complex **1** features an induction period: the time after the reagents had been mixed before H_2 was observed to evolve. In each case, the induction period is significant enough (~400–600 s) to suggest a period of time during which no dehydrogenation of $H_3B{\cdot}NMe_2H$ occurs rather than just a small delay before enough H_2 pressure builds up in the flask to cause a bubble of gas to evolve from the Teflon tube into the water-filled burette. These observations are consistent with catalysis in a closed system (sealed NMR tube) where an induction period is also observed. In this case, the induction period is defined as the time after the reagents have been mixed before $H_2B{=}NMe_2$ is observed by ^{11}B NMR spectroscopy.

The presence of an induction period at the onset of catalysis may indicate the formation of colloidal rhodium nanoparticles,[32,33] and therefore heterogeneous catalysis. However, another indication of the formation of rhodium nanoparticles would be the visual observation of a dark precipitate. During the induction period of the catalytic dehydrocoupling of $H_3B{\cdot}NMe_2H$ with complex **1**, the reaction mixture is a clear, light yellow that darkens slightly to orange immediately before H_2 evolution, however no dark precipitate is observed at any point during the reaction. This suggests a lack of colloidal rhodium and therefore implies homogeneous catalysis.

To probe the hetero- or homogeneous nature of the active catalyst further, tests for heterogeneity by catalyst poisoning developed by Finke were carried out.[32]

Elemental mercury has been shown to poison heterogeneous catalysts by forming an unreactive amalgam with the metal, and thus suppressing catalytic activity. For example, the addition of mercury to the catalytic dehydrocoupling of $H_3B{\cdot}NMe_2H$ with $[Rh(1,5\text{-cod})(\mu\text{-Cl})]_2$ was shown to halt catalysis.[9] This particular result suggested that the active catalyst was heterogeneous, which was confirmed by multiple other tests (TEM, filtration, analysis of reaction kinetics, etc.).[33]

The dehydrocoupling of $H_3B{\cdot}NMe_2H$ (72 mM, 1,2-$F_2C_6H_4$, 298 K) catalysed by complex **1** (2 mol%) was carried out under H_2 evolution conditions. After 0.25 equivalents of the expected total amount of H_2 (assumed to be one equivalent of H_2) had evolved, an excess of elemental mercury (2000 equivalents relative to complex

1) was added to the reaction mixture. Catalysis was observed to continue, as measured by H_2 evolution (**Figure 3.12**), with no significant effects in the temporal profile, consistent with a homogeneous system.

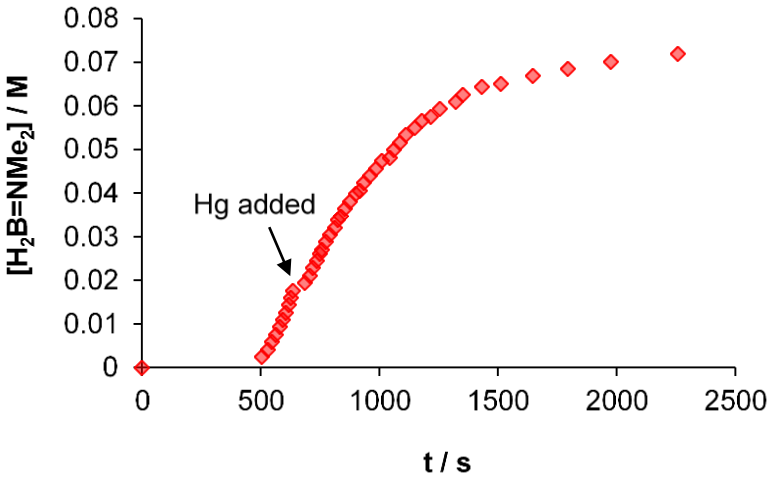


Figure 3.12 Time course plot for the dehydrocoupling of $H_3B{\cdot}NMe_2H$ (72 mM, 1,2-$F_2C_6H_4$, 298 K) with complex **1** (2 mol%) as measured by H_2 evolution with the addition of 2000 eq. Hg at 624 s.

Another test for heterogeneous catalysis is the fractional poisoning of the catalyst by the addition of the strongly coordinating ligand PPh_3. A homogeneous catalyst would require at least one equivalent of PPh_3 (relative to the catalyst) in order to bind to every metal site and completely suppress catalysis. Whereas, a heterogeneous catalyst can be completely poisoned by only a sub-stoichiometric amount of PPh_3. This is because for a heterogeneous catalyst, only the metal sites on the surface of the nanoparticles are available for catalysis and these constitute a fraction of the total amount of metal and so less than one equivalent of PPh_3 should block all catalytically active sites.

A repeat of the H_2 evolution experiment in which elemental mercury was added was carried out but this time 0.2 equivalents of PPh_3 (compared to complex **1**) were added (as a 0.2 mL 1,2-$F_2C_6H_4$ solution) to the reaction mixture after 0.25 equivalents of the total expected amount of H_2 had been evolved. The resulting time course plot is depicted in **Figure 3.13**, overlaid with the plot for the identical experiment without the addition of PPh_3. In order to compare these plots, equivalents of H_2 evolved is used rather than the normalised concentration of $H_2B{=}NMe_2$, as the process of normalisation assumes exactly one equivalent of H_2 is released, which may not be the case in the doped system where 20 % of the catalyst can be sequestered by PPh_3. The induction periods of both plots have also been removed to allow for an easier pictorial comparison. Overall, it can be seen from **Figure 3.13** that upon the addition of PPh_3, catalysis continues, consistent with homogeneous catalysis, albeit more slowly, consistent with partial sequestering of the catalyst.

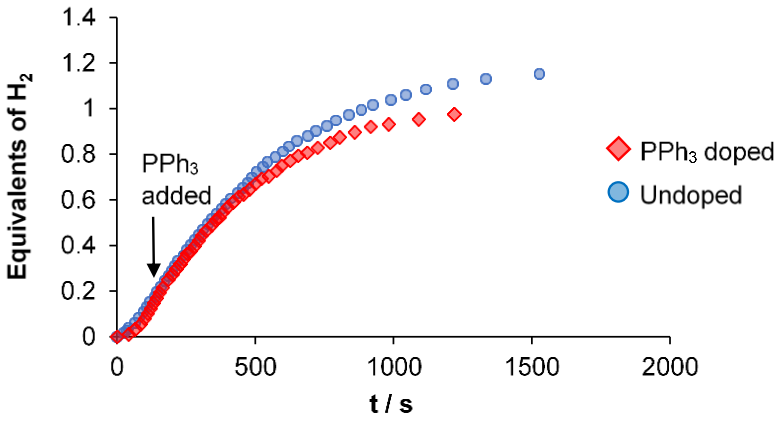


Figure 3.13 Time course plot for the dehydrocoupling of $H_3B{\cdot}NMe_2H$ (72 mM, 1,2-$F_2C_6H_4$, 298 K) with complex **1** (2 mol%) under H_2 evolution conditions (blue circles) with the addition of 0.2 eq. PPh_3 (red diamonds)at 0.25 eq. H_2 release.

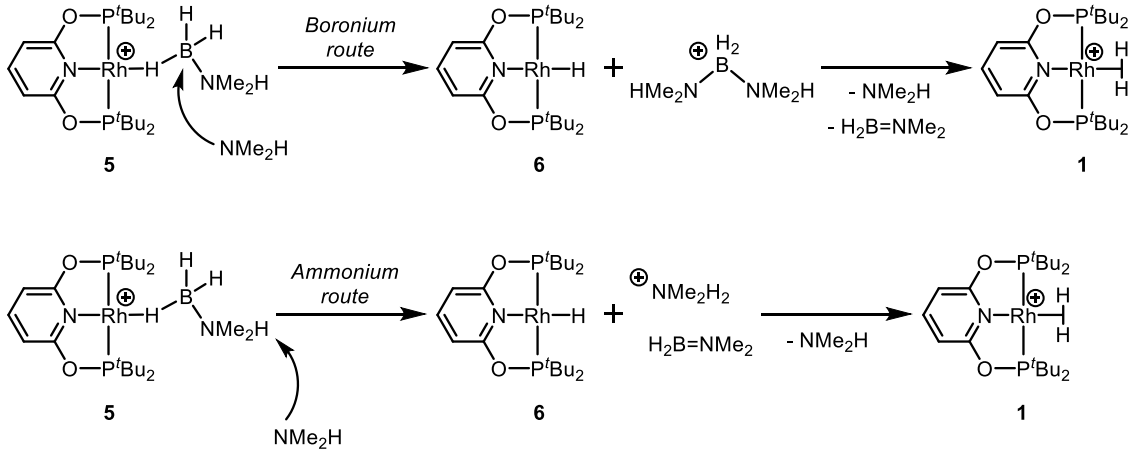
The lack of visible precipitate in the reaction mixture and the lack of catalyst suppression by the addition of excess elemental mercury or sub-stoichiometric PPh_3 suggests the catalytic dehydrocoupling of $H_3B{\cdot}NMe_2H$ with complex **1** proceeds via homogeneous catalysis. The homogeneous nature of the system encouraged further investigations into the mechanism of catalysis. Although the presence of an induction period initially indicated this may be a heterogeneous system, other homogeneous systems for the dehydropolymerisation of amine-boranes, such as with $\{Rh(PPh_2(CH_2)_3PPh_2)\}^{+}$[34] and $\{Rh(\kappa^2\text{-P,P-Xantphos-Ph})\}^{+}$[27], have also demonstrated induction periods. Therefore, explanations for the presence of an induction period other than heterogeneity were sought and discussed further in section 3.8.

3.6.3 Kinetic isotope effects

The amine-borane isotopologues $D_3B{\cdot}NMe_2H$ and $H_3B{\cdot}NMe_2D$ were employed to probe any kinetic isotope effects (KIE = ν_H/ν_D) in the dehydrocoupling of $H_3B{\cdot}NMe_2H$ using complex **1**. Catalysis was carried out under H_2 evolution conditions at a catalyst loading of 2 mol% (1,2-$F_2C_6H_4$, 298 K) with each isotopologue (72 mM). For each experiment, a maximum rate (ν_{max}) was calculated using the method described previously (see section 3.6) and compared to that obtained for the non-deuterated amine-borane (ν_H = 1.0 ± 0.06 × 10^{-4} M s^{-1}) to deduce a KIE value. On substituting B–H bonds for B–D bonds, a KIE of 1.2 ± 0.07 was calculated (ν_D = 0.9 × 10^{-4} M s^{-1}), and for N–H/N–D substitution and KIE of 2.0 ± 0.11 was calculated (ν_D = 0.5 × 10^{-4} M s^{-1}).

Deuterium incorporation at the boron in $H_3B{\cdot}NMe_2H$ yields a very small KIE that is close to unity suggesting that B–H bond cleavage is not directly involved in the rate-determining step. The larger KIE observed for N–H/N–D substitution implies that N–H bond cleavage is involved in the rate-determining step in catalysis. Many examples of N–H/N–D substitution KIEs for the dehydrocoupling of amine-boranes are larger than observed here. For example: the $[Cp_2Ti]$-catalysed dehydrocoupling of $H_3B{\cdot}NMe_2H$ has a KIE = 3.6 ± 0.3;[35] a KIE of 5.3 ± 1.2 is reported for dehydrocoupling using $Rh(PCy_3)_2(H)_2Cl$;[36] and the dehydropolymerisation of $H_3B{\cdot}NH_3$ catalysed by $Ru(H)_2(PMe_3)(HN\text{-}(CH_2CH_2P^iPr_2)_2)$ has a KIE = 5.3.[37] In all these examples, N–H activation is proposed to be involved in the turnover limiting step. However, there are also examples that show smaller N–H/N–D substitution KIEs, such as for the dehydrocoupling of $H_3B{\cdot}NMe_2H$ with $\{Rh(Xantphos\text{-}Ph)\}^+$ (KIE = 2.1 ± 0.2),[27] the dehydropolymerisation of $H_3B{\cdot}NH_3$ with $Fe(^{i\text{Pr}}POCOP\text{-}OMe)H(PMe_2Ph)_2$ (KIE = 2.0 ± 0.3),[38] and with a Ni-NHC-based system as described by Baker (KIE = 2.3).[39]

Earlier in this chapter (section 3.4), two routes were proposed as possible mechanistic pathways for the dehydrocoupling of $H_3B{\cdot}NMe_2H$ with complex **1** (**Scheme 3.6**).



Scheme 3.6 Possible mechanistic pathways for the formation of complex **6** from the reaction of complex **1** $H_3B{\cdot}NMe_2H$ in 1,2-$F_2C_6H_4$. $[BAr^F{}_4]^-$ anions omitted for clarity.

The boronium route involves B–H bond activation in complex **5** to generate complex **6** and $\{H_2B(NMe_2H)_2\}^+$, followed by N–H bond activation of $\{H_2B(NMe_2H)_2\}^+$ to protonate complex **5** and yield complex **1**. In contrast, the ammonium route requires initial N–H and B–H activation in complex **5** followed again by N–H activation of $\{NMe_2H_2\}^+$ to generate complex **1**. Therefore, if the rate determining step during catalysis was the protonation of complex **6**, then both routes would be expected to show a KIE for N–H/N–D substitution. As such a KIE is observed experimentally, this result does not distinguish between the two routes considered if the rate determining step is indeed the protonation of complex **6**. However, if the rate determining step of catalysis was the formation of complex **6** from complex **5**, then a KIE for N–H/N–D substitution indicates catalysis is occurring via the ammonium route rather than the boronium route.

As complex **5** is observed during the induction period and complex **6** is observed during catalytic turnover, then the formation of complex **6** from complex **5** is suggested to be the induction period limiting process, i.e. cause for the induction period. A significantly longer induction period was observed for catalysis with $H_3B{\cdot}NMe_2D$ (~1000 s) compared to that with $H_3B{\cdot}NMe_2H$ (~650 s) or $D_3B{\cdot}NMe_2H$ (~750 s), suggesting N–H activation is involved in the turnover limiting step during the induction period. This result can be explained if the ammonium route is in operation, as it requires initial N–H activation in complex **5** to yield complex **6**. The boronium route would require B–H activation for the same process and although reversible B–H bond activation during the induction period was revealed through deuterium studies as described in section 3.5, the lack of a significant KIE calculated for B–H/B–D substitution implies this bond activation is not relevant to the rate-determining step of catalysis.

3.6.4 Determining order in pre-catalyst 1 and $H_3B{\cdot}NMe_2H$

To gain further mechanistic insight into the catalytic cycle for complex **1** catalysed dehydrocoupling of $H_3B{\cdot}NMe_2H$, H_2 evolution experiments were used to determine the kinetic order for each reagent. However, the post-induction period kinetic data for any given H_2 evolution experiment did not agree with simple kinetic models, i.e. the plots in **Figure 3.14** do not exhibit a straight line.

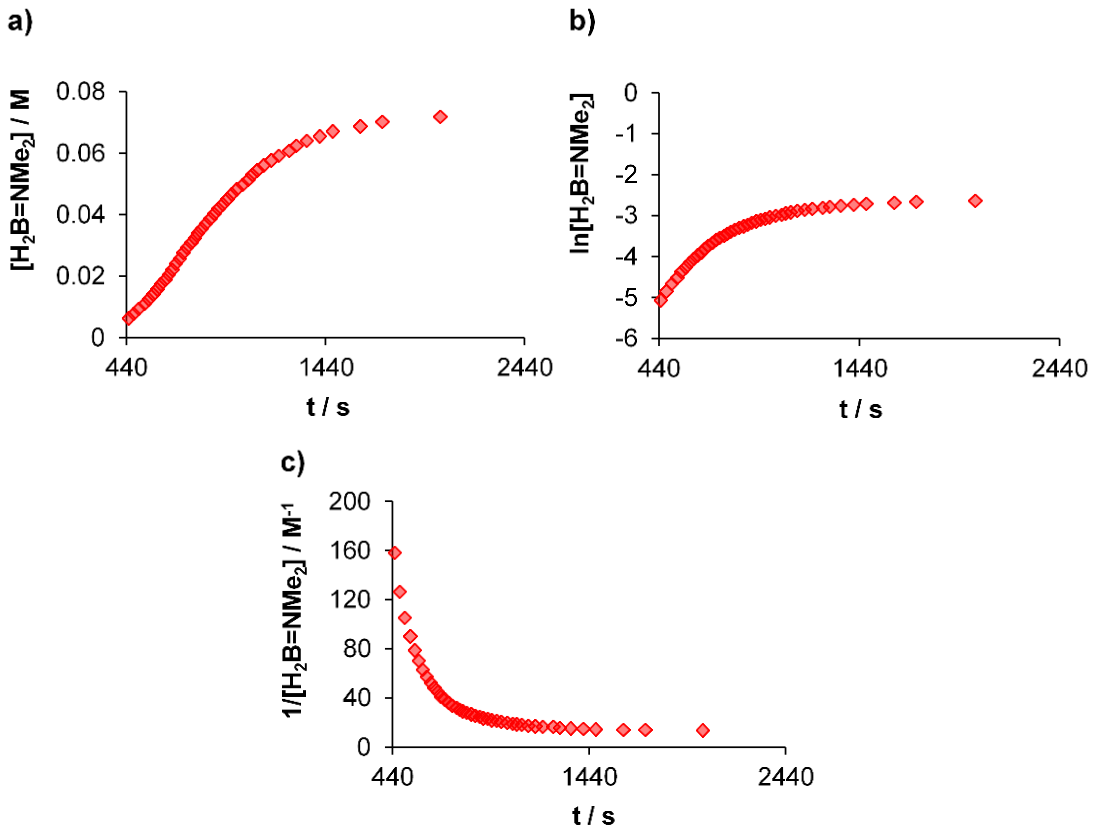


Figure 3.14 Kinetic data manipulation for the dehydrocoupling of $H_3B{\cdot}NMe_2H$ (72 mM, 1,2-$F_2C_6H_4$, 298 K) with complex **1** (2 mol%) under H_2 evolution conditions. a) Zero order plot, b) first order plot, c) second order plot. Induction period of 449 s is not shown.

Therefore, the effect of changing the concentration of complex **1** on the rate of catalysis was probed instead. Multiple H_2 evolution experiments were carried out where the initial concentration of $H_3B{\cdot}NMe_2H$ was kept the same (72 mM) and the concentration of complex **1** was varied between 0.14–2.9 mM (0.2 –4 mol% catalyst loading). The rate data from each of these experiments was manipulated as described previously (section 3.6) to identify a maximum rate that could be compared between experiments (**Figure 3.15**).

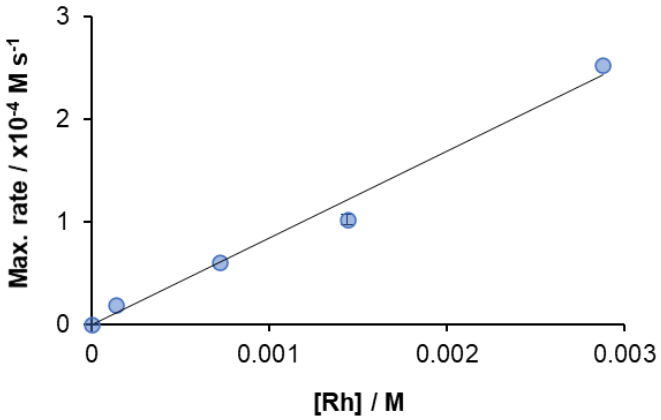


Figure 3.15 Maximum rate of catalysis vs. concentration of complex **1** for the catalytic dehydrocoupling of $H_3B{\cdot}NMe_2H$ (72 mM, 1,2-$F_2C_6H_4$, 298 K) with complex **1** (0.2–4 mol%) as measured by H_2 evolution.

The graphical data suggest the rate of catalysis is directly proportional to the concentration of complex **1** and therefore indicates an overall first order kinetic regime. This suggests there is no rapid rhodium monomer/dimer equilibrium involved in catalysis, which is often indicated by a half order regime.[40]

The first order dependency of the rate of catalysis on the concentration of complex **1** was also confirmed using Burés' graphical approach of Variable Time Normalisation Analysis (VTNA).[41,42] By plotting concentration against a normalised time scale for experiments at different catalyst loadings, the direct comparison of concentration profiles is possible (assuming the total concentration of catalyst remains constant throughout each experiment and that there is not a change in mechanism). The normalised time scale ($t[Rh]^n$) is derived by multiplying each time data point (t) by the total concentration of the catalyst ([Rh] in this case)

raised to a power (n), which is the proposed order of the catalyst. The value of n which allows all the concentration vs. normalised time plots for different catalyst loadings to overlay is the order in catalyst.

This approach has been applied to the same data sets that were used to generate **Figure 3.15** ([$H_3B{\cdot}NMe_2H$] = 72 mM, 0.2–4 mol% catalyst loadings) and the results for when n = 0.5, 1 and 2 are depicted in **Figure 3.16**. Each data set originally showed an induction period (~500 s), which has been removed to allow for direct comparison. As can been seen, when n = 1, i.e. $[Rh]^1$, the concentration profiles visually overlap the most suggesting catalysis is first order with respect to complex **1**. The non-perfect overlap of the data is suggested to be due to experimental variety partially due to using different batches of 1,2-$F_2C_6H_4$ solvent. GC-MS analysis of 1,2-$F_2C_6H_4$ has reportedly shown the presence of trace impurities such as 1-chloro-2-fluorobenzene, 2-fluorophenol and 2-chloro-4-fluorotoluene.[43–45] Such impurities have been shown to affect the length of induction periods prior to the onset of catalysis and also may act to modify a small amount of the catalyst.

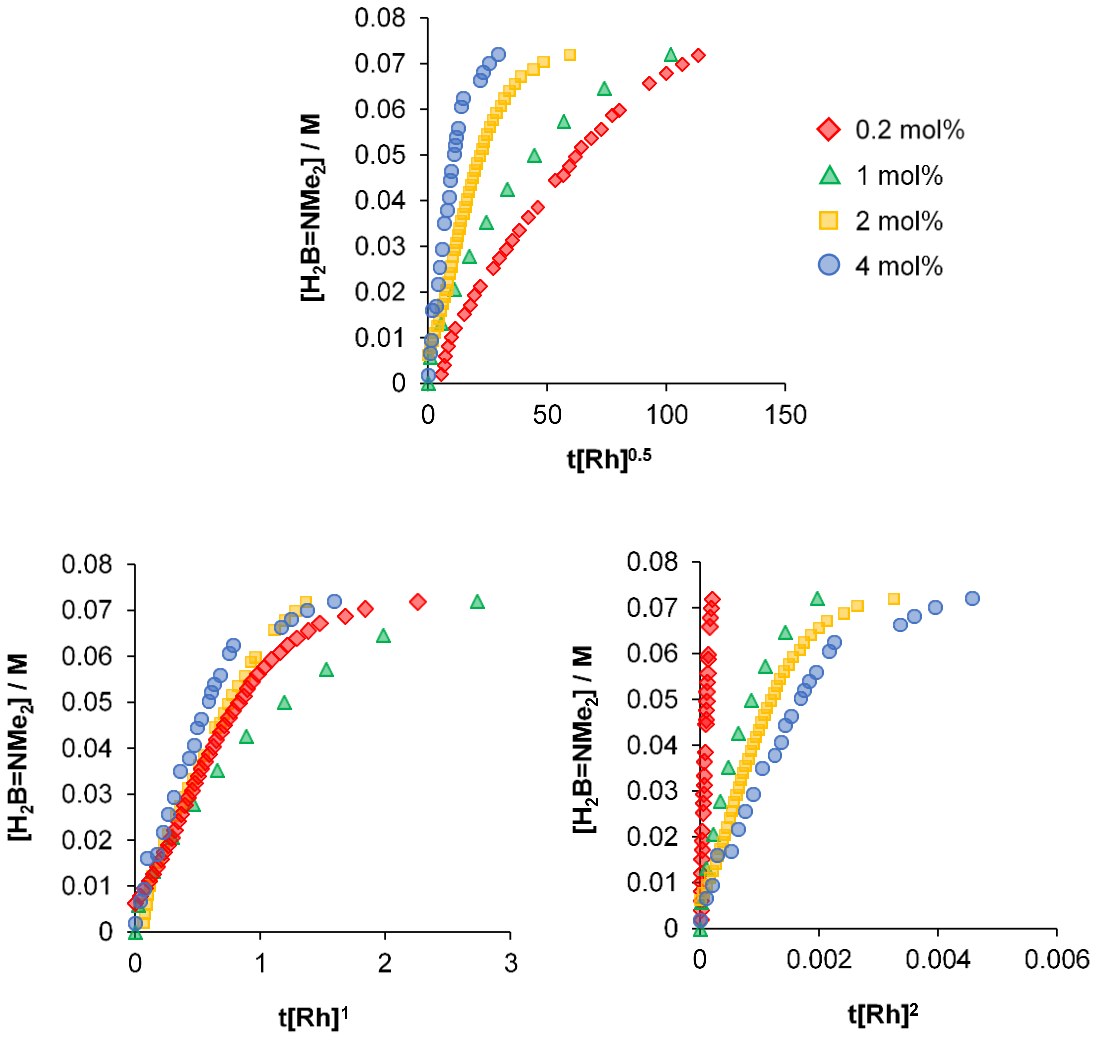


Figure 3.16 Variable Time Normalisation Analysis for the order in [Rh] (0.2–4 mol%) for the catalytic dehydrocoupling of $H_3B{\cdot}NMe_2H$ (72 mM, 1,2-$F_2C_6H_4$, 298 K) under H_2 evolution conditions.

The effect of varying the initial concentration of $H_3B{\cdot}NMe_2H$ upon the rate of catalysis was likewise investigated using the maximum rate method. Multiple H_2 evolution experiments were carried out where the concentration of complex **1** was kept the same (1.4 mM) and the initial concentration of $H_3B{\cdot}NMe_2H$ was varied between 0.014–0.72 M (10–0.2 mol% catalyst loading). From the data from each experiment, a maximum rate was identified (in the same way as determined when

varying the concentration of complex **1**) and these rates were compared for the different starting concentrations of $H_3B{\cdot}NMe_2H$ (**Figure 3.17**).

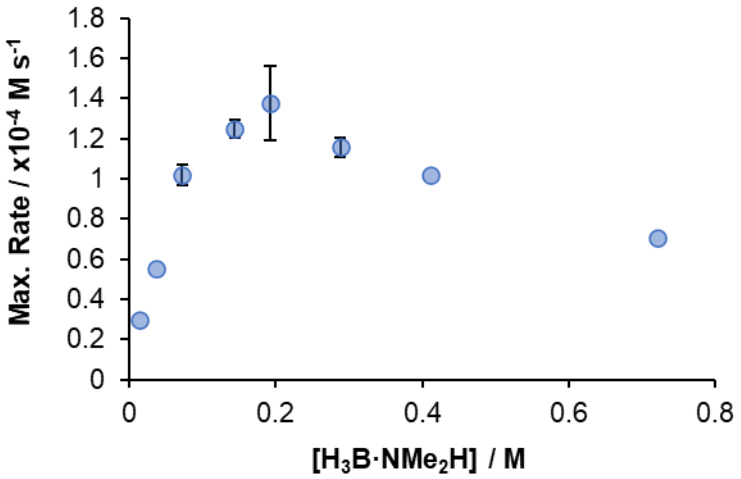


Figure 3.17 Maximum rate of catalysis v.s. starting concentration of $H_3B{\cdot}NMe_2H$ (0.014 – 0.72 M) as catalysed by complex **1** (1.4 mM, 1,2-$F_2C_6H_4$, 298 K) as measured by H_2 evolution.

The graphical data suggest that catalysis has a positive order in terms of $H_3B{\cdot}NMe_2H$ up to a limiting concentration of $H_3B{\cdot}NMe_2H$ (~0.2 M) at which point the rate of catalysis becomes inhibited with increasing concentration of $H_3B{\cdot}NMe_2H$. This trend suggests that $H_3B{\cdot}NMe_2H$ may be participating in an off-cycle equilibrium, which results in the sequestering of a species involved in the rate-determining step of catalysis.

VTNA was not employed to determine the order in [$H_3B{\cdot}NMe_2H$] as it was used for determining the order in [Rh] as [$H_3B{\cdot}NMe_2H$] does not remain constant throughout catalysis, unlike [Rh].

One possible scenario that may explain a decrease in rate of catalysis at higher initial concentrations of $H_3B{\cdot}NMe_2H$ is if the product of dehydrocoupling, $[H_2BNMe_2]_2$, is inhibiting catalysis. For example, $\{Rh(P^iBu_2P^tBu)_2\}^+$ catalyses the hydroboration of *tert*-butylethene with $H_3B{\cdot}NMe_3$; however, a maximum conversion of ~70 % is reached as the product ($Me_3N{\cdot}H_2BCH_2CH_2{}^tBu$) can compete with $H_3B{\cdot}NMe_3$ and bind to the metal centre.[46]

In order to probe the possibility of product inhibition, the catalytic dehydrocoupling of $H_3B{\cdot}NMe_2H$ (72 mM, 1,2-$F_2C_6H_4$, 298 K) with complex **1** (2 mol%) was carried out under H_2 evolution conditions with the addition of 50 equivalents of $[H_2BNMe_2]_2$ (compared to complex **1**). No change to the temporal profile, compared to without the addition of $[H_2BNMe_2]_2$, was observed and so any effects of the product on the rate of catalysis were discounted.

Other off-cycle equilibria that may explain the decrease in rate of catalysis observed for higher initial concentrations of $H_3B{\cdot}NMe_2H$ are investigated in more detail in the rest of this chapter.

3.7 Interactions of amine-borane with $[H_2B(NMe_2H)_2][BAr^F{}_4]$ and $[NMe_2H_2][BAr^F{}_4]$

Kinetic studies described in the previous section indicate that $H_3B{\cdot}NMe_2H$ may be participating in an off-cycle interaction with another species, leading to inhibition of catalysis.

One species that has been observed during catalysis and may be involved in the rate-determining step is boronium, $[H_2B(NMe_2H)_2][BAr^F_4]$. Interestingly, when boronium (38 mM, 1,2-$F_2C_6H_4$) is combined with one equivalent of either $H_3B{\cdot}NMe_3$ or $H_3B{\cdot}NMe_2H$, small chemical shift changes (<1 ppm) in the NH signals in the ^1H NMR spectra are observed, compared to NMR spectra of the individual species (**Figure 3.18**).

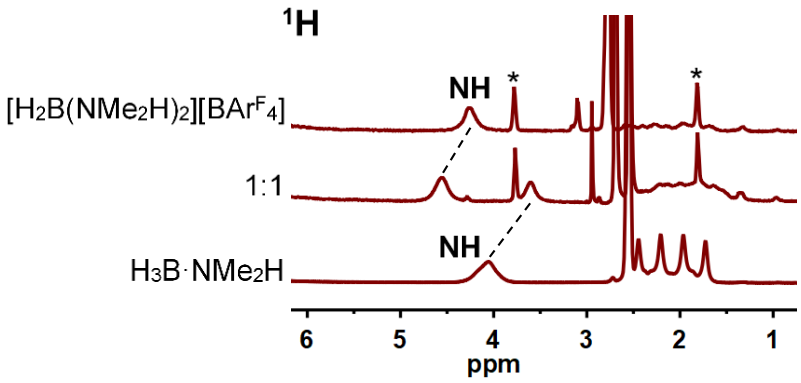


Figure 3.18 Stacked partial ^1H NMR spectra (400 MHz, 1,2-$F_2C_6H_4$, 298 K) of $[H_2B(NMe_2H)_2][BAr^F]$ (*top*), $H_3B{\cdot}NMe_2H$ (*bottom*) and a 1:1 mixture of these species (*middle*) showing the shift of the NH signals.

These chemical shift changes indicate the presence of a significant interaction, likely via dihydrogen bonding,[47] between boronium and amine-borane. If boronium is involved in the rate-determining step of catalysis, then an excess of $H_3B{\cdot}NMe_2H$ may sequester any boronium present in an off-cycle competing equilibrium, and thus lead to a decrease in the rate of catalysis as observed for high initial concentrations of $H_3B{\cdot}NMe_2H$ (**Figure 3.17**).

To further probe the interaction between amine-borane and boronium, both $H_3B{\cdot}NMe_3$ and $H_3B{\cdot}NMe_2H$ were each titrated against $[H_2B(NMe_2H)_2][BAr^F{}_4]$ in an effort to measure the association constants for these interactions. Successive aliquots of amine-borane (1.5 M, 1,2-$F_2C_6H_4$) were added to an NMR tube containing boronium (30 mM, 1,2-$F_2C_6H_4$) and the solution was analysed by ^1H NMR spectroscopy. The change in the chemical shift of the NH signal in boronium was monitored as a function of amine-borane concentration, allowing titration isotherms to be generated (**Figure 3.19**).

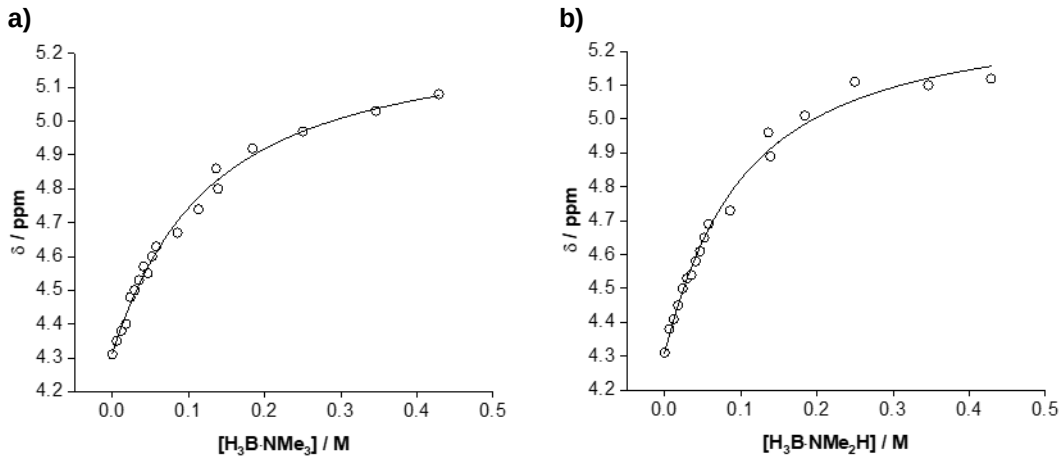


Figure 3.19 Titration binding curve of $[H_2B(NMe_2H)_2][BAr^F{}_4]$ (30 mM, 1,2-$F_2C_6H_4$, 298 K) with a) $H_3B{\cdot}NMe_3$ and b) $H_3B{\cdot}NMe_2H$. For a) the fitted binding isotherm is indicated by the line and K_a = 9.3(1) M^{-1}, calculated using WinEQNMR2[48] from monitoring the chemical shift data for NH protons in $[H_2B(NMe_2H)_2][BAr^F{}_4]$. For b) the attempted 1:1 binding isotherm is indicated by the line but results in substantial errors.

Figure 3.19 shows a notable chemical shift for the addition of the first five equivalents of amine-borane to boronium, after which both isotherms plateau. This

trend suggests a saturation point is reached and so implies the changes in chemical shifts observed are due to a set of genuine interactions.[49]

The titration data for boronium with $H_3B{\cdot}NMe_3$ was analysed using WinEQNMR2[48] by A. Docker (Beer group, University of Oxford) and a 1:1 stoichiometric association constant (K_a) of 9.3(1) M^{-1} was determined. This 1:1 interaction could be due to non-classical dihydrogen bonds occurring between the hydridic B–H protons of $H_3B{\cdot}NMe_3$ and the protic N–H hydrogens of boronium (**Figure 3.20**, *left*).[47] Similar interactions between the BH_2 fragment of one molecule of $H_3B{\cdot}NMe_2H$ and the NH fragment of adjacent $H_3B{\cdot}NMe_2H$ were reported after obtaining the solid state structure of molecules of $H_3B{\cdot}NMe_2H$ (**Figure 3.20**, *right*).[50] Analogous bisphosphine boronium salts have also been reported that demonstrate P–H···X hydrogen bonds between the boronium cation and the corresponding counteranion (X).[51]

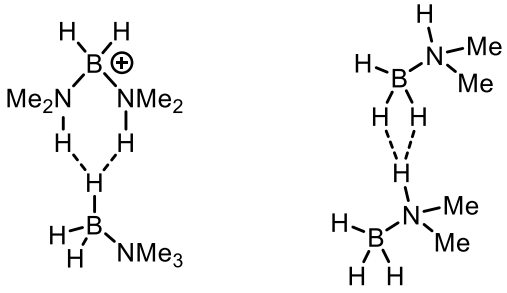


Figure 3.20 *Left:* Suggested adduct of $\{H_2B(NMe_2H)_2\}^+$ with $H_3B{\cdot}NMe_3$. $[BAr^F{}_4]^-$ anion omitted for clarity. *Right*: Schematic adaptation of the solid state structure of multiple molecules of $H_3B{\cdot}NMe_2H$ demonstrating non-classical dihydrogen bonds.

The isotherm generated from the titration of $H_3B{\cdot}NMe_2H$ against $[H_2B(NMe_2H)_2][BAr^F{}_4]$ follows a similar trend to the titration involving $H_3B{\cdot}NMe_3$

(**Figure 3.19**) and thus implies a similar interaction may be occurring. However, the situation is more complex than for $H_3B{\cdot}NMe_3$ as analysis of the titration data resulted in a poor fit to 1:1, 2:1 or 1:2 binding models and so an association constant could not be calculated. This implies that higher stoichiometry and/or complex equilibria are involved. Even so, the titration data demonstrate clearly that there is a significant interaction between $H_3B{\cdot}NMe_2H$ and boronium that may lead to off-cycle adducts and result in the sequestering of these species. If boronium is involved in the rate-determining step of catalysis, this would explain the inhibitory effect on the rate of catalysis as the initial concentration of $H_3B{\cdot}NMe_2H$ is increased.

In section 3.4, an alternative mechanistic pathway for catalysis was also proposed: the "ammonium route". This process would involve the deprotonation of complex **5** by free NMe_2H to yield $\{NMe_2H_2\}^+$, $H_2B{=}NMe_2$ and complex **6**, which could then be reprotonated by ammonium to regenerate complex **1** and NMe_2H. An analogous titration of $H_3B{\cdot}NMe_3$ against $[NMe_2H_2][BAr^F{}_4]$ (30 mM, 1,2-$F_2C_6H_4$) was carried out by A. Docker (Beer group, University of Oxford) and the chemical shifts for the NMe group in $H_3B{\cdot}NMe_3$ were monitored by ^1H NMR spectroscopy (**Figure 3.21**).[24] The data was analysed as before by A. Docker and a 1:1 stoichiometric association constant (K_a) of 28(2) M^{-1} was calculated, indicating the existence of a significant interaction between $H_3B{\cdot}NMe_3$ and $[NMe_2H_2][BAr^F{}_4]$ (more so than with $[H_2B(NMe_2H)_2][BAr^F{}_4]$, K_a = 9.3(1) M^{-1}). This interaction could again come from non-classical dihydrogen bonds between amine-borane and ammonium, forming an adduct as depicted in **Figure 3.21**.

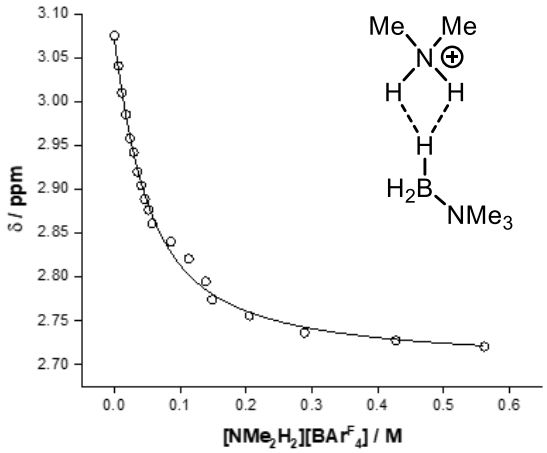


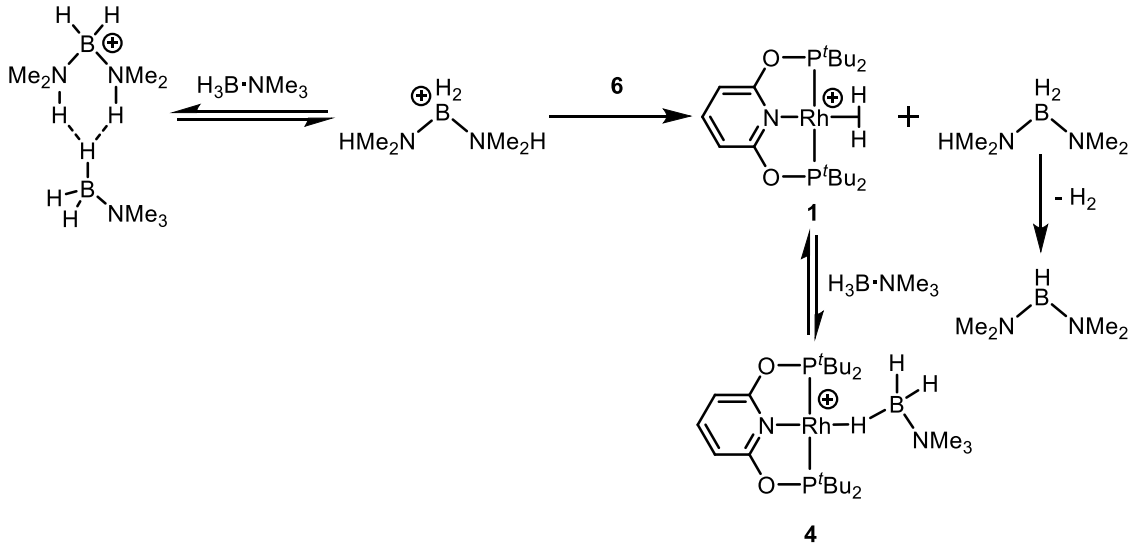
Figure 3.21 Titration binding curve of $[NMe_2H_2][BAr^F_4]$ (30 mM, 1,2-$F_2C_6H_4$, 298 K) with $H_3B{\cdot}NMe_3$. The fitted binding isotherm is indicated by the line and K_a = 28(2) M^{-1}, calculated using WinEQNMR2[48] from monitoring the chemical shift data for NMe protons in $H_3B{\cdot}NMe_3$. Suggested adduct of $\{NMe_2H_2\}^+$ with $H_3B{\cdot}NMe_3$ is also shown. $[BAr^F_4]^-$ anion omitted for clarity.

As for boronium, such an interaction between amine-borane and $[NMe_2H_2][BAr^F_4]$ may indicate a competing off-cycle equilibrium during catalysis in which amine-borane sequesters $\{NMe_2H_2\}^+$. If catalysis proceeds via the "ammonium route" and ammonium is involved in the rate-determining step, then this sequestering of ammonium would explain the decrease in rate of catalysis observed at high initial concentrations of $H_3B{\cdot}NMe_2H$. Thus, as for the KIE experiments described in section 3.6.3, these data do not allow us to discriminate between the two proposed routes.

A competing off-cycle equilibrium in which $H_3B{\cdot}NMe_2H$ sequesters either boronium or ammonium, depending on the mechanistic pathway, may explain another observation. Both the boronium route and ammonium route suggested in section 3.4 involve the protonation of complex **6** to regenerate complex **1**. Stoichiometric

reactions between complex **6** and either boronium or ammonium showed immediate formation of complex **1** with no complex **6** observed by NMR spectroscopy. In contrast, during speciation studies of catalysis, complex **6** was observed by NMR spectroscopy. This would not be expected if either boronium or ammonium were present, as is suggested in both proposed routes, as complex **6** would be rapidly protonated and therefore not observable on an NMR spectroscopy timescale. Therefore, a possible explanation for the observation of complex **6** during catalysis is if the protonating agent (boronium or ammonium) is sequestered rapidly upon production by excess $H_3B{\cdot}NMe_2H$, leading to only a small amount of the protonating species to be available. This effect would change as the concentration of $H_3B{\cdot}NMe_2H$ changes.

Boronium was used to probe this possibility. A 1:1 solution of $H_3B{\cdot}NMe_3$ and $[H_2B(NMe_2H)_2)][BAr^F{}_4]$ (10 mM, 1,2-$F_2C_6H_4$) was added to one equivalent of complex **6** in an NMR tube and the reaction was monitored by NMR spectroscopy (**Scheme 3.7**). $H_3B{\cdot}NMe_3$ was used rather than $H_3B{\cdot}NMe_2H$ in order to simplify the reaction products by preventing any onwards dehydrocoupling occurring.



Scheme 3.7 Proposed reactivity for the addition of complex **6** to a 1:1 solution of $H_3B{\cdot}NMe_3$ and $[H_2B(NMe_2H)_2][BAr^F{}_4]$ in1,2-$F_2C_6H_4$. $[BAr^F{}_4]^-$ anions omitted for clarity.

Initially, a mixture of complex **6** and complex **1** were observed in the $^{31}P\{^1H\}$ NMR spectra. In contrast, the reaction of complex **6** with $[H_2B(NMe_2H)_2][BAr^F{}_4]$ without amine-borane present yielded complete conversion to complex **1** immediately, without any observation of complex **6** (section 3.4). The slower protonation of complex **6** when amine-borane is present is consistent with a competing equilibrium between boronium and amine-borane. Such an equilibrium could therefore be occurring during catalysis, where the concentration of amine-borane is much higher than that of boronium (or ammonium) at any given time, and thus explains why complex **6** can be observed by NMR spectroscopy.

After one minute of reactivity, the $^{31}P\{^1H\}$ NMR spectra showed a mixture of complex **1** and $[Rh(PONOP)(\eta^1\text{-}H_3B{\cdot}NMe_3)][BAr^F{}_4]$ (**4**), with all complex **6** consumed. This observation is consistent with the reaction of complex **1** with

$H_3B{\cdot}NMe_3$ discussed in Chapter Two (section 2.4). The ^{11}B NMR spectra showed signals for unbound $H_3B{\cdot}NMe_3$ and complex **4**, consistent with a mixture of complex **1** and complex **4** being present. Also observed in the ^{11}B NMR spectra were signals for $H_2B(NMe_2)_2H$ and $HB(NMe_2)_2$, just as for the reaction of complex **6** with $[H_2B(NMe_2H)_2][BAr^F{}_4]$ (section 3.4).

In summary, it has been demonstrated that both $[H_2B(NMe_2H)_2][BAr^F{}_4]$ and $[NMe_2H_2][BAr^F{}_4]$ interact significantly with amine-boranes in solution. Therefore, it is proposed that $H_3B{\cdot}NMe_2H$ may sequester these species during catalysis in an off-cycle equilibrium. This process would account for the decrease in rate observed at high initial concentrations of $H_3B{\cdot}NMe_2H$ assuming either boronium or ammonium is involved in the rate-determining step. Furthermore, such an off-cycle equilibrium is proposed to explain the observation of complex **6** during catalysis, even though it has been demonstrated that the presence of either boronium or ammonium leads to immediate protonation of complex **6** to yield complex **1**. These results are consistent with both the ammonium route and boronium route proposed in section 3.4, but do not allow the discernment of which route is, in fact, occurring.

3.8 Role of NMe_2H in catalysis

As demonstrated earlier in this chapter, an induction period is observed for the catalytic dehydrocoupling of $H_3B{\cdot}NMe_2H$ with $[Rh(PONOP)(\eta^2\text{-}H_2)][BAr^F{}_4]$ (**1**), during which $[Rh(PONOP)(\eta^1\text{-}H_3B{\cdot}NMe_2H)][BAr^F{}_4]$ (**5**) is the sole organometallic species present. Two possible pathways for catalysis have been proposed: the "boronium route" and the "ammonium route". Both of these routes are proposed to

involve the initial reaction of free NMe_2H with complex **5**. Free NMe_2H may be present in catalysis due to the dissociation of $H_3B{\cdot}NMe_2H$ in solution.[22,23] Examples of similar reactivity of amine have been reported in the literature, including for the cationic rhodium-based systems $\{Rh(Xantphos)\}^+$[20] and $\{Rh(DPEphos)\}^+$.[21]

In order to probe the role of free NMe_2H in the catalytic dehydrocoupling of $H_3B{\cdot}NMe_2H$ with complex **1**, catalysis was carried out under closed and H_2 evolution conditions with the addition of NMe_2H to investigate any effects upon speciation and kinetics.

Catalysis of $H_3B{\cdot}NMe_2H$ (0.14 M, 1,2-$F_2C_6H_4$) with complex **1** (2 mol%) and one equivalent of NMe_2H (2 M in THF, relative to complex **1**) was carried out in a high pressure NMR tube and the reaction progress monitored by $^{31}P\{^1H\}$ NMR spectroscopy (**Figure 3.22**). The immediate formation of Rh(PONOP)H (**6**) was observed, with no trace of complex **5**, consistent with the proposal that NMe_2H reacts with complex **5** to generate complex **6**. This result suggests that the addition of NMe_2H moves the initial resting state of the organometallic species in catalysis from complex **5** (in undoped catalysis) to complex **6**. After approximately five minutes, a signal for dihydrogen complex **1** was observed, which became the major product as complex **6** was consumed via reprotonation.

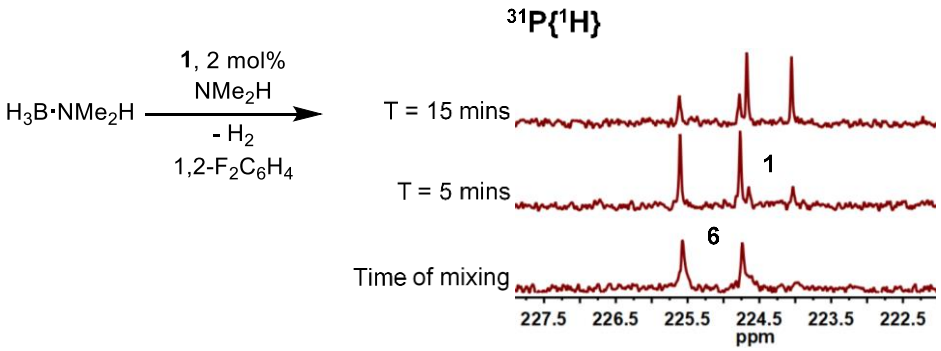


Figure 3.22 Stacked $^{31}P\{^{1}H\}$ NMR spectra (202 MHz, 1,2-$F_2C_6H_4$, 298 K) over time of the reaction of complex **1** (2 mol%) with $H_3B{\cdot}NMe_2H$ (0.14 M) in the presence of 1 eq. NMe_2H (c.f. **1**).

Catalysis doped with NMe_2H was repeated under the same conditions and followed *in situ* by ^{11} B NMR spectroscopy (**Figure 3.23**). The initial ^{11}B NMR spectrum shows signals for $H_2B(NMe_2)_2H$, $H_2B{=}NMe_2$, $[H_2BNMe_2]_2$ and $HB(NMe_2)_2$ indicating catalysis has begun. This suggests that the addition of NMe_2H removes the induction period, and therefore implies that the induction period observed in undoped catalysis depends on the lack of free NMe_2H in solution. Interestingly, the signals for $H_2B{=}NMe_2$ and $H_2B(NMe_2)_2H$ are both initially broad to the extent that there is no resolvable coupling, suggesting these species may be interacting or be in rapid equilibrium with each other. As catalysis progresses, these signals sharpen and coupling is resolved.

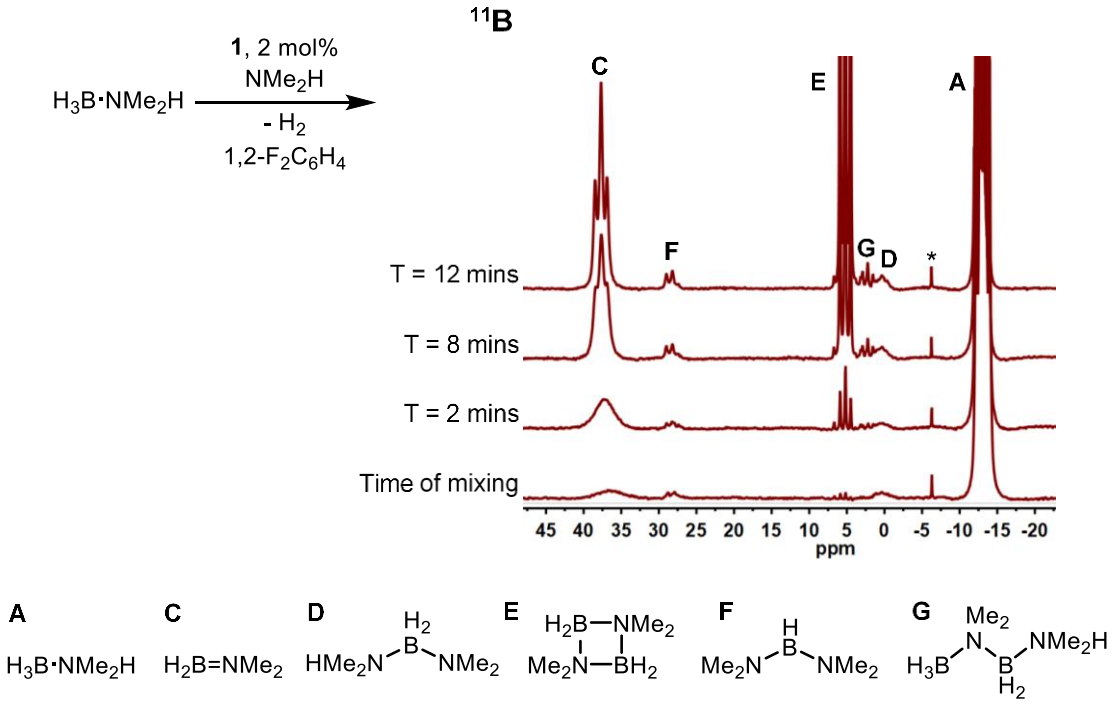
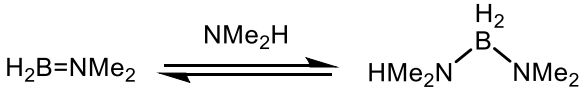


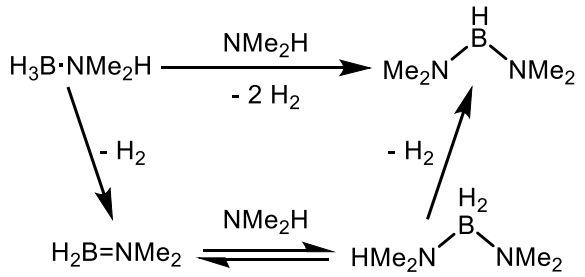
Figure 3.23 Stacked ^{11}B NMR spectra (160 MHz, 1,2-$F_2C_6H_4$, 298 K) over time for catalysis with complex **1** (2 mol%) and $H_3B{\cdot}NMe_2H$ (0.14 M) in the presence of 1 eq. NMe_2H (c.f. **1**).

To test whether this broadening effect is due to the added NMe_2H, catalysis was repeated initially without NMe_2H and ^{11}B NMR spectroscopy showed sharp signals for $H_2B{=}NMe_2$ and $H_2B(NMe_2)_2H$. One equivalent of NMe_2H was then added to the reaction mixture, which was analysed again by ^{11}B NMR spectroscopy. The signals for $H_2B{=}NMe_2$ and $H_2B(NMe_2)_2H$ were now broad, confirming the involvement of NMe_2H in this observation. Therefore, it is suggested that $H_2B{=}NMe_2$ and $H_2B(NMe_2)_2H$ are in equilibrium with each other (**Scheme 3.8**) in the presence of an excess of NMe_2H, leading to a broadening of the signals observed by ^{11}B NMR spectroscopy.



Scheme 3.8 Suggested equilibrium between $H_2B{=}NMe_2$ and $H_2B(NMe_2)_2H$.

When one equivalent of NMe_2H (relative to complex **1**) is added to catalysis, a larger proportion of $HB(NMe_2)_2$ is observed by ^{11}B NMR spectroscopy compared to undoped catalysis (~7 % compared to <1 %) and $HB(NMe_2)_2$ is observed from the start of catalysis rather than towards the end. $HB(NMe_2)_2$ is formed from the dehydrocoupling reaction between $H_3B{\cdot}NMe_2H$ and NMe_2H (**Scheme 3.9**).[17,19,52] In catalysis, this process competes with the dimerisation of $H_2B{=}NMe_2$ to form $[H_2BNMe_2]_2$ and so increasing the concentration of NMe_2H will favour the formation of $HB(NMe_2)_2$.



Scheme 3.9 Formation of $HB(NMe_2)_2$.

In order to probe the effect upon kinetics of the addition of NMe_2H, the catalytic dehydrocoupling of $H_3B{\cdot}NMe_2H$ (72 mM, 1,2-$F_2C_6H_4$, 298 K) with complex **1** (2 mol%) was carried out under H_2 evolution conditions with the addition of one equivalent of NMe_2H (2 M in THF, relative to complex **1**) 30 s after the reagents were combined. **Figure 3.24** shows the concentration of $H_2B{=}NMe_2$ as a function of time

for the doped reaction, overlaid with an undoped reaction under the same conditions.

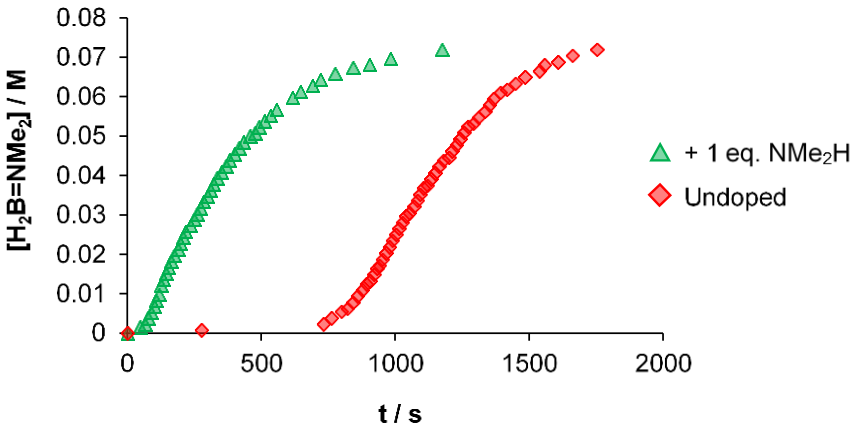


Figure 3.24 Time course plots for the dehydrocoupling of $H_3B{\cdot}NMe_2H$ (72 mM, 1,2-$F_2C_6H_4$, 298 K) with complex **1** (2 mol%) undoped and with the addition of 1 eq. NMe_2H, as measured under H_2 evolution conditions.

As can be seen in **Figure 3.24**, there is no observable induction period when catalysis is doped with one equivalent of NMe_2H (relative to **1**). This is consistent with what is observed in the closed system and suggests the induction period is dependent on the presence of NMe_2H in solution. From the H_2 evolution data, a maximum rate of catalysis (ν_{max}) was calculated to be 1.6×10^{-4} M s^{-1}, which is larger than that for undoped catalysis ($\nu_{max} = 1.0 \pm 0.06 \times 10^{-4}$ M s^{-1}), suggesting that free NMe_2H acts to promote catalysis and may be involved in the rate-determining step. Except for the removal of the induction period, catalysis with the addition of one equivalent of NMe_2H follows essentially the same temporal profile as undoped catalysis and again, the kinetics could not be reconciled with a simple kinetic model. Repeating catalysis under the same conditions except for adding 0.5 mL of THF

rather than NMe_2H (which is used as a 2 M solution in THF) generated an induction period of 720 s (undoped catalysis induction periods 450 – 650 s) and ν_{max} = 0.6 × 10^{-4} M s^{-1} (undoped ν_{max} = 1.0 × 10^{-4} M s^{-1}). Therefore, the lack of induction period and larger ν_{max} observed upon the addition of NMe_2H (2 M in THF) to catalysis can be assumed to be due to the presence of NMe_2H and not THF.

In summary, NMe_2H acts to promote catalysis by removing the induction period and increasing the maximum rate. Speciation studies have shown that addition of NMe_2H moves the initial organometallic resting state from complex **5** to complex **6**, which is consistent with both the proposed ammonium route and boronium route, which require NMe_2H to react with complex **5** in order to generate complex **6**.

3.9 Role of $[H_2B(NMe_2H)_2][BAr^F_4]$ and $[NMe_2H_2][BAr^F_4]$ in catalysis

As described in section 3.4, the observation of Rh(PONOP)H (**6**) during the catalytic dehydrocoupling of $H_3B{\cdot}NMe_2H$ with $[Rh(PONOP)(\eta^2\text{-}H_2)][BAr^F_4]$ (**1**) led to the proposal of two possible mechanistic routes: the boronium route and the ammonium route. Both routes require NMe_2H in solution to react with $[Rh(PONOP)(\eta^1\text{-}H_3B{\cdot}NMe_2H)][BAr^F_4]$ (**5**) to generate Rh(PONOP)H (**6**) along with either boronium, $[H_2B(NMe_2H)_2][BAr^F_4]$, or ammonium, $[NMe_2H_2][BAr^F_4]$. Both boronium and ammonium have been shown to rapidly protonate complex **6** to yield $[Rh(PONOP)(\eta^2\text{-}H_2)][BAr^F_4]$ (**1**), a key step proposed in catalysis. Boronium and ammonium have also demonstrated significant interactions with amine-borane, which thus explains several observations during catalysis (section 3.7). However,

further investigation is required in order to elucidate which pathway is in operation during catalysis.

In order to further probe the possible role of ammonium or boronium in catalysis, several experiments that involved the addition of $[NMe_2H_2][BAr^F_4]$ or $[H_2B(NMe_2H)_2][BAr^F_4]$ to catalysis were carried out and are described in this section.

The catalytic dehydrocoupling of $H_3B{\cdot}NMe_2H$ (72 mM, 1,2-$F_2C_6H_4$, 298 K) with complex **1** (2 mol%) was carried out under H_2 evolution conditions with the addition of one equivalent of $[NMe_2H_2][BAr^F_4]$ (relative to complex **1**) (**Figure 3.25**). An induction period of approximately 3600 s was observed, which is much longer than that observed for undoped catalysis (450 – 650 s).

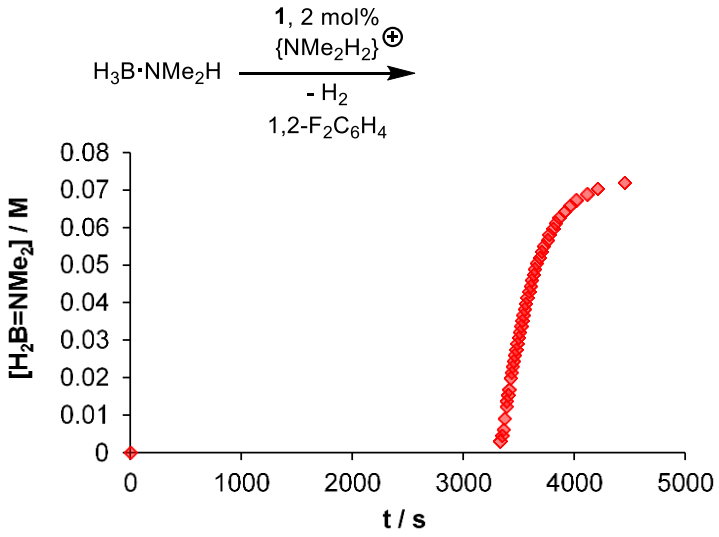


Figure 3.25 Temporal profile for the dehydrocoupling of $H_3B{\cdot}NMe_2H$ (72 mM, 1,2-$F_2C_6H_4$, 298 K) with complex **1** (2 mol%) with the addition of 1 eq. $[NMe_2H_2][BAr^F_4]$ (c.f. **1**) as measured by H_2 evolution.

Complex **5** has been shown to be the sole organometallic species present during the induction period prior to catalysis, with which free NMe_2H may react to generate complex **6** and start catalytic turnover. Therefore, the longer induction period observed when catalysis is doped with ammonium indicates that ammonium may interact with NMe_2H in such a way (e.g. via hydrogen bonding) that inhibits NMe_2H from reacting with complex **5**. Under these conditions, the induction period is proposed to extend until sufficient NMe_2H has been generated by B–N bond cleavage of $H_3B{\cdot}NMe_2H$ to overcome the competing off-cycle equilibrium between NMe_2H and ammonium.

In comparison, the dehydrocoupling of $H_3B{\cdot}NMe_2H$ (72 mM, 1,2-$F_2C_6H_4$, 298 K) catalysed by complex **1** (2 mol%) was carried out with the addition of differing amounts $[H_2B(NMe_2H)_2][BAr^F{}_4]$ (0.5 – 10 eq. compared to complex **1**) and was monitored under H_2 evolution conditions. The induction periods observed for the H_2 evolution experiments with the addition of 0.5 or 1 equivalent of $[H_2B(NMe_2H)_2][BAr^F{}_4]$ are within the same timescale as observed for catalysis under H_2 evolution conditions where no $[H_2B(NMe_2H)_2][BAr^F{}_4]$ has been added (450 – 650 s). However, on the addition of more $[H_2B(NMe_2H)_2][BAr^F{}_4]$, longer induction periods are observed; 760 s for 2 equivalents, 1200 s for 5 equivalents and 1600 s for 10 equivalents. Such an elongation of the induction period was also observed for catalysis with the addition of one equivalent of $[NMe_2H_2][BAr^F{}_4]$. The extended induction period was suggested to be due to a competing off-cycle equilibrium between $[NMe_2H_2][BAr^F{}_4]$ and free NMe_2H and therefore the same explanation is proposed in the case of doping with $[H_2B(NMe_2H)_2][BAr^F{}_4]$.

To probe the sequestering of NMe_2H, $[H_2B(NMe_2H)_2][BAr^F_4]$ (20 mM, 1,2-$F_2C_6H_4$) was added to one equivalent of NMe_2H (2M in THF) in an NMR tube and analysed by NMR spectroscopy. Notable changes in the chemical shift of the NH protons in $\{H_2B(NMe_2H)_2\}^+$ were observed in the ^1H NMR spectra, compared to control experiments (**Figure 3.26**). This observation is analogous to that observed for the interactions between amine-borane and boronium or ammonium (section 3.7) and is consistent with hydrogen bonding occurring between $[H_2B(NMe_2H)_2][BAr^F_4]$ and NMe_2H. This interaction is suggested to be responsible for the extended induction periods observed for the addition of boronium and, by extension, ammonium to catalysis.

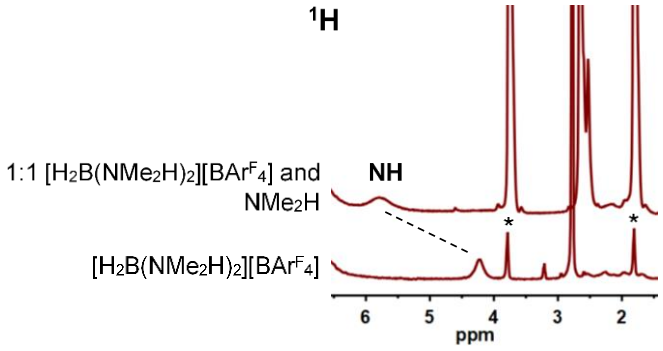


Figure 3.26 Stacked partial ^1H NMR spectra (400 MHz, 1,2-$F_2C_6H_4$, 298 K) of $[H_2B(NMe_2H)_2][BAr^F_4]$ (*bottom*) and a 1:1 mixture of $[H_2B(NMe_2H)_2][BAr^F_4]$ and NMe_2H (*top*). * = residual THF.

The fact that the addition of one equivalent of ammonium to catalysis extends the induction period by more than double that observed upon the addition of 10 equivalents of boronium indicates that ammonium is better able to sequester NMe_2H. This may be due to ammonium exhibiting a stronger interaction with NMe_2H than boronium. An analogous comparison is reflected in the stronger

association constant exhibited by $[NMe_2H_2][BAr^F{}_4]$ (K_a = 28(2) M^{-1}) than $[H_2B(NMe_2H)_2][BAr^F{}_4]$ (K_a = 9.3(1) M^{-1}) for $H_3B{\cdot}NMe_3$ (section 3.7).

When one equivalent of $[NMe_2H_2][BAr^F{}_4]$ was added to catalysis, a maximum rate (ν_{max}) of 2.0 × 10^{-4} M s^{-1} was calculated from the H_2 evolution data. This value is larger than that for undoped catalysis (ν_{max} = 1.0 ± 0.06 × 10^{-4} M s^{-1}). The increase in rate of catalysis with the addition of $[NMe_2H_2][BAr^F{}_4]$, indicates that once the induction period is over and catalytic turnover has begun, the additional ammonium present does not hinder catalysis. A similar increase in maximum rate was observed for catalysis with the addition of one equivalent of $[H_2B(NMe_2H)_2][BAr^F{}_4]$ (ν_{max} = 1.8 × 10^{-4} M s^{-1}). The maximum rates calculated for catalysis with added ammonium or boronium are the same within error to that when one equivalent of NMe_2H is added (ν_{max} = 1.6 × 10^{-4} M s^{-1}) (section 3.8). As both boronium and ammonium can act as a source of free NMe_2H upon reaction with complex **6**, it can be considered that the addition of one equivalent of ammonium or boronium to catalysis is effectively equivalent to adding one equivalent of NMe_2H. Thus, a corresponding increase in the rate of catalysis is achieved.

In section 3.4 it was demonstrated that complex **6** could be protonated to yield complex **1** using a stoichiometric amount of $[NMe_2H_2][BAr^F{}_4]$. To probe this process under catalytic conditions, catalysis under H_2 evolution conditions was carried out as before (72 mM $H_3B{\cdot}NMe_2H$, 2 mol%, one equivalent $[NMe_2H_2][BAr^F{}_4]$ relative to the catalyst) but with complex **6** rather than complex **1**. No induction period was observed and a maximum rate of catalysis (ν_{max}) of 1.6 × 10^{-4} M s^{-1} was calculated

from the H_2 evolution data. The identical ν_{max} and effect upon the induction period are observed for catalysis with complex **1** when one equivalent of NMe_2H (relative to the metal) is added (section 3.8). Therefore, these results are consistent with $[NMe_2H_2][BAr^F_4]$ immediately protonating complex **6** to yield complex **1** along with an equivalent of NMe_2H. Catalysis then occurs as it would do with complex **1** in the presence of one equivalent of NMe_2H.

The reaction of complex **6** with $[H_2B(NMe_2H)_2][BAr^F_4]$ has also been shown to immediately generate complex **1**, along with $H_2B(NMe_2)_2H$ and subsequently $HB(NMe_2)_2$ (section 3.4). $H_2B(NMe_2)_2H$ may reversibly form NMe_2H with $H_2B{=}NMe_2$, and so may act as a source of NMe_2H. Therefore analogous catalysis with complex **6** and one equivalent of $[H_2B(NMe_2H)_2][BAr^F_4]$ could also be expected to have no induction period and a ν_{max} ~1.6×10^{-4} M s^{-1}, just as observed for catalysis with complex **6** and one equivalent of $[NMe_2H_2][BAr^F_4]$ and for catalysis with complex **1** and NMe_2H. In order to probe this, catalysis was carried out with complex **6** (2 mol%), $H_3B{\cdot}NMe_2H$ (72 mM) and one equivalent of $[H_2B(NMe_2H)_2][BAr^F_4]$ (compared to **6**) under H_2 evolution conditions (1,2-$F_2C_6H_4$, 298 K). No induction period was observed, consistent with the protonation of complex **6** to complex **1** along with the generation of NMe_2H, which removes the induction period. However, a maximum rate of catalysis of 0.6×10^{-4} M s^{-1} was calculated from the H_2 evolution data. This value is significantly slower than for catalysis with complex **1** with NMe_2H and complex **6** with $[NMe_2H_2][BAr^F_4]$ ($\nu_{max} = 1.6 \times 10^{-4}$ M s^{-1}), although due to the lack of errors in these measurements from the lack of repeat experiments, this comparison in rates is only tentative. The slower rate for catalysis with complex **6**

and $[H_2B(NMe_2H)_2][BAr^F{}_4]$, along with the lack of induction period, could be explained by the partial sequestering of $[H_2B(NMe_2H)_2][BAr^F{}_4]$ with the excess of $H_3B{\cdot}NMe_2H$. In this case a portion of complex **6** would be protonated by the available boronium to generate **1** along with NMe_2H, hence the lack of induction period. But a portion of complex **6** would remain unprotonated and free to catalyse the dehydrocoupling of $H_3B{\cdot}NMe_2H$ directly at a very slow rate. Thus, the maximum rate of catalysis would be an average of the rate of catalysis with complex **1** and NMe_2H (ν_{max} = 1.6 × 10^{-4} M s^{-1}) and catalysis with complex **6** (ν_{max} = 0.1 × 10^{-4} M s^{-1}). The weighting of this average would depend upon the position of the off-cycle equilibrium between boronium and $H_3B{\cdot}NMe_2H$. Section 3.7 outlined a precedent for the interaction between boronium and amine-borane, with an association constant of 9.8(1) M^{-1} calculated for the interaction between $[H_2B(NMe_2H)_2][BAr^F{}_4]$ and $H_3B{\cdot}NMe_3$. The presence of $H_3B{\cdot}NMe_3$ in solution was also observed to delay the protonation of complex **6** with boronium. These results imply that under catalytic conditions, $[H_2B(NMe_2H)_2)][BAr^F{}_4]$ is not able to completely protonate complex **6**, and therefore the proposed "boronium route" may not be the mechanistic pathway in operation.

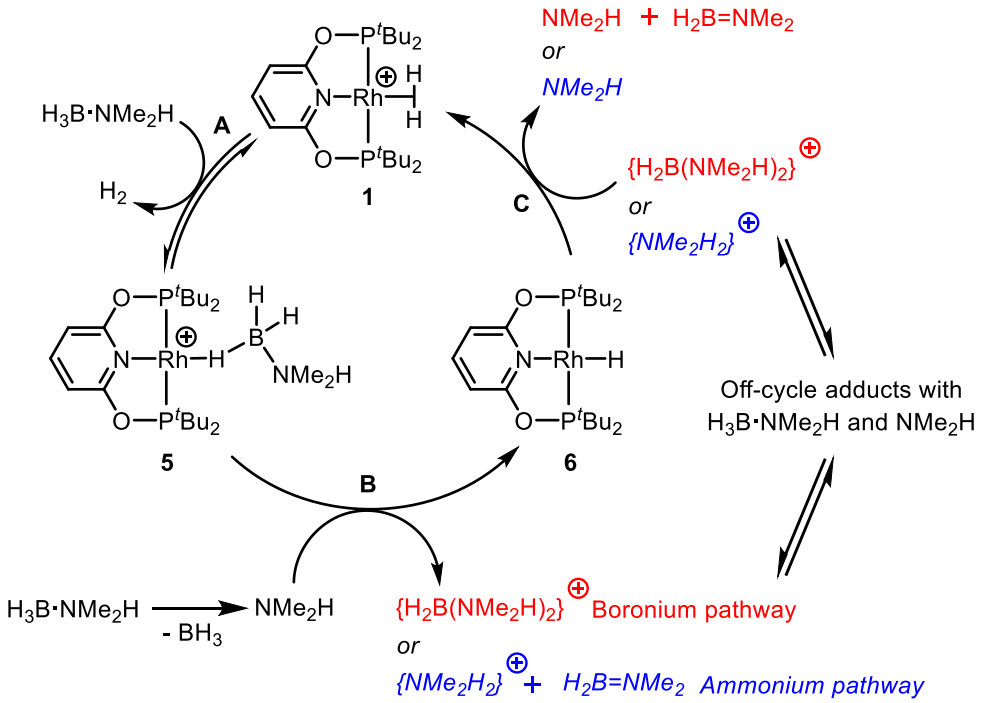
If a competing off-cycle equilibrium is occurring between $H_3B{\cdot}NMe_2H$ and $[H_2B(NMe_2H)_2)][BAr^F{}_4]$, then the same would be expected between $H_3B{\cdot}NMe_2H$ $[NMe_2H_2][BAr^F{}_4]$, especially as $[NMe_2H_2][BAr^F{}_4]$ has demonstrated a stronger interaction with the model amine-borane $H_3B{\cdot}NMe_3$ than $[H_2B(NMe_2H)_2][BAr^F{}_4]$ (K_a = 28(2) M^{-1} compared to K_a = 9.8(1) M^{-1}). Therefore, the same slow rate would be expected for catalysis with complex **6** and $[NMe_2H_2][BAr^F{}_4]$; however the maximum

rate for this reaction is calculated as 1.6×10^{-4} M s^{-1}. A possible explanation for the difference in reactivity observed could be if the protonation of complex **6** by $[NMe_2H_2][BAr^F_4]$ has a lower barrier and/or is more thermodynamically favoured than protonation by $[H_2B(NMe_2H)_2][BAr^F_4]$, to the extent that any off-cycle equilibrium between $[NMe_2H_2][BAr^F_4]$ and $H_3B{\cdot}NMe_2H$ does not inhibit the reactivity of $[NMe_2H_2][BAr^F_4]$ with complex **6**. If this is the case, the "ammonium route" may therefore be operating under catalytic conditions rather than the "boronium route".

To summarise, both the addition of $[NMe_2H_2][BAr^F_4]$ and $[H_2B(NMe_2H)_2][BAr^F_4]$ to catalysis with complex **1** lead to an increase in the maximum rate of catalysis. These effects are proposed to be due to both ammonium and boronium acting as a source of NMe_2H, which has been demonstrated to promote catalysis (section 3.8). Both the addition of ammonium and boronium have been shown to extend the induction period prior to catalysis, supposedly due to the sequestering of NMe_2H in a competing off-cycle equilibrium. As both the addition of ammonium and boronium show similar effects upon catalysis, discerning the mechanistic pathway is difficult. However, in this section it was indicated that $[NMe_2H_2][BAr^F_4]$ is able to protonate complex **6** under catalytic conditions more easily than $[H_2B(NMe_2H)_2][BAr^F_4]$, implying that the ammonium route may be more favourable during catalysis. Further discernment between the two proposed routes was made possible by DFT calculations and is discussed in section 3.11.

3.10 Proposed mechanism for the catalytic dehydrocoupling of $H_3B{\cdot}NMe_2H$ with $[Rh(PONOP)(\eta^2\text{-}H_2)][BAr^F{}_4]$ (1)

Drawing together all the observations described in Chapters Two and Three, a catalytic cycle can be proposed for the dehydrocoupling of $H_3B{\cdot}NMe_2H$ with $[Rh(PONOP)(\eta^2\text{-}H_2)][BAr^F{}_4]$ (**1**) and is depicted in **Scheme 3.10**.



Scheme 3.10 Proposed catalytic cycle for the dehydrocoupling of $H_3B{\cdot}NMe_2H$ with complex **1**. Both the "boronium route" (red) and the "ammonium route" (blue, italics) are depicted. $[BAr^F{}_4]^-$ anions omitted for clarity.

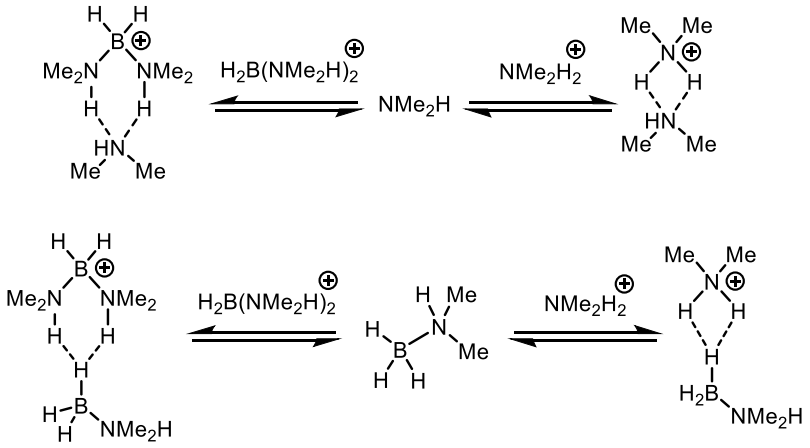
Step A: Complex **1** can react reversibly with $H_3B{\cdot}NMe_2H$ to form the amine-borane sigma complex $[Rh(PONOP)(\eta^1\text{-}H_3B{\cdot}NMe_2H)][BAr^F{}_4]$ (**5**), which is observed to be the resting state during the induction period and also the major product at the very start of catalysis. Deuterium labelling studies have shown that complex **5** can undergo reversible B–H bond activation; however, the lack of a significant KIE

measured for B–H/B–D substitution suggests that B–H bond cleavage is not involved in the rate-determining step. Therefore, we propose reversible B–H activation in complex **5** is not relevant to catalytic turnover.

Step B: Free NMe_2H in solution (generated from the slow, catalyst independent B–N bond dissociation of free $H_3B{\cdot}NMe_2H$) can rapidly react with complex **5** to generate the neutral monohydride Rh(PONOP)H (**6**) along with $[H_2B(NMe_2H)_2][BAr^F{}_4]$ (boronium route) or $[NMe_2H_2][BAr^F{}_4]$ and $H_2B{=}NMe_2$ (ammonium route). This signals the end of the induction period.

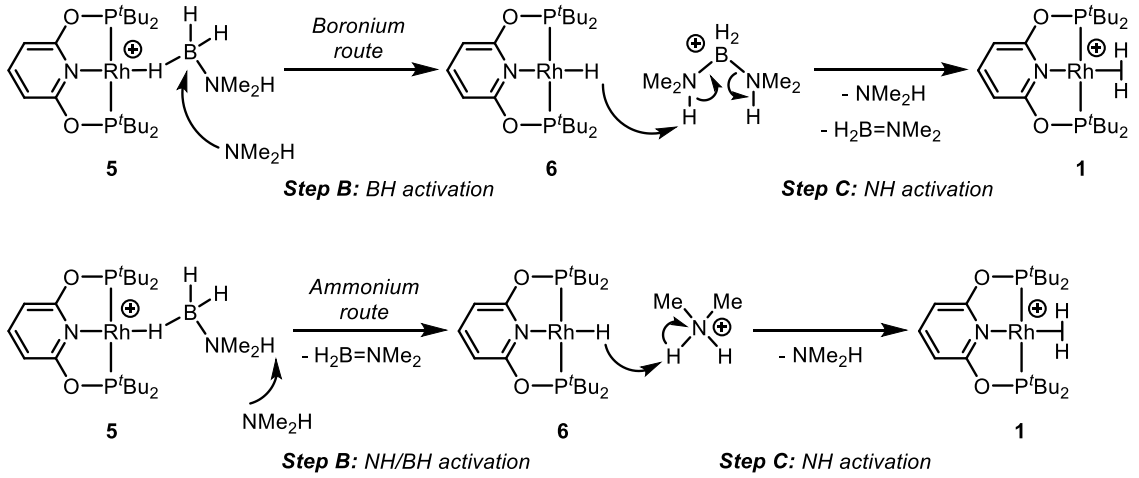
Step C: Protonation of complex **6** by either $[H_2B(NMe_2H)_2][BAr^F{}_4]$ or $[NMe_2H_2][BAr^F{}_4]$ regenerates complex **1** along with free NMe_2H (and $H_2B{=}NMe_2$ in the case of the boronium route). $H_2B{=}NMe_2$ undergoes relatively slow dimerisation to give the major product of $[H_2BNMe_2]_2$. A small amount of $H_2B{=}NMe_2$ may react with free NMe_2H and lose one equivalent of H_2 to generate the side product $HB(NMe_2)_2$.

Throughout catalysis, complex off-cycle equilibria may also operate to attenuate the available concentration of NMe_2H (**Scheme 3.11**, *top*) and either $[H_2B(NMe_2H)_2][BAr^F{}_4]$ or $[NMe_2H_2][BAr^F{}_4]$ (**Scheme 3.11**, *bottom*), thus effecting the species available for catalytic turnover.



Scheme 3.11 *Top:* Sequestering of NMe_2H with either boronium or ammonium. *Bottom:* Sequestering of either boronium or ammonium with $H_3B{\cdot}NMe_2H$. $[BAr^F{}_4]^-$ anions omitted for clarity.

A KIE of 2.0 ± 0.11 was calculated for N–H/N–D substitution in $H_3B{\cdot}NMe_2H$ indicating that N–H bond activation is involved in the rate-determining step. This could be due to **Step C** if the boronium route is operating, or **Step B** and **Step C** if catalysis is occurring via the ammonium route (**Scheme 3.12**). A much smaller KIE of 1.2 ± 0.07 was calculated upon B–H/B–D substitution at $H_3B{\cdot}NMe_2H$, and therefore it is proposed that B–H bond activation is not involved in the rate-determining step in catalysis.



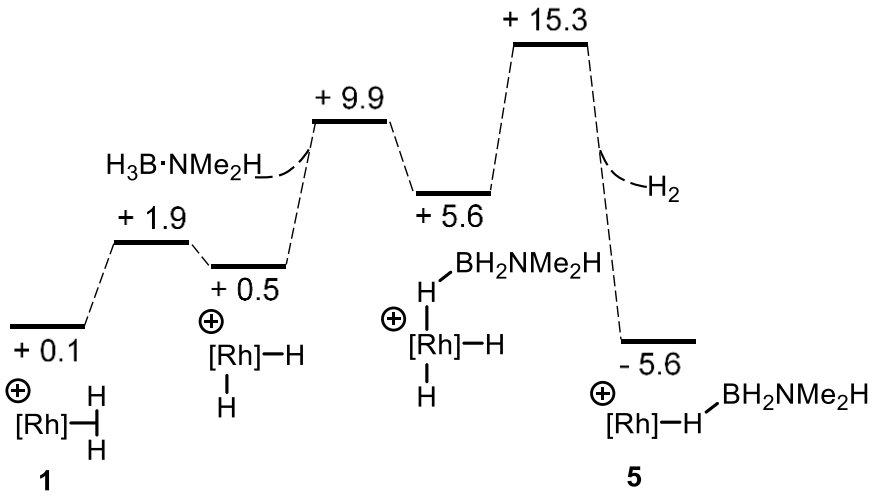
Scheme 3.12 Schematic depicting NH/BH bond activation during mechanistic steps **B** and **C** in both the proposed boronium and ammonium routes. $[BAr^F_4]^-$ anions omitted for clarity.

3.11 Computational studies of catalytic pathways

Two pathways have been proposed for the catalytic dehydrocoupling of $H_3B{\cdot}NMe_2H$ with $[Rh(PONOP)(\eta^2\text{-}H_2)][BAr^F_4]$ (**1**); the "boronium route" and the "ammonium route". Experimental studies discussed in this chapter have shown that both pathways are viable but have not been able to distinguish which pathway may be operating. Therefore, computational studies were undertaken by Dr Nicholas A. Beattie, Gregg Baillie, Rachel Reed and Professor Stuart A. Macgregor (Heriot-Watt University, Edinburgh) in order to provide insight as to the energetic feasibility of both pathways.[24]

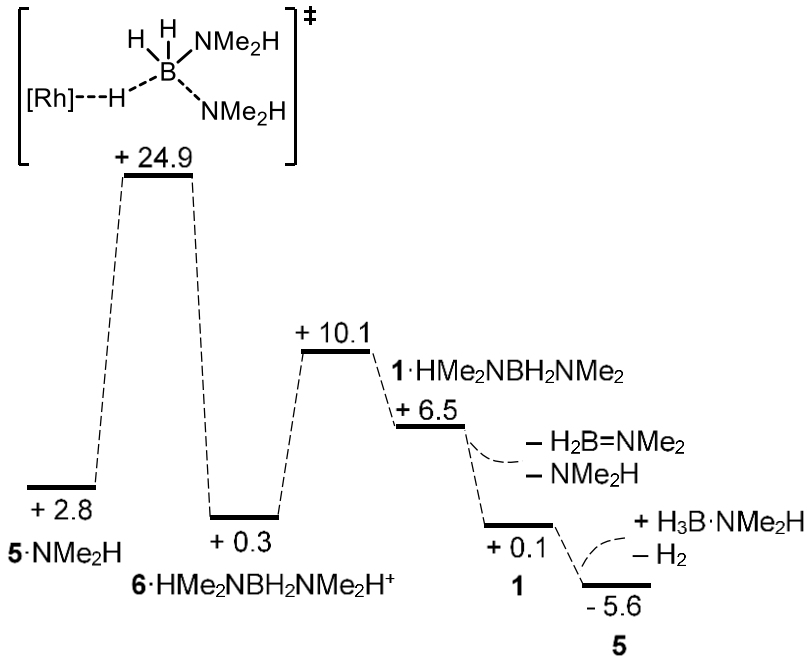
Formation of $[Rh(PONOP)(\eta^1\text{-}H_3B{\cdot}NMe_2H)][BAr^F_4]$ (**5**) from the reaction of complex **1** with $H_3B{\cdot}NMe_2H$ is supported by DFT calculations and is suggested to proceed via initial oxidative cleavage of H_2 in complex **1**, followed by the addition of $H_3B{\cdot}NMe_2H$ to yield a Rh^{III} adduct such as $\{Rh(PONOP)(H)_2(\eta^1\text{-}H_3B{\cdot}NMe_2H)\}^+$ (+5.6 kcal mol^{-1})

(**Scheme 3.13**). Reductive elimination of H_2 via a transition state at +15.3 kcal mol^{-1} is proposed to yield complex **5** (at –5.6 kcal mol^{-1}). This is an associative displacement mechanism rather than a simple dissociative loss of H_2.



Scheme 3.13 Computed free energy profiles (kcal mol^{-1}) for the reaction of complex **1** with $H_3B{\cdot}NMe_2H$ to yield complex **5**. Energies are quoted relative to **5** + free $H_3B{\cdot}NMe_2H$ + free NMe_2H set to 0.0 kcal mol^{-1}.[Rh] = Rh(PONOP).

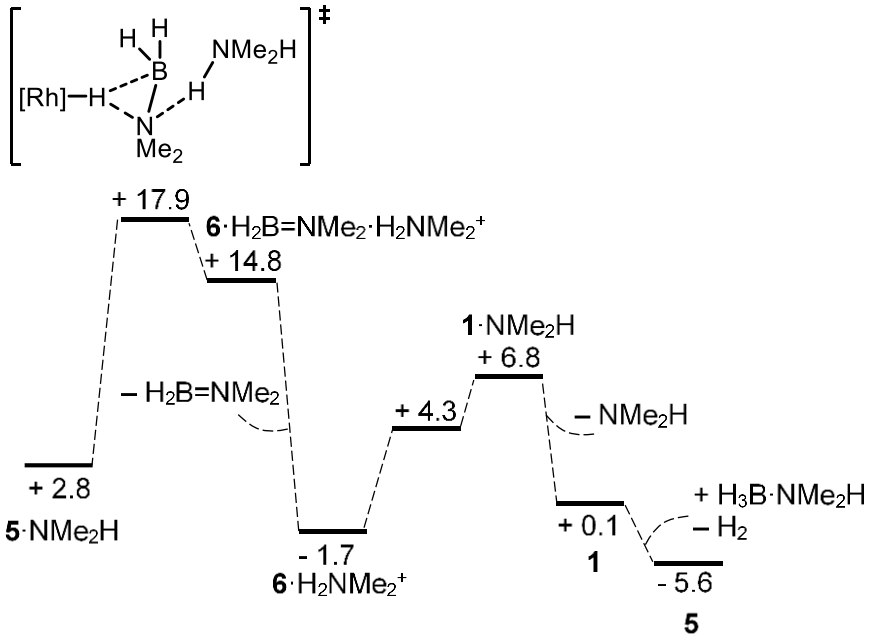
From complex **5** (now set to 0.0 kcal mol^{-1}), a hydrogen-bonded adduct with NMe_2H is proposed to form (+2.8 kcal mol^{-1}). The "boronium route" was then calculated involving nucleophilic attack of NMe_2H at boron in complex **5** resulting in Rh(PONOP)H (**6**) and $\{H_2B(NMe_2H)_2\}^+$, which are proposed to interact via a strong dihydrogen bond (via N–H). Facile proton transfer regenerates complex **1**, initially as a dihydrogen bonded adduct with $H_2B(NMe_2)_2H$, followed by release of $H_2B{=}NMe_2$ and NMe_2H. Complex **5** is reformed upon the addition of $H_3B{\cdot}NMe_2H$. The energy span for this pathway is 24.9 kcal mol^{-1} (**Scheme 3.14**).



Scheme 3.14 Computed free energy profiles (kcal mol^{-1}) for the dehydrocoupling of $H_3B{\cdot}NMe_2H$ from the H-bonded adduct of **5** and NMe_2H via the "boronium route" i.e. initial nucleophilic attack at B. Energies are quoted relative to **5** set to 0.0 kcal mol^{-1}. [Rh] = Rh(PONOP).

The alternative "ammonium route" from the adduct of complex **5** with NMe_2H is proposed to occur via concomitant deprotonation and B–H bond cleavage of complex **5** to yield complex **6** as a weakly bound adduct with $H_2B{=}NMe_2$ and $\{NMe_2H_2\}^+$. Removal of $H_2B{=}NMe_2$ leaves a stable adduct (–1.7 kcal mol^{-1}) of complex **6** and $\{NMe_2H_2\}^+$ containing strong dihydrogen bonds. Facile proton transfer yields complex **1**, initially as an adduct with NMe_2H, which loses NMe_2H and undergoes displacement of H_2 to regenerate complex **5**. The overall energy span for this pathway is calculated to be 17.9 kcal mol^{-1}, which is a smaller barrier than calculated for the boronium route. Although the difference in the calculated overall energy span between the ammonium route and the boronium route is small (7 kcal

mol^{-1}) and therefore does not suggest a large mechanistic difference, these results may indicate that the ammonium route is favoured under catalytic conditions.



Scheme 3.15 Computed free energy profiles (kcal mol^{-1}) for the dehydrocoupling of $H_3B{\cdot}NMe_2H$ from the H-bonded adduct of **5** and NMe_2H via the "ammonium route", i.e. initial deprotonation at N. Energies are quoted relative to **5** set to 0.0 kcal mol^{-1}. [Rh] = Rh(PONOP).

Experimentally, a very small KIE of 1.2 ± 0.07 was calculated upon B–H/B–D substitution and a larger KIE of 2.0 ± 0.11 was calculated for N–H/N–D substitution. For the boronium route, the computed geometries of the rate-determining transition state of nucleophilic attack at boron in complex **5** (**Scheme 3.14**) feature significant B–H bond stretching (calc. 1.73 Å) as complex **6** is formed. This would therefore imply a significant KIE for B–H/B–D bond substitutions; however, this is not seen experimentally. For the ammonium route, the computed transition state (**Scheme 3.15**) before forming complex **6** with $H_2B{=}NMe_2$ and $\{NMe_2H_2\}^+$ exhibits a

later geometry where the proton and hydride transfers have already mostly occurred. For this transition a small KIE would be expected for N–H/N–D substitution, which is observed experimentally. The transition state discussed for the ammonium route is also more energetically favoured (+17.9 kcal mol^{-1}) than for the boronium route (+24.9 kcal mol^{-1}). These studies therefore again imply that the ammonium route is occurring during catalysis.

Complexes **1** and **5** are calculated to be most stable as isolated species, rather than adducts with other species. In contrast, for the ammonium route, complex **6** is calculated to exist as a dihydrogen bonded adduct with $\{NMe_2H_2\}^+$. This interaction therefore explains the slight differences in chemical shift observed for complex **6** during catalysis (^{1}H NMR δ –10.13 ppm) compared to when synthesised independently (^{1}H NMR δ –9.6 ppm). The computed adduct with complex **6**, along with complex **1** and complex **5** are all calculated to be within 1.8 kcal mol^{-1} of each other, consistent with the fact that all three species are observed in catalysis.

As it was demonstrated experimentally that complex **5** was able to undergo B–H activation (section 3.5), computational studies were carried out to probe a viable mechanistic pathway without the involvement of boronium or amine. Such a process based upon unassisted B–H and/or N–H activation of complex **5** was calculated to be much higher in energy: transition states for concerted N–H/B–H activation at +28.5 and +32.3 kcal mol^{-1}; transition state for N–H activation at +50.0 kcal mol^{-1}; no intermediates for B–H activation were located. Therefore, such pathways were deemed energetically unfavourable.

Finally, catalytic dehydrocoupling of $H_3B{\cdot}NMe_2H$ with complex **6** was studied and a transition state involving concomitant B–H transfer to the Rh–H ligand and N–H transfer to the rhodium centre was calculated at +26.2 kcal mol^{-1}. This would be followed by release of $H_2B{=}NMe_2$ and H_2 and the regeneration of complex **6**. The high energy barrier associated with this process is consistent with complex **6** being a poor catalyst and explains why the amine-assisted pathway occurs instead when complex **6** is generated in catalysis starting from complex **1**.

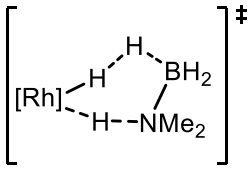


Figure 3.27 Computed geometry of the transition state (+ 26.2 kcal mol^{-1}) for the dehydrogenation of $H_3B{\cdot}NMe_2H$ with complex **6**. Energies quoted relative to **6** + free $H_3B{\cdot}NMe_2H$ set to 0.0 kcal mol^{-1}. [Rh] = Rh(PONOP).

3.12 Conclusions

This chapter has built upon the stoichiometric studies outlined in Chapter Two and has detailed an in-depth study into the mechanism of the dehydrocoupling of $H_3B{\cdot}NMe_2H$ with the cationic pincer complex [Rh(PONOP)(η^2-H_2)][$BAr^F{}_4$] (**1**). A multitude of speciation and kinetic studies have been carried out, resulting in the proposal of a mechanism for catalysis.

At the centre of the catalytic cycle is a hydride transfer process to form the neutral monohydride Rh(PONOP)H (**6**), followed by protonation to regenerate complex **1**. This general process has been proposed for a handful of other cationic systems.[19,20]

Two viable pathways for this hydride transfer/reprotonation process have been proposed: the boronium route and the ammonium route. The boronium route is suggested to occur via nucleophilic attack of NMe_2H at boron in [Rh(PONOP)(η^1-$H_3B{\cdot}NMe_2H$)][$BAr^F{}_4$] (**5**); whereas, the ammonium route consists of deprotonation of the sigma-bound amine-borane in complex **5** by NMe_2H. Both pathways were experimentally demonstrated to be viable; however computational studies carried out on this system suggested that the ammonium route is more energetically favourable under catalytic conditions.

Free NMe_2H in solution has been proposed to promote the formation of complex **6** in catalysis and has been demonstrated to have a positive effect on the rate of catalysis, implying its involvement in the rate-determining step. Similar effects of the addition of amine to catalysis have been recently reported.[21,53]

These studies of the dehydrocoupling of the secondary amine-borane $H_3B{\cdot}NMe_2H$ with the cationic pincer complex **1** allow the opportunity to investigate the elementary processes occurring during the dehydrogenation of amine-boranes in general. The catalytic cycle proposed for the dehydrocoupling of the model amine-borane $H_3B{\cdot}NMe_2H$ may contribute towards the elucidation of a universal mechanism for the more complex dehydropolymerisation of primary amine-boranes, such as $H_3B{\cdot}NMeH_2$.

3.13 Epilogue: further studies involving $[H_2B(NMe_2H)_2][BAr^F_4]$

Throughout this chapter, both the "boronium route" and "ammonium route" proposed for the dehydrocoupling of $H_3B{\cdot}NMe_2H$ with complex **1** have been shown to be experimentally viable. Computational studies described in section 3.11 have aided in discerning which route operates under catalytic conditions, with the ammonium route calculated to be more energetically favourable. However, due to the initial observation of $[H_2B(NMe_2H)_2][BAr^F_4]$ in the stoichiometric reaction between complex **1** and $H_3B{\cdot}NMe_2H$, many more studies were carried out with $[H_2B(NMe_2H)_2][BAr^F_4]$ than with $[NMe_2H_2][BAr^F_4]$. A few of these extra studies involving the addition of $[H_2B(NMe_2H)_2][BAr^F_4]$ to catalysis with complex **1** are discussed below.

Dehydrogenation of $H_3B{\cdot}NMe_2H$ (72 mM, 1,2-$F_2C_6H_4$) catalysed by complex **1** (2 mol%) with the addition of 10 equivalents of $[H_2B(NMe_2H)_2][BAr^F_4]$ (relative to complex **1**) was carried out in an NMR tube (i.e. under closed conditions). The reaction progress was monitored *in situ* using $^{31}P\{^1H\}$ NMR spectroscopy. Speciation observed was the same as for catalysis without the doping of boronium (see section 3.3), except no signal for complex **6** was observed in the $^{31}P\{^1H\}$ NMR spectra for this reaction. This can be explained by the rapid protonation of complex **6** to form complex **1** by $[H_2B(NMe_2H)_2][BAr^F_4]$, as demonstrated in section 3.4. However, as described in section 3.7, competing off-cycle equilibria may sequester boronium, explaining why complex **6** is observed early on in catalysis under undoped conditions. When catalysis is doped with excess boronium, the

concentration of boronium is much higher and so any competing off-cycle equilibrium with $H_3B{\cdot}NMe_2H$ would have less effect, explaining the lack of observed complex **6** under such conditions.

Catalysis with the addition of 10 equivalents of $[H_2B(NMe_2H)_2][BAr^F{}_4]$ under closed conditions was repeated and the reaction progress was monitored *in situ* using ^{11}B NMR spectroscopy. During the induction period (i.e. before $H_2B{=}NMe_2$ is observed), a signal for $[H_2B(NMe_2H)_2][BAr^F{}_4]$ was observed along with unreacted $H_3B{\cdot}NMe_2H$. The speciation then observed during catalytic turnover follows the same trends as observed for undoped catalysis (section 3.3) with the only differences being an increased signal for $H_2B(NMe_2)_2H$ (maximum of 15 % compared to 2 %) and the consumption of $[H_2B(NMe_2H)_2][BAr^F{}_4]$, implying that $H_2B(NMe_2)_2H$ is formed in catalysis from $[H_2B(NMe_2H)_2][BAr^F{}_4]$. This result does not discount the ammonium route, even though $H_2B(NMe_2)_2H$ is always observed during catalysis, as $H_2B(NMe_2)_2H$ may also be formed from the reaction between $H_2B{=}NMe_2$ and NMe_2H, both of which are yielded in the ammonium route.

As discussed in section 3.9, the dehydrocoupling of $H_3B{\cdot}NMe_2H$ (72 mM, 1,2-$F_2C_6H_4$, 298 K) catalysed by complex **1** (2 mol%) with the addition of differing amounts $[H_2B(NMe_2H)_2][BAr^F{}_4]$ (0.5 – 10 eq. compared to complex **1**) was monitored under H_2 evolution conditions. For each experiment, a maximum rate (ν_{max}) was calculated from the H_2 evolution data as described in section 3.6, a comparison of which is depicted in **Figure 3.28**.

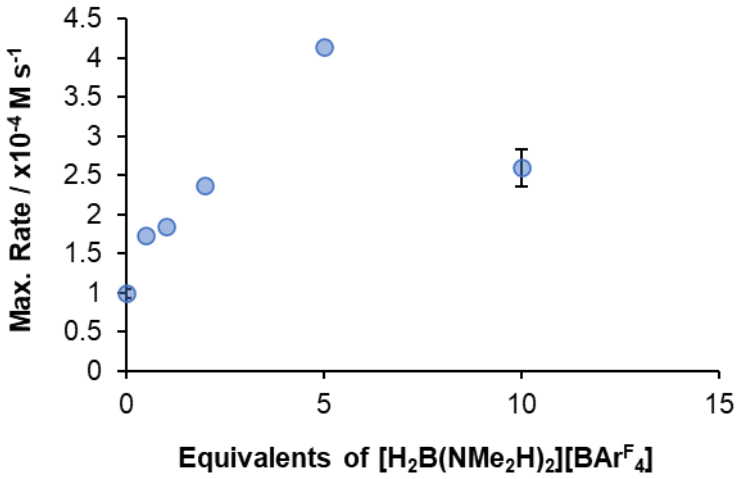


Figure 3.28 Maximum rates of catalysis vs. equivalents of $[H_2B(NMe_2H)_2][BAr^F_4]$ (compared to **1**) added to the catalytic dehydrocoupling of $H_3B{\cdot}NMe_2H$ (72 mM, 1,2-$F_2C_6H_4$, 298 K) with complex **1** (2 mol%) as measured under H_2 evolution conditions.

As can be seen in **Figure 3.28**, the addition of increasing amounts of $[H_2B(NMe_2H)_2][BAr^F_4]$ leads to an increase in ν_{max}, up to a limiting amount of $[H_2B(NMe_2H)_2][BAr^F_4]$ (between 5 – 10 equivalents). The increase in rate observed may be explained by the addition of boronium acting as a source of free NMe_2H upon protonation of complex **6**. Free NMe_2H has been shown to promote catalysis in section 3.8. The decrease in rate of catalysis observed upon the addition of 10 equivalents of $[H_2B(NMe_2H)_2][BAr^F_4]$ compared to 5 equivalents is proposed to be due the sequestering of NMe_2H by $[H_2B(NMe_2H)_2][BAr^F_4]$ in a competing off-cycle equilibrium as described in section 3.9. Therefore, at high concentrations of $[H_2B(NMe_2H)_2][BAr^F_4]$, free NMe_2H may be sequestered and its reaction with complex **5** inhibited to an extent that affects the rate of catalysis.

Data from the H_2 evolution experiments involving the addition of $[H_2B(NMe_2H)_2][BAr^F_4]$ were further analysed using the VTNA method as introduced in section 3.6.4. The concentration profiles for the experiments with the addition of 0.5, 1 and 5 equivalents of $[H_2B(NMe_2H)_2][BAr^F_4]$ are shown in **Figure 3.29**. To achieve overlap, the time scales have been normalised to an overall order of 0.28. This partial order in $[H_2B(NMe_2H)_2][BAr^F_4]$ suggests a mixture of a positive involvement in the promotion of catalysis (source of NMe_2H) along with a secondary, less dominant process that affects the inhibition of catalysis (competing off-cycle equilibrium with NMe_2H).

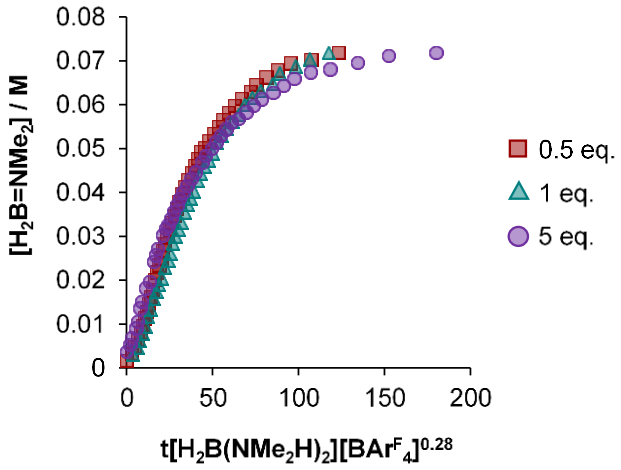


Figure 3.29 Variable Time Normalisation Analysis for the order in $[H_2B(NMe_2H)_2][BAr^F_4]$ for the catalytic dehydrocoupling of $H_3B{\cdot}NMe_2H$ (72 mM, 1,2-$F_2C_6H_4$, 298 K) with complex **1** (2 mol%) with added $[H_2B(NMe_2H)_2][BAr^F_4]$ (0.5 – 5 eq. compare to complex **1**) as measured by H_2 evolution. Induction periods removed for comparison.

In summary, addition of $[H_2B(NMe_2H)_2][BAr^F_4]$ to the catalytic dehydrocoupling of $H_3B{\cdot}NMe_2H$ with complex **1** increases the rate of catalysis, supposedly due to boronium acting as a source of rate-promoting NMe_2H. After a limiting point

(between 5 and 10 equivalents of boronium compared to **1**), the addition of boronium acts to decrease the rate of catalysis. This is proposed to be due to the sequestering of rate-promoting NMe_2H by boronium. Overall, the dependence of the rate of catalysis upon the concentration of boronium includes a complex set of competing off-cycle equilibrium. These studies are consistent with the proposed boronium route and, although the analogous studies have not been carried out with $[NMe_2H_2][BAr^F{}_4]$, similar results would be expected. Computational studies calculate the ammonium route to be more favourable under catalytic conditions; however, the boronium route may still operate under other conditions (e.g. stoichiometric).

3.14 References

[1] H. C. Johnson, T. N. Hooper, A. S. Weller, *Top.Organomet.Chem* **2015**, 153.
[2] A. Staubitz, A. Presa Soto, I. Manners, *Angewandte Chemie International Edition* **2008**, *47*, 6212–6215.
[3] A. L. Colebatch, A. S. Weller, *Chem. Eur. J.* **2019**, *25*, 1379–1390.
[4] C. J. Stevens, R. Dallanegra, A. B. Chaplin, A. S. Weller, S. A. Macgregor, B. Ward, D. McKay, G. Alcaraz, S. Sabo-Etienne, *Chem. Eur. J.* **2011**, *17*, 3011–3020.
[5] O. J. Metters, A. M. Chapman, A. P. M. Robertson, C. H. Woodall, P. J. Gates, D. F. Wass, I. Manners, *Chem. Commun.* **2014**, *50*, 12146–12149.
[6] T. M. Douglas, A. B. Chaplin, A. S. Weller, X. Yang, M. B. Hall, *J. Am. Chem. Soc.* **2009**, *131*, 15440–15456.
[7] T. M. Douglas, A. B. Chaplin, A. S. Weller, *J. Am. Chem. Soc.* **2008**, *130*, 14432–14433.
[8] H. Nöth, H. Vahrenkamp, *Chemische Berichte* **1966**, *99*, 1049–1067.
[9] C. A. Jaska, K. Temple, A. J. Lough, I. Manners, *J. Am. Chem. Soc.* **2003**, *125*, 9424–9434.
[10] H. C. Johnson, A. P. M. Robertson, A. B. Chaplin, L. J. Sewell, A. L. Thompson, M. F. Haddow, I. Manners, A. S. Weller, *J. Am. Chem. Soc.* **2011**, *133*, 11076–11079.
[11] A. P. M. Robertson, R. Suter, L. Chabanne, G. R. Whittell, I. Manners, *Inorg. Chem.* **2011**, *50*, 12680–12691.
[12] L. J. Sewell, G. C. Lloyd-Jones, A. S. Weller, *J. Am. Chem. Soc.* **2012**, *134*, 3598–3610.
[13] N. V. Belkova, L. M. Epstein, O. A. Filippov, E. S. Shubina, *Chem. Rev.* **2016**, *116*, 8545–8587.

[14] R. Kumar, B. R. Jagirdar, *Inorg. Chem.* **2013**, *52*, 28–36.
[15] A. Rossin, M. Caporali, L. Gonsalvi, A. Guerri, A. Lledós, M. Peruzzini, F. Zanobini, *European Journal of Inorganic Chemistry* **2009**, *2009*, 3055–3059.
[16] A. Telleria, C. Vicent, V. San Nacianceno, M. A. Garralda, Z. Freixa, *ACS Catal.* **2017**, *7*, 8394–8405.
[17] M. Roselló-Merino, R. J. Rama, J. Díez, S. Conejero, *Chem. Commun.* **2016**, *52*, 8389–8392.
[18] S. Pal, S. Kusumoto, K. Nozaki, *Organometallics* **2018**, *37*, 906–914.
[19] M. Roselló-Merino, J. López-Serrano, S. Conejero, *J. Am. Chem. Soc.* **2013**, *135*, 10910–10913.
[20] G. M. Adams, A. L. Colebatch, J. T. Skornia, A. I. McKay, H. C. Johnson, G. C. Lloyd−Jones, S. A. Macgregor, N. A. Beattie, A. S. Weller, *J. Am. Chem. Soc.* **2018**, *140*, 1481–1495.
[21] G. M. Adams, D. E. Ryan, N. A. Beattie, A. I. McKay, G. C. Lloyd-Jones, A. S. Weller, *ACS Catal.* **2019**, *9*, 3657–3666.
[22] D. Pun, E. Lobkovsky, P. J. Chirik, *Chem. Commun.* **2007**, *0*, 3297–3299.
[23] M. C. Denney, V. Pons, T. J. Hebden, D. M. Heinekey, K. I. Goldberg, *J. Am. Chem. Soc.* **2006**, *128*, 12048–12049.
[24] E. A. K. Spearing-Ewyn, N. A. Beattie, A. L. Colebatch, A. J. Martinez-Martinez, A. Docker, T. M. Boyd, G. Baillie, R. Reed, S. A. Macgregor, A. S. Weller, *Dalton Trans.* **2019**, *48*, 14724–14736.
[25] Peter. J. Hore, *Nuclear Magnetic Resonance*, Oxford University Press, Oxford, New York, **1994**.
[26] R. N. Perutz, S. Sabo-Etienne, *Angewandte Chemie International Edition* **2007**, *46*, 2578–2592.
[27] H. C. Johnson, E. M. Leitao, G. R. Whittell, I. Manners, G. C. Lloyd-Jones, A. S. Weller, *J. Am. Chem. Soc.* **2014**, *136*, 9078–9093.
[28] A. A. Mikhailine, M. I. Maishan, A. J. Lough, R. H. Morris, *J. Am. Chem. Soc.* **2012**, *134*, 12266–12280.
[29] Python Software Foundation. Python Language Reference, Version 3.7.1 Available at Http://Www.Python.Org.
[30] Anaconda Software Distribution. Computer Software. Version 2-2.4.0. Anaconda, November 2016. Available at Https://Anaconda.Com.
[31] Jones E, Oliphant E, Peterson P, et al. SciPy: Open Source Scientific Tools for Python, 2001. Available at Http://Www.Scipy.Org/ [Online; Accessed 2019-05-14].
[32] J. A. Widegren, R. G. Finke, *Journal of Molecular Catalysis A: Chemical* **2003**, *198*, 317–341.
[33] C. A. Jaska, I. Manners, *J. Am. Chem. Soc.* **2004**, *126*, 9776–9785.
[34] R. Dallanegra, A. P. M. Robertson, A. B. Chaplin, I. Manners, A. S. Weller, *Chem. Commun.* **2011**, *47*, 3763–3765.
[35] M. E. Sloan, A. Staubitz, T. J. Clark, C. A. Russell, G. C. Lloyd-Jones, I. Manners, *J. Am. Chem. Soc.* **2010**, *132*, 3831–3841.
[36] L. J. Sewell, M. A. Huertos, M. E. Dickinson, A. S. Weller, G. C. Lloyd-Jones, *Inorg. Chem.* **2013**, *52*, 4509–4516.
[37] A. N. Marziale, A. Friedrich, I. Klopsch, M. Drees, V. R. Celinski, J. Schmedt auf der Günne, S. Schneider, *J. Am. Chem. Soc.* **2013**, *135*, 13342–13355.

[38] P. Bhattacharya, J. A. Krause, H. Guan, *J. Am. Chem. Soc.* **2014**, *136*, 11153–11161.
[39] R. J. Keaton, J. M. Blacquiere, R. T. Baker, *J. Am. Chem. Soc.* **2007**, *129*, 1844–1845.
[40] A. Kumar, J. S. A. Ishibashi, T. N. Hooper, T. C. Mikulas, D. A. Dixon, S.-Y. Liu, A. S. Weller, *Chemistry – A European Journal* **2016**, *22*, 310–322.
[41] J. Burés, *Angewandte Chemie International Edition* **2016**, *55*, 2028–2031.
[42] J. Burés, *Angewandte Chemie International Edition* **2016**, *55*, 16084–16087.
[43] S. D. Pike, M. R. Crimmin, A. B. Chaplin, *Chem. Commun.* **2017**, *53*, 3615–3633.
[44] A. L. Colebatch, A. I. McKay, N. A. Beattie, S. A. Macgregor, A. S. Weller, *European Journal of Inorganic Chemistry* **2017**, *2017*, 4533–4540.
[45] G. M. Adams, POP-Type Rhodium Complexes in Amine Borane Dehydropolymerisation, Oxford, **2018**.
[46] L. J. Sewell, A. B. Chaplin, A. S. Weller, *Dalton Trans.* **2011**, *40*, 7499–7501.
[47] X. Chen, J.-C. Zhao, S. G. Shore, *Acc. Chem. Res.* **2013**, *46*, 2666–2675.
[48] M. J. Hynes, *J. Chem. Soc., Dalton Trans.* **1993**, 311–312.
[49] P. Thordarson, *Chem. Soc. Rev.* **2011**, *40*, 1305–1323.
[50] S. Aldridge, A. J. Downs, C. Y. Tang, S. Parsons, M. C. Clarke, R. D. L. Johnstone, H. E. Robertson, D. W. H. Rankin, D. A. Wann, *J. Am. Chem. Soc.* **2009**, *131*, 2231–2243.
[51] T. A. Shuttleworth, M. A. Huertos, I. Pernik, R. D. Young, A. S. Weller, *Dalton Trans.* **2013**, *42*, 12917–12925.
[52] P. Bellham, M. S. Hill, G. Kociok-Köhn, D. J. Liptrot, *Chem. Commun.* **2013**, *49*, 1960–1962.
[53] A. Glüer, M. Förster, V. R. Celinski, J. Schmedt auf der Günne, M. C. Holthausen, S. Schneider, *ACS Catal.* **2015**, *5*, 7214–7217.

4 Reactivity of Rh(PONOP)H

4.1 Introduction

Chapters Two and Three discussed the dehydrocoupling of $H_3B{\cdot}NMe_2H$ catalysed by the cationic pincer complex [Rh(PONOP)(η^2-H_2)][$BAr^F{}_4$] (**1**). A mechanistic cycle was proposed and the neutral monohydride Rh(PONOP)H (**6**) was determined to be a key intermediate. During catalysis, it was suggested that free NMe_2H reacts with the amine-borane sigma complex [Rh(PONOP)(η^1-$H_3B{\cdot}NMe_2H$)][$BAr^F{}_4$] (**5**) to yield complex **6**, along with $\{NMe_2H_2\}^+$ and $H_2B{=}NMe_2$. Complex **6** can then be protonated to regenerate the starting complex **1**, thus closing the catalytic cycle. This mechanistic pathway was determined by a mixture of experimental and computational analysis.

Complex **6** can be synthesised more simply, and cleanly isolated, following the method described in Chapter Two, section 2.7: Rh(PONOP)Cl is reacted with $Li[H_3B{\cdot}NMe_2]$ in pentane. In Chapter Three, isolated Rh(PONOP)H was shown to be a poor catalyst for the direct dehydrocoupling of $H_3B{\cdot}NMe_2H$ ($TOF_{25\%}$ = 12 h^{-1} at 2 mol%, 298 K). However, the range of activity of other transition metal monohydrides for the dehydrogenation of amine-boranes is wide, for example: Rh(κ^3-P,O,P-Xantphos-*i*Pr)H ($TOF_{50\%}$ = 1725 h^{-1} at 1 mol%, 304 K),[1] Ru(κ^3-P,O,P-Xantphos-Ph)(H)(H_2O)(PPh_3)][$BAr^F{}_4$] ($TOF_{48\%}$ = 0.1 h^{-1} at 5 mol%, 298 K)[2] and [Fe(*i*PrPOCOP-OMe)(H)(PMe_2Ph)$_2$ ($TOF_{100\%}$ = 13 h^{-1} at 5 mol%, 333 K, for $H_3B{\cdot}NH_3$)[3] (**Figure 4.1**).

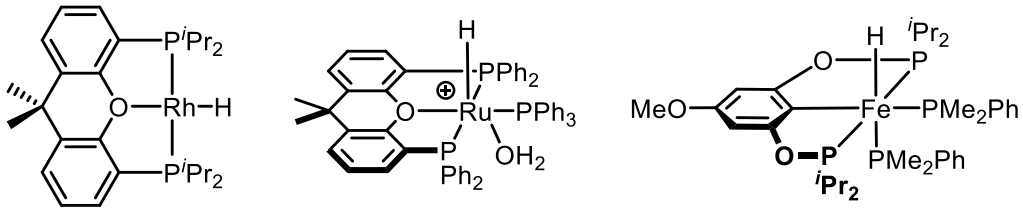


Figure 4.1 *Left:* Rh(κ³-P,O,P-Xantphos-*i*Pr)H;[1] *middle:* Ru(κ³-P,O,P-Xantphos-Ph)(H)(H_2O)(PPh_3)][BAr^F_4][2] and *right:* [Fe($^{i\text{Pr}}$POCOP-OMe)(H)(PMe_2Ph)$_2$.[3]

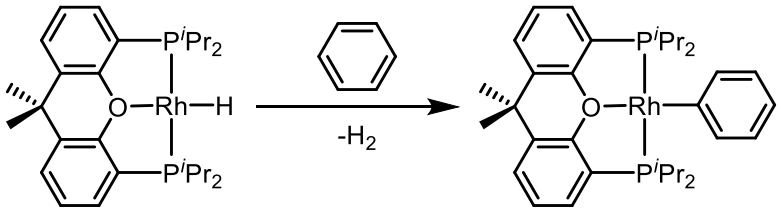
Transition metal hydrides have also been shown to demonstrate other interesting reactivity. For example, Milstein *et al*. have shown an acetone-stabilised Rh^{III} monohydride, [Rh($^{i\text{Pr}}$PCP)(H)((CH_3)$_2$CO)$_2$][BF_4], to coordinate up to two molecules of CO to give [Rh($^{i\text{Pr}}$PCP)(H)(CO)$_2$][BF_4].[4] Other hydrides, such as [Rh($^{t\text{Bu}}$PNP)(H)][5] and [Ir($^{i\text{Pr}}$PNP)(H_3)],[6,7] have been reported to reductively hydrogenate CO_2 using H_2 to yield formic acid. Further applications of transition metal hydrides include olefin hydrogenation,[8,9] ketone hydrogenation[10] and hydrosilylation.[11]

This chapter explores the reactivity of Rh(PONOP)H (**6**), including its potential as a catalyst for the reduction of CO_2. The novel complexes Rh(PONOP)OCOH (**11**), Rh(PONOP)OAc (**14**) and Rh(PONOP)OTf (**15**) are reported, and the reactivity of complex **11** with amine-boranes is probed.

4.2 Solubility and stability of Rh(PONOP)H (6)

Neutral transition metal hydride complexes have been reported to undergo C–H bond activation of arenes and fluoroarenes. For example, Esteruelas *et al*. have

reported the C–H bond activation of benzene with Rh(κ³-P,O,P-Xantphos-^{i}Pr)H leading to the formation of the aryl sigma-coordinated analogue (**Scheme 4.1**).[12]

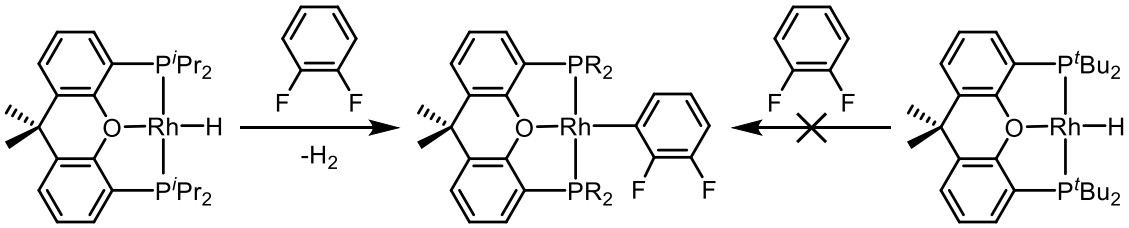


Scheme 4.1 C–H bond activation of benzene using a rhodium monohydride complex.[12]

Prior to investigating the reactivity of Rh(PONOP)H (**6**), its stability in different solvents was probed in order to understand the species that may result from any baseline reactivity.

Upon synthesis, complex **6** was characterised by NMR spectroscopy and the solvent used for this process was C_6D_6. The hydride signal in the ^{1}H NMR spectrum (td, δ –9.60 ppm, $^{1}J_{RhH}$ = 20 Hz and $^{1}J_{PH}$ = 23 Hz) was clearly evident and fully integrated to 1 H (compared to signals for aromatic protons), consistent with there being no C–D bond activation of C_6D_6 at room temperature. Analysing the same solution by NMR spectroscopy two days later showed no change or reactivity. The lack of reactivity of complex **6** with benzene compared to Rh(κ³-P,O,P-Xantphos-^{i}Pr)H may be explained by the increased steric bulk of the ^{t}Bu groups compared to ^{i}Pr, as observed in the following example.

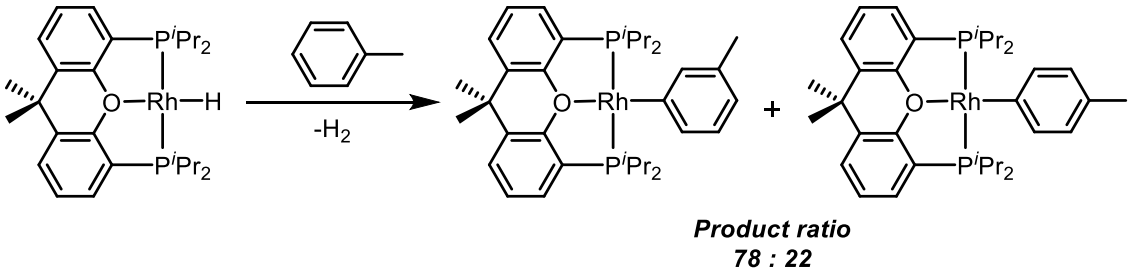
As well as with benzene, Rh(κ³-P,O,P-Xantphos-^{i}Pr)H has been reported to undergo C–H bond activation with fluoroarenes (**Scheme 4.2**).[12–14] However, substitution of the ^{i}Pr groups for bulkier ^{t}Bu groups renders the monohydride complex inactive for the C–H bond activation of 1,2-$F_2C_6H_4$.



Scheme 4.2 C–H bond activation in 1,2-$F_2C_6H_4$ with a rhodium monohydride complex, where R = ^{i}Pr.[13]

Unsurprisingly, the NMR spectra of a 1,2-$F_2C_6H_4$ solution of complex **6** indicated no reaction. Again, this may be due to the presence of sterically bulky ^{t}Bu groups.

Esteruelas *et al*. have also reported the C–H activation of toluene with Rh(κ³-P,O,P-Xantphos-^{i}Pr)H to yield two isomeric sigma-toluene complexes (**Scheme 4.3**).[12]



Scheme 4.3 C–H bond activation of toluene with a rhodium monohydride complex.[12]

$^{31}P\{^{1}H\}$ NMR spectroscopy of a toluene solution of complex **6** showed the formation of two new species in very small amounts (~5 % each) over three days (d, δ 197.0 ppm, $^{1}J_{RhP}$ = 165 Hz and d, δ 198.3 ppm, $^{1}J_{RhP}$ = 153 Hz). Potentially these new signals are due to the formation of analogous sigma-toluene complexes, as in **Scheme 4.3**, or potentially from C–H bond activation of the CH_3 group in toluene to form a benzyl complex, Rh(PONOP)($CH_2C_6H_5$). Assignment of these new species could not be corroborated by the ^{1}H NMR spectrum as any new signals were obscured by those for the toluene solvent, and these products were not characterised further. Although only slight reactivity occurred, these results indicate that complex **6** is not completely stable in toluene.

THF and pentane were also probed as suitable solvents for use with complex **6**. Solutions of complex **6** with both solvents led to no decomposition or reaction as observed by NMR spectroscopy.

To summarise, there is no C–H activation of benzene or 1,2-$F_2C_6H_4$ with complex **6** at room temperature; however, there is some reactivity observed with toluene to give undetermined products. Complex **6** is easily dissolved and stable in benzene, 1,2-$F_2C_6H_4$, THF and pentane and therefore these solvents were employed for the reactivity studies described in this chapter.

4.3 Protonation of Rh(PONOP)H (6)

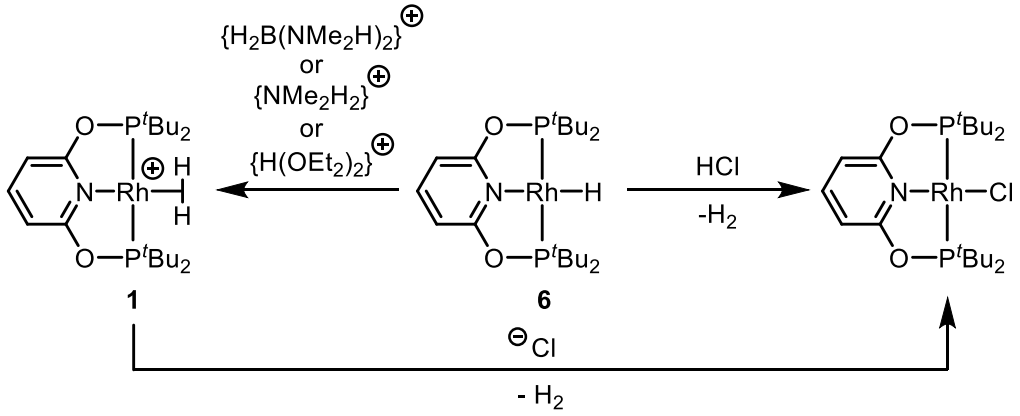
As described in Chapter Three, Rh(PONOP)H (**6**) can be protonated to give {Rh(PONOP)(η^2-H_2)}$^+$ (**1**). It was shown that the addition of a stoichiometric amount

of boronium, $[H_2B(NMe_2H)_2][BAr^F_4]$, or ammonium, $[NMe_2H_2][BAr^F_4]$, salts to a 1,2-$F_2C_6H_4$ solution of complex **6** led to immediate protonation of complex **6**.

Transition metal monohydrides have also been reportedly protonated using Brookhart's acid, $[H(OEt_2)_2][BAr^F_4]$. For example, reaction of Pt(POCOP)H with $[H(OEt_2)_2][BAr^F_4]$ in CD_2Cl_2 at –78 °C yielded $[Pt(POCOP)(\eta^2\text{-}H_2)][BAr^F_4]$.[15] Reaction of complex **6** (20 mM, 1,2-$F_2C_6H_4$) with one equivalent of Brookhart's acid also immediately yielded the analogous protonated product, complex **1**, as observed by NMR spectroscopy.

The reaction of complex **6** with HCl was also studied. A solution of complex **6** (20 mM, C_6H_6) was reacted with one equivalent of HCl (2 M in Et_2O) to immediately yield the known complex Rh(PONOP)Cl,[16] as determined by NMR spectroscopy. This result is consistent with complex **6** being protonated by HCl to give complex **1** as expected, followed by rapid replacement of the η^2-H_2 ligand with chloride indicating the chloride anion is more strongly coordinating than H_2.

To summarise, complex **6** is readily protonated by boronium, ammonium and Brookhart's acid, but in the case of HCl, the end products are Rh(PONOP)Cl and H_2 rather than complex **1** (**Scheme 4.4**).



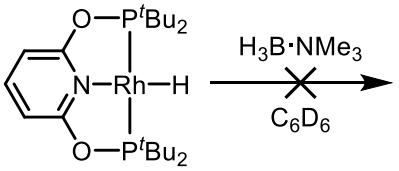
Scheme 4.4 Reactivity of complex **6** with different proton sources. $[BAr^{F}_{4}]^{-}$ anions and the co-products from the reaction of **6** to **1** are omitted for clarity.

4.4 Reaction of Rh(PONOP)H (6) with amine-boranes

In 2016, Rh(κ³-P,O,P-Xantphos-^{i}Pr)H was shown to catalyse the rapid dehydrocoupling of both $H_3B{\cdot}NH_3$ (TOF = 3, 150 h^{-1}) and $H_3B{\cdot}NMe_2H$ (TOF = 1, 725 h^{-1}). The mechanism, as probed by DFT studies, was proposed to operate via decoordination of the oxygen donor in the Xantphos ligand from the metal centre to allow coordination of the respective amine-borane.[1] Three years later, Rh(κ³-P,O,P-Xantphos-R)H (R = ^{i}Pr, ^{t}Bu) was reported to catalyse the dehydropolymerisation of $H_3B{\cdot}NMeH_2$, with the sterically bulkier ^{t}Bu-analogue leading to significantly slower catalysis.[13] Other transition metal hydride complexes have been reported to catalyse the dehydrogenation of amine-boranes, including Ru(κ³-P,O,P-Xantphos-Ph)(H)(H_2O)(PPh_3)][BAr^{F}_{4}],[2] [Ru($^{i\text{Pr}}$POSOP)(H)(Cl)(Py)],[17] and [Fe($^{i\text{Pr}}$POCOP-OMe)(H)(PMe_2Ph)$_2$.[3] With these examples in mind, the reactivity of Rh(PONOP)H (**6**) with amine-boranes was explored.

4.4.1 Reaction of complex 6 with $H_3B{\cdot}NMe_3$

The tertiary amine-borane $H_3B{\cdot}NMe_3$ was used in order to probe the potential for amine-borane coordination to the metal centre of complex **6** without the complication of subsequent dehydrogenation. In an NMR tube, a solution of complex **6** (20 mM, C_6D_6) was combined with one equivalent of $H_3B{\cdot}NMe_3$ (**Scheme 4.5**) and the reaction mixture monitored *in situ* using NMR spectroscopy. No reaction with $H_3B{\cdot}NMe_3$ was observed in the ^{11}B NMR spectra after 24 hours. The sample was then heated to 60 °C for 48 hours and still no reaction was observed by ^{11}B NMR spectroscopy; however, a small amount (~5 %) of decomposition to Rh(PONOP)Cl was observable in the $^{31}P\{^1H\}$ NMR spectrum, presumably from the presence of adventitious chloride.



6

Scheme 4.5 Attempted reaction of complex **6** with $H_3B{\cdot}NMe_3$.

Similar to these results, Rh(κ^3-P,O,P-Xantphos-^{t}Bu)H was reported to not undergo complexation with $H_3B{\cdot}NMe_3$.[13] However, upon reaction with $D_3B{\cdot}NMe_3$, H/D exchange occurred to yield the deuteride analogue, Rh(κ^3-P,O,P-Xantphos-^{t}Bu)D (10 % conversion in 10 minutes), demonstrating reversible B–H activation at the metal centre is possible. Presumably this occurs via a short-lived amine-borane sigma complex intermediate.

To probe whether complex **6** is able to similarly interact with $H_3B{\cdot}NMe_3$, even though no amine-borane complex is observed, a solution of complex **6** (20 mM, C_6D_6) was reacted with one equivalent of $D_3B{\cdot}NMe_3$ and the reaction monitored by NMR spectroscopy. The initial $^{31}P\{^1H\}$ spectrum shows the formation of a small amount (~4 %) of the deuteride analogue of complex **6**, Rh(PONOP)D (**6-D**) (225.9 ppm, dt, $^1J_{RhP}$ = 171 Hz, $^2J_{PD}$ = 3 Hz). The assignment for complex **6-D** comes from the distinctive isotopic perturbation of chemical shift towards the low frequency region compared to the NMR spectroscopic data for Rh(PONOP)H (**6** i.e. **6-H**) in C_6D_6 (226.2 ppm, d, $^1J_{RhP}$ = 171 Hz). The $^{31}P\{^1H\}$ NMR spectrum signal for complex **6-D** also shows $^2J_{PD}$ coupling as a 1:1:1 triplet (**Figure 4.2**). The assignment of complex **6-D** is also consistent with the observation of a signal in the ^2H NMR spectrum at –9.6 ppm, which is of the same chemical shift as observed for **6-H** by ^1H NMR spectroscopy. In addition, when a solution of Rh(PONOP)H is placed under one atmosphere of D_2, the same species assigned as complex **6-D** is observed by NMR spectroscopy, as discussed further in section 4.5.

The signal for **6-D** observed in the $^{31}P\{^1H\}$ NMR spectra increases in intensity to ~70 % after five days (**Figure 4.2**), as the signal for Rh(PONOP)H decreases and a small amount (total ~8 %) of decomposition to Rh(PONOP)Cl is observed (proposed to be due to the presence of adventitious chloride).

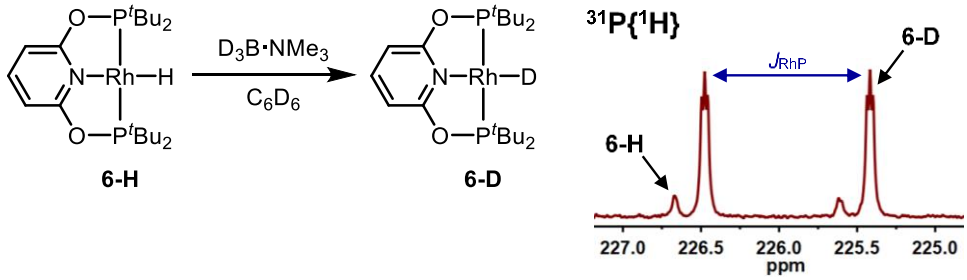
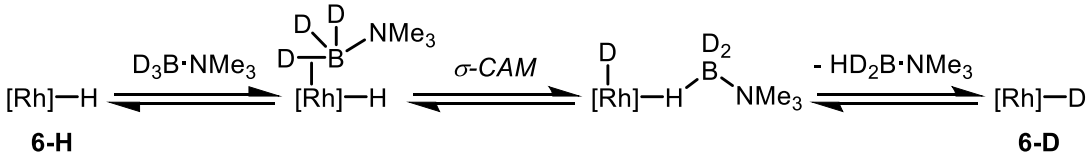


Figure 4.2 Partial $^{31}P\{^1H\}$ NMR spectrum (162 MHz, C_6D_6, 298 K) of the reaction of complex **6-H** with $D_3B{\cdot}NMe_3$ after 5 days. J_{RhP} = 171 Hz.

During the reaction, ^1H NMR spectroscopy reveals a decrease in the integration of the hydride signal for complex **6-H** as the deuteride signal for **6-D** in the ^2H NMR spectra increases. In the ^{11}B NMR spectra, the broad peak at δ –7.7 ppm for $D_3B{\cdot}NMe_3$ shows an asymmetric broadening towards a higher frequency shift as the reaction progress, which is proposed to be due to the slow substitution of B–D for B–H in $D_3B{\cdot}NMe_3$ causing the chemical shift of the signal to be isotopically perturbed.

These results suggest that H/D exchange may occur, albeit slowly, at the metal centre of complex **6** indicating the ability of $H_3B{\cdot}NMe_3$ to undergo B–H activation with complex **6**, proposed to be via a σ-CAM type mechanism[18] (**Scheme 4.6**).



Scheme 4.6 One proposed mechanism for H/D exchange between complex **6-H** and $D_3B{\cdot}NMe_3$ via a σ-CAM mechanism. Not all pathways and H/D combinations are shown. [Rh] = Rh(PONOP).

The reaction of complex **6-H** with one equivalent of $D_3B{\cdot}NMe_3$ was repeated in 1,2-$F_2C_6H_4$, again leading to the slow formation of Rh(PONOP)D (**6-D**) indicating that this reactivity is independent of whether a proto- or deutero-solvent is used.

4.4.2 Reaction of complex 6 with $H_3B{\cdot}NMe_2H$

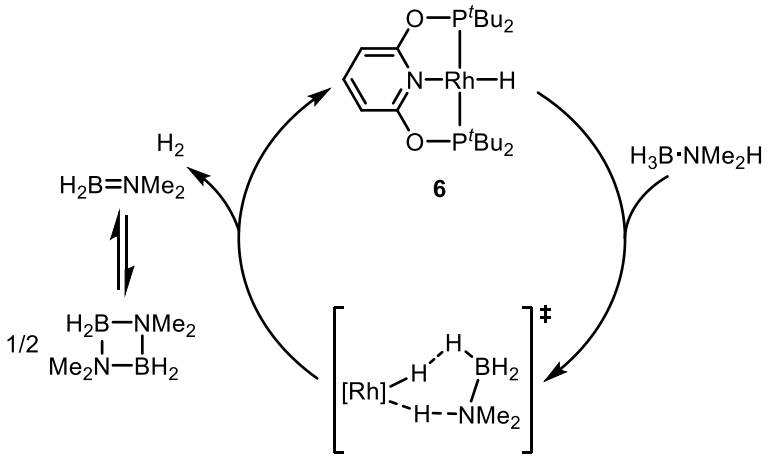
Chapter Three discussed in detail the catalytic dehydrocoupling of $H_3B{\cdot}NMe_2H$ with the cationic complex **1** (ν_{max} = 1.0 ± 0.06 × 10^{-4} M s^{-1}). Neutral complex **6** was identified to be a key intermediate in this process, but was found to be a poor dehydrocoupling catalyst, compared to **1**, when taken with $H_3B{\cdot}NMe_2H$ directly (ν_{max} = 0.12 × 10^{-4} M s^{-1}). The slow reactivity of complex **6** with $H_3B{\cdot}NMe_2H$ was consistent with a higher energy barrier of +26.2 kcal mol^{-1} being calculated for this process, in the absence of NMe_2H.[19]

Other differences between the catalytic activity between complex **1** and complex **6** were observed by speciation studies, as detailed in section 3.4. The organometallic resting state observed throughout catalysis with neutral complex **6** was observed to be solely complex **6**, rather than a cationic amine-borane sigma complex (**5**) as observed for catalysis with complex **1**. Furthermore, the only boron-containing species observed for catalysis with complex **6** are $H_2B{=}NMe_2$ and $[H_2BNMe_2]_2$; whereas, $H_2B(NMe_2)_2H$ and $HB(NMe_2)_2$ were also observed for catalysis with complex **1**.

Another difference between the reactivity of complex **6** and complex **1** with $H_3B{\cdot}NMe_2H$ is that no induction period is observed for catalysis with complex **6**;

whereas, as an induction period between 450 – 650 s is observed for catalysis with complex **1**. The lack of induction period when complex **6** is employed again indicates a different mechanism is occurring than when complex **1** is used.

A proposed mechanism for the catalytic dehydrocoupling of $H_3B{\cdot}NMe_2H$ with complex **6** is depicted in **Scheme 4.7**. Computational studies discussed in section 3.11 revealed a transition state involving concomitant B–H transfer to the Rh–H ligand and N–H transfer to the rhodium centre upon reaction of complex **6** with $H_3B{\cdot}NMe_2H$. This would release $H_2B{=}NMe_2$ and H_2 in a single step and regenerate **6**, thus closing the cycle. This mechanistic pathway is simpler than that proposed for the catalytic dehydrocoupling of $H_3B{\cdot}NMe_2H$ with cationic complex **1** in section 3.10, but more energetically unfavourable. This route is unavailable to $H_3B{\cdot}NMe_3$ due to the lack of N–H bonds.

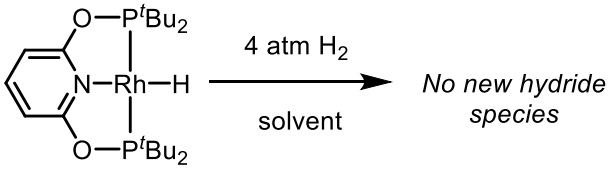


Scheme 4.7 Proposed catalytic cycle for the catalytic dehydrocoupling of $H_3B{\cdot}NMe_2H$ with complex **1**. [Rh] = Rh(PONOP).

4.5 Reaction of complex 6 with H_2 and D_2

Several neutral transition metal pincer complexes have been reported to oxidatively add H_2 leading to an increase in the oxidation state of the metal by two. Such examples include: the reaction of Rh(κ^3-P,O,P-Xantphos-^{t}Bu)Cl and Rh(κ^3-P,O,P-fur-^{t}Bu)Cl (fur-^{t}Bu = 2,5-bis((di-*tert*-butylphosphino)methyl)furan) with H_2 to yield *cis*-Rh(κ^3-P,O,P-Xantphos-^{t}Bu)$(H)_2$Cl and *cis*-Rh(κ^3-P,O,P-fur-^{t}Bu)$(H)_2$Cl respectively;[20] the reaction of Ir($^{t\text{Bu}}$PNP)Ph with H_2 to yield *trans*-Ir($^{t\text{Bu}}$PNP)$(H)_2$Ph;[21] and the addition of H_2 to Ir($^{t\text{Bu}}$PONOP)(CH_3) to yield *trans*-Ir($^{t\text{Bu}}$PONOP)$(H)_2(CH_3)$.[22] The ability of neutral pincer complex Rh(PONOP)H (**6**) to oxidatively add H_2 and access the Rh^{III} oxidation state was subsequently probed.

Complex **6** (5 mg) was added to three high pressure NMR tubes and each sample was dissolved in a different solvent (THF, 1,2-$F_2C_6H_4$ and pentane) before being placed under four atmospheres H_2 and monitored by NMR spectroscopy (**Scheme 4.8**). No initial reaction was observed by NMR spectroscopy; however, after 24 hours a small amount (~15 %) of a mixture of other products were observed in the $^{31}P\{^1H\}$ NMR spectra for the samples in THF and 1,2-$F_2C_6H_4$. The ^1H NMR spectra did not exhibit any corresponding signals in the hydride region indicating these new species are not products from the oxidative addition of H_2. These species were not characterised further.



6

Scheme 4.8 Reaction of complex **6** with H_2. Solvent = THF, 1,2-$F_2C_6H_4$ or pentane.

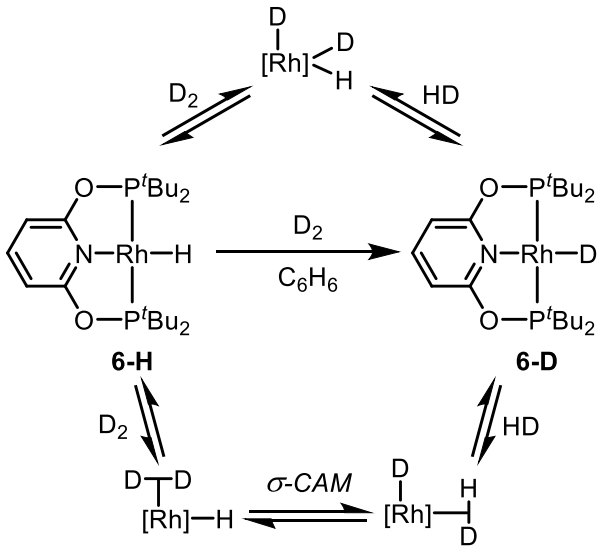
This lack of reactivity is consistent with the fact that the neutral monohydride Rh(κ^3-P,O,P-Xantphos-^{t}Bu)H also undergoes no reaction with H_2 at room temperature.[20] This difference in reactivity compared to Rh(κ^3-P,O,P-Xantphos-^{t}Bu)Cl is proposed to be due to oxidative addition being disfavoured by an increase in sigma-donation to the metal from the hydride ligand compared to the chloride ligand, thus destabilising intermediate species. This reasoning may therefore suggest that Rh(PONOP)Cl may oxidatively add H_2. However, upon reacting a 1,2-$F_2C_6H_4$ solution of Rh(PONOP)Cl with four atmospheres of H_2, no reaction took place. As the *trans*-influence of the X metal-coordinating group in the general pincer "PXP" ligand has been reported to have a significant effect upon the ability of a complex to undergo oxidative addition,[20] the lack of reactivity of Rh(PONOP)Cl compared to Rh(κ^3-P,O,P-Xantphos-^{t}Bu)Cl can be explained by the N-group in the PONOP ligand being more sigma-donating than the O-group in the POP ligand and thus disfavouring oxidative addition.

Although no new species were observed to form when complex **6** was placed under four atmospheres of H_2, a reversible reaction may still be occurring that is biased on

the side of starting materials. This possibility, and thus the possibility of H/D exchange, was probed using D_2.

A solution of complex **6** (i.e. **6-H**) (0.01 mmol, 25 mM, C_6H_6) in a high pressure NMR tube was freeze-pump-thaw degassed and then placed under one atmosphere of D_2 (~0.06 mmol) (**Scheme 4.9**). After three hours, $^{31}P\{^1H\}$ NMR spectroscopy revealed 85 % conversion (relative integral compared to signal for complex **6-H**, assuming no phosphorus leaching) to the deuterium analogue Rh(PONOP)D (**6-D**) (δ 225.9 ppm, dt, $^1J_{RhP}$ = 171 Hz, $^2J_{PD}$ = 3 Hz). The ^2H spectrum exhibited a signal at –9.6 ppm, consistent with **6-D** (for assignment see section 4.4.1), and the ^1H NMR spectrum revealed an ~85 % reduction in the integration of the hydride signal for complex **6-H**. The head space in the NMR tube was then recharged with one atmosphere of D_2, yielding an increase to 92 % conversion to complex **6-D** as observed by $^{31}P\{^1H\}$ NMR spectroscopy. No change in conversion was observed during the next 24 hours, indicating multiple recharges of D_2 would be necessary for full conversion. As H/D exchange had been demonstrated, further recharges in attempt to further push the equilibrium between **6-H** and **6-D** were not attempted.

Two viable mechanistic pathways for the activation of D_2 by complex **6-H** may be via a σ-CAM type mechanism[18] or via a tri-hydride/deuteride complex (**Scheme 4.9**). Due to the lack of observation of a trihydride species when complex **6-H** was placed under H_2, such a trihydride complex is presumed to be unstable; however, DFT calculations would be required to elucidate the exact mechanism.



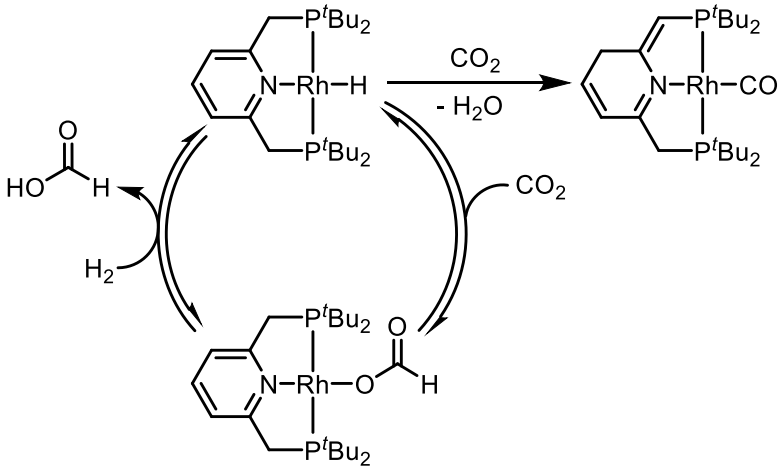
Scheme 4.9 Formation of complex **6-D** from the reaction of complex **6-H** with D_2. *Top:* possible pathway via a tri-hydride/deuteride complex. *Bottom:* possible pathway via a σ-CAM mechanism.

To summarise, while complex **6** does not appear to undergo reaction with H_2, this reaction is shown to be reversible as it does react quickly with D_2 to generate Rh(PONOP)D (**6-D**) as the major product showing, H/D exchange can occur at the metal centre.

4.6 Reaction of Rh(PONOP)H (6) with CO_2

The catalytic reduction of CO_2 to yield other carbon-containing, potentially higher value materials is an important process.[23–26] CO_2 has been reported to insert into transition metal hydride bonds to yield formate complexes, which are proposed as intermediates during the metal-catalysed reduction of CO_2 to formic acid.[27,28] For example, Takase *et al*. have reported CO_2 insertion into Ni^{II} and Pd^{II} hydride complexes to yield the corresponding formate complexes, such as M(^{R}PCP)(OCOH) (M = Ni, Pd; R = $^{t}Bu_2$, Cy_2).[29] Milstein *et al*. also reported the ability of Rh($^{t\text{Bu}}$PNP)H

to undergo rapid insertion of CO_2 into the Rh–H bond to give the formate complex Rh($^{t\text{Bu}}$PNP)(OCOH) (**Scheme 4.10**).[5] In this case, hydrogenation of Rh($^{t\text{Bu}}$PNP)(OCOH) returned Rh($^{t\text{Bu}}$PNP)H alongside formic acid. However, attempts to make this process catalytic were hindered by CO_2 cleavage to form the dearomatised product Rh($^{t\text{Bu}}$PNP')(CO) and water. In 2009, the dehydrogenation of CO_2 was successfully catalysed by an Ir^{III} trihydride complex, Ir($^{i\text{Pr}}$PNP)$(H)_3$, in the presence of 1 M KOH.[6,7]



Scheme 4.10 Proposed mechanism for the catalytic reduction of CO_2 with Rh($^{t\text{Bu}}$PNP)H.[5]

CO_2 was also reported to be catalytically reduced by Ni($^{t\text{Bu}}$PONOP)H via hydroboration of catecholborane.[30] During this process, initial CO_2 insertion into the Ni–H bond of the monohydride is observed, yielding the formate complex, Ni($^{t\text{Bu}}$PONOP)(OCOH).

The literature precedent of the reactivity of transition metal hydride complexes with CO_2 led to the investigation of the reactivity of Rh(PONOP)H (**6**) with CO_2, as described in this section.

4.6.1 Formation of Rh(PONOP)OCOH (11)

Initially, the ability of CO_2 to insert into the Rh–H bond of complex **6** was probed. In a high pressure NMR tube, a solution of Rh(PONOP)H (**6**) (25 mM, C_6D_6) was freeze-pump-thaw degassed three times, following which one atmosphere of CO_2 was admitted to the system. Upon shaking of the sample, the reaction mixture underwent an immediate colour change from red to orange. The $^{31}P\{^1H\}$ NMR spectrum of the sample initially showed 97 % conversion to a new species (**11**), as signalled by the observation of a doublet at 200.3 ppm ($^1J_{RhP}$ = 163 Hz) (**Figure 4.3**). This new species shows a similar decrease in chemical shift (~20 ppm) and coupling constant (~10 Hz) compared to complex **6** (d, 226.2 ppm, $^1J_{RhP}$ = 171 Hz) as reported for the comparison of the complexes Rh(PNP)H (d, 83.2 ppm, $^1J_{RhP}$ = 166 Hz)[31] and Rh(PNP)(OCOH) (d, 60.0 ppm, $^1J_{RhP}$ = 154 Hz).[5] The ^1H NMR spectrum of complex **11** exhibits a signal at 8.63 ppm, integrating to 1H and assigned to the formyl proton. This is similar to that observed for Rh(PNP)(OCOH) (8.58 ppm, dt). Upon comparison with the NMR spectroscopic data for the reported formate complex Rh(PNP)(OCOH), the novel complex **11** was assigned as the analogous formate complex Rh(PONOP)(OCOH).

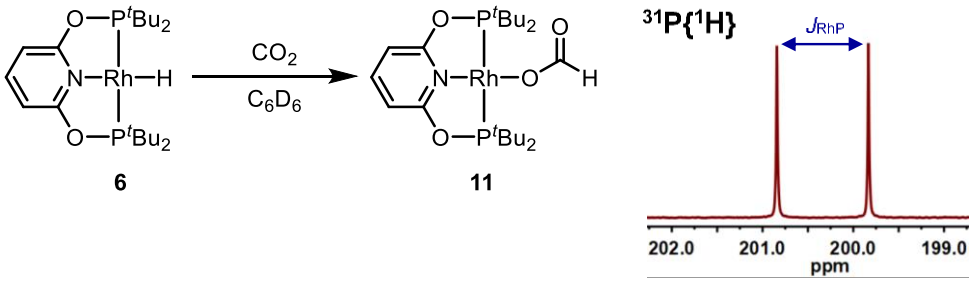


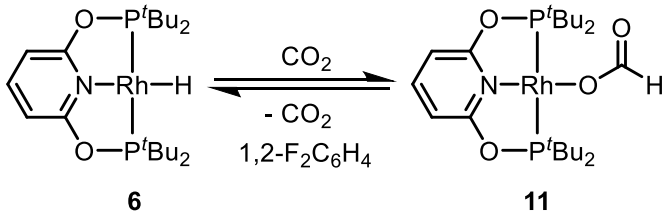
Figure 4.3 Synthesis and partial $^{31}P\{^1H\}$ NMR spectrum of complex **11** (162 MHz, C_6D_6, 298 K). J_{RhP} = 163 Hz.

$^{31}P\{^1H\}$ NMR spectroscopy of the sample one hour after CO_2 had been added showed a decrease in the signal for complex **11** from 97 % to 93 %, with multiple other species present, indicating complex **11** is unstable in solution. After 24 hours, only 32 % of the phosphorus containing species present was complex **11**. Milstein *et al*. reported similar instability of Rh(PNP)(OCOH) in solution, with gradual conversion to Rh(PNP')(CO) (PNP' = deprotonated ligand) observed.[5] The PONOP ligand is unable to be deprotonated in the same way as the PNP ligand, and no analogous CO complex, $\{Rh(PONOP)(CO)\}^+$,[32] was observed by $^{31}P\{^1H\}$ NMR spectroscopy. Therefore, the decomposition observed of complex **11** in solution must be occurring via a different route than that reported for Rh(PNP)(OCOH). The multiple decomposition products were not characterised further.

The reaction with complex **6** and CO_2 was repeated under the same conditions but in 1,2-$F_2C_6H_4$ rather than C_6D_6 solvent. In this case, the initial $^{31}P\{^1H\}$ NMR spectrum indicated 100 % conversion to complex **11**, with decomposition to 96 % after one hour and only 16 % of **11** remaining after 24 hours. This result indicates that the use of 1,2-$F_2C_6H_4$ as a solvent rather than C_6D_6 yields better reactivity, but faster

decomposition. However, due to the complete conversion to complex **11** observed, all future reactions involving complex **11** were carried out in 1,2-$F_2C_6H_4$, using a freshly prepared solution.

Attempts to isolate complex **11** were carried out by the removal of solvent *in vacuo* immediately after complex **11** had been formed. The NMR spectrum of a solution of the resulting orange solid indicated that CO_2 had been extruded to yield complete conversion back to complex **6** (**Scheme 4.11**), showing that insertion of CO_2 into the Rh–H bond is reversible. The same result was reported when vacuum was applied to Rh(PNP)(OCOH).[5]



Scheme 4.11 Reversible reaction of CO_2 with complex **6**.

However, complex **11** was able to be isolated using recrystallisation techniques as follows. A methylcyclohexane solution of complex **6** (15 mM) was freeze-pump-thaw degassed three times and one atmosphere of CO_2 was added to the system. The reaction mixture was immediately cooled to 5 °C for one hour and then left at –20 °C for three days, after which dark orange crystals suitable for single crystal X-ray diffraction had formed. The solid state structure of complex **11** is depicted in **Figure 4.4**.

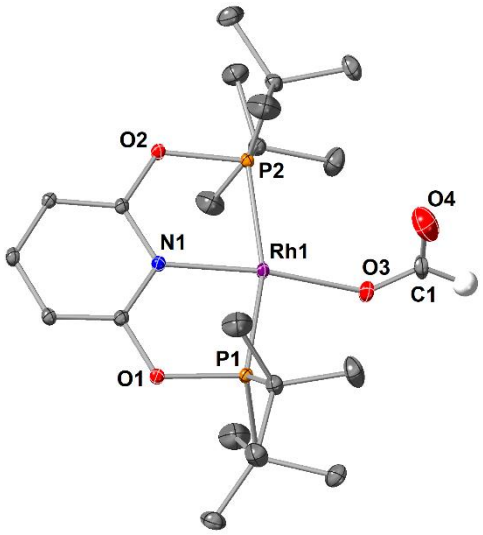


Figure 4.4 Solid state structure of complex **11**. Displacement ellipsoids are drawn at the 30 % probability level. Carbon-bound hydrogens are omitted for clarity. Selected bond lengths (Å) and angles (°): Rh1–O3, 2.0713(18); Rh1–P1, 2.2399(6); Rh1–P2, 2.2570(6); Rh1–N1, 2.002(2); C1–O3, 1.266(4); C1–O4, 1.225(4); P1–Rh1–P2, 163.17(2); N1–Rh1–O3, 169.88(8).

The solid state structure of complex **11** indicates an η^1-OCOH binding mode with a Rh–O distance of 2.0713(18) Å, analogous to that reported for Rh(PNP)(OCOH)[5] (Rh–O, 2.075(2) Å) and for a cobalt-based formate complex, Co(PNP)(OCOH)[33] (Co–O, 1.9120(15) Å). A pseudo-square planar geometry around the rhodium centre is observed, with near linear bond angles around the metal centre (N–Rh–O, 169.88(8)° and P–Rh–P, 163.17(2)°). Similar geometry is observed for Rh(PNP)(OCOH) (N–Rh–O, 169.02(6)° and P–Rh–P, 167.62(2)°) and Co(PNP)(OCOH) (N–Co–O, 166.43(6)° and P–Co–P, 165.86(2)°). The C1–O4 bond exhibits a shorter bond distance (1.225(4) Å) than for C1–O3 (1.266(4) Å) consistent with C1–O4 bond having more double bond character as expected. An analogous difference in bond lengths is reported for Rh(PNP)(OCOH) (C=O = 1.214(4) Å and C–O = 1.270(4) Å).[5]

4.6.2 Catalytic hydrogenation of CO_2 to form formic acid

As described previously, the Ir^{III} complex $Ir(^{i}PrPNP)(H)_3$ has been reported to successfully catalyse the hydrogenation of CO_2 under basic conditions to yield formic acid via the insertion of CO_2 into an Ir–H bond.[6,7] Milstein *et al*. have also shown that, after the rapid insertion of CO_2 into Rh(PNP)H to yield Rh(PNP)(OCOH), the addition of H_2 reforms Rh(PNP)H alongside formic acid (depicted earlier in **Scheme 4.10**).[5] However, efficient hydrogenation is hindered by deprotonation of the PNP ligand and CO_2 cleavage to yield Rh(PNP')(CO). The PONOP ligand is unable to be deprotonated in the same way as the PNP ligand and therefore Rh(PONOP)H (**6**) may allow for efficient hydrogenation of CO_2.

In order to probe the potential of complex **6** as a catalyst for the hydrogenation of CO_2, the reaction of Rh(PONOP)(OCOH) (**11**) with H_2 was investigated. In a high pressure NMR tube, a solution of complex **6** (25 mM, 1,2-$F_2C_6H_4$) was freeze-pump-thaw degassed three times before being placed under one atmosphere of CO_2. NMR spectroscopy confirmed immediate full conversion to complex **11** as expected. The sample was then freeze-pump-thaw degassed again and backfilled with one atmosphere of H_2. Initially, NMR spectroscopy indicated no immediate reaction; however, $^{31}P\{^{1}H\}$ NMR spectroscopy after 10 minutes showed the presence of 6 % complex **6** (calculated from relative integrals), with the remaining 94 % the signal for complex **11**. The ^{1}H NMR spectrum also showed a small, new signal at 8.83 ppm, tentatively assigned to the C–H proton in formic acid.[5] However, after three hours

of reactivity, although complex **11** remained the major species (53 %), many new species were present in the $^{31}P\{^{1}H\}$ NMR spectrum indicating decomposition.

To prevent the presence of formic acid reacting with the organometallic complexes in solution and potentially leading to decomposition, the addition of H_2 to complex **11** was repeated but in the presence of NEt_3 (1:5 NEt_3:solvent). The role of NEt_3 is to react with any formic acid produced *in situ* to yield $[HNEt_3][OCOH]$. Initially, a small amount (~2 %) of conversion to complex **6** was observed in the $^{31}P\{^{1}H\}$ NMR spectrum. However, NMR spectroscopy after four hours showed no more formation of complex **6** and decomposition to multiple species was again observed, but complex **11** remained the major product (~72 %). A lower conversion to complex **6** but less decomposition was observed than without the presence of NEt_3.

The same reaction in the presence of NEt_3 was repeated in C_6D_6 and in THF. Similarly, a small amount of initial conversion to complex **6** was observed after the addition of one atmosphere of H_2 (5 % and 4 % respectively), followed by decomposition of complex **11** after four hours (85 % and 72 % remaining complex **11**, respectively).

In order to carry out the hydrogenation of CO_2 under catalytic conditions, both CO_2 and H_2 are required to be present in order to constantly regenerate complex **11** (the formate) and complex **6** (the hydride) respectively. Even though addition of H_2 to complex **11** had only yielded small conversions to complex **6**, an attempt at catalysis was carried out. In a high pressure NMR tube, complex **6** (10 mg, 0.02 mmol) was

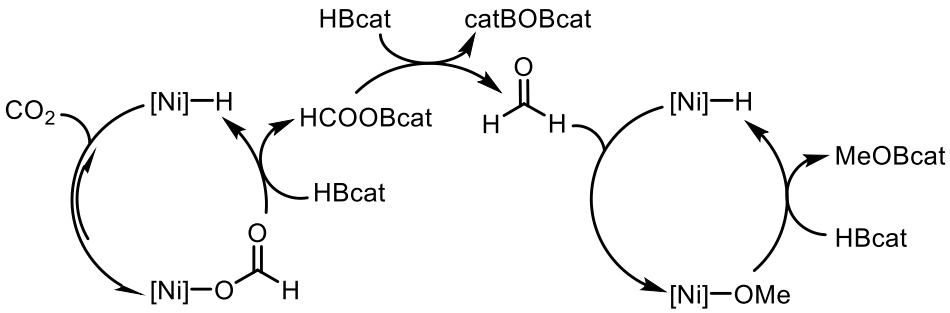
dissolved in a 1:5 mixture of NEt_3:THF (0.6 mL in total) and freeze-pump-thaw degassed three times. The sample was then placed under one atmosphere of 1:1 H_2:CO_2 for 45 minutes. $^{31}P\{^1H\}$ NMR spectroscopy showed complex **11** to be the major complex (~88 %), along with a small amount of complex **6** (~5 %) and multiple other unknown species (~7 %). At this point, ^1H NMR spectroscopy showed no signal for formic acid or [$HNEt_3$][OCOH]. $^{31}P\{^1H\}$ NMR spectroscopy after 24 hours showed complete decomposition.

To summarise, upon reaction of complex **6** with CO_2, rapid insertion of CO_2 into the Rh–H bond to yield the formate complex Rh(PONOP)(OCOH) (**11**) is observed. This complex is not stable in solution nor can it be easily isolated from the reaction solution. The addition of H_2 to complex **11** resulted in a very limited conversion back to complex **6**. Complex **6** did not catalyse the hydrogenation of CO_2 to yield formic acid at room temperature under one atmosphere of 1:1 H_2:CO_2. However, successful catalysis using transition metal hydrides has been reported to occur at pressures between 35–80 atm of 1:1 H_2:CO_2 and temperatures of up to 200 °C.[5–7,25,26] Therefore, complex **6** may still have potential as a catalyst for the hydrogenation of CO_2, but the use of higher pressures and temperatures may be required. Reactivity under these conditions is not explored in this thesis.

4.7 Reaction of Rh(PONOP)OCOH (11) with amine-boranes

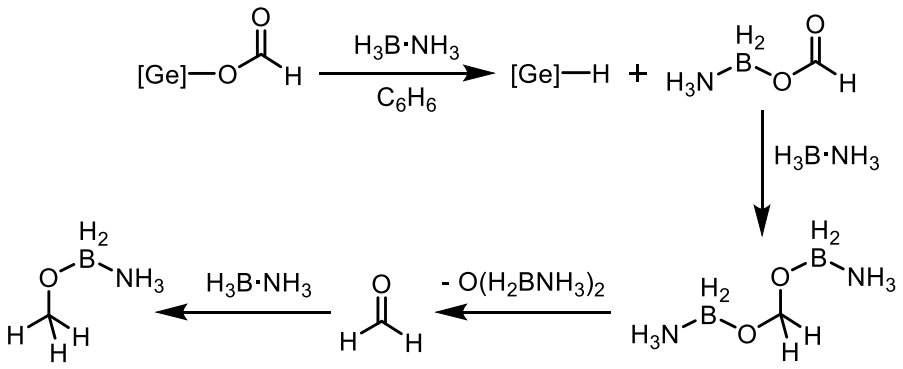
Following on from the successful insertion of CO_2 into the Rh–H bond of Rh(PONOP)H (**6**) to yield the formate complex Rh(PONOP)(OCOH) (**11**), the reactivity of complex **11** with amine-boranes was explored. There is a literature

precedent for the reaction of metal-formate complexes with boranes. For example, in 2010 Ni(PONOP)H was reported to catalyse the reduction of CO_2 via hydroboration using catecholborane (HBcat) (**Scheme 4.12**).[30] Initial CO_2 insertion into the Ni–H bond gave Ni(PONOP)(OCOH), which then reacted with HBcat to return Ni(PONOP)H along with HCOOBcat. Further reaction of HCOOBcat with HBcat yielded formaldehyde, which could be hydroborated by Ni(PONOP)H to yield MeOBcat.



Scheme 4.12 Catalytic reduction of CO_2 with Ni($^{t\text{Bu}}$PONOP)H ([Ni] = Ni($^{t\text{Bu}}$PONOP)).[30]

In the same year, the reaction of a Ge^{II}-formate complex, Ge(L)(OCOH) (L = CH{(CMe)(2,6-$^{i\text{Pr}2}C_6H_3N$)}$_2$) with $H_3B{\cdot}NH_3$ was reported.[34] The reaction yielded complete formation of Ge(L)H; however, no intermediates were identified by NMR spectroscopy. Repeats with ^{13}C-labelled formate led to the observation of ^{13}C-labelled acetone and thus the following mechanism was proposed (**Scheme 4.13**).

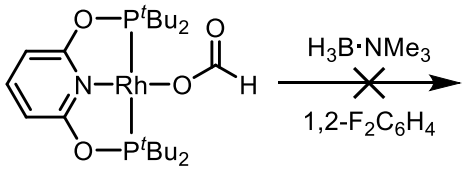


Scheme 4.13 Proposed mechanism for the reaction of Ge(L)(OCOH) with $H_3B{\cdot}NH_3$. [Ge] = Ge[CH{(CMe)(2,6-^{i}Pr2C_6H_3N)}$_2$)].[34]

With these examples in mind, the reaction of complex **11** with amine-boranes was probed. Complex **11** is not stable in solution, especially in the absence of CO_2 (section 4.6.1), and so for each reaction described in this section, complex **11** was formed *in situ* from the rapid reaction of Rh(PONOP)H (**6**) with CO_2, and the resulting solution used immediately.

4.7.1 Reaction of complex 11 with $H_3B{\cdot}NMe_3$

In a high pressure NMR tube, a solution of complex **6** (0.01 mmol, 25 mM, 1,2-$F_2C_6H_4$) was combined with one equivalent of $H_3B{\cdot}NMe_3$ and the sample placed under one atmosphere of CO_2 (~0.06 mmol) (**Scheme 4.14**). The colour of the reaction mixture changed from red to orange upon shaking, consistent with formation of complex **11**. $^{31}P\{^{1}H\}$ NMR spectroscopy showed complete formation of complex **11**; however, ^{11}B NMR spectroscopy indicated no reaction of the amine-borane had taken place.



11

Scheme 4.14 Attempted reaction of complex **11** (formed *in situ*) with $H_3B{\cdot}NMe_3$.

4.7.2 Reaction of complex 11 with $H_3B{\cdot}NMe_2H$

The reaction with $H_3B{\cdot}NMe_3$ described in the previous section was repeated under the same conditions, but with one equivalent of $H_3B{\cdot}NMe_2H$ rather than $H_3B{\cdot}NMe_3$ (**Figure 4.5**). The initial $^{31}P\{^1H\}$ NMR spectrum of the sample showed complete formation of complex **11**. In contrast to the reaction with $H_3B{\cdot}NMe_3$, the ^{11}B NMR spectrum showed two new species along with some unreacted $H_3B{\cdot}NMe_2H$ (~13 %); a triplet (**12**) at –0.63 ppm ($^1J_{BH}$ = 114 Hz) and a doublet (**13**) at 2.19 ppm ($^1J_{BH}$ = 132 Hz). After 15 minutes, complex **11** remained the sole organometallic species observable in the $^{31}P\{^1H\}$ NMR spectrum, while the ^{11}B spectrum showed nearly complete consumption of $H_3B{\cdot}NMe_2H$ and **12**, to form the doublet species at 2.19 ppm as the major product (~90 %).

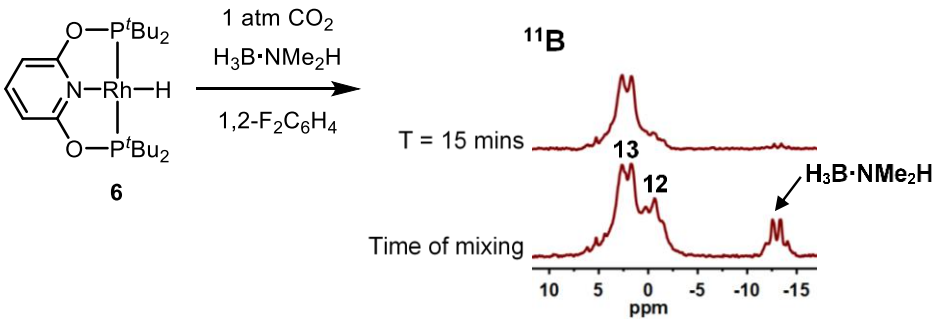
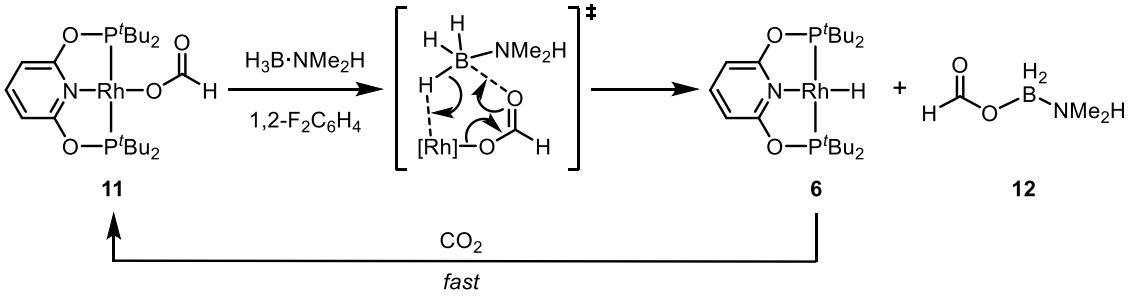


Figure 4.5 Stacked ^{11}B NMR spectra (128 MHz, 1,2-$F_2C_6H_4$, 298 K) over time for the reaction of complex **11** (formed *in situ* from complex **6** and CO_2) with 1 eq. $H_3B{\cdot}NMe_2H$. **12** = unknown triplet, **13** = unknown doublet.

The ^{1}H NMR spectrum at this time showed the expected signal at 8.43 ppm for the formate proton in complex **11**. Two other similar signals are also observed at 8.46 ppm and 8.40 ppm (in the approximate ratio 4:1 at T = 15 mins) implying two other formate signals in slightly different chemical environments are present.

These results imply **12** is an intermediate on the path to forming **13** (**Figure 4.5**) and that complex **11** is a catalyst in the process. The triplet (**12**) signal observed in the ^{11}B NMR spectra indicates the presence of a species containing a BH_2 group. The first intermediate proposed, but not observed, for the reaction of Ge(L)(OCOH) with $H_3B{\cdot}NH_3$ is $H_3N{\cdot}BH_2OCOH$, which also contains a BH_2 group (**Scheme 4.13**).[34] Thus signal **12**, observed at early stages in the reaction of complex **11** with $H_3B{\cdot}NMe_2H$, may be due to the formation of $HMe_2N{\cdot}BH_2OCOH$ from hydroboration across the Rh–O bond (**Scheme 4.15**). This reactivity is analogous to the hydroboration observed across the Ni–O bond with HBCat and as depicted in **Scheme 4.12**. The formation of $HMe_2N{\cdot}BH_2OCOH$ may proceed via a six-membered transition state as depicted.



Scheme 4.15 Proposed initial reactivity of complex **11** with $H_3B{\cdot}NMe_2H$.

The ^{11}B NMR spectroscopic data observed for **12** are similar to analogous species containing a BH_2 group reported in the literature (**Figure 4.6**). For example, a triplet at –0.4 ppm ($^1J_{BH}$ = 121 Hz, CD_2Cl_2) is observed in the ^{11}B NMR spectrum of $HMe_2N{\cdot}BH_2OTf$.[35] The reaction of $H_3B{\cdot}NMeH_2$ with oxalic acid initially yields $H_2MeN{\cdot}BH_2O(CO)_2OH$, as observed as a broad triplet at –4 ppm in the ^{11}B NMR spectrum (THF-d_8).[36] The anion $[H_2B(OCOH)_2]^-$ also exhibits a triplet in the ^{11}B NMR spectrum at 1.2 ppm ($^1J_{BH}$ = 112 Hz, CD_3CN).[37]

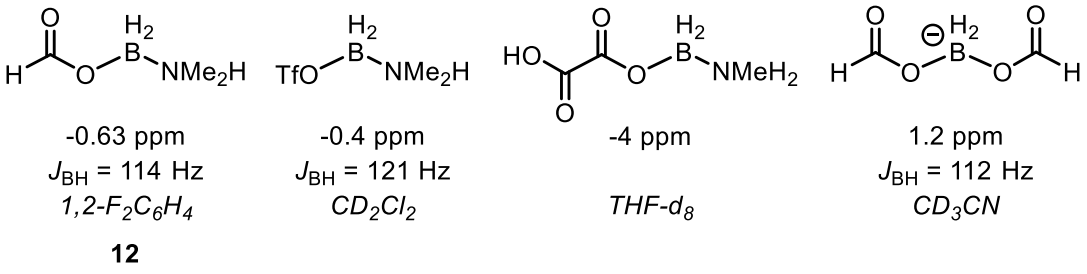
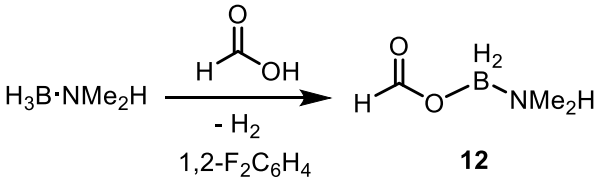


Figure 4.6 Comparison of ^{11}B NMR spectroscopic data of selected BH_2-containing molecules.

To further probe the exact species forming upon reaction of complex **11** with $H_3B{\cdot}NMe_2H$ and giving rise to a triplet signal in the ^{11}B NMR spectrum, independent synthesis of $HMe_2N{\cdot}BH_2OCOH$ was undertaken via two different synthetic routes.

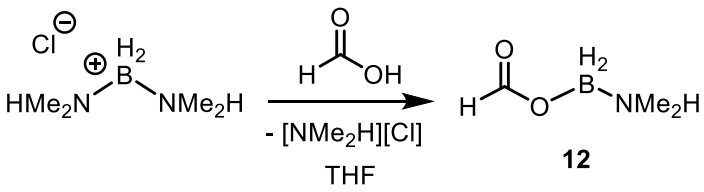
Firstly, a solution of $H_3B{\cdot}NMe_2H$ (0.3 M, 1,2-$F_2C_6H_4$) was reacted with approximately 1.1 equivalent of formic acid and the reaction mixture stirred at room temperature for 24 hours (**Scheme 4.16**). The solvent was removed *in vacuo* to give a colourless oil that was washed in cold hexane and dried again *in vacuo*. ^{11}B NMR spectroscopy of a 1,2-$F_2C_6H_4$ solution of the product gave a triplet at –0.63 ppm ($^1J_{BH}$ = 114 Hz), which is identical to that observed in the reaction of complex **11** with $H_3B{\cdot}NMe_2H$. A very small amount of an overlapping doublet at 2.21 ppm ($^1J_{BH}$ = 134 Hz) was also observed, which is very similar to the doublet signal observed for the reaction of complex **11** with $H_3B{\cdot}NMe_2H$ (d, 2.19 ppm, $^1J_{BH}$ = 132 Hz). The ^1H NMR spectrum of the oil product in 1,2-$F_2C_6H_4$ yielded a sharp singlet at 8.4 ppm (1H), a broad singlet at 6.2 ppm (1H), a broad obscured quartet at 2.9 ppm and a doublet at 2.5 ppm ($^3J_{HH}$ 6 Hz, 6H), integration consistent with the product being $HMe_2N{\cdot}BH_2OCOH$. A signal at 8.4 ppm was also observed in the ^1H NMR spectra for the reaction of **11** with $H_3B{\cdot}NMe_2H$.



Scheme 4.16 Synthetic pathway 1 for $HMe_2N{\cdot}BH_2OCOH$ (**12**).

A second route to independently synthesise the unknown triplet product from the reaction of complex **11** with $H_3B{\cdot}NMe_2H$ consisted of the reaction of $[H_2B(NMe_2H)_2][Cl]$ with one equivalent of formic acid in THF (**Scheme 4.17**). ^{11}B NMR spectroscopy of the reaction mixture after 10 minutes of stirring revealed a

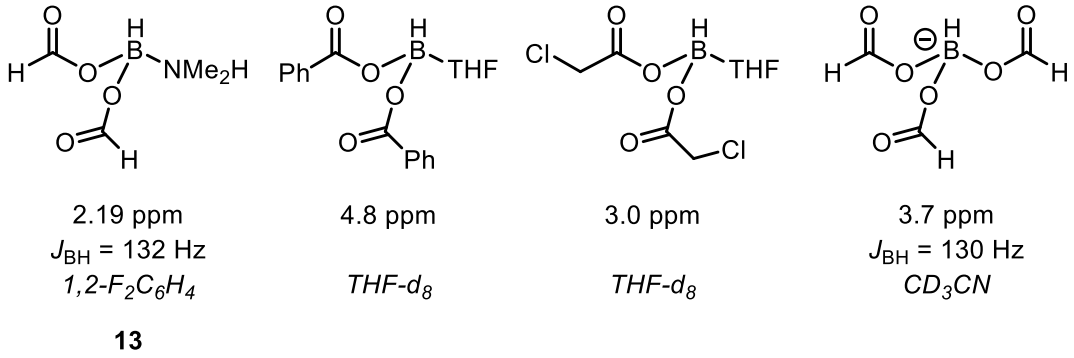
triplet at –0.66 ppm ($^1J_{BH}$ = 113 Hz) as the sole product. ^{11}B NMR spectroscopy of the same product in 1,2-$F_2C_6H_4$ gives a triplet at –0.63 ppm ($^1J_{BH}$ = 114 Hz) and ^{1}H NMR spectroscopy exhibits a signal at 8.4 ppm. These signals are identical to those observed for **12** in the reaction of complex **11** with $H_3B{\cdot}NMe_2H$ and from the reaction of $H_3B{\cdot}NMe_2H$ with formic acid. The ^{1}H NMR spectrum was more easily integrated in C_6D_6 and yielded signals at 8.31 ppm (s, 1H), 5.75 ppm (br s, 1H), 2.87 ppm (dd, $^1J_{BH}$ = 122 Hz, 101 Hz, 2H) 1.87 ppm (d, $^3J_{HH}$ = 6 Hz, 6H), all consistent with the formation of $HMe_2N{\cdot}BH_2OCOH$. ^{1}H NMR signals were also present for $\{NMe_2H_2\}^+$, a possible side product (8.85 ppm, br s, NH_2 and 2.12 ppm, s, NMe_2). ESI-MS analysis of the sample yielded a signal *m/z* = 126.06, which is consistent with $HMe_2N{\cdot}BH_2OCOH + Na^+$ (calc. 126.07, fragment showing the correct isotope pattern).



Scheme 4.17 Synthetic pathway 2 for $HMe_2N{\cdot}BH_2OCOH$ (**12**).

These results strongly suggest that the initial product **12** from the reaction of complex **11** with $H_3B{\cdot}NMe_2H$ is $HMe_2N{\cdot}BH_2OCOH$. Following on from this, the assignment of the doublet observed in the ^{11}B NMR spectra of the later stages of the reaction of complex **11** with $H_3B{\cdot}NMe_2H$ (**13**, 2.19 ppm, $^1J_{BH}$ = 132 Hz) may be $HMe_2N{\cdot}BH(OCOH)_2$. Other similar complexes containing a BH group in the literature are reported at similar chemical shifts in ^{11}B NMR spectra: 4.8 ppm for

$(PhCO_2)_2BH{\cdot}THF$;[38] 3.0 ppm for $(ClCH_2CO_2)_2BH{\cdot}THF$;[38] and 3.7 ppm ($^1J_{BH}$ = 130 Hz, CD_3CN) for $\{HB(OCOH)_3\}^-$ (**Figure 4.7**).[39]



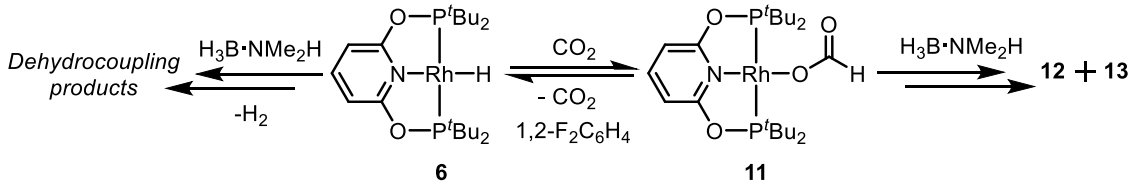
13

Figure 4.7 Comparison of ^{11}B NMR spectroscopic data of selected BH-containing molecules.

In order to make a confident assignment of the unknown BH species, attempts to isolate this species were carried out. The reaction between complex **11** and $H_3B{\cdot}NMe_2H$ was investigated further and probed under catalytic conditions in order to generate enough BH product **13** for characterisation.

In a high pressure NMR tube, a solution of complex **6** (0.01 mmol, 25 mM, 1,2-$F_2C_6H_4$) was reacted with 10 equivalents of $H_3B{\cdot}NMe_2H$ (i.e. 10 mol% catalyst loading) and the sample placed under one atmosphere of CO_2 (~0.06 mmol). Initially, $^{31}P\{^1H\}$ NMR spectroscopy showed complete formation of complex **11** as expected from stoichiometric experiments. The initial ^{11}B NMR spectrum showed the presence of the same triplet from **12** and doublet from **13** observed in the stoichiometric reaction assigned to $HMe_2N{\cdot}BH_2OCOH$ and $HMe_2N{\cdot}BH(OCOH)_2$ respectively, alongside unreacted $H_3B{\cdot}NMe_2H$. However, after 10 minutes, the ^{11}B

NMR showed a mixture of signals including those for $H_2B{=}NMe_2$, $HB(NMe_2)_2$ and boric acid and the $^{31}P\{^1H\}$ NMR spectrum showed the reformation of complex **6** along with a small amount of the known fragment, $\{Rh(PONOP)(CO)\}^{+}$[32] (219.1 ppm, $^1J_{RhP}$ = 127 Hz). These observations are consistent with the fact only a 6x equivalents of CO_2 (compared to **6**) were contained in the headspace of the NMR tube, i.e. not enough CO_2 to maintain the presence of complex **11** in solution upon reaction with 10 equivalents of $H_3B{\cdot}NMe_2H$. Therefore, complex **6** is reformed and this may directly dehydrocouple $H_3B{\cdot}NMe_2H$ slowly (**Scheme 4.18**).



Scheme 4.18 Simplified route for the reaction of complex **6** with CO_2. With excess CO_2, complex **11** is favoured and so reacts with $H_3B{\cdot}NMe_2H$ and *vice versa*.

In light of this, catalysis was repeated in a J. Young flask (volume = 472 cm^3) rather than an NMR tube (1.9 cm^3), in order to increase the headspace in the reaction vessel and therefore the amount of CO_2 present in the closed system and thus ensure complex **11** is continuously present to react with $H_3B{\cdot}NMe_2H$. Under these conditions, catalysis could not be followed *in situ* by NMR spectroscopy and so multiple catalytic runs were carried out with different catalyst loadings and for different lengths of time. Catalysis carried out with 25 equivalents of $H_3B{\cdot}NMe_2H$ (i.e. 4 mol% catalyst loading, 3.40 mmol) added to a solution of complex **6** (0.14 mmol, 27 mM, 1,2-$F_2C_6H_4$) under one atmosphere of CO_2 (~19 mmol, i.e. an excess)

was found to yield complete conversion from $H_3B{\cdot}NMe_2H$ to species **13** (assumed to be $HMe_2N{\cdot}BH(OCOH)_2$) in 24 hours. NMR spectroscopy at this time revealed **13** as the only boron-containing species and $\{Rh(PONOP)(CO)\}^+$[32] as the only phosphorus-containing species. Cold hexane was added to the reaction mixture to yield a brown/yellow precipitate, which was isolated by filtration and washed further with hexane before being dried *in vacuo* to yield an off-white oily solid. $^{31}P\{^1H\}$ NMR spectroscopy of the product in CD_2Cl_2 revealed that $\{Rh(PONOP)(CO)\}^+$ was still present. ^1H NMR spectra of the product mixture in CD_2Cl_2 revealed the following data for **13**: a broad singlet at 8.22 ppm (2H), a broad singlet at 5.98 ppm (1H), an obscured signal at 3.27 ppm (dd, $^1J_{BH}$ = 128 Hz, 107 Hz, 1H) and a doublet at 2.48 ppm ($^3J_{HH}$ = 6 Hz, 6H), with integration all consistent with the boron-containing product being $HMe_2N{\cdot}BH(OCOH)_2$. Upon ^{11}B decoupling, the obscured multiplet at 3.27 ppm for the BH group becomes a sharp singlet, consistent with a signal for a B–H bond. The ^{11}B NMR signal for the product in CD_3CN is a doublet at 2.03 ppm ($^1J_{BH}$ = 132 Hz), which is different to that reported for $\{BH(OCOH)_3\}^-$ (3.7 ppm, $^1J_{BH}$ = 130 Hz, CD_3CN).[39]

To probe the reaction between complex **11** and $H_3B{\cdot}NMe_2H$ further, speciation studies were undertaken under catalytic conditions. Smaller amounts of **6** and $H_3B{\cdot}NMe_2H$ were used than before, along with a larger NMR tube and a slightly higher pressure of CO_2, in order to ensure an excess of CO_2. In a high pressure NMR tube, catalysis at 5 mol% catalyst loading with a solution of complex **6** (1.3 μmol, 3.2 mM, 1,2-$F_2C_6H_4$) and 20 equivalents of $H_3B{\cdot}NMe_2H$ (0.03 mmol, 63.6 mM) was carried out. The system was placed under 1.2 atmospheres of CO_2 (~0.09 mmol) and

the reaction monitored by ^{11}B NMR spectroscopy. **Figure 4.8** depicts a time course plot for the fate of $H_3B{\cdot}NMe_2H$, $HMe_2N{\cdot}BH_2OCOH$ and $HMe_2N{\cdot}BH(OCOH)_2$ as determined from relative integrals in the ^{11}B NMR spectra (assuming no leaching of boron).

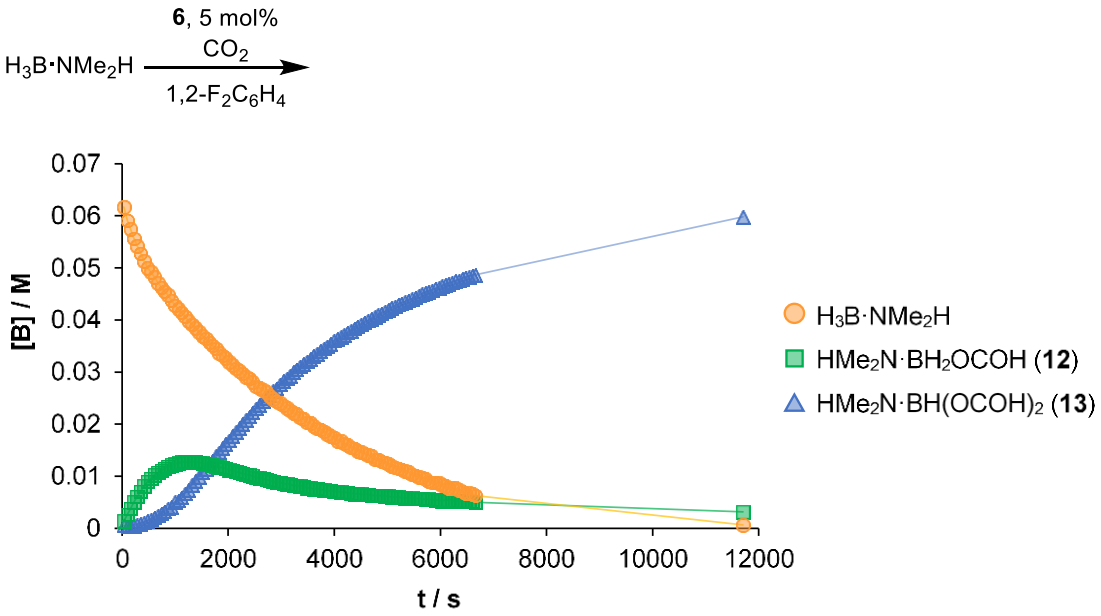
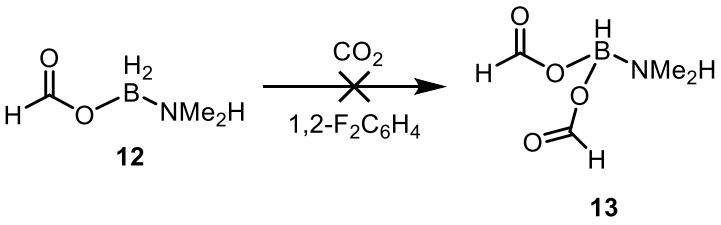


Figure 4.8 Time course plot for the catalytic reduction of CO_2 with $H_3B{\cdot}NMe_2H$ (64 mM, 1,2-$F_2C_6H_4$, 298 K) and complex **11** (5 mol%) as measured *in situ* by ^{11}B NMR spectroscopy.

A ^{11}B NMR spectrum was recorded every minute for 105 minutes (6300 s), at which point a $^{31}P\{^1H\}$ NMR spectrum was recorded that showed complex **11** to be the sole organometallic species. Catalysis was still occurring at this point and so further analysis by NMR spectroscopy was carried out ~1h30 later to show complete consumption of $H_3B{\cdot}NMe_2H$, as seen in the ^{11}B NMR spectrum, and both complexes **11** (~75 %) and $\{Rh(PONOP)(CO)\}^+$ (~25 %) present, as observed in the $^{31}P\{^1H\}$ NMR spectrum. Therefore, the data implies that complex **11** is the sole resting state

during catalysis and that $\{Rh(PONOP)(CO)\}^+$ is formed towards the end/after catalysis (i.e. at low concentration of $H_3B{\cdot}NMe_2H$). The temporal profile of $HMe_2N{\cdot}BH_2OCOH$ (**12**) is that of an intermediate, with $HMe_2N{\cdot}BH(OCOH)_2$ (**13**) being the boron-containing product, and thus confirms the supposition that **12** reacts to form **13** during catalysis.

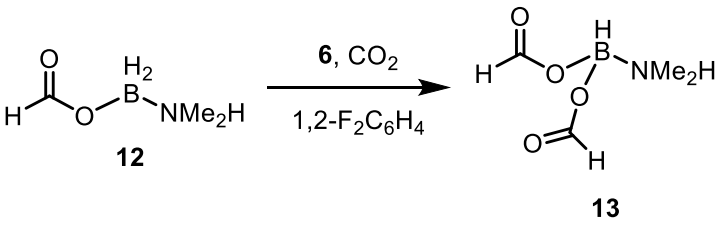
In 1985 it was reported that the addition of CO_2 to $\{H_2B(OCOH)_2\}^-$ in CH_2Cl_2 at –50 °C yielded $\{HB(OCOH)_3\}^-$, where the cation is $\{Cu(PH_3P)_2(phen)\}^+$.[37] This reaction was reversed upon the heating of $\{HB(OCOH)_3\}^-$ to 45 °C. To probe whether the conversion of $HMe_2N{\cdot}BH_2OCOH$ (**12**) to $HMe_2N{\cdot}BH(OCOH)_2$ (**13**) is metal-mediated, a 1,2-$F_2C_6H_4$ solution of **12** in an NMR tube was placed under one atmosphere of CO_2 and monitored by NMR spectroscopy. The sample was monitored continuously using ^{11}B NMR spectroscopy for 25 minutes, during which time no reaction of **12** occurred (**Scheme 4.19**).



Scheme 4.19 Attempted reaction of $HMe_2N{\cdot}BH_2OCOH$ (**12**) with CO_2.

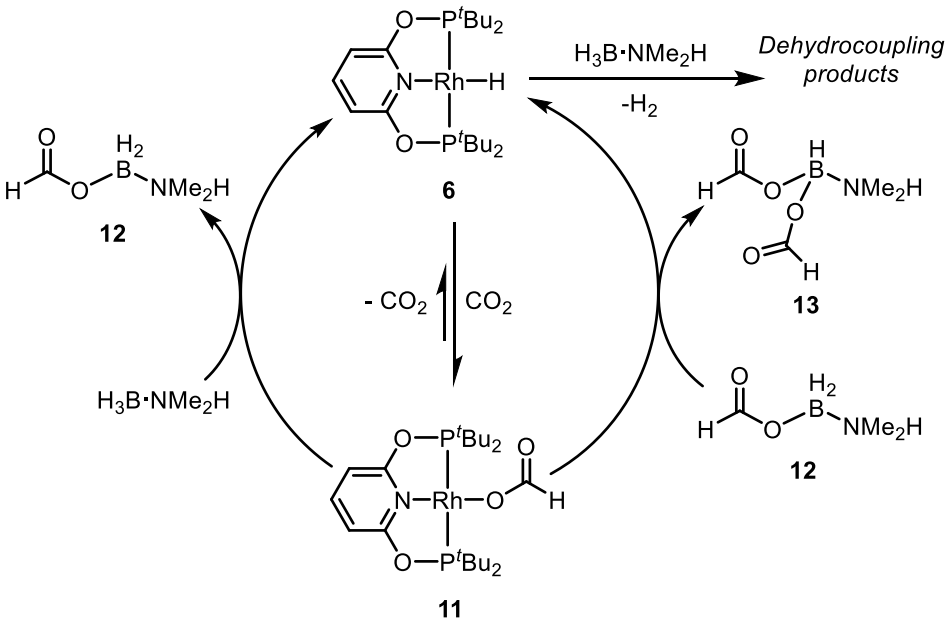
Complex **6** (0.5 mg) was then added to the reaction mixture and the sample backfilled again with one atmosphere of CO_2 (**Scheme 4.20**). ^{11}B NMR spectroscopy

revealed the slow consumption of **12** and formation of **13**. These results indicate that the conversion of **12** to **13** under the conditions of catalysis is metal-mediated.



Scheme 4.20 Reaction of $HMe_2N{\cdot}BH_2OCOH$ (**12**) with CO_2 and complex **6**, i.e. complex **11**.

With the results described in mind, a mechanism for the catalytic reduction of CO_2 with complex **6** and $H_3B{\cdot}NMe_2H$ was proposed (**Scheme 4.21**).

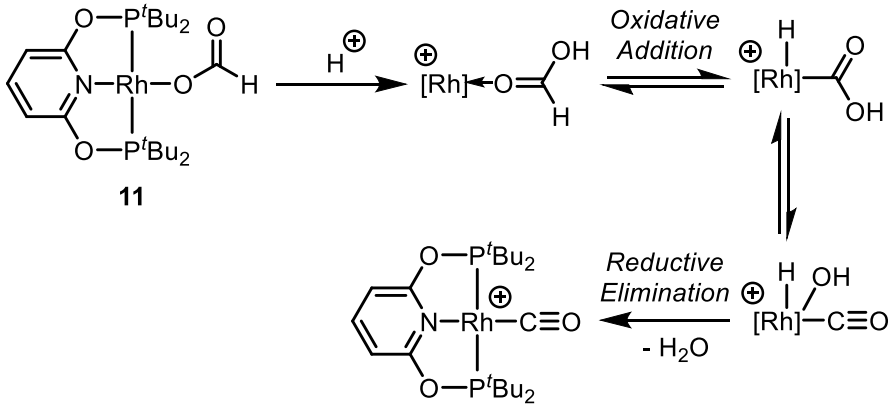


Scheme 4.21 Proposed mechanism for the catalytic reduction of CO_2 with complex **6** and $H_3B{\cdot}NMe_2H$.

Complex **6** and CO_2 immediately react via insertion of CO_2 into the Rh–H bond to yield complex **11**. Complex **11** can then react with $H_3B{\cdot}NMe_2H$ leading to cleavage of the Rh–O bond and reformation of complex **6** along with $HMe_2N{\cdot}BH_2OCOH$. $HMe_2N{\cdot}BH_2OCOH$ is observed in the ^{11}B NMR as a triplet at –0.63 ppm ($^1J_{BH}$ = 114 Hz). Complex **6** can react immediately with another equivalent of CO_2 to generate complex **11** again. Complex **11** can either repeat the reaction with $H_3B{\cdot}NMe_2H$ or may react with $HMe_2N{\cdot}BH_2OCOH$ to cleave the Rh–O bond again and generate $HMe_2N{\cdot}BH(OCOH)_2$, which is observed as a doublet at 2.19 ppm ($^1J_{BH}$ = 132 Hz) in the ^{11}B NMR spectra. This is the final boron-containing product observed in catalysis, which is proposed to be due to increased sterics around the boron centre preventing further reaction.

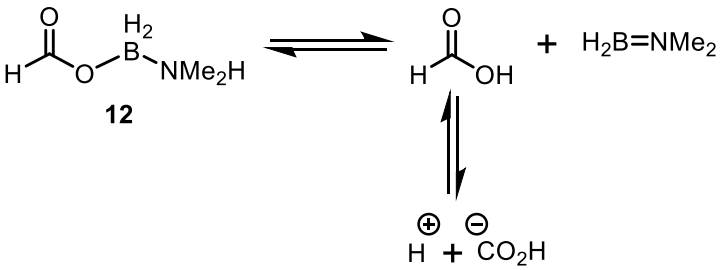
When the concentration of CO_2 in the system is too low to regenerate complex **11** (i.e. CO_2 not in excess), complex **6** is observed via $^{31}P\{^1H\}$ NMR spectroscopy and products of the slow reaction of complex **6** with $H_3B{\cdot}NMe_2H$ are then observed. If CO_2 is reintroduced to the system, complex **11** is reformed and no more complex **6** is observed, consistent with the proposed mechanism.

$\{Rh(PONOP)(CO)\}^+$ is often observed via $^{31}P\{^1H\}$ NMR spectroscopy as the final organometallic product at the end of catalysis. The mechanism explaining this observation has not been explored; however, one possible route to form $\{Rh(PONOP)(CO)\}^+$ is outlined in **Scheme 4.22**.



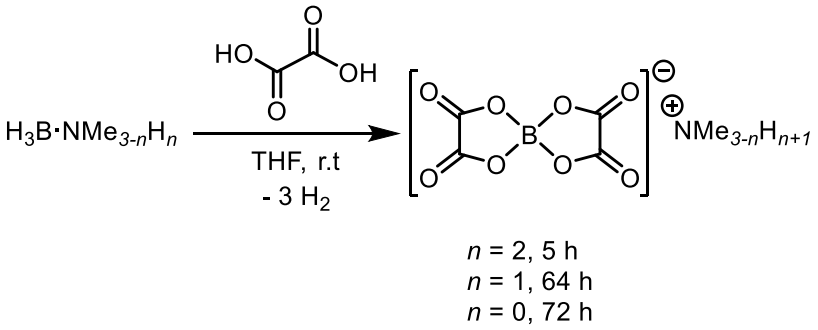
Scheme 4.22 Suggested pathway for the formation of {Rh(PONOP)(CO)}$^+$ from complex **11**. H^+ = acidic proton. Anions, proposed to be $COOH^-$, not shown.

The suggested mechanistic pathway outlined in **Scheme 4.22** is analogous to that proposed for the catalytic decarbonylation of different formates using rhodium diphosphine complexes reported by Kwong *et al*.[40] In the case of complex **11**, coordination of the formate is followed by oxidative addition and subsequent reductive elimination to yield {Rh(PONOP)(CO)}$^+$. The acidic proton required for this process may be present in the system if formic acid is generated, which could come from the decomposition/generation of $HMe_2N{\cdot}BH_2OCOH$ (**12**) (**Scheme 4.23**). If this process was occurring, it would be expected that small amounts of $H_2B{=}NMe_2$ (and therefore $[H_2BNMe_2]_2$) and also H_2O would be observable by NMR spectroscopy towards the end of catalysis; however, no such evidence has been found. Therefore the exact explanation for the formation of {Rh(PONOP)(CO)}$^+$ at the end of catalysis is still under consideration.



Scheme 4.23 Suggested formation of H^+ during the catalytic reduction of CO_2 with $H_3B{\cdot}NMe_2H$ and complex **11**.

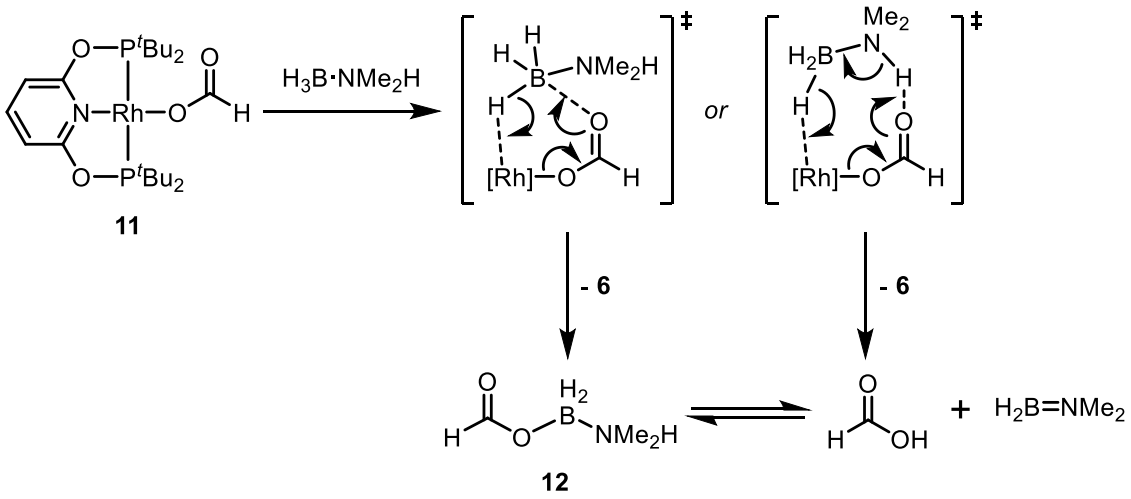
At the beginning of this section it was shown that there is no reaction between complex **11** and $H_3B{\cdot}NMe_3$. This may simply be explained by $H_3B{\cdot}NMe_3$ being more sterically bulky than $H_3B{\cdot}NMe_2H$ and thus preventing any reaction. For example, the increasing steric requirements between $H_3B{\cdot}NMeH_2$, $H_3B{\cdot}NMe_2H$ and $H_3B{\cdot}NMe_3$ led to a significant decrease in reaction rates for the reaction of amine-boranes with oxalic acid (**Scheme 4.24**).[36]



Scheme 4.24 Reaction of different amine-boranes with oxalic acid.[36] Reaction completion times quoted in hours for each amine-borane.

Alternatively, the lack of reaction of complex **11** with $H_3B{\cdot}NMe_3$ may indicate that the presence of a N–H is necessary for reactivity. This may be the case if the initial

reaction of complex **11** with $H_3B{\cdot}NMe_2H$ involves breaking of the N–H bond, rather than reaction solely via the BH group (**Scheme 4.25**).



Scheme 4.25 Comparison of the two transition states proposed for the reaction of complex **11** with $H_3B{\cdot}NMe_2H$.

Reaction between complex **11** and $H_3B{\cdot}NMe_2H$ involving breaking of the N–H bond would lead to the generation of $H_2B{=}NMe_2$ and formic acid. Reaction of these two products with each other could then yield $HMe_2N{\cdot}BH_2OCOH$ (**12**), as observed in catalysis. In order to probe the feasibility of this route, formic acid was reacted with one equivalent of $H_2B{=}N^iPr_2$ (an isolatable aminoborane) in THF. ^{11}B NMR spectroscopy revealed a triplet at –4.1 ppm ($^1J_{BH}$ = 113 Hz), similar to that for **12** (–0.63 ppm, $^1J_{BH}$ = 114 Hz) and to reported boronium-like complexes such as $H^iPr_2N{\cdot}BH_2R$ where R = Cl (–6.7 ppm), OTf (–3.7 ppm) and OMs (–4.1 ppm).[41] A signal for $H_3B{\cdot}N^iPr_2H$ (–20.9 ppm, $^1J_{BH}$ = 97 Hz)[42] was also observed in the ^{11}B NMR, along with a triplet at 1.1 ppm ($^1J_{BH}$ = 116 Hz), tentatively assigned as $\{H_2B(N^iPr_2H)(THF)\}^+$ due to the similarity to other analogous cations. Thus,

catalysis between complex **11** and $H_3B{\cdot}NMe_2H$ may indeed occur via formation of $H_2B{=}NMe_2$ and formic acid.

To further probe which pathway the reaction of complex **11** with $H_3B{\cdot}NMe_2H$ occurs by, labelling studies with $D_3B{\cdot}NMe_2H$ and $H_3B{\cdot}NMe_2D$ were carried out. In a high pressure NMR tube, a solution of complex **6** (1.3 μmol, 3.2 mM, 1,2-$F_2C_6H_4$) was combined with 20 equivalents of $D_3B{\cdot}NMe_2H$ (0.03 mmol, 63.6 mM, i.e. 5 mol% catalyst loading) and the system was placed under 1.2 atmospheres of CO_2 (~0.09 mmol). The reaction was followed by ^{11}B NMR spectroscopy, the relative integrals analysed and a time course plot depicting the consumption of $D_3B{\cdot}NMe_2H$ is shown in **Figure 4.9**. The reaction was repeated under identical conditions with $H_3B{\cdot}NMe_2D$ and the resulting time course plot overlaid with that for $D_3B{\cdot}NMe_2H$. The analogous plot for the reaction with the undeuterated isotopologue, $H_3B{\cdot}NMe_2H$, is also shown for comparison. The data from this reaction was discussed in more detail earlier in this section.

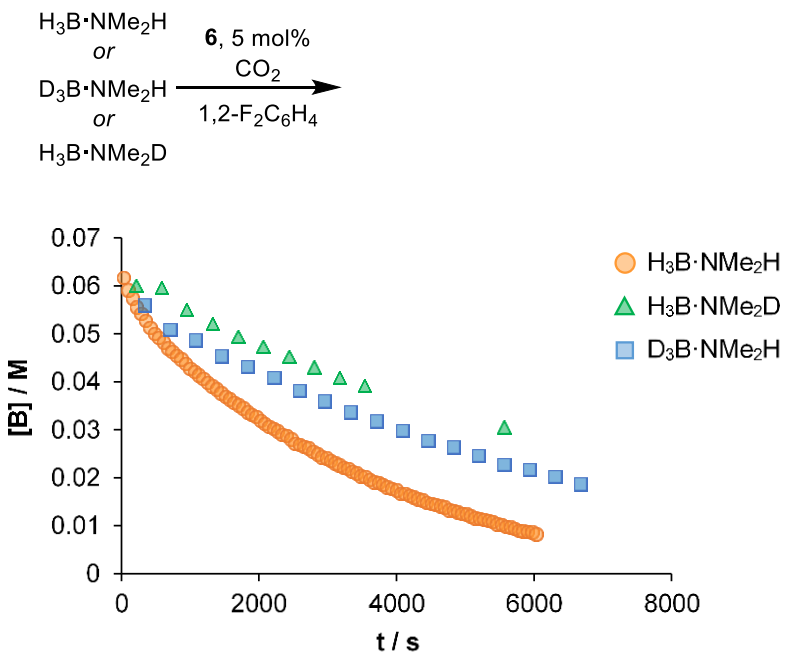
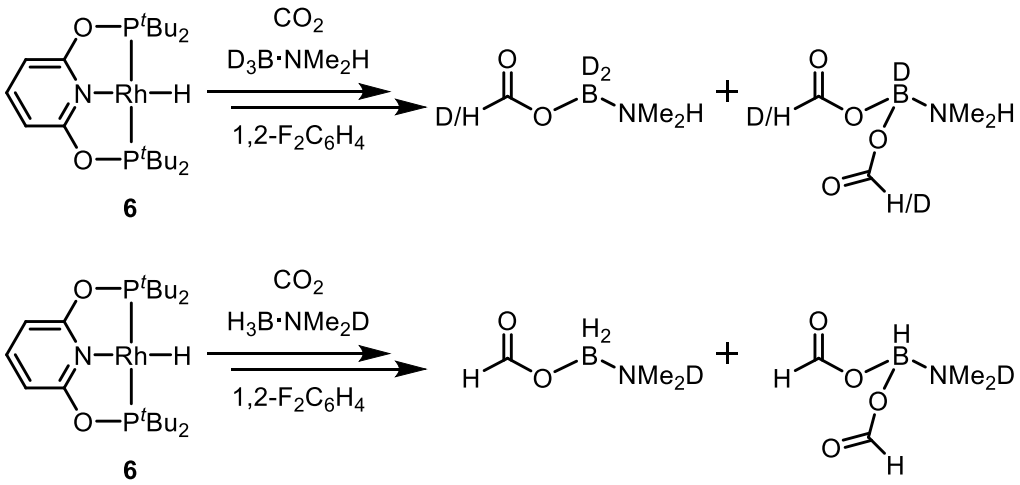


Figure 4.9 Partial time course plot for the catalytic reduction of CO_2 with $H_3B{\cdot}NMe_2H$, $H_3B{\cdot}NMe_2D$ or $D_3B{\cdot}NMe_2H$ (64 mM, 1,2-$F_2C_6H_4$, 298 K) and complex **11** (5 mol%) as measured *in situ* by ^{11}B NMR spectroscopy.

As can be seen in **Figure 4.9**, the rate of consumption of amine-borane is slower for both the reaction with $D_3B{\cdot}NMe_2H$ and $H_3B{\cdot}NMe_2D$, compared to the reaction with $H_3B{\cdot}NMe_2H$, implying a kinetic isotope effect for both B–H and N–H bond activation during catalysis with complex **11** and $H_3B{\cdot}NMe_2H$. Out of the two transition states proposed during catalysis (**Scheme 4.25**), only the one leading to the formation of formic acid and $H_2B{=}NMe_2$ involves both B–H and N–H bond activation. Therefore, these results are also consistent with catalysis occurring via the initial formation of formic acid and $H_2B{=}NMe_2$ rather than the direct formation of **12**.

^{11}B NMR spectroscopy of the reaction with $D_3B{\cdot}NMe_2H$ shows broad signals throughout catalysis for $D_3B{\cdot}NMe_2H$ as well as **12** and **13**. This is consistent with

there being no significant H/D exchange at the boron centre, which is consistent with the proposed mechanism. Similarly, the signals in the ^{11}B NMR spectra for catalysis with $H_3B{\cdot}NMe_2D$ remain sharp with resolvable coupling, consistent with no significant N–D/B–H exchange. With this in mind, for catalysis with $D_3B{\cdot}NMe_2H$, a varied amount of H/D substitution in the formate groups of **11** and **12** would be expected due to generation of Rh(PONOP)D (**6-D**) during catalysis (**Scheme 4.26**, *top*). In line with this, the ^{1}H NMR spectrum when half the starting $D_3B{\cdot}NMe_2H$ had been consumed revealed reductions of ~45 % for the formate signal of **12** and ~53 % for **13** upon integration and comparison to the respective Me group signals.

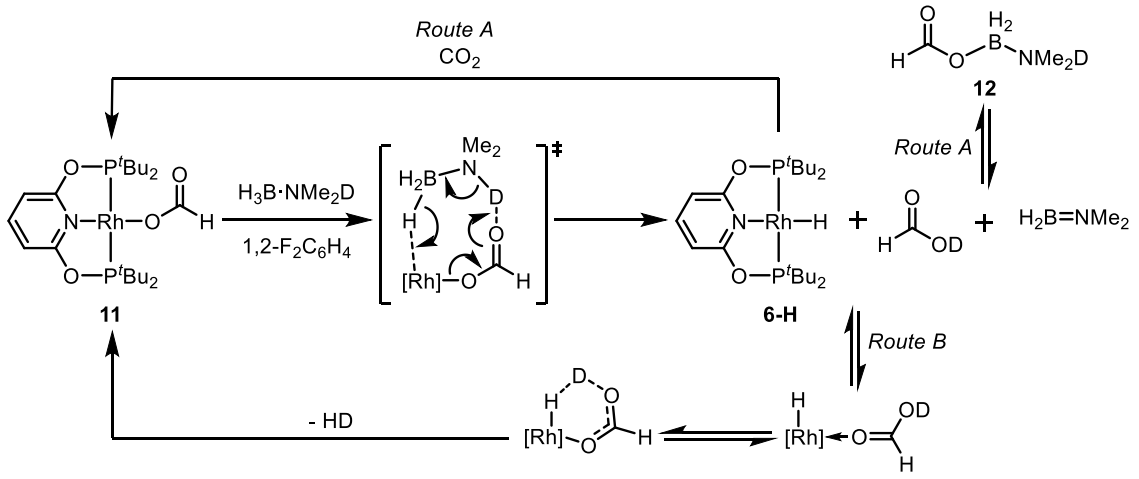


Scheme 4.26 Proposed boron-containing products from catalysis of $D_3B{\cdot}NMe_2H$ (*top*) or $H_3B{\cdot}NMe_2D$ (*bottom*) with complex **11** (formed *in situ* from **6** and CO_2).

In contrast, no deuteration of the formate protons in **12** and **13** would be expected for catalysis with $H_3B{\cdot}NMe_2D$ (**Scheme 4.26**, *bottom*). However, the ^{1}H NMR spectrum when half the starting $D_3B{\cdot}NMe_2H$ had been consumed revealed a reduction of ~13 % for formate signal for **12** and ~17 % reduction was observed

for **13**. Furthermore, signals for the NH group in both **12** and **13** were also observed in the ^{1}H NMR spectra. These unexpected reductions in signal intensity and observation of NH signals for catalysis with $H_3B{\cdot}NMe_2D$ imply a small amount of H/D substitution is occurring during catalysis. It should be noted that the signal for the formate proton in complex **11** is observed at 8.43 ppm in the ^{1}H NMR spectra at the beginning of catalysis in all cases ($H_3B{\cdot}NMe_2H$, $D_3B{\cdot}NMe_2H$ or $H_3B{\cdot}NMe_2D$); however, this signal exhibits a low frequency shift during catalysis and becomes obscured by the formate signal for **13**. Therefore, any reduction in signal for the formation of Rh(PONOP)(OCOD) cannot be analysed.

A further indication of the occurrence of H/D scrambling during catalysis is the observation of HD in the ^{1}H NMR spectra for both catalysis with $D_3B{\cdot}NMe_2H$ and $H_3B{\cdot}NMe_2D$. This result, along with the observation of H/D exchange in **12** and **13** during catalysis with $H_3B{\cdot}NMe_2D$, may be explained if catalysis is proceeding via the proposed transition state that leads to the formation of formic acid and $H_2B{=}NMe_2$ (**Scheme 4.27**).



Scheme 4.27 Simplified mechanism for H/D scrambling and HD production during catalysis of $H_3B{\cdot}NMe_2D$ with complex **11**. Not all H/D combinations and pathways are shown. [Rh] = Rh(PONOP).

Once complex **11** has reacted with $H_3B{\cdot}NMe_2D$, the deuterated formic acid formed alongside $H_2B{=}NMe_2$ may react to give **12** as expected and complex **6** would react with CO_2 to regenerate **11** (**Scheme 4.27**, *Route A*). However, complex **6** may also react with formic acid to regenerate **11** and evolve HD (**Scheme 4.27**, *Route B*). Such a reaction has recently been reported by Ryzhov *et al*. where $[Zn(tpy)H]^+$ (tpy = 2,2';6',2''-terpyridine) reacts rapidly with formic acid to generate $[Zn(tpy)(OCOH)]^+$ and H_2.[43]

The mechanistic pathway depicted in **Scheme 4.27** for the reaction of complex **6** with formic acid suggests reversible oxidative cleavage of formic acid at the rhodium centre. This pathway would allow the evolution HD, explaining the observation of these species during catalysis. This route may also lead to the generation of proto-formic acid (HCOOH) rather than the deuterated analogue (DCOOH) and thus lead to the formation of complex **12** and **13** with an NH group

rather than ND, thus explaining the observation of NH signals in the ^{1}H NMR spectra. Finally, this pathway would allow the formation of Rh(PONOP)D (**6-D**) and therefore Rh(PONOP)(OCOD) (**11-D**), and subsequently H/D substitution in the formate signals of **12** and **13**, thus explaining the reduction of the intensity of these signals in the ^{1}H NMR spectra. Therefore, it is proposed that the catalysis of $H_3B{\cdot}NMe_2H$ with complex **11** occurs via the formation of formic acid and $H_2B{=}NMe_2$. DFT calculations would be a suitable technique for confirming this proposed mechanism. It follows that, by increasing the pressure of CO_2 in the system, rapid reaction of complex **6** with CO_2 to generate complex **11** would be favoured and thus *Route B* in the suggested mechanism may be suppressed.

To summarise, complex **11** has been shown to react catalytically with $H_3B{\cdot}NMe_2H$ to form $HMe_2N{\cdot}BH_2OCOH$ (**12**) initially, and subsequently $HMe_2N{\cdot}BH(OCOH)_2$ (**13**). A mechanism for this process has been proposed and complex **11** has been shown to be the resting state of the organometallic species during catalysis, when CO_2 is present. After amine-borane consumption, complete formation of $\{Rh(PONOP)(CO)\}^+$ is observed.

4.8 Reaction of Rh(PONOP)H (6) with acetic acid

In section 4.3, the protonation of Rh(PONOP)H (**6**) to yield [Rh(PONOP)(η^2-H_2)][BAr^F_4] (**1**) using Brookhart's acid, [$H(OEt_2)_2$][BAr^F_4], was described. In contrast, the known complex Rh(PONOP)Cl was generated upon reaction of complex **6** with HCl, an acid with a stronger conjugate base. In this, and the following

section, the reactivity of complex **6** with acetic acid and trifluoromethanesulfonic acid (triflic acid) are probed, respectively.

In a J. Young flask, 1.2 equivalents of degassed acetic acid were added to a solution of complex **6** (20 mM, C_6H_6) and the reaction mixture was stirred for 30 minutes, during which a colour change of red to orange was observed. The reaction mixture was filtered and the solvent removed *in vacuo* to yield an orange powder. $^{31}P\{^1H\}$ NMR spectroscopy of the product in C_6D_6 revealed a doublet at 200.0 ppm ($^1J_{RhP}$ = 162 Hz) (**Figure 4.10**). This signal is very similar to that observed for Rh(PONOP)OCOH (**11**) (200.3 ppm, $^1J_{RhP}$ = 163 Hz) and so the product was initially assigned as the analogous acetate complex, Rh(PONOP)OAc (**14**).

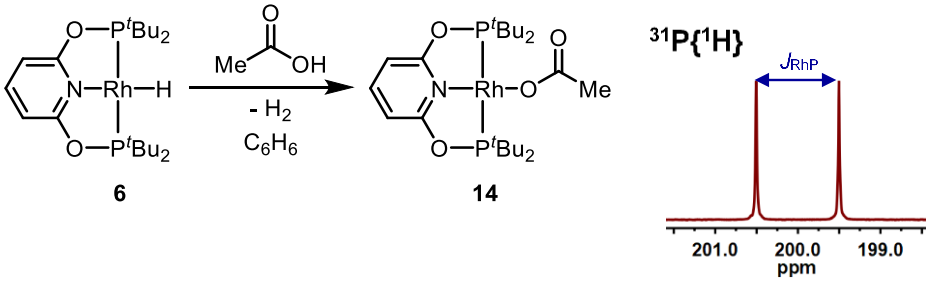


Figure 4.10 Synthesis and partial $^{31}P\{^1H\}$ NMR spectrum (162 MHz, C_6D_6, 298 K) of complex **14**. J_{RhP} = 162 Hz.

The ^1H NMR spectral data confirmed the assignment of complex **14**, with analogous signals for the PONOP ligand in complex **11**, a lack of signal at 8.63 ppm for the OCOH group in complex **11** and the presence of a singlet at 2.28 ppm (3 H) for the methyl group on OCOMe in complex **14**.

Dark orange crystals suitable for X-ray diffraction were formed from a concentrated solution of complex **14** in methylcyclohexane at –21 °C for three days. The solid state structure is shown in **Figure 4.11** and is consistent with the assignment of complex **14** as Rh(PONOP)OAc.

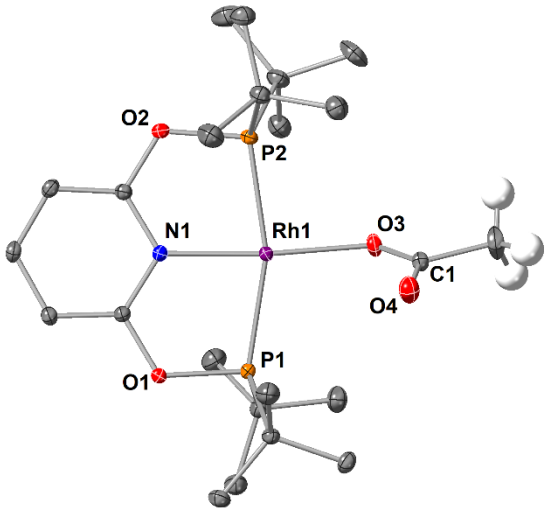
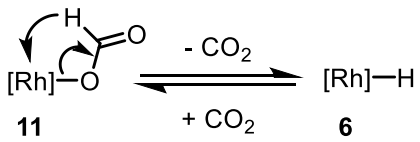


Figure 4.11 Solid state structure of complex **14**. Displacement ellipsoids are drawn at the 30 % probability level. Most carbon-bound hydrogens are omitted for clarity. Selected bond lengths (Å) and angles (°): Rh1–O3, 2.0670(13); Rh1–P1, 2.2535(4); Rh1–P2, 2.2382(4); Rh1–N1, 2.0061(14); C1–O3, 1.274(2); C1–O4, 1.225(3); P1–Rh1–P2, 162.844(17); N1–Rh1–O3, 171.30(6).

The solid state structure of complex **14** indicates an η^1-OCOMe binding motif, analogous to that observed for complex **11**. Complex **14** exhibits a very similar Rh–O bond distance of 2.0670(13) Å compared to that observed for complex **11** (2.0713(18) Å) and the bond angles for N–Rh–O (171.30(6) °) and P–Rh–P (162.844(17) °) are also comparable to those for complex **11** (169.88(8) ° and 163.17(2) ° respectively). Such near linear bond angles indicate a pseudo-square planar geometry around the rhodium centre.

Due to the similarity between complex **14** and complex **11**, interconversion between the two species was probed. In a high pressure NMR tube, a solution of complex **14** (25 mM, C_6D_6) was placed under one atmosphere of CO_2; however, no reaction was observed to occur even after 24 hours indicating complex **14** is stable to reaction with CO_2. This can be explained due to the lack of a β-H for β-H elimination in complex **14**, compared to **11**, which allows the extrusion of CO_2 to yield complex **6**, which has been shown to react rapidly with CO_2 to form complex **11** (**Scheme 4.28**).



Scheme 4.28 Interconversion between complex **11** and **6** via β-H elimination and CO_2 insertion.

To summarise, Rh(PONOP)OAc (**14**) can be synthesised from the reaction of Rh(PONOP)H (**6**) with acetic acid and simply isolated. By comparison of NMR spectroscopic data and solid state structures, complex **14** has a very similar geometry to the analogous formate complex **11**. Complex **14** exhibits no reaction with CO_2.

4.9 Reaction of Rh(PONOP)H (6) with triflic acid

Following on from section 4.8, the analogous reactivity of Rh(PONOP)H (**6**) with triflic acid was explored.

In a J. Young flask, 1.2 equivalents of triflic acid were added to a solution of complex **6** (20 mM, C_6H_6) and the reaction mixture was stirred for 30 minutes, during which time a colour change was observed from red to orange. The solution was filtered before the solvent was removed *in vacuo* to give a light orange powder. $^{31}P\{^1H\}$ NMR spectroscopy of the product in C_6D_6 gave a doublet at 203.5 ppm ($^1J_{RhP}$ = 152 Hz), which was assigned to the triflate complex Rh(PONOP)OTf (**15**) upon comparison to the formate complex **11** (200.3 ppm, $^1J_{RhP}$ = 163 Hz) and the acetate complex **14** (200.0 ppm, $^1J_{RhP}$ = 162 Hz) (**Figure 4.12**).

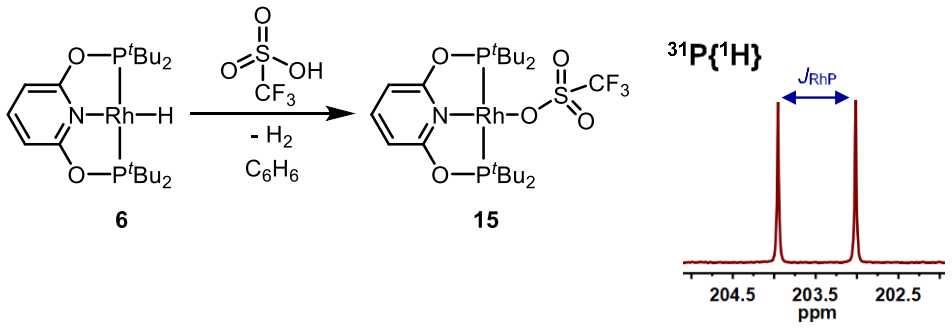


Figure 4.12 Synthesis and partial $^{31}P\{^1H\}$ NMR spectrum (162 MHz, C_6D_6, 298 K) of complex **15**.

The ^{19}F NMR spectrum of the product revealed a singlet at –77.1 ppm consistent with the presence of Rh(PONOP)OTf (**15**). The ^1H NMR spectrum of complex **15** exhibited analogous signals for the PONOP ligand as observed for complex **11** and complex **14**.

A concentrated solution of complex **15** in methylcyclohexane stored at –21 °C for three days yielded light orange crystals suitable for single crystal X-ray diffraction and the solid state structure of complex **15** is shown in **Figure 4.13**.

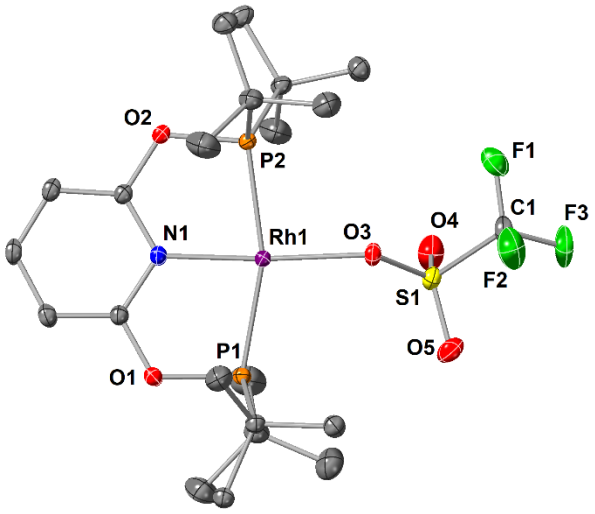


Figure 4.13 Solid state structure of complex **15**. Displacement ellipsoids are drawn at 30 % probability level. Carbon-bound hydrogens are omitted for clarity. Selected bond lengths (Å) and angles (°): Rh1–O3, 2.1285(14); Rh1–P1, 2.2720(5); Rh1–P2, 2.2553(5); Rh1–N1, 2.0013(16); S1–O3, 1.4661(16); S1–O4, 1.4237(19); S1–O5, 1.4310(19); P1–Rh1–P2, 162.414(19); N1–Rh1–O3, 174.64(7).

The solid state structure for complex **15** is consistent with the assignment of Rh(PONOP)OTf and, as for complexes **11** and **14**, an η^1-binding mode of the triflate to the rhodium centre is exhibited. A pseudo-square planar geometry around the rhodium centre is indicated by near linear bond angles of 174.64(7) ° for N–Rh–P and 162.414(19) ° for P–Rh–P. Complex **15** has a similar, if slightly longer Rh–O bond distance of 2.1285(14) Å compared to that for complex **11** (2.0713(18) Å) and complex **14** (2.0670(13) Å).

As with complex **14**, complex **15** exhibited no reactivity with CO_2 when a high pressure NMR tube containing a solution of complex **15** in C_6D_6 (40 mM) was backfilled with one atmosphere of CO_2.

4.10 Conclusions

This chapter has provided an initial overview of the reactivity of the neutral monohydride pincer complex, Rh(PONOP)H (**6**). Complex **6** has been shown to be stable in solvents such as C_6H_6 and 1,2-$F_2C_6H_4$; whereas, analogous monohydride complexes with less bulky ligands, such as Rh(κ^3-P,O,P-Xantphos-^{i}Pr)H, have been reported to initiate C–H activation with such solvents.[12]

Continuing on from the work described in Chapter Three, the reactivity of complex **6** with various amine-boranes has been further explored. No reaction was observed between complex **6** and the tertiary amine-borane, $H_3B{\cdot}NMe_3$, which is as expected due to the lack of NH bonds present. H/D exchange was shown to occur at the metal centre in the presence of $D_3B{\cdot}NMe_3$ indicating reversible B–H/D activation is possible; however, no amine-borane sigma complex was observed, most likely due to the increased steric bulk of the tertiary amine-borane. Complex **6** has already been shown to successfully catalyse the dehydrocoupling of $H_3B{\cdot}NMe_2H$, albeit rather slowly ($\nu_{max} = 0.12 \times 10^{-4}$ M s^{-1}). A mechanism was proposed for this process that involves the concomitant B–H transfer to the Rh–H ligand and N–H transfer to the rhodium centre, which would release $H_2B{=}NMe_2$ and H_2 in a single step, regenerating complex **6**.

In Chapter Three, complex **6** was shown to be protonated by $[H_2B(NMe_2H)_2][BAr^F{}_4]$ or $[NMe_2H_2][BAr^F{}_4]$ to give [Rh(PONOP)(η^2-H_2)][$BAr^F{}_4$] (**1**) and the same outcome was observed in this chapter on reaction of complex **6** with Brookhart's acid, $[H(OEt_2)_2][BAr^F{}_4]$. However, different reactivity was observed when hydrochloric

acid, acetic acid or triflic acid was used resulting in the formation of Rh(PONOP)Cl, Rh(PONOP)OAc (**14**) and Rh(PONOP)OTf (**15**) respectively. Complexes **14** and **15** are novel complexes and their characterisation has been discussed.

Analogous to complexes **14** and **15**, the novel formate complex Rh(PONOP)OCOH (**11**) has been synthesised from the reaction of complex **6** with CO_2. The formation of this complex has been discussed in the context of catalytic formic acid production and initial studies carried out. This system shows some potential however large pressures of H_2:CO_2 and high temperatures are required to investigate fully.

The reactivity of complex **11** with amine-boranes has also been probed and complex **11** has been found to catalytically react with $H_3B{\cdot}NMe_2H$. It was found that complex **11** remained the organometallic resting state during active catalysis. The product of catalysis was identified as $HMe_2N{\cdot}BH(OCOH)_2$ and a mechanism proposed for this process.

4.11 References

[1] M. A. Esteruelas, P. Nolis, M. Oliván, E. Oñate, A. Vallribera, A. Vélez, *Inorg. Chem.* **2016**, *55*, 7176–7181.
[2] A. E. W. Ledger, C. E. Ellul, M. F. Mahon, J. M. J. Williams, M. K. Whittlesey, *Chemistry – A European Journal* **2011**, *17*, 8704–8713.
[3] P. Bhattacharya, J. A. Krause, H. Guan, *J. Am. Chem. Soc.* **2014**, *136*, 11153–11161.
[4] M. Montag, L. Schwartsburd, R. Cohen, G. Leitus, Y. Ben-David, J. M. L. Martin, D. Milstein, *Angewandte Chemie* **2007**, *119*, 1933–1936.
[5] A. Anaby, M. Feller, Y. Ben-David, G. Leitus, Y. Diskin-Posner, L. J. W. Shimon, D. Milstein, *Journal of the American Chemical Society* **2016**, *138*, 9941–9950.
[6] R. Tanaka, M. Yamashita, L. W. Chung, K. Morokuma, K. Nozaki, *Organometallics* **2011**, *30*, 6742–6750.
[7] R. Tanaka, M. Yamashita, K. Nozaki, *J. Am. Chem. Soc.* **2009**, *131*, 14168–14169.
[8] D. Evans, J. A. Osborn, F. H. Jardine, G. Wilkinson, *Nature* **1965**, *208*, 1203.

[9] C. O'Connor, G. Wilkinson, *J. Chem. Soc. A* **1968**, 2665–2671.
[10] R. Langer, G. Leitus, Y. Ben-David, D. Milstein, *Angewandte Chemie International Edition* **2011**, *50*, 2120–2124.
[11] P. Bhattacharya, J. A. Krause, H. Guan, *Organometallics* **2011**, *30*, 4720–4729.
[12] M. A. Esteruelas, M. Oliván, A. Vélez, *Organometallics* **2015**, *34*, 1911–1924.
[13] G. M. Adams, A. L. Colebatch, J. T. Skornia, A. I. McKay, H. C. Johnson, G. C. Lloyd−Jones, S. A. Macgregor, N. A. Beattie, A. S. Weller, *J. Am. Chem. Soc.* **2018**, *140*, 1481–1495.
[14] M. A. Esteruelas, M. Oliván, A. Vélez, *Inorg. Chem.* **2013**, *52*, 5339–5349.
[15] B. F. M. Kimmich, R. M. Bullock, *Organometallics* **2002**, *21*, 1504–1507.
[16] W. H. Bernskoetter, C. K. Schauer, K. I. Goldberg, M. Brookhart, *Science* **2009**, *326*, 553–556.
[17] M. J. Sgro, D. W. Stephan, *Dalton Trans.* **2013**, *42*, 10460–10472.
[18] R. N. Perutz, S. Sabo-Etienne, *Angewandte Chemie International Edition* **2007**, *46*, 2578–2592.
[19] E. A. K. Spearing-Ewyn, N. A. Beattie, A. L. Colebatch, A. J. Martinez-Martinez, A. Docker, T. M. Boyd, G. Baillie, R. Reed, S. A. Macgregor, A. S. Weller, *Dalton Trans.* **2019**, *48*, 14724–14736.
[20] M. C. Haibach, D. Y. Wang, T. J. Emge, K. Krogh-Jespersen, A. S. Goldman, *Chem. Sci.* **2013**, *4*, 3683–3692.
[21] M. A. Iron, E. Ben-Ari, R. Cohen, D. Milstein, *Dalton Trans.* **2009**, 9433–9439.
[22] M. Findlater, W. H. Bernskoetter, M. Brookhart, *J. Am. Chem. Soc.* **2010**, *132*, 4534–4535.
[23] E. V. Kondratenko, G. Mul, J. Baltrusaitis, G. O. Larrazábal, J. Pérez-Ramírez, *Energy Environ. Sci.* **2013**, *6*, 3112–3135.
[24] M. Cokoja, C. Bruckmeier, B. Rieger, W. A. Herrmann, F. E. Kühn, *Angewandte Chemie International Edition* **2011**, *50*, 8510–8537.
[25] E. Graf, W. Leitner, *J. Chem. Soc., Chem. Commun.* **1992**, *0*, 623–624.
[26] W. Leitner, E. Dinjus, F. Gaßner, *Journal of Organometallic Chemistry* **1994**, *475*, 257–266.
[27] P. G. Jessop, F. Joó, C.-C. Tai, *Coordination Chemistry Reviews* **2004**, *248*, 2425–2442.
[28] M. Feller, U. Gellrich, A. Anaby, Y. Diskin-Posner, D. Milstein, *J. Am. Chem. Soc.* **2016**, *138*, 6445–6454.
[29] H.-W. Suh, T. J. Schmeier, N. Hazari, R. A. Kemp, M. K. Takase, *Organometallics* **2012**, *31*, 8225–8236.
[30] S. Chakraborty, J. Zhang, J. A. Krause, H. Guan, *Journal of the American Chemical Society* **2010**, *132*, 8872–8873.
[31] L. Schwartsburd, M. A. Iron, L. Konstantinovski, E. Ben-Ari, D. Milstein, *Organometallics* **2011**, *30*, 2721–2729.
[32] G. M. Adams, F. M. Chadwick, S. D. Pike, A. S. Weller, *Dalton Trans.* **2015**, *44*, 6340–6342.
[33] M. L. Scheuermann, S. P. Semproni, I. Pappas, P. J. Chirik, *Inorg. Chem.* **2014**, *53*, 9463–9465.
[34] A. Jana, G. Tavčar, H. W. Roesky, M. John, *Dalton Trans.* **2010**, *39*, 9487–9489.

[35] O. J. Metters, A. M. Chapman, A. P. M. Robertson, C. H. Woodall, P. J. Gates, D. F. Wass, I. Manners, *Chem. Commun.* **2014**, *50*, 12146–12149.
[36] Q. Zhao, J. Li, N.-N. Ma, C.-G. Wei, T. Xu, B. Li, J. Zhang, X. Chen, *European Journal of Inorganic Chemistry* **2018**, *2018*, 2659–2665.
[37] G. La Monica, G. A. Ardizzoia, F. Cariati, S. Cenini, M. Pizzotti, *Inorg. Chem.* **1985**, *24*, 3920–3923.
[38] H. C. Brown, T. P. Stocky, *J. Am. Chem. Soc.* **1977**, *99*, 8218–8226.
[39] I. Knopf, C. C. Cummins, *Organometallics* **2015**, *34*, 1601–1603.
[40] H. W. Lee, A. S. C. Chan, F. Y. Kwong, *Chem. Commun.* **2007**, 2633–2635.
[41] H. D. S. Guerrand, M. Vaultier, S. Pinet, M. Pucheault, *Advanced Synthesis & Catalysis* **2015**, *357*, 1167–1174.
[42] C. A. Jaska, K. Temple, A. J. Lough, I. Manners, *J. Am. Chem. Soc.* **2003**, *125*, 9424–9434.
[43] E. L. Piacentino, K. Parker, T. M. Gilbert, R. A. J. O'Hair, V. Ryzhov, *Chemistry – A European Journal* **2019**, *25*, 9959–9966.

5 Summary and future outlook

This thesis explored the reactivity of the {Rh(PONOP)}$^+$ fragment with amine-boranes, with an aim of increasing the understanding of the mechanistic pathways of the transition metal-catalysed dehydrocoupling of amine-boranes. An in-depth study into the dehydrocoupling of $H_3B{\cdot}NMe_2H$ with the {Rh(PONOP)}$^+$ fragment has been conducted and a mechanism for this process has been proposed. At the centre of the catalytic cycle is a hydride transfer process to form the neutral monohydride Rh(PONOP)H, which may be protonated by either a boronium or ammonium cation to close the catalytic cycle. Computational studies revealed protonation via the ammonium cation to be the energetically favourable route under catalytic conditions. Free NMe_2H in solution was also shown to promote catalysis. Future work in this area would be to apply the knowledge of the reactivity of {Rh(PONOP)}$^+$ with $H_3B{\cdot}NMe_2H$ to reactivity with the primary amine-borane $H_3B{\cdot}NMeH_2$ under comparable conditions. These studies may contribute towards the elucidation of a universal mechanism for the more complex dehydropolymerisation of primary amine-boranes.

The final chapter of this thesis explored the synthesis and reactivity of the novel formate complex Rh(PONOP)OCOH. Preliminary studies into the catalytic reduction of CO_2 to yield formic acid were carried out; however, to investigate the potential of Rh(PONOP)OCOH in this context further, higher pressures of H_2 and CO_2 would be required. Rh(PONOP)OCOH was also found to react catalytically with $H_3B{\cdot}NMe_2H$ and a mechanistic pathway for this process was proposed. A natural next step would be to

explore the reactivity of Rh(PONOP)OCOH with the primary amine-borane $H_3B{\cdot}NMeH_2$, in order to probe the potentially more complex, CO_2–containing products.

Finally, in all cases of the reactivity discussed in this thesis, an interesting comparison would be to substitute the bulky ^{t}Bu groups in the PONOP ligand with the less bulky ^{i}Pr groups as this may reduce the steric bulk around the rhodium centre and may lead to faster, and more varied reactivity.

6 Experimental

6.1 Experimental techniques

All manipulations, unless otherwise stated, were performed under an argon atmosphere using standard Schlenk line and glovebox techniques. Glassware was oven dried at 130 °C overnight and flame dried under vacuum prior to use. Pentane, hexane, toluene, Et_2O, C_6H_6 and CH_2Cl_2 were dried using a Grubbs-type solvent purification system (MBraun SPS-800) and degassed by three successive freeze-pump-thaw cycles.[1] THF was dried over Na/benzophenone, vacuum distilled, degassed by three successive freeze-pump-thaw cycles and stored over 3.0 Å molecular sieves. 1,2-$F_2C_6H_4$ (pre-treated with alumina) and CD_2Cl_2 were dried over CaH_2, vacuum distilled, degassed by three successive freeze-pump-thaw cycles and stored over 3.0 Å molecular sieves. C_6D_6 and methylcyclohexane were dried over Na, vacuum distilled, degassed by three successive freeze-pump-thaw cycles and stored over 3.0 Å molecular sieves.

6.2 Procedure for the addition of $H_2/N_2/D_2/CO_2$ to a reaction mixture

To achieve the addition of one atmosphere of H_2, N_2, D_2 or CO_2, the sample was freeze-pump-thaw degassed three times and backfilled with one atmosphere of the desired gas at 298 K. To achieve the addition of four atmospheres of gas, the same procedure for one atmosphere was carried out except the sample was cooled to 77 K by the immersion in liquid N_2 for the duration of the addition of the desired gas. The

sample flask was then closed and warmed to 298 K, yielding an internal pressure of approximately four atmospheres.

6.3 Nuclear Magnetic Resonance (NMR) spectroscopy

NMR spectra were recorded on a Bruker AVIIIHD 500 or Bruker AVIIIHD 400 nanobay spectrometer at room temperature, unless otherwise stated. Residual protio solvent was used as a reference for ^{1}H NMR and ^{13}C NMR spectra in deuterated solvent samples. For samples in 1,2-$F_2C_6H_4$ solvent, the NMR spectrometer was pre-locked and shimmed to a sample of C_6D_6 (25 %) and 1,2-$F_2C_6H_4$ (75 %) and referenced to the centre of the high frequency multiplet, δ 7.07 ppm. ^{31}P and ^{11}B NMR spectra were referenced externally against 85 % H_3PO_4 and $BF_3{\cdot}OEt_2$, respectively. Chemical shifts (δ) are quoted in ppm and coupling constants (*J*) in Hz, with the multiplicities of the NMR signals reported as follows: s, singlet; d, doublet; t, triplet; q, quartet; m, multiplet and br, broad.

6.4 Mass spectrometry

Electrospray ionisation mass spectrometry (ESI-MS) of organometallic complexes were recorded using a Bruker MicrOTOF instrument directly connected to a modified Innovative Technology glovebox.[2] The mass spectrometer was calibrated in positive ion mode using a 10.0 ng mL^{-1} mixture of tetraalkylammonium bromide salts $[N(C_nH_{2n+1})_4]Br$ (n = 2 – 8, 12, 16, 18) in CH_2Cl_2. Typical experimental acquisition parameters were as follows: sample flow rate, 4.0 μL min^{-1}; nebuliser gas pressure, 0.4 bar; drying gas (argon) at 60 °C flowing at 4.0 L min^{-1}; capillary voltage, 4.5 kV; funnel voltage, 200 Vpp. Samples were diluted in 1,2-$F_2C_6H_4$ to a

concentration of approximately 1.0×10^{-6} M and filtered (0.2 μm pore size) before analysis.

6.5 Elemental microanalysis

Elemental microanalyses were performed by Stephen Boyer at London Metropolitan University.

6.6 Infrared spectroscopy

Infrared spectra were recorded as thin films in Nujol oil between NaCl discs on a Bruker Tensor 27 FT-IR spectrometer (resolution < 1 cm^{-1}).

6.7 Synthesis and characterisation

6.7.1 Starting materials

$H_3B{\cdot}NMe_3$ and $H_3B{\cdot}NMe_2H$ were purchased from Sigma-Aldrich and sublimed once and twice prior to use respectively (5.0×10^{-2} mbar, 298 K). Hg (99.9995 %) was purchased from Sigma-Aldrich, washed with 1,2-$F_2C_6H_4$ and dried *in vacuo* prior to use. PPh_3, n-BuLi (2.5 M in hexanes), HCl (2.0 M in Et_2O), D_2 and CO_2 were purchased from Sigma-Aldrich and used as received. NMe_2H (2.0 M in THF) was purchased from Fisher Scientific and used as received to form solutions in 1,2-$F_2C_6H_4$ of the desired concentrations. Formic, acetic and triflic acid were purchased from Sigma-Aldrich and small batches were bubbled degassed with argon prior to use. $Na[BAr^F{}_4]$,[3] $D_3B{\cdot}NMe_3$,[4] $H_3B{\cdot}NMe_2D$,[5] $D_3B{\cdot}NMe_2D$,[5] $H_2B{=}N^iPr_2$,[6] $[H_2BNMe_2]_2$,[6] $[H_2B(NMe_2H)_2][Cl]$,[7] $[H_2B(NMe_2H)_2][BAr^F{}_4]$,[7,8] $H_3B{\cdot}NMe_2H_2B{\cdot}NMe_2H$,[6] $[H(OEt_2)_2][BAr^F{}_4]$,[9] $[Rh(COE)_2Cl]_2$,[10] Rh(PONOP)Cl,[11] [Rh(PONOP)(η²-

H_2)][BAr^F_4] (**1**),[12] [Rh(PONOP)(κ^1-N_2)][BAr^F_4] (**2**)[13] and [Rh(PONOP)(κ^1-$ClCH_2Cl$)][BAr^F_4] (**3**)[13] were prepared according to literature methods. [NMe_2H_2][BAr^F_4] was synthesised according to the literature procedure for ammonium BAr^F_4 salts.[14] ^{Cy}PONOP had been previously synthesised by F. M. Chadwick following the literature procedure for other PONOP ligands[15] and was available for group use as a solution in hexane (0.407 M).

6.7.2 Synthesis of [Rh(PONOP)(η^1-$H_3B{\cdot}NMe_3$)][BAr^F_4] (4)

[Rh(PONOP)(η^2-H_2)][BAr^F_4] (**1**) (50 mg, 0.036 mmol) and $H_3B{\cdot}NMe_3$ (2.62 mg, 0.036 mmol) were dissolved in 1,2-$F_2C_6H_4$ (2 mL) and the reaction mixture stirred at room temperature for 24 hours. The solution was then concentrated *in vacuo* to ~1 mL, cooled to 0 °C and pentane (5 mL) was added to give a precipitate. The solid was isolated by filtration and washed with pentane (2 mL × 2) before being dried under vacuum to give the product as a yellow powder. An isolated yield of 32.8 mg (63 %) was obtained. Layering a 1,2-$F_2C_6H_4$ solution of complex **4** with pentane and storing at 5 °C overnight yielded dark yellow crystals suitable for single crystal X-ray diffraction.

^{1}H NMR (500 MHz, CD_2Cl_2, 298 K): δ 7.73 (br s, 8H, [BAr^F_4]-*o*-CH), 7.69 (obscured tr, $^3J_{HH}$ 8, 1H, C_5H_3N), 7.56 (br s, 4H, [BAr^F_4]-*p*-CH), 6.67 (d, $^3J_{HH}$ 8, 2H, C_5H_3N), 2.72 (s, 9H, NMe_3), 1.42 (vt, J_{PH} 8, 36H, P(^{t}Bu)$_2$), –2.55 (br d, $^1J_{BH}$ 90, 3H, RhH_3B).

^{11}B NMR (160 MHz, CD_2Cl_2, 298 K): δ –6.61 (s, [BAr^F_4]$^-$), –15.24 (br s, RhH_3B).

^{31}P{^{1}H} NMR (202 MHz, CD_2Cl_2, 298 K): δ 208.9 (d, $^1J_{RhP}$ 142).

ESI-MS (1,2-$F_2C_6H_4$, 60 °C, 4.5 kV): *m/z* 575.26 (calc. 575.26 for {Rh(PONOP)(η^1-$H_3B{\cdot}NMe_3$)}$^+$ fragment, showing the correct isotope pattern).

Elemental Microanalysis: Calc. $C_{56}H_{63}B_2F_{24}N_2O_2P_2Rh$ (1438.57 gmol^{-1}) C, 46.76; H, 4.41; N, 1.95. Found: C, 46.90; H, 4.27; N, 2.01.

6.7.3 Spectroscopic data for [Rh(PONOP)(η^1-$H_3B{\cdot}NMe_2H$)][BAr^F_4] (5)

^{1}H NMR (500 MHz, 1,2-$F_2C_6H_4$, 298 K): δ 8.32 (br s, 8H, [BAr^F_4]-*o*-CH), 7.69 (br s, 4H, [BAr^F_4]-*p*-CH), 7.61 (tr, $^3J_{HH}$ 8, 1H, C_5H_3N), 6.67 (d, $^3J_{HH}$ 8, 2H, C_5H_3N), 3.25 (br s, 1H, NH), 2.76 (d, $^3J_{HH}$ 6, 6H, NMe_2), 1.42 (vt, J_{PH} 7, 36H, P(^{t}Bu)$_2$), –1.98 (br s, 3H, RhH_3B).

^{11}B NMR (160 MHz, 1,2-$F_2C_6H_4$, 298 K): δ –6.22 (s, [BAr^F_4]$^-$), –21.36 (br s, RhH_3B).

^{31}P{^{1}H} NMR (202 MHz, 1,2-$F_2C_6H_4$, 298 K): δ 212.9 (d, $^1J_{RhP}$ 138).

6.7.4 Synthesis of Li[$H_3B{\cdot}NMe_2$]

Adapted from literature.[16]

Hexane (20 mL) was added to $H_3B{\cdot}NMe_2H$ (400 mg, 6.79 mmol) to give a white suspension, which was then cooled to –78 °C. *n*-Butyllithium (2.5 M in hexanes, 3 mL, 7.5 mmol) was added dropwise by syringe over 15 minutes. The reaction was stirred at –78 °C for 1 hour and then allowed to come to room temperature and stirred for an additional hour. The solution was then filtered, leaving a white solid which was washed with hexane (3 × 10 mL). The solid was dried cold *in vacuo* for 2 hours to yield a white powder (412.9 mg, 94% yield).

^{11}B NMR (128 MHz, THF, 298 K): δ –14.45 (q, $^1J_{BH}$ 87).

$^{11}B\{^{1}H\}$ NMR (128 MHz, THF, 298 K): δ –14.83 (s).

6.7.5 Synthesis of Rh(PONOP)H (6)

Rh(PONOP)Cl (150 mg, 0.279 mmol) and Li[$H_3B{\cdot}NMe_2$] (36.2 mg, 0.558 mmol) were dissolved in pentane (5 mL) to give an orange/red solution which was stirred at room temperature for 24 hours. The solution was filtered and the solvent removed *in vacuo* to yield a red powder. An isolated yield of 113.3 mg (81 %) was obtained. A concentrated solution of complex **6** in methylcyclohexane was stored at 5 °C for 1 hour and then at –20 °C for 3 days, after which red crystals suitable for single crystal X-ray diffraction were formed.

^{1}H NMR (400 MHz, C_6D_6, 298 K): δ 6.92 (tr, $^{3}J_{HH}$ 8, 1H, C_5H_3N), 6.27 (d, $^{3}J_{HH}$ 8, 2H, C_5H_3N), 1.41 (vt, J_{PH} 7, 36H, P(^{t}Bu)$_2$), –9.60 (td, J_{PH} 23, J_{RhH} 20, 1H, RhH).

$^{1}H\{^{31}P\}$ NMR (400 MHz, C_6D_6, 298 K): δ 6.92 (tr, $^{3}J_{HH}$ 8, 1H, C_5H_3N), 6.28 (d, $^{3}J_{HH}$ 8, 2H, C_5H_3N), 1.42 (s, 36H, P(^{t}Bu)$_2$), –9.60 (d, J_{RhH} 20, 1H, RhH).

$^{31}P\{^{1}H\}$ NMR (162 MHz, C_6D_6, 298 K): δ 226.2 (d, $^{1}J_{RhP}$ 171).

$^{13}C\{^{1}H\}$ NMR (100 MHz, C_6D_6, 298 K): δ 28.7 (vt, J_{CP} 5, 12C, P-C(CH$_3$)$_3$), 39.0 (vq, J_{CPRh} 4, 4C, P-C(CH$_3$)$_3$), 100.8 (d, J_{CP} 2, 2C, C_5H_3N), 135.9 (s, 1C, C_6H_5N), 163.4 (vt, J_{CP} 5, 2C, C_6H_5N).

Elemental Microanalysis: Calc. $C_{21}H_{40}NO_2P_2Rh$ (503.41 gmol^{-1}) C, 50.10; H, 8.01; N, 2.78. Found: C, 49.99; H, 8.09; N, 2.86.

6.7.6 Synthesis of Rh(^{Cy}PONOP)Cl (7)

A hexane solution of ^{Cy}PONOP (0.49 mL, 0.407 M, 0.2 mmol) was added to a toluene solution of $[Rh(COE)_2Cl]_2$ (7.10 mg, 0.1 mmol) and stirred at room temperature for 24 hours. The solvent was then removed *in vacuo* and the resulting solid cooled to –78 °C and washed with –78 °C pentane (3 × 10 mL). The solid was then dried under vacuum overnight to yield a dark orange powder (73.0 mg, 57 % yield).

^{1}H NMR (500 MHz, C_6D_6, 298 K): δ 6.82 (tr, $^3J_{HH}$ 8, 1H, C_5H_3N), 6.16 (d, $^3J_{HH}$ 8, 2H, C_5H_3N), 2.4–1.2 (m, 44H, $P(Cy)_2$).

^{31}P{^{1}H} NMR (202 MHz, C_6D_6, 298 K): δ 187.8 (d, $^1J_{RhP}$ 154).

6.7.7 Spectroscopic data for [Rh(^{Cy}PONOP)(κ^1-N_2)][BAr^F_4] (8)

^{31}P{^{1}H} NMR (162 MHz, 1,2-$F_2C_6H_4$, 298 K): δ 194.5 (d, $^1J_{RhP}$ 132).

ESI-MS (1,2-$F_2C_6H_4$, 60 °C, 4.5 kV): *m/z* 634.23 (calc. 634.22 for {Rh(^{Cy}PONOP)(κ^1-N_2)}$^+$ fragment, showing the correct isotope pattern).

6.7.8 Spectroscopic data for [Rh(^{Cy}PONOP)(η^2-H_2)][BAr^F_4] (9)

^{1}H NMR (500 MHz, 1,2-$F_2C_6H_4$, 298 K): δ 8.33 (br s, 8H, [BAr^F_4]-*o*-CH), 7.84 (tr, $^3J_{HH}$ 8, 1H, C_5H_3N), 7.69 (br s, 4H, [BAr^F_4]-*p*-CH), 2.7–1.2 (m, 44H, $P(Cy)_2$), –8.16 (d, $^1J_{RhH}$ 28, 2H, RhH_2).

^{31}P{^{1}H} NMR (202 MHz, 1,2-$F_2C_6H_4$, 298 K): δ 208.0 (d, $^1J_{RhP}$ 127).

ESI-MS (1,2-$F_2C_6H_4$, 60 °C, 4.5 kV): *m/z* 608.22 (calc. 608.23 for {Rh(^{Cy}PONOP)(η^2-H_2)}$^+$ fragment, showing the correct isotope pattern).

6.7.9 Synthesis of [Rh(^{Cy}PONOP)(η^1-$H_3B{\cdot}NMe_3$)][BAr^F_4] (10)

Rh(^{Cy}PONOP)Cl (**7**) (30 mg, 0.047 mmol), $NaBAr^F_4$ (45.6 mg, 0.051 mmol) and $H_3B{\cdot}NMe_3$ (3.75 mg, 0.051 mmol) were dissolved in 1,2-$F_2C_6H_4$ (2 mL) to give a dark brown solution and the reaction stirred at room temperature for 2 hours. The solution was then filtered, cooled to 0 °C and pentane (5 mL) was added to give a precipitate. The solid was isolated by filtration, washed with pentane (2 mL x 3) and then dried under vacuum to give a brown oil. No yield was obtained as the product was immediately dissolved in 1,2-$F_2C_6H_4$ (0.4 mL) and layered with pentane. After two days, orange crystals were obtained suitable for single crystal X-ray diffraction. The product was also characterised *in situ* by NMR spectroscopy:

^{1}H NMR (400 MHz, CD_2Cl_2, 298 K): δ 7.72 (br s, 8H, [BAr^F_4]-*o*-CH), 7.65 (tr, $^3J_{HH}$ 8, 1H, C_5H_3N), 7.57 (br s, 4H, [BAr^F_4]-*p*-CH), 6.62 (d, $^3J_{HH}$ 8, 2H, C_5H_3N), 2.2–1.2 (m, 44H, $P(Cy)_2$), –2.47 (br s, 3H, RhH_3B).

^{11}B NMR (128 MHz, CD_2Cl_2, 298 K): δ –6.62 (s, [BAr^F_4]$^-$), –14.01 (br s, RhH_3B).

^{31}P{^{1}H} NMR (162 MHz, CD_2Cl_2, 298 K): δ 199.5 (d, $^1J_{RhP}$ 142).

6.7.10 Synthesis of $D_3B{\cdot}NMe_2H$

Adapted from literature.[4]

$D_3B{\cdot}NMe_3$ (200 mg, 2.6 mmol, 99% D) was added to a J. Young flask and cooled to –78 °C. NMe_2H (2.0 M in THF, 7 mL, 132.0 mmol) was added to $D_3B{\cdot}NMe_3$ and the solution was allowed to warm to room temperature and stirred for 72 hours. The volatiles were removed *in vacuo* at 0 °C and the resulting solid purified by

sublimation (5.0×10^{-2} mbar, 303 K) to give a white solid (130 mg, 80 % yield). NMR spectroscopic data as reported in the literature.[6]

6.7.11 *In situ* synthesis of Rh(PONOP)(OCOH) (11)

A high pressure J. Young NMR tube containing a solution of Rh(PONOP)H (**6**) (15 mg, 0.03 mmol) in C_6D_6 (0.4 mL) was freeze-pump-thaw degassed three times before placed under 1 atm CO_2. An immediate colour change from red to orange was observed upon shaking of the sample. NMR spectroscopy of the reaction mixture confirmed the complete formation of Rh(PONOP)(OCOH) (**11**). Dark orange crystals of complex **11** suitable for single crystal X-ray diffraction were obtained by the addition of 1 atm CO_2 to a degassed solution of complex **6** (15 mg, 0.03 mmol) in methylcyclohexane (2 mL) followed by immediate cooling of the sample to 5 °C for 1 hour and then leaving the sample at –20 °C for 3 days.

^{1}H NMR (400 MHz, C_6D_6, 298 K): δ 8.63 (m, 1H, COH), 6.72 (tr, $^3J_{HH}$ 8, 1H, C_5H_3N), 5.99 (d, $^3J_{HH}$ 8, 2H, C_5H_3N), 1.46 (vt, J_{PH} 7, 36H, P(^{t}Bu)$_2$).

^{31}P{^{1}H} NMR (162 MHz, C_6D_6, 298 K): δ 200.3 (d, $^1J_{RhP}$ 163).

^{13}C{^{1}H} NMR (100 MHz, C_6D_6, 298 K): δ 27.8 (vt, J_{CP} 5, 12C, P-C(CH_3)$_3$), 39.8 (vq, J_{CPRh} 3, 4C, P-C(CH_3)$_3$), 101.6 (s, 2C, C_5H_3N), 135.7 (s, 1C, C_6H_5N), 165.6 (vt, J_{CP} 5, 2C, C_6H_5N), 167.6 (s, 1C, OCOH).

Elemental Microanalysis: Calc. $C_{22}H_{40}NO_4P_2Rh$ (547.42 g mol^{-1}) C, 48.27; H, 7.37; N, 2.56. Found: C, 48.16; H, 7.19; N, 2.56.

IR (Nujol): ν_{CO} = 1965 cm^{-1}.

6.7.12 Synthesis of $HMe_2N{\cdot}BH_2OCOH$ (12)

Route A: Formic acid (38 µL, 0.9 mmol), that had been bubble degassed with argon, was added dropwise to a 3 mL 1,2-$F_2C_6H_4$ solution of $H_3B{\cdot}NMe_2H$ (50 mg, 0.8 mmol) in a Schlenk and stirred at room temperature for 24 hours. The reaction was filtered and the solvent removed *in vacuo* to give a colourless oil, which was then washed with –78 °C hexane and dried *in vacuo* to give the product as an oil (51.3 mg, 59 %).

Route B: THF (5 mL) was added to a Schlenk containing $H_2B(NMe_2H)_2Cl$ (60 mg, 0.4 mmol) to form a white suspension. Formic acid (16.4 µL, 0.4 mmol), that had been bubble degassed with argon, was added dropwise to the suspension and the resulting mixture was stirred for 10 minutes at room temperature. The reaction mixture was filtered and the solvent removed *in vacuo* to give a colourless oil (28.0 mg, 63 %).

^{1}H NMR (400 MHz, C_6D_6, 298 K): δ 8.31 (s, 1H, OCOH), 5.75 (br s, 1H, NH), 2.87 (dd, $^1J_{BH}$ 122, 101, 2H, BH_2), 1.87 (d, $^3J_{HH}$ 7, 6H, NMe_2).

^{1}H{^{11}B} NMR (400 MHz, C_6D_6, 298 K): δ 8.31 (s, 1H, COH), 5.75 (br s, 1H, NH), 2.87 (s, 2H, BH_2), 1.87 (d, $^3J_{HH}$ 7, 6H, NMe_2).

^{11}B NMR (128 MHz, C_6D_6, 298 K): δ –0.54 (t, $^1J_{BH}$ 114).

^{11}B{^{1}H} NMR (128 MHz, C_6D_6, 298 K): δ –0.54 (s).

^{11}B NMR (128 MHz, 1,2-$F_2C_6H_4$, 298 K): δ –0.63 (t, $^1J_{BH}$ 114).

$^{11}B\{^1H\}$ NMR (128 MHz, 1,2-$F_2C_6H_4$, 298 K): δ –0.63 (s).

ESI-MS (1,2-$F_2C_6H_4$, 60 °C, 4.5 kV): *m/z* 126.06 (calc. 126.07 for $\{HMe_2N{\cdot}BH_2OCOH.Na\}^+$ fragment, showing the correct isotope pattern).

6.7.13 Synthesis of $HMe_2N{\cdot}BH(OCOH)_2$ (13)

In a J. Young flask, complex **6** (68.5 mg, 0.14 mmol) and $H_3B{\cdot}NMe_2H$ (200 mg, 3.40 mmol) were dissolved in 1,2-$F_2C_6H_4$ (5 mL) and the flask immersed immediately in liquid N_2. The solution was freeze-pump-thaw degassed three times before being backfilled with 1 atm of CO_2 (19 mmol) at room temperature and stirred for 24 hours. Cold hexane (0 °C, 15 mL) was then added to the reaction mixture to yield a brown/yellow precipitate, which was isolated by filtration and washed with more hexane (2 × 10 mL) and then dried *in vacuo* to yield an off-white oily solid (11.6 mg, 58 %). NMR spectroscopy of the product indicated the additional presence of $\{Rh(PONOP)CO\}^+$.

^1H NMR (400 MHz, CD_2Cl_2, 298 K): δ 8.22 (s, 2H, $(OCOH)_2$), 5.98 (br s, 1H, NH), 3.27 (obs. dd, $^1J_{BH}$ 128, 107, 1H, BH), 2.48 (d, $^3J_{HH}$ 6, 6H, NMe_2).

$^1H\{^{11}B\}$ NMR (400 MHz, CD_2Cl_2, 298 K): δ 8.22 (s, 1H, COH), 5.98 (br s, 1H, NH), 3.27 (s, 2H, BH_2), 2.48 (d, $^3J_{HH}$ 7, 6H, NMe_2).

^{11}B NMR (128 MHz, CD_2Cl_2, 298 K): δ 2.15 (d, $^1J_{BH}$ 132).

$^{11}B\{^1H\}$ NMR (128 MHz, CD_2Cl_2, 298 K): δ 2.15 (s).

^{11}B NMR (128 MHz, 1,2-$F_2C_6H_4$, 298 K): δ 2.19 (d, $^1J_{BH}$ 132).

$^{11}B\{^1H\}$ NMR (128 MHz, 1,2-$F_2C_6H_4$, 298 K): δ 2.19 (s).

6.7.14 Synthesis of Rh(PONOP)OAc (14)

Acetic acid (6.8 μL, 0.12 mmol) that had been bubble degassed was added to a 5 mL C_6H_6 solution of Rh(PONOP)H (**6**) (50 mg, 0.10 mmol) in a J. Young flask and stirred for 30 minutes, during which a colour change from red to orange was observed. The solution was filtered and solvent removed *in vacuo* overnight to yield Rh(PONOP)OAc (**14**) as an orange powder (26.5 mg, 48 % yield). A concentrated solution of **14** in methylcyclohexane was stored at 5 °C for 1 hour and then at –21 °C and after 3 days, dark orange crystals suitable for single crystal X-ray diffraction were yielded.

^{1}H NMR (400 MHz, C_6D_6, 298 K): δ 6.69 (tr, $^3J_{HH}$ 8, 1H, C_5H_3N), 5.95 (d, $^3J_{HH}$ 8, 2H, C_5H_3N), 2.28 (s, 3H, CH_3), 1.42 (vt, J_{PH} 7, 36H, P(^{t}Bu)$_2$).

^{31}P{^{1}H} NMR (162 MHz, C_6D_6, 298 K): δ 200.0 (d, $^1J_{RhP}$ 162).

^{13}C{^{1}H} NMR (100 MHz, C_6D_6, 298 K): δ 24.1 (s, 1C, OCH_3), 27.7 (vt, J_{CP} 5, 12C, P-C(CH_3)$_3$), 39.7 (vq, J_{CPRh} 4, 4C, P-C(CH_3)$_3$), 100.98 (d, J_{CP} 3, 2C, C_5H_3N), 135.4 (s, 1C, C_6H_5N), 165.6 (vt, J_{CP} 5, 2C, C_6H_5N), 175.2 (s, 1C, COMe).

Elemental Microanalysis: Calc. $C_{23}H_{42}NO_4P_2Rh$ (561.45 g mol^{-1}) C, 49.20; H, 7.54; N, 2.49. Found: C, 49.31; H, 7.63; N, 2.48.

IR (Nujol): ν_{CO} = 1610 cm^{-1}.

6.7.15 Synthesis of Rh(PONOP)OTf (15)

Triflic acid (8.8 μL, 0.1 mmol) that had been bubble degassed was added to a 5 mL C_6H_6 solution of Rh(PONOP)H (**6**) (50 mg, 0.1 mmol) in a J. Young flask and stirred for 30 minutes, during which time a colour change from red to yellow was observed.

The solution was filtered and the volatiles removed *in vacuo* overnight to yield Rh(PONOP)OTf (**15**) as a light orange powder (38.5 mg, 60 % yield). A concentrated solution of **15** in methylcyclohexane was stored at 5 °C for 1 hour and then at –21 °C and after 3 days, light orange crystals suitable for single crystal X-ray diffraction were yielded.

^{1}H NMR (400 MHz, C_6D_6, 298 K): δ 6.61 (tr, $^{3}J_{HH}$ 8, 1H, C_5H_3N), 5.85 (d, $^{3}J_{HH}$ 8, 2H, C_5H_3N), 1.41 (vt, J_{PH} 7, 36H, P(^{t}Bu)$_2$).

^{31}P{^{1}H} NMR (162 MHz, C_6D_6, 298 K): δ 203.5 (d, $^{1}J_{RhP}$ 152).

^{19}F{^{1}H} NMR (377 MHz, C_6D_6, 298 K): δ –77.07 (s, 3H, CF_3).

^{13}C{^{1}H} NMR (100 MHz, C_6D_6, 298 K): δ 27.7 (vt, J_{CP} 4, 12C, P-C(CH_3)$_3$), 40.1 (1, J_{CPRh} 5, 4C, P-C(CH_3)$_3$), 101.2 (d, J_{CP} 3, 2C, C_5H_3N), 119.8 (q, J_{CF} 320, 1C, CF_3), 137.7 (s, 1C, C_6H_5N), 166.0 (vt, J_{CP} 4, 2C, C_6H_5N).

Elemental Microanalysis: Calc. $C_{22}H_{39}F_3NO_5P_2RhS$ (651.46 g mol^{-1}) C, 40.56; H, 6.03; N, 2.15. Found: C, 40.39; H, 6.14; N, 2.07.

6.8 General procedures for the catalytic dehydrogenation of $H_3B{\cdot}NMe_2H$

6.8.1 Under closed/NMR tube conditions

In a typical experiment (e.g. 2 mol% catalyst loading), $H_3B{\cdot}NMe_2H$ (3.4 mg, 57.7 μmol) was dissolved in 1,2-$F_2C_6H_4$ (0.4 mL) in a Schlenk flask and 0.2 mL of this solution was added to a J. Young high-pressure NMR tube. In a separate flask, complex **1** (2 mg, 1.4 μmol) was dissolved in 1,2-$F_2C_6H_4$ (0.5 mL) and 0.2 mL of this solution was added to the same NMR tube, which was immediately sealed and then

frozen in liquid N_2. When the NMR spectrometer was set up appropriately, the NMR tube was thawed, shaken thoroughly and immediately inserted into the NMR spectrometer for analysis.

6.8.2 Under H_2 evolution measurement conditions

In typical experiment (e.g. 2 mol% catalyst loading), $H_3B{\cdot}NMe_2H$ (21.2 mg, 0.36 mmol) was dissolved in 1,2-$F_2C_6H_4$ (4 mL) in a jacketed two-neck Schlenk flask connected to a recirculating cooler and the temperature set to 25 °C. In a separate Schlenk flask, complex **1** (11.8 mg, 8.6 μmol) was dissolved in 1,2-$F_2C_6H_4$ (1.2 mL). The flask containing amine-borane was sealed off from the argon supply and connected to a water-filled 100.0 mL gas burette. 1 mL of the catalyst solution was added to the reaction mixture and the resultant solution was stirred at 400 rpm. The volume of gas evolved was then recorded as function of time, starting from the addition of catalyst to amine-borane.

6.9 Computational details

The computational work described in this thesis was carried out by Professor Stuart A. Macgregor and Dr Nicholas A. Beattie at Heriot-Watt University, Edinburgh. The calculations were run with Gaussian 09 Revision D.01[17] and geometry optimisations were performed using the BP86 functional.[18,19] Rh and P centres were described via Stuttgart RECPs and associated basis sets[20] (with additional d-orbital polarisation on P)[21] and 6-31G** basis sets[22,23] for all other atoms. Stationary points were fully characterised via analytical frequency calculations as either minima (no imaginary frequencies) or transition states (a single imaginary

frequency). Transition states were further characterised through IRC calculations and subsequent geometry optimisations. SFC energies were re-computed at the BP86-optimised geometries with the def2-tzvp basis sets[24,25] on all atoms, including a correction for 2-hexanone solvent (ε = 14.14, employed as solvent in the absence of parameters for 1,2-$F_2C_6H_4$, ε = 13.81) via the PCM approach[26] and dispersion using Grimme's D3 parameter set with Becke-Johnson damping.[27]

6.10 X-ray crystallography

Structure determinations were carried out by Dr Annie L. Colebatch (**4**) and Dr Antonio J. Martínez-Martínez (**6**, **10**, **11**, **14** and **15**). Crystallographic data were collected (ω-scans) on a Nonius Kappa-CCD with Mo-*Kα* radiation (λ = 0.71073 Å) for **4** and Oxford Diffraction/Agilent SuperNova diffractometer with Cu-*Kα* radiation (λ = 1.54184 Å) equipped with a nitrogen gas Oxford Cryosystems Cryostream unit for all other structures reported.[28] Raw frame data were reduced using CrysAlisPro, including unit cell determination and refinement, integration of intensities and associated correction, or the DENZO-SMN package.[29] The structures were solved using direct methods with SIR92[30] for **4** and SHELXT[31] for all other structures; and then refined using full-matrix least squares refinement on all F^2 data using the CRYSTALS program suite[32,33] for **4**, and SHELXL[31] using the interface GUI OLEX2[34] for all other structures. Some of the CF_3 groups in the $[BAr^F{}_4]^-$ anion refined to give highly prolate[35] displacement ellipsoids. For each structure a split site model was used and the same distance restraints were applied to maintain a sensible geometry. Thermal similarity and vibrational restraints were also used to

ensure the displacement ellipsoids behaved as expected. For **4**, the hydrogen atoms were located in the difference Fourier maps and refined independently using soft restraints.[33] Hydrogen atoms were refined in this way at intervals following inclusion in the refinement using a riding model. For **6**, the hydrogen atoms were set at geometric positions with the exception of the hydride H atoms, which were located using the difference Fourier map, refined and the Rh–H bond lengths were restrained to refine similar lengths for the six independent molecules present in the asymmetric unit. In addition, **6** was refined as a 2-component twin, rotated by –179.9 ° around 0.00 0.45–0.89 (reciprocal space) or –0.05 0.71–0.71 (direct space) and BASF refined to 0.4203(7).

The relevant crystallographic data are summarised in the following tables.

6.10.1 Crystallographic data

Complex	4	6
CCDC number	1917326	1917160
Formula	$C_{24}H_{51}BN_2O_2P_2Rh \cdot C_{32}H_{12}BF_{24}$	$C_{21}H_{40}NO_2P_2Rh$
Formula weight	1438.55	503.39
Temperature (K)	150	150
Crystal system	Monoclinic	Triclinic
Space group	$P2_1/c$	P-1
a (Å)	12.6670(1)	9.2325(2)
b (Å)	18.7076(2)	26.6707(4)
c (Å)	26.9666(3)	33.1426(6)
α (°)	90	68.569(2)
β (°)	94.9435(5)	89.805(2)
γ (°)	90	88.221(10)
V (Å^3)	6366.48(11)	7592.7(3)
Z	4	12
ρ (calcd) (g cm^{-1})	1.501	1.321
μ (mm^{-1})	0.43	6.76
Reflections collected	22651	51748
Unique reflections	14142	51748
Restraints/parameters	924/1072	36/1555
R_{int}	0.029	0.097
R_1 [$I > 2\sigma(I)$]	0.050	0.059
wR_2 [$I > 2\sigma(I)$]	0.135	0.189
GoF	0.92	1.09
Residual electron density (e Å^{-3})	1.17, –1.11	1.83, –2.10

Table 6.1 Crystallographic data for complexes **4** and **6**.

Complex	**10**	**11**
CCDC number	-	-
Formula	$C_{32}H_{59}BN_2O_2P_2Rh \cdot C_{32}H_{12}BF_{24}$	$C_{22}H_{40}NO_4P_2Rh$
Formula weight	1542.71	547.40
Temperature (K)	150	150
Crystal system	Triclinic	Triclinic
Space group	*P*-1	*P*-1
a (Å)	14.3741(3)	8.3782(4)
b (Å)	14.4138(3)	12.0810(4)
c (Å)	18.2481(4)	13.4501(5)
α (°)	85.3254(18)	100.518(3)
β (°)	69.033(2)	97.491(3)
γ (°)	83.3425(16)	104.067(3)
V (Å^3)	3503.33(14)	1276.39(9)
Z	2	2
ρ (calcd) (g cm^{-1})	1.462	1.424
μ (mm^{-1})	3.36	6.81
Reflections collected	37809	15302
Unique reflections	14510	5260
Restraints/parameters	456/930	0/283
R_{int}	0.020	0.031
R_1 [$I > 2\sigma(I)$]	0.043	0.028
wR_2 [$I > 2\sigma(I)$]	0.109	0.069
GoF	0.90	1.04
Residual electron density (e Å^{-3})	1.66, –1.16	1.94, –0.74

Table 6.2 Crystallographic data for complexes **10** and **11**.

Complex	**14**	**15**
CCDC number	-	-
Formula	$C_{23}H_{42}NO_4P_2Rh$	$C_{22}H_{39}F_3NO_5P_2RhS$
Formula weight	561.42	651.45
Temperature (K)	150	150
Crystal system	Monoclinic	Monoclinic
Space group	$P2_1/c$	$P2_1/n$
a (Å)	17.2801(2)	10.8548(1)
b (Å)	10.7562(1)	19.8340(1)
c (Å)	15.1424(1)	14.2251(1)
α (°)	90	90
β (°)	108.434(1)	110.608(1)
γ (°)	90	90
V (Å^3)	2670.07(5)	2866.61(4)
Z	4	4
ρ (calcd) (g cm^{-1})	1.397	1.509
μ (mm^{-1})	6.52	7.01
Reflections collected	35540	74141
Unique reflections	5562	5978
Restraints/parameters	0/293	0/328
R_{int}	0.041	0.057
R_1 [$I > 2\sigma(I)$]	0.024	0.026
wR_2 [$I > 2\sigma(I)$]	0.066	0.070
GoF	0.99	1.04
Residual electron density (e Å^{-3})	0.52, –0.35	0.45, –0.67

Table 6.3 Crystallographic data for complexes **14** and **15**.

6.11 References

[1] A. B. Pangborn, M. A. Giardello, R. H. Grubbs, R. K. Rosen, F. J. Timmers, *Organometallics* **1996**, *15*, 1518–1520.
[2] A. T. Lubben, J. S. McIndoe, A. S. Weller, *Organometallics* **2008**, *27*, 3303–3306.
[3] A. J. Martínez-Martínez, A. S. Weller, *Dalton Trans.* **2019**, *48*, 3551–3554.
[4] A. L. Colebatch, B. W. Hawkey Gilder, G. R. Whittell, N. L. Oldroyd, I. Manners, A. S. Weller, *Chemistry – A European Journal* **2018**, *24*, 5450–5455.
[5] M. E. Sloan, A. Staubitz, T. J. Clark, C. A. Russell, G. C. Lloyd-Jones, I. Manners, *J. Am. Chem. Soc.* **2010**, *132*, 3831–3841.
[6] C. A. Jaska, K. Temple, A. J. Lough, I. Manners, *J. Am. Chem. Soc.* **2003**, *125*, 9424–9434.
[7] O. J. Metters, A. M. Chapman, A. P. M. Robertson, C. H. Woodall, P. J. Gates, D. F. Wass, I. Manners, *Chem. Commun.* **2014**, *50*, 12146–12149.
[8] M. Roselló-Merino, J. López-Serrano, S. Conejero, *J. Am. Chem. Soc.* **2013**, *135*, 10910–10913.
[9] M. Brookhart, B. Grant, A. F. Volpe, *Organometallics* **1992**, *11*, 3920–3922.
[10] A. Van Der Ent, A. L. Onderdelinden, R. A. Schunn, in *Inorganic Syntheses*, John Wiley & Sons, Inc., **1990**, pp. 90–92.
[11] W. H. Bernskoetter, C. K. Schauer, K. I. Goldberg, M. Brookhart, *Science* **2009**, *326*, 553–556.
[12] M. Findlater, K. M. Schultz, W. H. Bernskoetter, A. Cartwright-Sykes, D. M. Heinekey, M. Brookhart, *Inorg. Chem.* **2012**, *51*, 4672–4678.
[13] G. M. Adams, F. M. Chadwick, S. D. Pike, A. S. Weller, *Dalton Trans.* **2015**, *44*, 6340–6342.
[14] L. Carreras, L. Rovira, M. Vaquero, I. Mon, E. Martin, J. Benet-Buchholz, A. Vidal-Ferran, *RSC Adv.* **2017**, *7*, 32833–32841.
[15] S. Kundu, W. W. Brennessel, W. D. Jones, *Inorg. Chem.* **2011**, *50*, 9443–9453.
[16] G. B. Fisher, J. C. Fuller, J. Harrison, S. G. Alvarez, E. R. Burkhardt, C. T. Goralski, B. Singaram, *J. Org. Chem.* **1994**, *59*, 6378–6385.
[17] M. J. Frisch, G. W. Trucks, H. B. Schlegel, G. E. Scuseria, M. A. Robb, J. R. Cheeseman, G. Scalmani, V. Barone, B. Mennucci, G. A. Petersson, et al., *Gaussian 09 Revision D.01*, Wallingford CT, **2014**.
[18] A. D. Becke, *Phys. Rev. A* **1988**, *38*, 3098–3100.
[19] J. P. Perdew, *Phys. Rev. B* **1986**, *33*, 8822–8824.
[20] D. Andrae, U. Häußermann, M. Dolg, H. Stoll, H. Preuß, *Theoret. Chim. Acta* **1990**, *77*, 123–141.
[21] A. Höllwarth, M. Böhme, S. Dapprich, A. W. Ehlers, A. Gobbi, V. Jonas, K. F. Köhler, R. Stegmann, A. Veldkamp, G. Frenking, *Chemical Physics Letters* **1993**, *208*, 237–240.
[22] W. J. Hehre, R. Ditchfield, J. A. Pople, *J. Chem. Phys.* **1972**, *56*, 2257–2261.
[23] P. C. Hariharan, J. A. Pople, *Theoret. Chim. Acta* **1973**, *28*, 213–222.
[24] F. Weigend, R. Ahlrichs, *Phys. Chem. Chem. Phys.* **2005**, *7*, 3297–3305.
[25] F. Weigend, *Phys. Chem. Chem. Phys.* **2006**, *8*, 1057–1065.
[26] J. Tomasi, B. Mennucci, R. Cammi, *Chem. Rev.* **2005**, *105*, 2999–3094.

[27] S. Grimme, S. Ehrlich, L. Goerigk, *Journal of Computational Chemistry* **2011**, *32*, 1456–1465.
[28] J. Cosier, A. M. Glazer, *J Appl Cryst* **1986**, *19*, 105–107.
[29] Z. Otwinowski, W. Minor, in *Methods in Enzymology*, Academic Press, **1997**, pp. 307–326.
[30] A. Altomare, G. Cascarano, C. Giacovazzo, A. Guagliardi, M. C. Burla, G. Polidori, M. Camalli, *J Appl Cryst* **1994**, *27*, 435–435.
[31] G. M. Sheldrick, *Acta Cryst A* **2015**, *71*, 3–8.
[32] P. W. Betteridge, J. R. Carruthers, R. I. Cooper, K. Prout, D. J. Watkin, *J Appl Cryst* **2003**, *36*, 1487–1487.
[33] R. I. Cooper, A. L. Thompson, D. J. Watkin, *J Appl Cryst* **2010**, *43*, 1100–1107.
[34] O. V. Dolomanov, L. J. Bourhis, R. J. Gildea, J. a. K. Howard, H. Puschmann, *J Appl Cryst* **2009**, *42*, 339–341.
[35] I. A. Guzei, M. Wendt, *Dalton Trans.* **2006**, 3991–3999.